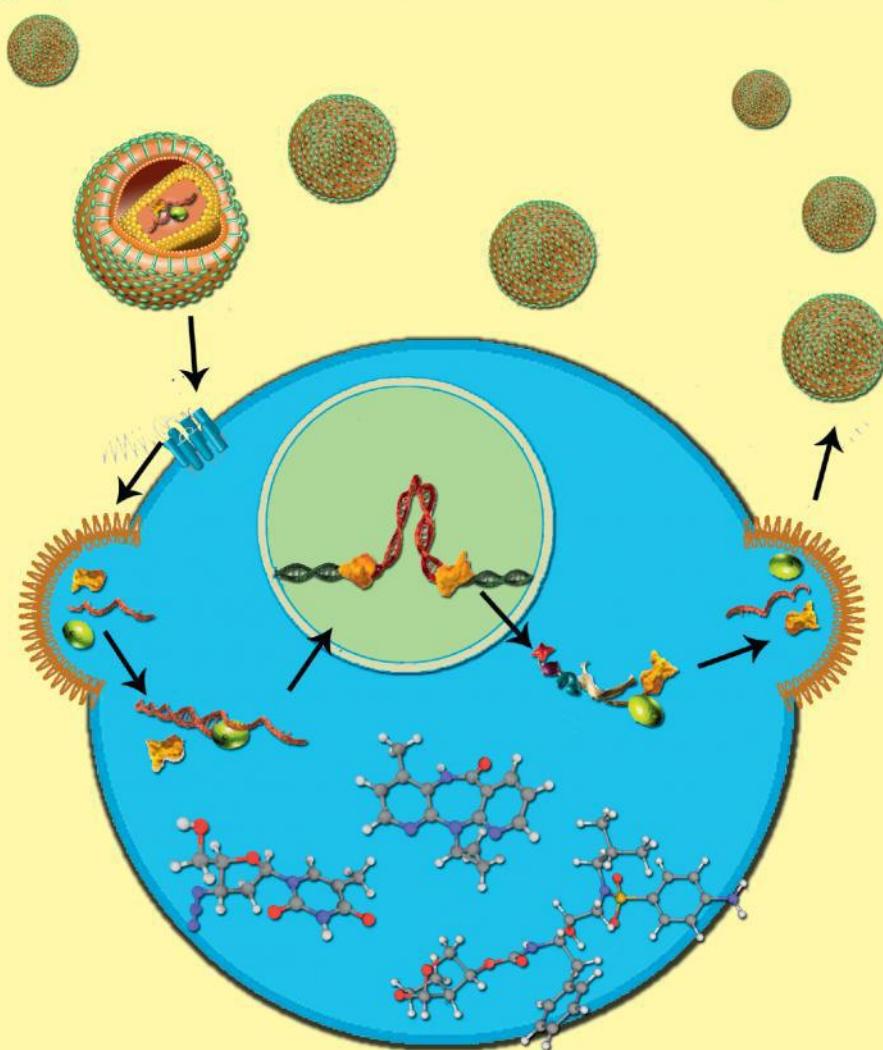


Acta Naturae

Therapy of HIV Infection: Current Approaches and Prospects



**PECULIARITIES
OF YEASTS AND
HUMAN
TELOMERASE RNAs
PROCESSING**
P. 14

**SYNTHETIC
FLUOROPHORES
FOR VISUALIZING
BIOMOLECULES IN
LIVING SYSTEMS**
P. 33

**THE ROLE OF BAR
DOMAIN PROTEINS
IN REGULATION
OF MEMBRANE
DYNAMICS**
P. 60

CHEMRAR Hi-Tech Center is a unique pharma and biotech cluster built in Russian Federation by highly innovative life science R&D organizations, discovering, developing and commercializing novel drugs for partners in Russia and worldwide.


We see **our mission** in bringing novel therapies for unmet needs in treating CNS, oncology, cardiovascular, metabolic and infection diseases through using novel post genomic technology platforms.

CHEMRAR`s companies offer a broad range of services and flexible partnering models in the following areas:

- S** Streamlined drug discovery preclinical and clinical development;
- P** Partnering for innovative drug combinations;
- F** Formulation, nano-based delivery technologies for improved pharmacokinetics and efficacy;
- C** Co-partnering of innovative molecules from target to market.

CHEMRAR`s companies invite financial and development partners for collaboration on pharmaceutical market in Russia!

Letter from the Editors



Dear readers of ActaNaturae, As we move towards the end of year 2016, we can state with certainty that the *Acta Naturae* journal has become one of the highest-ranking Russian periodicals. The impact factor of our journal has increased to 1.77. Along with the fundamental research, we manage to publish other interesting materials in the “Forum” section. Thus, in this issue we present an analytical review focused on revision of the regulatory framework for genetically modified organisms (GMOs) and GMO products, as well as the approaches for assessing their safety and the related potential risks.

The Editorial Board has elaborated and is currently launching the electronic manuscript submission system, which is expected to bring the process of preparing and monitoring the publications to a new technological level. We hope that our journal will maintain high ranking positions and the high impact factor due to the quality of our publications.

We sincerely wish you a happy New Year 2017 and will be glad to see you reading the next issue of Acta Naturae! ●

The Editorial Board

INNOVATION RUSSIA

Discussion club

We create a dialogue between all socially active groups of people: students, scientists, lecturers, businessmen, managers, innovators, investors, designers, art critics, architects, photographers.

Learn more
at WWW.STRF.RU

Everyone with something to say and
ideas to share is welcome to visit
our events

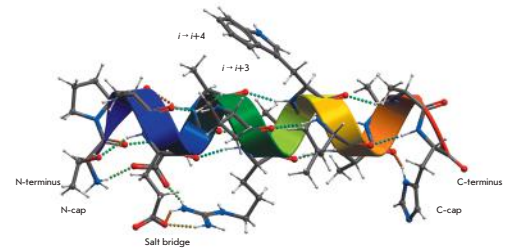


Tel.: +7 (495) 930-87-07, 930-88-50
E-mail: seminar@strf.ru

Design of stable α -helical peptides and thermostable proteins in biotechnology and biomedicine

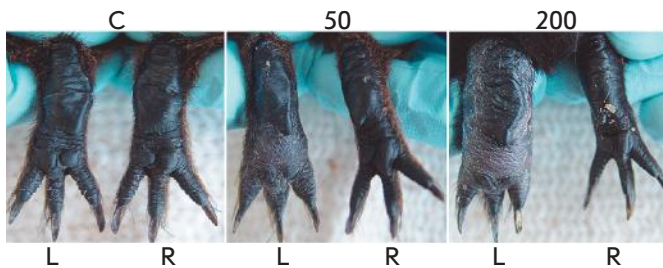
A.P. Yakimov, A.S. Afanaseva, M.A. Khodorkovskiy, M.G. Petukhov

Designing highly stable α -helical peptides used as highly active and specific inhibitors of protein–protein and other interactions have recently found more applications in medicine. In this review, we discuss the approaches to increasing the conformational stability of α -helical peptides, the methods to improve the permeability of peptides and proteins across cellular membranes and their resistance to intracellular protease activity.



Structure and factors influencing the conformational stability of α -helices in proteins and monomeric peptides

Adjuvant-induced arthritis in guinea pigs



Appearance of the hind limbs of guinea pigs on day 37 after CFA injection

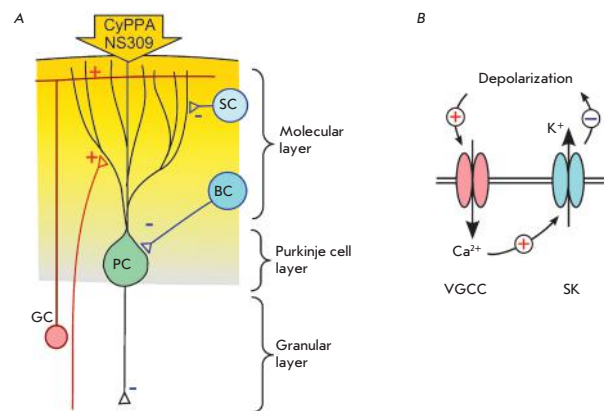
O.S. Taranov, S.N. Yakubitskiy, T.S. Nepomnyashchikh, A.E. Nesterov, and S.N. Shchelkunov

We propose a model of rheumatoid arthritis induced in outbred guinea pigs using a single subcutaneous injection of complete Freund's adjuvant to the hind paw. The high reproducibility of arthritis induction in this RA model is demonstrated. The proposed model is promising for the assessment of anti-arthritis drugs and dosage regimens.

Downregulation of activity of Purkinje cells by modulators of small conductance calcium-activated potassium channels in rat cerebellum

T. V. Karelina, Yu. D. Stepanenko, P. A. Abushik, D. A. Sibarov, S. M. Antonov

Activators of SK channels NS309 and CyPPA are shown to reduce simple spike frequency in Purkinje cells in rat cerebellum. The maximum effect was age-independent but was achieved faster in old animals. A direct effect of NS309 and CyPPA on potassium channels in Purkinje cells was revealed, which enhanced trace hyperpolarization of the Purkinje cells and increased the interspike interval. The use of SK channel activators can possibly compensate for age-related changes in autorhythmic functions of the cerebellum.



The scheme of action of SK channel modulators on Purkinje cells upon application to the cerebellum surface

Founders

Ministry of Education and
Science of the Russian Federation,
Lomonosov Moscow State University,
Park Media Ltd

Editorial Council

Chairman: A.I. Grigoriev
Editors-in-Chief: A.G. Gabibov, S.N. Kochetkov

V.V. Vlassov, P.G. Georgiev, M.P. Kirpichnikov,
A.A. Makarov, A.I. Miroshnikov, V.A. Tkachuk,
M.V. Ugryumov

Editorial Board

Managing Editor: V.D. Knorre
Publisher: K.V. Kiselev

K.V. Anokhin (Moscow, Russia)
I. Bezprozvanny (Dallas, Texas, USA)
I.P. Bilenkina (Moscow, Russia)
M. Blackburn (Sheffield, England)
S.M. Deyev (Moscow, Russia)
V.M. Govorun (Moscow, Russia)
O.A. Dontsova (Moscow, Russia)
K. Drauz (Hanau-Wolfgang, Germany)
A. Friboulet (Paris, France)
M. Issagouliants (Stockholm, Sweden)
A.L. Konov (Moscow, Russia)
M. Lukic (Abu Dhabi, United Arab Emirates)
P. Masson (La Tronche, France)
K. Nierhaus (Berlin, Germany)
V.O. Popov (Moscow, Russia)
I.A. Tikhonovich (Moscow, Russia)
A. Tramontano (Davis, California, USA)
V.K. Švedas (Moscow, Russia)
J.-R. Wu (Shanghai, China)
N.K. Yankovsky (Moscow, Russia)
M. Zouali (Paris, France)

Project Head: N.V. Soboleva

Editor: N.Yu. Deeva

Designer: K.K. Oparin

Art and Layout: K. Shnaider

Copy Chief: Daniel M. Medjo

Address: 119234 Moscow, Russia, Leninskiye Gory, Nauchny
Park MGU, vlad.1, stroeniye 75G.
Phone/Fax: +7 (495) 727 38 60
E-mail: vera.knorre@gmail.com, actanaturae@gmail.com

Reprinting is by permission only.

© ACTA NATURAE, 2016

Номер подписан в печать 27 октября 2016 г.

Тираж 200 экз. Цена свободная.

Отпечатано в типографии «МИГ ПРИНТ»

Indexed in Pubmed, Web of Science,
Scopus, and RISC

CONTENTS

Letter from the Editors 1

RESEARCH ARTICLES

I. V. Korobko, P. G. Georgiev, K. G. Skryabin,
M. P. Kirpichnikov

GMOs in Russia: Research, Society and
Legislation 6

REVIEWS

M.P. Rubtsova, D.P. Vasilkova, Yu.V. Naraykina,
O.A. Dontsova

Peculiarities of Yeasts and Human
Telomerase RNAs Processing 14

M. M. Prokofjeva, S. N. Kochetkov,
V. S. Prassolov

Therapy of HIV Infection: Current
Approaches and Prospects 23

V. I. Martynov, A. A. Pakhomov,
N. V. Popova, I. E. Deyev, A. G. Petrenko

Synthetic Fluorophores for Visualizing
Biomolecules in Living Systems 33

B. S. Shenkman

From Slow to Fast: Hypogravity-Induced
Remodeling of Muscle Fiber Myosin
Phenotype 47

CONTENTS

T.B. Stanishneva-Konovalova, N.I. Derkacheva,
S.V. Polevova, O.S. Sokolova

**The Role of BAR Domain Proteins in Regulation
of Membrane Dynamics.....60**

A.P. Yakimov, A.S. Afanaseva,
M.A. Khodorkovskiy, M.G. Petukhov

**Design of Stable α -Helical Peptides and
Thermostable Proteins in Biotechnology
and Biomedicine70**

RESEARCH ARTICLES

R. S. Esipov, Yu. A. Abramchik, I. V. Fateev,
I. D. Konstantinova, M. A. Kostromina,
T. I. Muravyova, K. G. Artemova, A. I.
Miroshnikov

**A Cascade of Thermophilic Enzymes As
an Approach to the Synthesis of Modified
Nucleotides82**

T. V. Karelina, Yu. D. Stepanenko, P. A.
Abushik, D. A. Sibarov, S. M. Antonov

**Downregulation of Purkinje Cell Activity
by Modulators of Small Conductance
Calcium-Activated Potassium Channels In Rat
Cerebellum91**

S. Yu. Smirnova, Yu. V. Sidorova, N. V.
Ryzhikova, K. A. Sychevskaya, E. N.
Parovichnikova, A. B. Sudarikov

**Evolution of Tumor Clones in Adult Acute
Lymphoblastic Leukemia100**

O.S. Taranov, S.N. Yakubitskiy, T.S.
Nepomnyashchikh, A.E. Nesterov, and S.N.
Shchelkunov

**Adjuvant-Induced Arthritis
in Guinea Pigs110**

E.I. Shramova, G.M. Proshkina, S.P. Chumakov,
Yu.M. Khodarovich, S.M. Deyev

**Flavoprotein Nimisog Cytotoxicity Can Be
Induced By Bioluminescence Resonance Energy
Transfer118**

Guidelines for Authors.....124

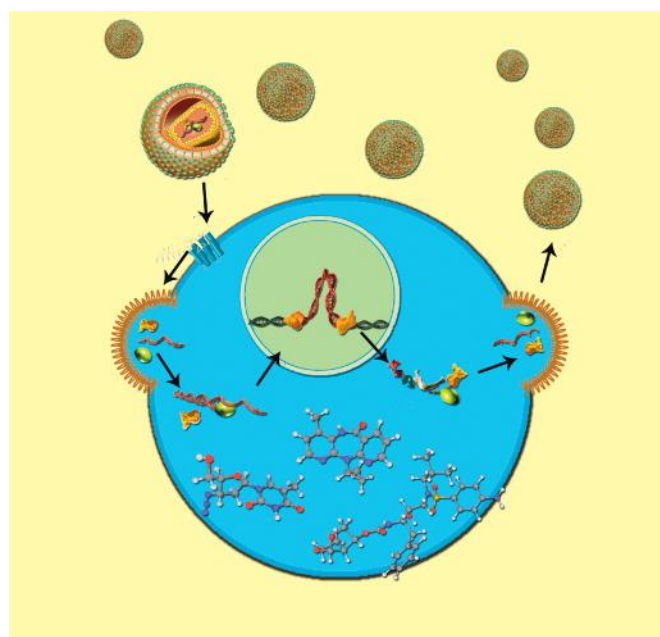


IMAGE ON THE COVER PAGE
(see the article by Prokofjeva *et al.*)

GMOs in Russia: Research, Society and Legislation

I. V. Korobko^{1*}, P. G. Georgiev¹, K. G. Skryabin², M. P. Kirpichnikov³

¹Institute of Gene Biology RAS, Vavilova Str. 34/5, 119334, Moscow, Russia

²The Federal Research Centre "Fundamentals of Biotechnology" RAS, Leninskii prospect Str. 33, build. 2, 119071, Moscow, Russia

³Moscow State University, Leninskie gory 1, 119991, Moscow, Russia

*E-mail: igorvk@igb.ac.ru

Russian legislation lags behind the rapid developments witnessed in genetic engineering. Only a scientifically based and well-substantiated policy on the place of organisms that are created with the use of genetic engineering technologies and an assessment of the risks associated with them could guarantee that the breakthroughs achieved in modern genetic engineering technologies are effectively put to use in the real economy. A lack of demand for such breakthroughs in the practical field will lead to stagnation in scientific research and to a loss of expertise.

The history of mankind is closely linked to the selection of plants and animals in an effort to reinforce favorable traits for practical use. With scientific progress, the methods of selection have been fine tuned for an expedited generation and selection of varieties with the desired traits. The arrival of genetic engineering techniques marked another milestone in the field, representing a major breakthrough from a selection among random genetic changes to the targeted generation of organisms with the desired traits through a pre-designed modification of their genomes. Targeted genome editing technologies, besides enabling the highly efficient generation of organisms with the desired characteristics, opened up the possibility of producing foreign for organism metabolites and proteins for application in various fields, including the pharmaceutical and food industries, veterinary medicine and agriculture, as well as biotechnology and environmental protection.

The importance of genetically modified organisms (GMOs) cannot be overemphasized, as exem-

plified by modern pharmaceuticals, in particular recombinant proteins and vaccines, as well as by the increased efficiency in agriculture that has contributed to the drive to solve the problem of food supply, etc. Genetically modified (GM) animals are carving a place for themselves in biotechnology: in particular, as bioreactors for recombinant protein production [1]. Along with industrial use, GMOs are also invaluable tools in scientific research, from gene function studies to serving as models of human diseases. Overall, the role of GMOs in our modern world continues to grow. Meanwhile, the increasing importance of GMOs in human life and the development of targeted genome editing technologies requires that we develop well-coordinated approaches to the handling and usage of GMOs and GMO-derived products (*i.e.*, products containing or produced with the aim of or using GMOs) (GM products). Such approaches should ensure not only an optimal use of GMOs from the social and economic standpoint, but also safety in their handling.

It is important to note that circulation in the real economy of GMOs and GM products and the demand for them are closely linked to fundamental and applied research focused on the development of novel, targeted genome editing technologies and the optimization of existing ones: under conditions of a lack of demand for GMOs or prohibitive GMO turnover legislation, research in the field becomes irrelevant and atrophies. This, in turn, reinforces the dependence of transgenic research and research in targeted genome editing on the legislative framework that regulates GMO turnover and state policy in this regard. The development of biotechnology is a priority for the Russian Federation, as stated in "The Program of Development of Biotechnologies Through 2020" approved by the Government of the Russian Federation in 2012, and the companion roadmap "Development of Biotechnology and Genetic Engineering." Genetic engineering is also in focus in the roadmap, which includes measures aiming at eliminating current inconsistencies in GMO regulation, to improve GMO-

related risk assessment, and to introduce cutting-edge techniques for GMO generation. Put together, these measures should sustain progress in genetic engineering, both in fundamental research and through vigorous demand in the applied sector. Owing to the initiatives contained in the Program, in the Russian Federation attention is given today to genetic engineering through the funding of research in key areas of bioeconomics in the form of programs of fundamental research, federal target programs, grants, etc. For example, in the framework of the state project “The Development of Biotechnologies and Industrial Adaptation of High-Reproduction Agricultural Plant GM Seed Production,” the first transgenic (*Bt*) potato varieties were developed in Russia, including the resistant-to-the-colorado-potato-beetle varieties Elizaveta Plus and Lugovskoi Plus. The benefits of the Russian *Bt*-potato lines are their stability, cost-efficiency, easy cultivation, and the environmental benefits of not needing insecticides. The two potato varieties have been approved for marketing by the Government (2005 and 2006, respectively). The varieties are listed in the State Registry of Varieties and Selection Achievements (2009) and covered by patents of the Russian Federation [2–10]. In 2015, The Russian Science Foundation (RSF) announced a call for research proposals that addressed various research priorities, among which was the development of techniques for the production of pharmaceuticals in eukaryotic systems, including plants and animals as bioreactors. Following a review of the applications, three proposals received financial support, which, along with other goals, aimed to develop novel approaches in animal transgenesis on the basis of existing best practices in the field. This will make it possible not just to generate animals

producing recombinant proteins for practical use, firstly in medicine and pharmaceutical applications, but also improve the safety of the recombinant proteins and minimize the potential risks to consumers associated with them. These examples clearly indicate an orientation of the state’s policy towards both preserving and building up expertise in this field. However, in contrast to the priorities set forth in the Complex Program and the Roadmap, the current legislative framework does not support the practical use of GM animals and plants, whereas the anticipated changes in it and the proposed solutions have some significant drawbacks. If ignored, this situation will not encourage the adoption of practical decisions in this sector of the economy, which is at the moment characterized by legislative uncertainty and anemic growth, while it is an innovative and hi-tech sector.

THE GMO LEGISLATIVE FRAMEWORK IN THE RUSSIAN FEDERATION

As of today, circulation of GMOs in the Russian Federation is regulated by Federal Law dated June 05, 1996, No. 86-FZ (edit. on June 19, 2011) “On the State Regulation in Genetic Engineering” (hereafter “86-FZ”) and by Government Decree of the Russian Federation dated February 16, 2001, No. 120 “On the State Registration of Genetically Modified Organisms”. In addition, turnover of GMOs for some particular use, such as food, feeds, and feed supplements, is regulated by national normative documents or recent acts of the Customs Union, such as Customs Union Technical Regulations TR CU 021/2011, TR CU 022/2011, TR CU 027/2012, TR CU 029/2012. However, mechanisms of state registration of GMOs intended for release into the environment, bylaws, and normative documents guiding the state regis-

tration process are lacking. Under these conditions, cultivation and breeding of GMOs, for example in agriculture, is ruled out. Furthermore, since the adoption of 86-FZ, genetic engineering techniques have undergone significant progress. The methods currently used allow for targeted genome editing without leaving foreign DNA sequences behind, collectively known as scarless genome editing, such as CRISPR (Clustered Regularly Interspaced Short Palindromic Repeats), TALEN (Transcription Activator-Like Effector Nucleases), and ZFN (Zinc Finger Nucleases) [11–14]. Also, there is a trend away from first- and second-generation GM plants, which are generated through the introduction of foreign DNA sequences into a recipient organism, toward third- and fourth-generation GMOs that lack foreign genetic material in their genomes. These trends definitely require an unambiguous legislative definition and positioning. This situation, which *de facto* makes impossible state registration of GMOs and the obtaining of approval for field farming, is supposed to be addressed by Government Decree of September, 2013, No. 839 “On the State Registration of Genetically Modified Organisms Intended for Release into the Environment, As Well As Products Obtained with the Use of Such Organisms or Containing Such Organisms” (hereinafter Decree No. 839), slated to enter into force on July 01, 2017. Decree No. 839 regulates the procedures of state registration and approval for a permitted use of GMOs intended for release into the environment, as well as products containing or produced with the use of such organisms. Yet, Decree No. 839 nullifies Decree No. 120 of the Russian Federation dated February 16, 2001. Decree No. 839 differentiates GMOs based on their intended use, subject to the implementation of proce-

dures developed by a corresponding body of executive power for conducting assessments suitable for each type of intended use. It is now clear that the list of intended uses of GMOs stated in Decree No. 839 (manufacturing of human and veterinary pharmaceuticals, medical devices, food, feeds and feed supplements, breeding and/or cultivation on the territory of the Russian Federation of GM plants, animals, and agricultural microorganisms) is far from comprehensive, thus potentially raising hurdles in the future for GMO use in certain applications. Namely, today several field trials of GM mosquitoes designed to eliminate mosquito-transmitted human diseases, such as Dengue fever, are underway [15–17]. Clearly, neither of the types of GMO intended use listed in Decree No. 839 covers this example, which can be defined as “environmental modification.” Also, Decree No. 839 does not specify the possibility of registration of GMOs and GMO products in such a dynamically developing and economically important sector as “technical use,” such as biofuel production, GM cotton, etc.

Decree No. 839 implies that state registration of GMOs is contingent on issuing a permit for its intended use. In other words, if an application for a permit is rejected, there is no state registration of the GMO and the GMO does not get listed in the state registry. At the same time, we believe that one of the vital objectives in the regulations of GMO turnover in the Russian Federation is the collection of information on GMOs that hold potential for practical use (even despite the absence of a permit for use), which would allow for their identification and, if required, monitoring. In the case of a lack of GMO record-keeping, irrelevant of the issuing of a permit for use, there is a risk of their illegal use with no technical capability for their identifica-

tion and revealing facts of unauthorized use. In this regard, it is possible to introduce GMO record-keeping (for example, in the form of a consolidated GMO registry) which would be independent of the outcome of the state registration process and supposed accumulation of data on GMOs, their genetic modification, and methods of identification and monitoring.

A possible drawback of the state registration process in its current form is the execution of an expertise of GMO molecular genetic study results by several federal bodies, depending on the type of intended use. Therefore, depending on the type of intended use of a GMO and the body of executive power responsible for its registration, the required experimental data and proofs might vary. There is no doubt that the workload in testing and the type of laboratory assays should account for GMO type specifics, details of its exploitation, and the intended use. However, it would be rational to harmonize and standardize molecular genetic characterization independently of the intended use of a GMO, and to identify molecular genetic expertise as a unified step that presupposes the deposition of information on the GMO into the united GMO registry within the procedure of GMO state registration, notwithstanding whether a permit for use is granted or not.

Finally, Decree No. 839 addresses only the question of state registration of GMOs intended for release into the environment. At the same time, Decree No. 839 (as well as TR CU 021/2011 “On the Safety of Food Products”) requires state registration of a GMO as a mandatory condition for the registration of products obtained with the use of that GMO, regardless of whether the GMO is released into the open environment or used in a closed system (*i.e.*, not assuming contact

of the GMO with the environment). Therefore, GM products derived from GMOs grown and bred in a closed system without a release into the environment cannot be registered due to the lack of regulations covering the registration of GMOs not intended for release into the environment. Thus, there is now an objective need for a legal basis for state registration of GMOs used for production purposes which are not intended for release into the environment.

The third milestone in GMO legislation, besides FZ-86 and Decree No. 839, is the recently introduced Federal Law of July 3, 2016 No. 358-FZ “On the Amendments to Individual Legislative Acts of the Russian Federation Improving State Regulation in Genetic Engineering” (hereafter – 358-FZ). These amendments prohibit the cultivation and breeding of GM plants and animals, except for research and laboratory purposes. Importantly, Federal Law 358 only bans GM animals and plants “whose genetic program has been altered using genetic engineering methods and containing genetically engineered material whose appearance cannot be the result of natural processes” (358-FZ, Article 4). Therefore, third- and fourth-generation GMOs, whose genome alteration theoretically can occur naturally without genetic engineering intervention, are exempt from the prohibition, which requires a greater effort to adopt an unambiguous legal definition of such organisms and products containing such organisms or obtained with the use of such organisms.

Despite the fact that some organisms generated with the use of genetic engineering are not banned by 358-FZ, prohibitive measures might have a negative impact on this sector of the economy, which is one of the drivers of innovation. The current situation is made worse

by a lack of prohibitive measures for GM products, along with the ban on the cultivation and breeding of GM plants and animals. In a case of a need for a GM plant- or animal-derived product, there is a risk of becoming fully dependent on external sources of GMOs.

The current ban on the cultivation and breeding of GM plants and animals could also affect research in the field of plant and animal transgenesis (and, accordingly, their financial support), both fundamental and translational ones. In such a situation, the Russian Federation can quickly lose its position and expertise in this area, finally falling into a dependence on external sources of GMO supply. In particular, should the ban be adopted, it would make impossible GM animal-derived pharmaceutical (and other) recombinant protein production from milk, which, according to the RAND Corp., a highly authoritative analytical entity, will become one of the leading trends in biotechnology, bionanotechnology and biomedicine to 2020 [18]. This opinion is supported by the presence on the market of the ATryn® and Ruconest® pharmaceuticals, which are based on the recombinant human antithrombin III and C1-esterase inhibitors, which are derived from GM goat and rabbit milk, respectively [1].

WHAT IS A GMO!

The term “GMO” is the cornerstone of the field, since it defines the subject of regulation. As of today, Federal Law 86-FZ defines a GMO as “an organism or several organisms, any non-cellular, cellular and multicellular formation capable of reproduction or transmission of its own genetic material, different from wild-type [natural] organisms, generated using genetic engineering methods and carrying genetically engineered material,

including genes, their fragments, or combinations of genes.” On the one hand, this definition is very broad, and, based on it, plasmids, actually being vectors whose propagation is possible only in permissive host cells, also fall under this definition. On the other hand, the requirement of reproducing and transmitting genetic material exempts infertile GMOs, such as the hybrids of fertile GMOs. At the same time, the transfer of genetic modification on a novel genetic background occurring as a result of crossing can affect its manifestations and requires a separate assessment of the risks and safety aspects. For this reason, the definition of a GMO should also cover such organisms. Finally, with the arrival of scareless genome editing technologies not assuming the introduction of foreign genetic material, a legal status for organisms obtained with the use of such technologies should be defined. Such organisms, classified as third- and fourth-generation GMOs (see section “GMO classification”), are indeed products of genetic engineering. However, they can in theory appear through natural selection, thus meaning full principal identity of a genetic engineering manipulation to natural processes in this case, and a scientifically substantiated classification of such organisms as being non-GMOs. Along with that, because the genome of such organisms carries no scarring sequences, the GM origin of such organisms is impossible to objectively prove, unlike in the case of “classical” GMOs of the first and second generations, which bear foreign DNA in their genomes serving as proof of their genetic modification. Evidently, the impossibility of proving usage of genetic engineering methods in the generation of such organisms can lead to legal ambiguity. In light of the abovementioned concerns,

it appears rational to lump organisms with genetically engineered genomes but lacking foreign DNA with those obtained through a classical selection process, while the notion of GMO should be restricted to those bearing in their genetic material foreign DNA sequences. This view is also shared by the international scientific community [19].

To summarize, there is currently a need for amendments to the definition of “a genetically modified organism,” which should, on the one hand, address the shortcomings of the existing definition (both its redundancy and insufficiency) illustrated above, and on the other, unambiguously situate in the legal realm organisms generated with the use of scarless genome editing methods, which have the potential to appear as a result of natural processes. Federal Law 358-FZ which exempts genetically engineered organisms in which genetic modifications can result from natural processes implicitly treats such organisms as outside the GMO classification, which, however, must be evidently specified in normative acts. As alluded to above, GMOs could be defined as “non-cellular, single-cellular or multicellular formations generated with the use of genetic engineering and containing foreign DNA sequences that cannot appear as a result of natural mating and horizontal gene transfer between non-GMO organisms, and/or as a result of recombination events or mutations (deletions and insertion of endogenous genetic material, single nucleotide substitutions, chromosome rearrangements).” Other organisms generated with the use of genetic engineering technologies shall not be considered as GMOs.

THE SAFETY OF GMOS

One of the obstacles in the use of GMOs is the concerns related to their safety. The safety of GMOs

and GM-products can be divided into the safety for consumers and environmental safety.

Today, there is a belief, mainly related to food products, that the presence of a genetic modification *a priori* makes GM products dangerous for humans. However, no scientific study has revealed negative effects related to the consumption of GM food products ostensibly caused by the presence of a genetic modification *per se*. As for the published results of studies apparently demonstrating the side effects related to GMO consumption and which are used as reference, a detailed analysis of such studies reveals scientific and methodological flaws and, consequently, shaky findings [20]. Indeed, the presence of foreign DNA in a host's genome contained in a food product by no means affects the safety of such a product for consumers: (i) first, the lack of horizontal DNA transfer upon ingestion has been experimentally demonstrated for mammals [21]; (ii) second, human diets contain huge amounts of foreign DNA from plants and animals and no horizontal transfer has yet been documented.

Interestingly, GMOs have constituted a portion of our diet for the last several thousand years according to recent studies. Namely, the genome of the sweet potato plant domesticated approximately 8,000 years ago has been shown to contain two stretches of DNA derived from the genome of *Agrobacterium*, one of which, in the authors' opinion, conferred the desirable traits that warranted the domestication of this particular variety [22]. At the same time, *Agrobacterium* T-DNA-based vectors are widely used today in plant genetic engineering [23]. Overall, the consumption of naturally transgenic sweet potato for a thousand years demonstrates that transgenic food crops are safe for humans from the dietary per-

spective, which is a very sensitive subject in society.

Put together, the only threat posed by a product obtained with the use of a GMO or containing a GMO is the new characteristics that the new phenotype might possess. However, any risk assessment should be based on our common regulations for new non-GMO products, which carry risks just as well [24]. The potato variety Lenape, which was withdrawn from the market due to excessive accumulation of natural potato toxins eventually formed during random selection is a good example of the risks associated with organisms obtained through natural selection [25].

In summary, the risks related to genetic modifications *per se* are negligible, whereas organisms obtained without the use of genetic engineering, similarly to GMOs, may also be unsafe.

CLASSIFICATION OF GMO

GMO classification is of practical importance since monitoring strategies and risk assessments studies of GMOs and GM products should be guided by their intrinsic characteristics.

One of the common classification schemes is by generation. It has been historically used for GM plants (and is fully applicable to GM animals). The first-generation GMO group includes organisms that carry a fragment of exogenous DNA in their genome. The organisms that belong to the second-generation GMOs are similar to those of the first group but carry several transformation events and can be obtained by crossing first-generation GMOs. Owing to the presence of foreign DNA in the genome of first- and second-generation GMOs, these organisms can be unambiguously identified [26], and scarring sequences unequivocally provide evidence of past ge-

netic manipulations. Third- and fourth-generation GMOs, which are nearly intragenic (*i.e.*, carry endogenous DNA sequences with minimal modifications), intragenic and *cis*-genic organisms (modified essentially with authentic endogenous genetic material), should be treated differently from the abovementioned GMOs [26]. The prominent feature of these organisms is the defining possibility of natural occurrence of such genetic modifications in the wild or during selection through mutations and/or chromosome rearrangements. This, in turn, leads to the impossibility of proving objectively that genetic engineering has been used to generate such an organism. Having said that, it would seem logical that third- and fourth-generation GMOs should be treated within the legal framework as those obtained through a classical selection process.

For GMOs ascribed to the first and second generations, safety and risk assessments and applicable constraints are mostly identical, with the requirement for more than one transformation event analysis for second-generation GMO identification and monitoring. In our opinion, from a practical point of view, more important in GMO and GM product classification are the following criteria:

- cultivation and breeding in a closed system (*i.e.*, assuming no contact with the environment) or in an open environment;
- presence or absence of viable or inactivated GMOs in GMO-derived products; and
- presence or absence of GMO-derived DNA in GM products.

The abovementioned criteria allow for shaping optimal and well calibrated principles of both GMO characterization from the molecular genetics standpoint and risk assessment for GMOs and GM products.

APPROACHES TO THE RISK ASSESSMENT OF GMO AND GM PRODUCTS

GMO indented for cultivation and breeding in a closed system

A GMO of this type primarily has no contact with the environment, while contacts with humans are restricted to the manufacturing process this organism is used in, and the personnel involved in GMO processing. In this respect, there is a no need for an assessment of the impact of GMOs on the environment and of the related risks, which might exist only for manufacture waste. The potential risks to personnel during GMO handling are comparable to those faced when handling similar non-GMOs, with additional requirements to assess the risks linked to the presence of genetic modifications. Keeping in mind that GMOs may spill into the environment in an emergency situation, there should be pre-established strategies for GMO identification and monitoring based on unique transgene detection, as well as measures to eliminate the consequences of a release into the environment. At the same time, the necessity for a molecular characterization of the transformation event in a given GMO (a transformation event refers to the incorporation of an exogenous DNA fragment into a particular site of an organism's genome) should depend on the type of GMO-derived product (see below).

GMO intended for cultivation and breeding in an open environment

This type of GMO requires that the risks be assessed in terms of the interactions of such organisms with the environment and the potential impact on it. These risks can be divided into two groups. The first is related to the novel phenotypic features acquired by an organism as a result of a genetic modification, as well as to the intrinsic properties

of the recipient organism if introduced into an extrinsic ecosystem. The second relates to the risk of uncontrolled propagation of the genetic modification in the ecosystem. To evaluate the first group of risks, it would be rational to implicate the approaches, methods, and criteria used in the evaluation when a similar non-GMO is introduced into the ecosystem as a novel species. Such an evaluation could also incorporate an assessment of the risks arising from the production by the GMO of extrinsic proteins and metabolites as a result of the genetic modification. However, as of today, ecological expertise of novel breeds and varieties is not stipulated by the law, while experience in such types of expertise applicable to cases of novel species introduction is very limited. This lack of appropriate knowledge and experience hinders an efficient application of such an approach and needs to be remedied by scientifically proven guidelines to assess the environmental impact of GMOs, which would also be fully applicable to non-GMOs. Indeed, regardless of whether the resistance of an organism to environmental factors (for example, to a particular pathogen) was conferred by a genetic manipulation or occurred naturally, the risks associated with the release of such an organism into the environment are similar, and the assessment of the environmental impact of an introduction should be done for both GM and non-GM organisms. In this case, it is rational to build the assessment on the basis of a comparative analysis with a similar organism (for GMO – with the recipient organism).

The presence of a transgene adds additional requirements to the risk assessment strategy. This includes uncontrolled horizontal or vertical transgene transfer (importantly, the risks of a spread of traits (for example, resistance to pathogens and pests) acquired under classical

selection are the same, but they are not covered by the current rules). It is possible to conduct an assessment of the risks of uncontrollable transgene expansion in the ecosystem depending on the specific properties of the GMO and type of genetic modification. For instance, GM animals show negligible risks of horizontal transgene transfer, whereas the risks associated with vertical inheritance of a transgene following inbreeding should be taken into account. In contrast, for GM microorganisms the assessment of horizontal transgene transfer is a must. In order to avoid bias, studies and methods aimed at evaluating horizontal or vertical transgene transfer risks should be standardized as much as possible for different taxonomy groups of GMOs and their intended use.

In compliance with Decree No. 839, the safety of a GM organism is the only factor that affects the decision on the release of such an organism into the environment (except for GMOs intended for the production of pharmaceuticals and medical devices). At the same time, all newly acquired properties, regardless of the mechanism of acquisition, *a priori* act as risk factors due to the fact that a comprehensive analysis of the environmental impact is impossible, thus prompting an unconditional ban in order to exclude all possible risks. Having said that, the decision on the cultivation and breeding of GMOs should consider not only identified or potential environmental risks, but other factors also should be taken into account, such as technological, social, economic factors, etc., and the final decision should be based on a comprehensive multifactorial “risks versus benefits” analysis.

The strategy regarding GMOs intended for cultivation and breeding in an open environment, in particular GM plants and animals,

requires not only unambiguous identification tools enabling their monitoring, but also methods allowing for an analysis of transformation events (if the latter are present). The transformation event unambiguously identifies the line of the GMO and permits its differentiation from related lines carrying the same transgene. In this case, the transformation event can also serve as a unique feature identifying the GMO.

GMO-derived products

It is deemed logical that GMO-derived products deserve a differential approach taking into account the specific risks associated with the described-above product types. Along with that, a general approach to safety evaluation should be based on principles applicable to similar non-GM products, with an additional evaluation of the specific risks associated with the presence of a transgene, if any.

As discussed above, we believe appropriate to single out three subtypes of GM products. The first one is defined as “products obtained with the aim of GMOs” and covers products manufactured from GMOs or their “waste products,” or the latter themselves, which are free of GMO genetic material (the maximally allowed residual DNA content should be settled in this case and controlled). Recombinant proteins and target metabolites (amino acids, etc.) are examples of such products. When compared to similar non-GM products, such GM-derived products pose no additional risks because of the absence of transgenic material. On these grounds, such products can and should be treated as non-GM. The only parameter worth monitoring is ensuring that there is no residual transgenic material in a manner similar to the regulatory standards of quality control for biopharmaceuticals, implying a maxi-

mally allowed residual host strain DNA content. For GMOs used for the manufacturing of this type of products and not supposed to be released into the environment, there is no need for transformation event description, if the latter exists.

The second type of GM products consists of “products obtained with the use of GMOs” which contain whole non-viable GMOs or products of their processing not assuming the removal of host DNA. The additional risks posed by such GM products are linked to the presence of GMO DNA and the associated potential risks of a horizontal transfer, which should govern risk assessment in conjunction with screening for viable organisms.

Finally, the third type of GM products can be defined as “products containing or being viable GMOs,” thus presupposing the presence of viable GMOs. The greater number of additional risks is associated with this type of products if compared to analogous non-GM products. In this case, an assessment of the risk of uncontrolled expansion of the GMO derived from the product in the environment should be performed, and if significant, necessitate a whole complex of risk assessment tools suited to GMOs intended for release into the environment.

Modern technologies of targeted genome editing and GMO's molecular genetic characterization and safety evaluation

As noted above, the legal framework for GMO and GM product turnover could directly influence research in the field of genetic engineering. At the same time, advances in targeted genome editing technologies, along with their practical applications aiming at generating socioeconomically significant GMOs, could be of importance for GMO and GM product characterization and safety evaluation, some-

thing especially applicable to GMOs bearing a transgene integrated into the host genome.

Earlier techniques of plant and animal transgenesis resulted in random integration of transgene into the host genome at variable copy numbers. Along with significant variations in transgene expression efficiency and stability, it technically complicates the precise localization of the transgene integration site in the genome (*i.e.*, transformation event), especially in the case of tandem integration of multiple transgene copies. In addition, random incorporation of a transgene can potentially lead to side effects that affect the safety of such organisms. For example, altered protein isoforms might appear, or some metabolic pathways could be altered, etc. Current methods of targeted genome editing, such as those based on CRISPR-mediated homologous recombination, along with its combination with site-directed recombination (using Cre, Flp and other recombinases) to increase the efficiency of transgenesis, allow one to achieve a targeted integration of a transgene with single-nucleotide precision. This approach enables the selection of an optimal integration site in the recipient's genome. For example, the β -casein locus may be an optimal one for transgene insertion to efficiently produce recombinant proteins in milk, owing to its high endogenous expression level and the dispensability of β -casein for normal lactation [27, 28]. Other attractive loci are those capable of supporting transgenic expression upon insertion but whose integrity is indispensable for the normal growth and development of an organism, such as *ROSA26* locus [29–32]. Besides the efficient generation of transgenic organisms with ensured stability and efficiency of transgene expression and a minimized

likelihood of eventual adverse effects on the host due to transgene insertion, which is of importance in ensuring the organism's safety, targeted genome editing technologies allow one to control the transgene copy number and makes the description of the transformation event a routine task. Over all, the use of state-of-the art methods of targeted genome editing simplifies the essential, for state registration, molecular genetic research aimed at characterizing the generated organisms and contributes to the minimization of the risks associat-

ed with the influence of a genetic modification on the GMO safety profile compared to its non-GMO counterpart (recipient).

Conclusion

To summarize, today it is vital to revisit our legal framework and guidelines related to the safety and risk assessment of GMOs and GM products in the Russian Federation. The suggested herein concept enables to conduct an efficient evaluation, while eliminating wasteful studies depending on the specific features of a GMO, the conditions

of its intended handling, and the features of the derived GM product. The creation of a system that enables a broad involvement of GMOs in the real economy will also provide incentives for research in this dynamic and growing field, where the Russian Federation today has sufficient expertise and potential [33]. However, if the situation with the regulatory system remains unchanged, with a total ban on GM plants and GM animals remaining in place, the existing expertise might be rapidly lost because it won't be needed. ●

REFERENCES

- Maksimenko O.G., Deykin A.V., Khodarovich Y.M., Georgiev P.G. // *Acta Naturae*. 2013. V. 5. № 1. P. 33–46.
- Kamionskaya A.M., Kuznetsov B.B., Skryabin K.G. Patent RF № 2286385. IPC C12N15/00 (2006.01), C12N15/09 (2006.01), C12N15/82 (2006.01), A01H1/06 (2006.01), A01H4/00 (2006.01). 2006.
- Kamionskaya A.M., Kuznetsov B.B., Skryabin K.G. Patent RF № 2286386. IPC C12N15/00, C12N15/09, C12N15/82, A01H1/06, A01H4/00. 2006.
- Starodubtseva (Kamionskaya) A.M., Belousova M.B., Shulga O.A., Konov A.L., Skryabin K.G. Patent RF № 2231551. IPC C12N15/82, A01H4/00. 2004.
- Starodubtseva (Kamionskaya) A.M., Belousova M.B., Shulga O.A., Konov A.L., Skryabin K.G. Patent RF № 2231550. IPC C12N15/82, A01H4/00. 2004.
- Starodubtseva (Kamionskaya) A.M., Belousova M.B., Shulga O.A., Konov A.L., Skryabin K.G. Patent RF № 2231549. IPC C12N15/82, A01H4/00. 2004.
- Starodubtseva (Kamionskaya) A.M., Belousova M.B., Shulga O.A., Konov A.L., Skryabin K.G. Patent RF № 2231251. IPC C12N15/82, A01H4/00. 2004.
- Starodubtseva (Kamionskaya) A.M., Belousova M.B., Shulga O.A., Konov A.L., Skryabin K.G. Patent RF № 2231548. IPC C12N15/82, A01H4/00. 2004.
- Shestibratov K.A., Dolgov S.V. Patent RF № 2261275. IPC C12N15/00, C12N15/29, C12N15/82, A01H5/00, A01H1/06. 2002.
- Maksimenko O.G., Dolgova A.S., Bonchuk A.N., Tikhonov M.V., Gasanov N.B., Zarayskiy Ye.I., Dolgov S.V., Georgiev P.G. Patent RF № 2507736. IPC A01H1/00. 2014.
- Petersen B., Niemann H. // *Transgenic Res.* 2015. V. 24. № 3. P. 381–396.
- Osakabe Y., Osakabe K. // *Plant Cell Physiol.* 2015. V. 56. № 3. P. 389–400.
- Nemudryi A.A., Valetdinova K.R., Medvedev S.P., Zakian S.M. // *Acta Naturae*. 2014. V. 6. № 3. P. 19–40.
- Gaj T., Gersbach C.A., Barbas C.F. 3rd. // *Trends Biotechnol.* 2013. V. 31. № 7. P. 397–405.
- Favia G. // *Bioengineered*. 2015. V. 6. № 1. P. 5–7.
- Lacroix R., McKemey A.R., Raduan N., Kwee Wee L., Hong Ming W., Guat Ney T., Rahidah A.A.S., Salman S., Subramaniam S., Nordin O., et al. // *PLoS One*. 2012. V. 7. № 8. P. e42771.
- Harris A.F., Nimmo D., McKemey A.R., Kelly N., Scaife S., Donnelly C.A., Beech C., Petrie W.D., Alphey L. // *Nat. Biotechnol.* 2011. V. 29. № 11. P. 1034–1037.
- Silberglitt R., Ant n P.S., Howell D.R., Wong A. *The Global Technology Revolution 2020, In-Depth Analyses. Bio/Nano/Materials/Information Trends, Drivers, Barriers, and Social Implications. Technical Report.* Santa Monica, Calif.: RAND Corporation, 2006. 281 c.
- Huang S., Weigel D., Beachy R.N., Li J. // *Nat. Genet.* 2016. V. 48. № 2. P. 109–111.
- Xia J., Song P., Xu L., Tang W. // *Biosci. Trends.* 2015. V. 9. № 2. P. 134–137.
- Rizzi A., Raddadi N., Sorlini C., Nordgrd L., Nielsen K.M., Daffonchio D. // *Crit. Rev. Food Sci. Nutr.* 2012. V. 52. № 2. P. 142–161.
- Kyndt T., Quispe D., Zhai H., Jarret R., Ghislain M., Liu Q., Gheysen G., Kreuze J.F. // *Proc. Natl. Acad. Sci. USA.* 2015. V. 112. № 18. P. 5844–5849.
- Lacroix B., Citovsky V. // *Int. J. Dev. Biol.* 2013. V. 57. № 6–8. P. 467–481.
- Tagliabue G. // *EMBO Rep.* 2016. V. 17. № 1. P. 10–13.
- Beier R.C. // *Rev. Environ. Contam. Toxicol.* 1990. V. 113. P. 47–137.
- Lin C.-H., Pan T.-M. // *J. Food Drug. Anal.* 2016. V. 24. № 1. P. 1–8.
- Cosenza G., Pauciullo A., Colimoro L., Mancusi A., Rando A., Di Bernardino D., Ramunno L. // *Anim. Genet.* 2007. V. 38. № 6. P. 655–658.
- Kumar S., Clarke A.R., Hooper M.L., Horne D.S., Law A.J., Leaver J., Springbett A., Stevenson E., Simons J.P. // *Proc. Natl. Acad. Sci. USA.* 1994. V. 91. № 13. P. 6138–6142.
- Chen S.X., Osipovich A.B., Ustione A., Potter L.A., Hipkens S., Gangula R., Yuan W., Piston D.W., Magnuson M.A. // *Dis. Model. Mech.* 2011. V. 4. № 4. P. 537–547.
- Friedrich G., Soriano P. // *Genes Dev.* 1991. V. 5. № 9. P. 1513–1523.
- Soriano P. // *Nat. Genet.* 1999. V. 21. № 1. P. 70–71.
- Tchorz J.S., Suply T., Ksiazek I., Giachino C., Cloëtta D., Danzer C.P., Doll T., Isken A., Lemaistre M., Taylor V., et al. // *PLoS One*. 2012. V. 7. № 1. P. e30011.
- Skryabin K.G. // *New. Biotechnology.* 2010. V. 27. № 5. P. 593–595.

Peculiarities of Yeasts and Human Telomerase RNAs Processing

M.P.Rubtsova^{1,2*}, D.P.Vasilkova¹, Yu.V.Naraykina³, O.A.Dontsova^{1,2,4}

¹Lomonosov Moscow State University, Chemistry Department, Leninskie gory, 1, bld. 3, Moscow, 119991, Russia

²Lomonosov Moscow State University, Belozersky Institute of physico-chemical biology, Leninskie gory, 1, bld. 40, Moscow, 119991, Russia

³Skolkovo Institute of Science and Technology, Skolkovo Innovation Center, bld. 3, Moscow, 143026, Russia

⁴Lomonosov Moscow State University, Faculty of bioengineering and bioinformatics, Leninskie gory, 1, bld. 73, Moscow, 119991, Russia

*E-mail: mprubtsova@gmail.com

Received July 28, 2016; in final form, September 13, 2016

Copyright © 2016 Park-media, Ltd. This is an open access article distributed under the Creative Commons Attribution License, which permits unrestricted use, distribution, and reproduction in any medium, provided the original work is properly cited.

ABSTRACT Telomerase is one of the major components of the telomeres — linear eukaryotic chromosome ends — maintenance system. Linear chromosomes are shortened during each cell division due to the removal of the primer used for DNA replication. Special repeated telomere sequences at the very ends of linear chromosomes prevent the deletion of genome information caused by primer removal. Telomeres are shortened at each replication round until it becomes critically short and is no longer able to protect the chromosome in somatic cells. At this stage, a cell undergoes a crisis and usually dies. Rare cases result in telomerase activation, and the cell gains unlimited proliferative capacity. Special types of cells, such as stem, germ, embryonic cells and cells from tissues with a high proliferative potential, maintain their telomerase activity indefinitely. The telomerase is inactive in the majority of somatic cells. Telomerase activity *in vitro* requires two key components: telomerase reverse transcriptase and telomerase RNA. In cancer cells, telomerase reactivates due to the expression of the reverse transcriptase gene. Telomerase RNA expresses constitutively in the majority of human cells. This fact suggests that there are alternative functions to telomerase RNA that are unknown at the moment. In this manuscript, we review the biogenesis of yeasts and human telomerase RNAs thanks to breakthroughs achieved in research on telomerase RNA processing by different yeasts species and humans in the last several years.

KEYWORDS exosome, processing, splicing telomerase, telomerase RNA, transcription

ABBREVIATIONS TER – telomerase RNA, hTR – human telomerase RNA, TLC1 – *S.cerevisiae* telomerase RNA, TERT – telomerase reverse transcriptase, snRNA – small nuclear RNA.

INTRODUCTION

Telomerase is a ribonucleoprotein complex comprising a reverse transcriptase (TERT) – a protein subunit enabling polymerase activity, and telomerase RNA (TER) [1, 2]. Telomerase RNA contains a template for the synthesis of telomeres and has an important architectural function: it acts as a structural framework for the formation of the active enzyme [3]. Different elements of the complex spatial structure of telomerase RNA are involved in the formation of the active telomerase center, promoting the effective addition of nucleotides during the synthesis of a telomeric repeat, as well as the translocation of the enzyme at the telomere required for the processive synthesis of a long telomeric sequence [4]. Additional protein factors interact with different domains of telomerase RNA and are necessary for its stabilization, efficient assembly,

and the regulation of enzyme activity, localization, and transport within the cell.

STRUCTURE OF TELOMERASE RNA

Despite the high degree of variation in term of their sizes and nucleotide sequences, telomerase RNAs in yeast and mammals share four conserved structural elements necessary for the formation and functioning of the enzyme [5–11]. The template region, as its name implies, serves as a template for telomere synthesis [3], pseudoknot is involved in the positioning of the template region in the active site of the enzyme [12], and together with the STE-element (stem-terminus element) it interacts with TERT, whereas the species-specific 3'-terminal element ensures the stability of telomerase RNA [13] and is required for its proper intracellular localization [14–16] (*Fig. 1*).

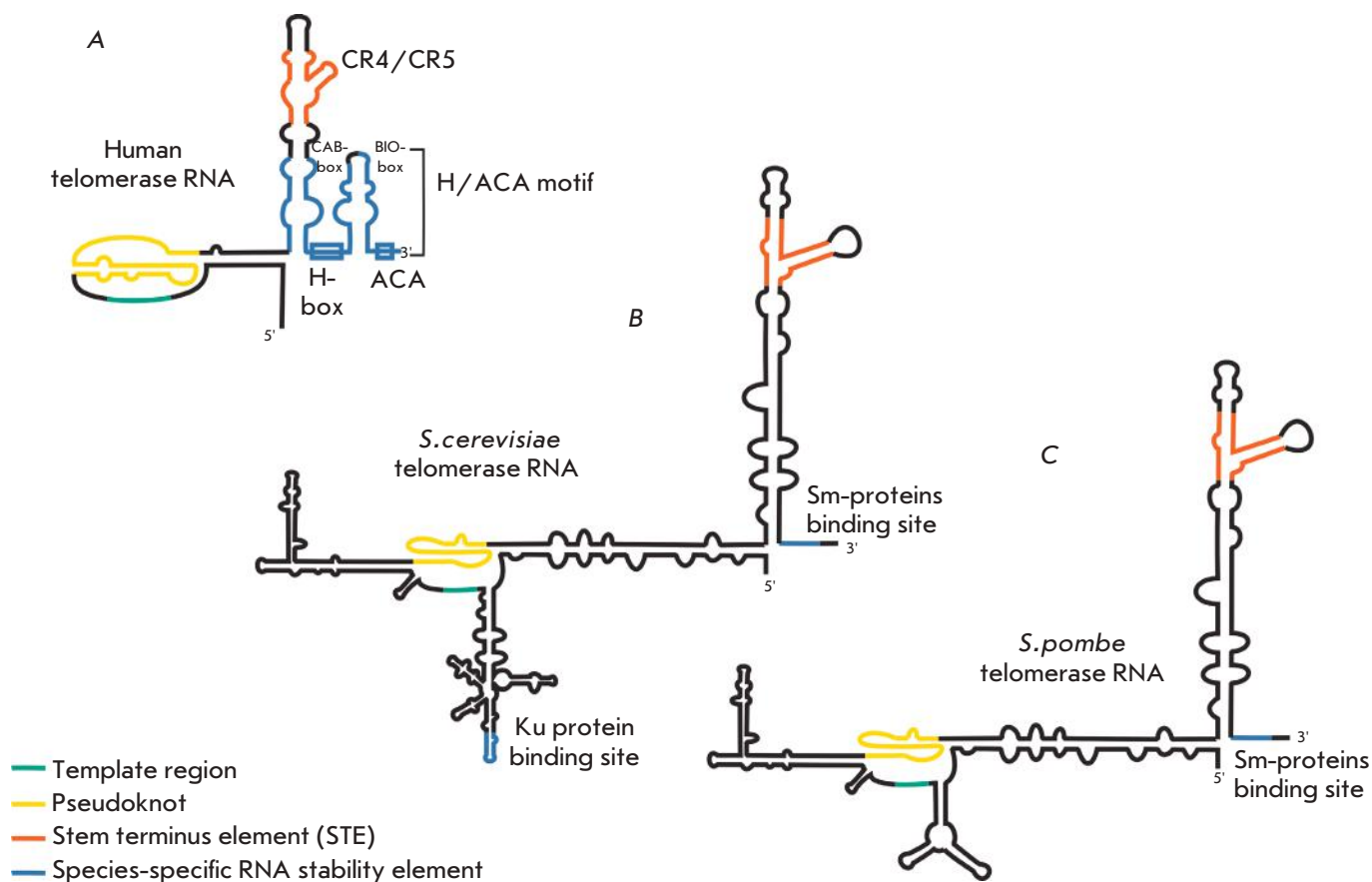


Fig. 1. Structures of yeasts and human telomerase RNAs. A. Schematic model of human telomerase RNA secondary structure. B. Schematic model of *S. cerevisiae* telomerase RNA secondary structure. C. Schematic model of *S. pombe* telomerase RNA secondary structure.

PROCESSING AND LOCALIZATION OF TELOMERASE RNA

Processing and localization of telomerase RNA of *Saccharomyces cerevisiae* (TLC1)

In the process of RNA transcription, polymerase II synthesizes two forms of telomerase RNA: a long polyadenylated one and a short non-polyadenylated one. The fate of the long polyadenylated form is poorly understood at the moment. It is known that this form accounts for 10% of the total telomerase RNA in a cell, but it is not associated with the active telomerase [17]. It is assumed that the long polyadenylated telomerase RNA can be processed to the “mature” catalytically active form. The expression of TLC1 in *S. cerevisiae* yeast is known to be regulated by a strong promoter (pGal4), which directs the expression of protein-encoding genes and leads to the accumulation of the polyadenylated form, but it does not affect the content of the non-polyadenylated one, whereas disruption of the polyadenylation system prevents the formation of the

polyadenylated form and greatly reduces the content of “mature” TLC1 in a cell [17, 18]. These data suggest that the long polyadenylated primary transcript may undergo processing to yield mature telomerase RNA, although there are no experimental data to support such a mechanism yet.

In yeast cells, different transcriptional complexes associated with RNA polymerase II participate in the formation of the two forms of the telomerase RNA primary transcript. At the transcription initiation step, RNA polymerase II forms a complex with termination and processing factors, i.e. the promoter determines the mechanism of termination. It has been demonstrated that the polyadenylated and non-polyadenylated forms of the primary transcript of *S. cerevisiae* telomerase RNA form independently. Disruption of polyadenylation signaling leads to the disappearance of the long polyadenylated form of TLC1, but it does not affect the formation of the non-polyadenylated mature form [18]. TLC1 is associated with Nrd1-Nab3-Sen1 transcription

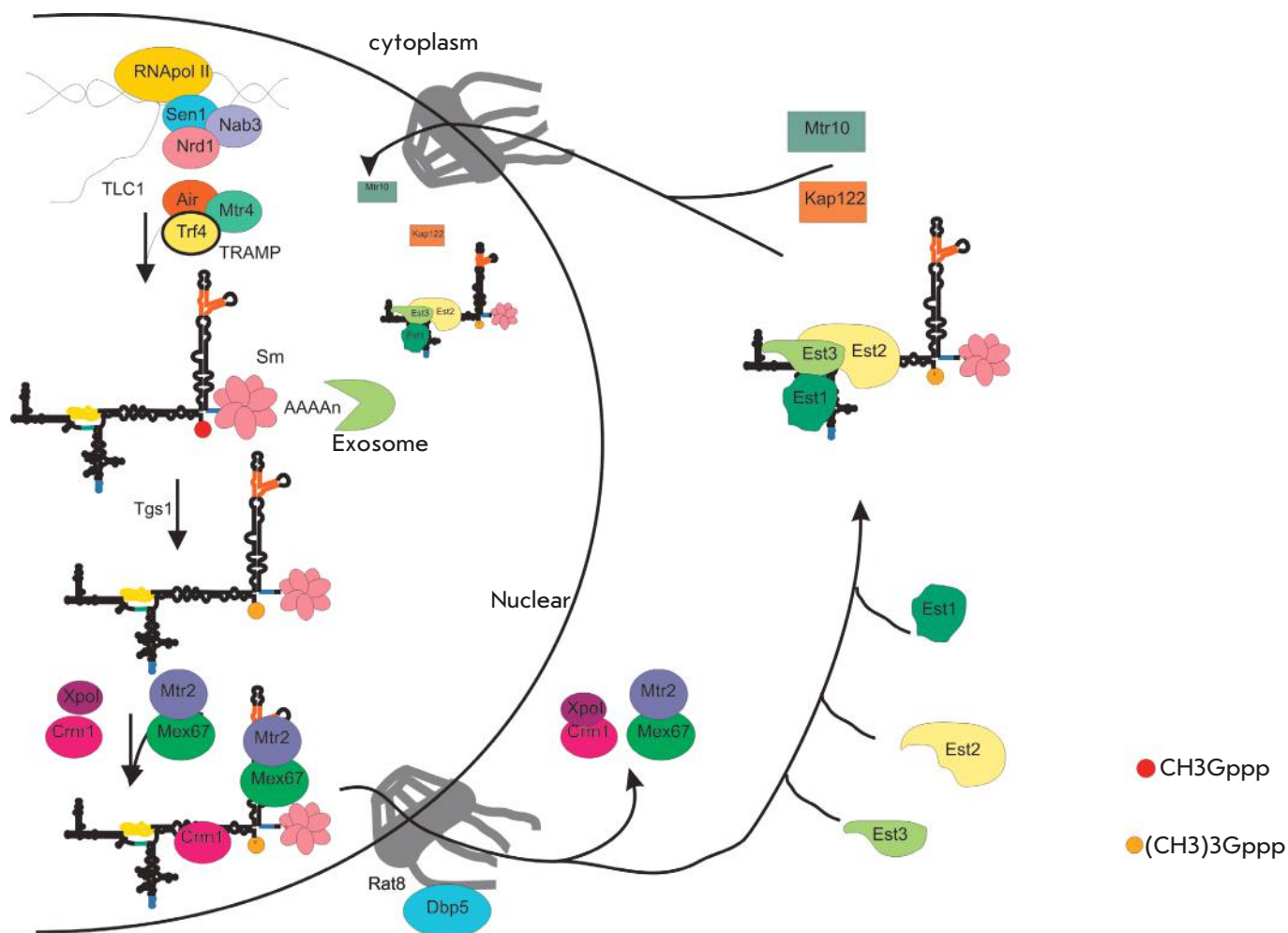


Fig. 2. Model of processing and localization of *S. cerevisiae* telomerase RNA.

termination factors, specific for noncoding RNA [19]. The 3'-terminal region of the *TLC1* gene contains binding sites for the termination factors Nab3 and Nrd1, whose deletion results in the accumulation of the polyadenylated primary transcript [18, 19]. The termination factors Nrd1, Nab3, and Sen1 are known to be associated with a complex consisting of RNA polymerase II, the cap-binding complex (CBP80, CBP20), an exosome, and TRAMP [20]. TRAMP includes TRF4/5 proteins (non-canonical poly(A) polymerase), Air1/2 (RNA-binding protein), and RNA-helicase MTR4 [21, 22]. TRF4 adds a short oligo(A) sequence, forming an unstructured 3'-terminus for noncoding RNAs as small nuclear, nucleolar, and TLC1, which can be processed by exosomes [18, 23–26]. Exosomes activity is limited by the Sm-proteins associated with the 3'-terminal portion of mature telomerase RNA. If an exosome does not encounter an obstacle in its path in the form of a Sm-

proteins complex, it fully degrades small nuclear and nucleolar RNA, as well as telomerase RNA [27] (Fig. 2).

Cellular localization and assembly of the active telomerase complex of *S. cerevisiae*

One of the important stages in the biogenesis of telomerase RNA and telomerase itself is the proper intracellular localization of their components (Fig. 2). As has been stated previously, the primary transcript of telomerase RNA in both yeast and human cells is subjected to co-transcription processing, followed by maturation or degradation by exosomes. In *S. cerevisiae*, properly matured telomerase RNA localizes in the nucleolus, where its cap is hypermethylated by the Tgs1 enzyme [28]. The trimethylated processed form of TLC1 is exported from the nucleus by a nuclear-cytoplasmic transport system [29]. The Crm1/Xpo1 and mRNA export factors Mex67 and Dbp5/Rat8 are

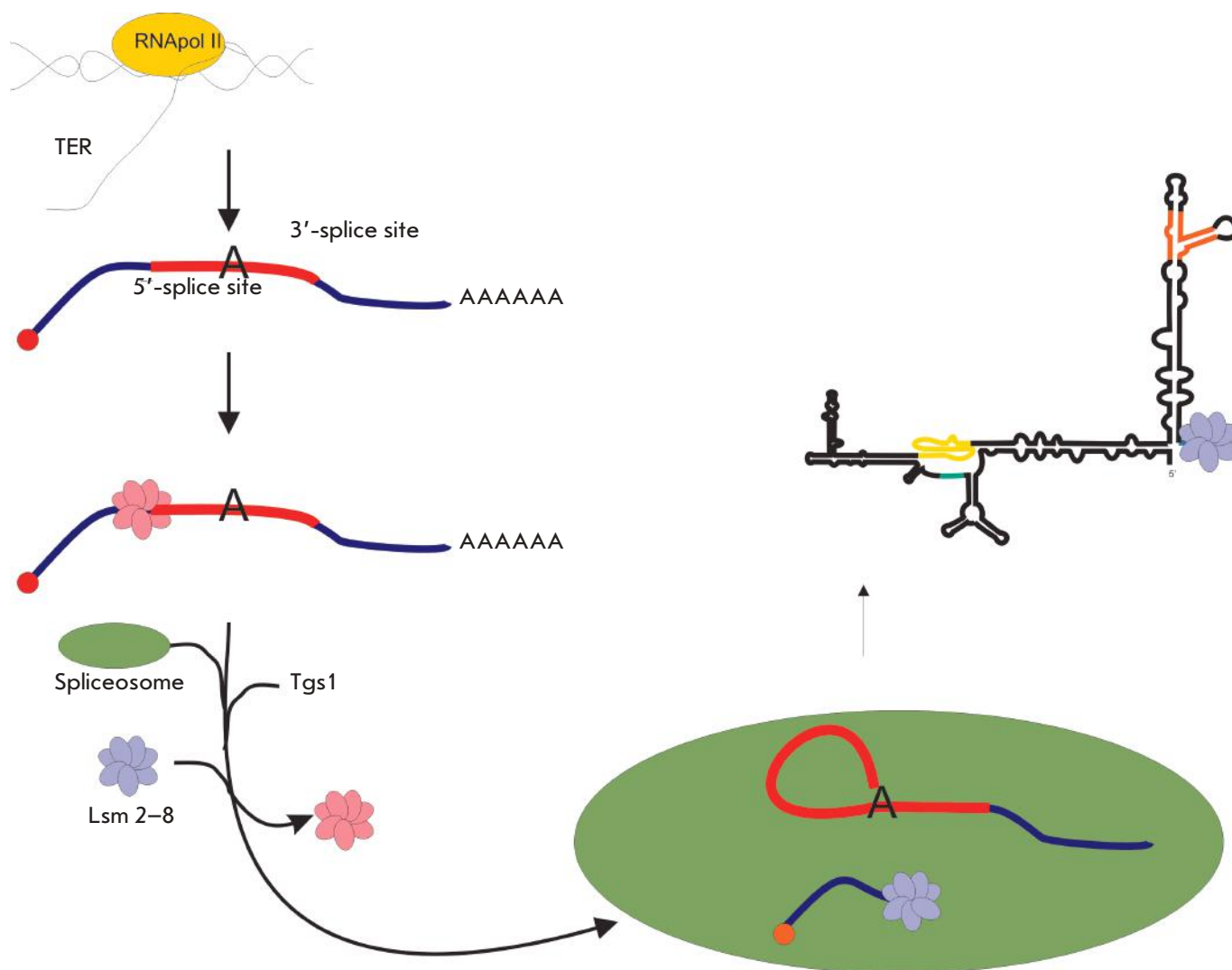


Fig. 3. Model of processing of *S. pombe* telomerase RNA.

responsible for the export of telomerase RNA. In the cytoplasm, telomerase RNA forms a complex with the protein subunits of telomerase Est1, Est2 and Est3, and afterwards the Mtr10 and Kap22 factors responsible for import into the nucleus transfer the enzyme back into the nucleus [29–31], where it interacts with telomeres and lengthens them in the late S-phase.

Processing of telomerase RNA in fission yeast

Telomerase RNA has undergone significant changes over the course of evolution, which have affected both its structure and processing mechanism. At the moment, there is no doubt that telomerase RNA is synthesized in all organisms as a long precursor whose correct processing results in mature catalytically active telomerase RNA. Telomerase RNA is involved in the fine regulation of the state of a cell; therefore, the

content of telomerase RNA must be maintained at the physiological level for its proper functioning in a cell. In fission yeast (*Schizosaccharomycetes*) [32], *Hansenula polymorpha* yeast (*Saccharomycetaceae*) [33], and other fungi (*Sordariaceae*, *Trichocomaceae*) [34], a precursor of telomerase RNA is synthesized by RNA polymerase II as a polyadenylated transcript (Fig. 3). The primary transcript of telomerase RNA in the cells of these organisms contains two exons, an intron, and a 3'-terminus poly(A) sequence. The processing of the primary transcript is carried out by a spliceosome. The first step in the splicing (cut in 5'-splicing site) produces a mature form of telomerase RNA. Processing by a spliceosome was first discovered in the cells of *Schizosaccharomyces pombe* yeast [32]. The splicing is a tightly coordinated process: all its stages occur very quickly and in a very specific order. In the first step, the 2'-hydroxyl

group of adenosine at the branching point located in the middle of the branching site attacks the 5'-terminal splicing site at its sugar phosphate backbone. The result is an intermediate with a lasso structure, wherein the 5'-terminus of the intron is attached to the branching point through a 2'-5'-linkage. The freed 3'-hydroxyl group of the 5'-terminus of the exon attacks the 3'-terminal splicing site, which leads to a joining of exons and the excision of the intron as a lariat. The spliceosome contains small nuclear RNA (snRNA) U1, U2, U4, U5 and U6, which direct and enable a quick and accurate splicing process through complementary interactions with different parts of pre-mRNA [35]. It has been shown that a slowdown of TER precursor splicing after the effective first stage is caused by the peculiarities of the regulatory regions of telomerase RNA itself [32, 36]. In *S. pombe*, the distance between the branching point and 3'-terminal splicing site of telomerase RNA is 22 nucleotides [32], which is about two times greater than in the majority of introns in this organism [37]. Shortening the intron to 14 nucleotides leads to complete splicing and degradation of telomerase RNA [32]. Further analysis of the splicing sites has revealed some interesting features [31, 35]. It turns out that incomplete complementarity of the 5'-terminal splicing site of U1 snRNA [32], high degree of complementarity between the branching site and U2 snRNA, and a long distance between the branching point and the 3'-terminal splicing site, as well as weak polypyrimidine tract synergistically reduce the rate of transition to the second stage of splicing [36]. The PrP22 and PrP43 proteins (helicases with DExD/H-box) are involved in the processing of *S. pombe* telomerase RNA [36]. These proteins use the energy of ATP hydrolysis to release splicing intermediates during deceleration in the second stage (exon ligation). Therefore, when transition to the second stage of splicing is arduous, the spliceosomes frozen on intermediates are released [38]. The mutations inhibiting the ATPase activity of these proteins significantly increase the content of the fully spliced TER1 form [36].

Sm-proteins are known to be associated with the telomerase RNA of *S. cerevisiae* yeast [39], and they also interact with U1, U2, U4, and U5 snRNA [40, 41]. The Sm-proteins binding site is located a few nucleotides away from the 3'-terminus of the mature form [39]. In *S. pombe* cells, a spliceosome cuts TER1 at a distance of one nucleotide from the Sm-proteins binding site and therefore, may decrease the stability of the complex. It has been discovered that Sm-proteins interact with the polyadenylated TER1 precursor and facilitate its sectioning by the spliceosome [42]. Smd2 attracts Tgs1, which carries out post-transcriptional hypermethylation of TER1 to produce 2,2,7-trimethylguanine

5'-cap. After the sectioning and hypermethylation of TER1, Sm-proteins dissociate and are replaced by Lsm-proteins (Fig. 3), which protect telomerase RNA against degradation by exosome [42].

Later, it was shown that other types of fission yeast and fungi maintain telomerase RNA processing by splicing its precursor with a spliceosome. In *S. cryophilus* and *S. octoporus*, the 5'-terminal splicing site comprises a cytosine residue in the third position, which stabilizes the interaction with U6 of snRNA in the first stage and slow transition to the second [43]. In *Aspergillus* sp. and *Neurospora crassa*, the first nucleotide of the 5'-terminal splicing site, adenine, is important for the release of the processed product after the first step of splicing [33, 42]. The formation of non-canonical interactions between the first and last guanosine in the intron is believed to be necessary for the positioning of the 3'-terminal splicing site in the second reaction of transesterification and ligation of exons [44], whereas replacement of guanosine with adenine in the telomerase RNA of the fungi families *Pezizomycotina* and *Taphrinomycotina*, which are the closest to the common ancestor, prevents the formation of a proper three-dimensional structure and stops the splicing after the first transesterification reaction and subsequent dissociation of the frozen spliceosome [34, 36, 43].

The dramatic differences in the mechanism of telomerase RNA processing in evolutionarily related organisms do not affect the strict control of the quantity and quality of the telomerase RNA in their cells. In yeast cells, exosome degrades improperly processed telomerase RNA as well as RNA which had not form complexes with the proteins that regulate its localization and activity.

Processing and localization of human telomerase RNA

Yeast and human telomerase RNA differ considerably in length and structure, but they share the main conservative components important for the formation and functioning of the telomerase complex. Mature human telomerase RNA (hTR) consists of 451 nucleotides [45]. Transcription of the *hTR* gene is carried out by RNA polymerase II [46]. The promoter of the *hTR* gene is well mapped, but the terminator region is poorly understood [47]. The length of the primary transcript of hTR remains to be determined. The 541-nucleotide elongated form of human telomerase RNA was first identified by reverse transcription, followed by PCR amplification [45]. More recent data obtained by high-throughput sequencing indicate the existence of a primary transcript of telomerase RNA up to 1,451 nucleotides in length [48]. The 3'-terminal domain of human telomerase RNA forms a structure similar to

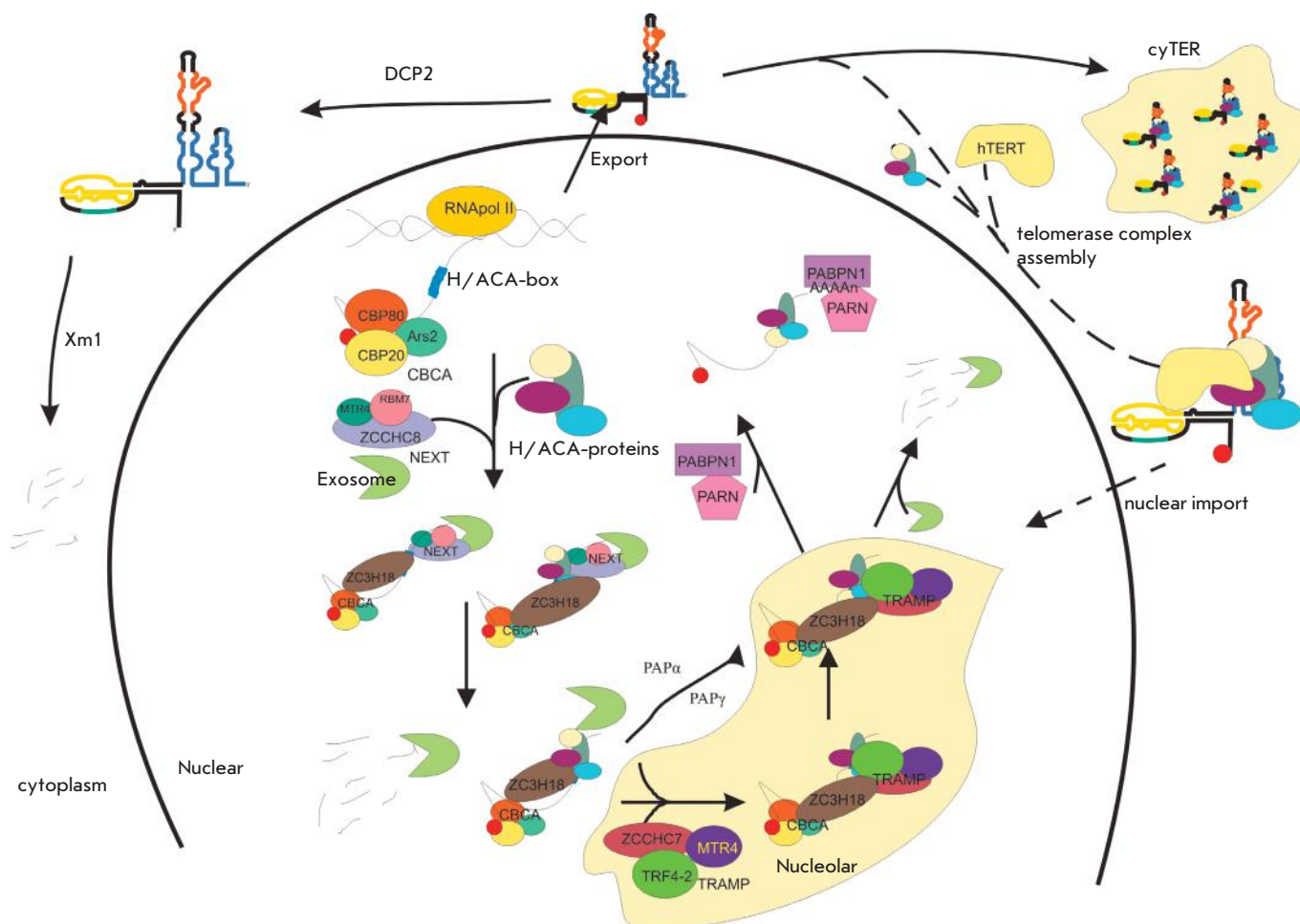


Fig. 4. Model of processing and localization of human telomerase RNA.

structures common to the H/ACA RNA family [49]. This structure consists of two hairpins connected by a single stranded loop H, and it contains a single stranded 5'-ACA-3' motif located 3 nucleotides before from the 3'-terminus of the mature telomerase RNA (Fig. 1). H/ACA hairpins are associated with a set of four proteins: dyskerin, NHP2, NOP10, and GAR1 [13]. H/ACA hairpins and the proteins associated with it provide stability to telomerase RNA, as well as to other H/ACA RNA. It is known that H/ACA RNAs serve as guides for the directional pseudouridylation of ribosomal RNA, but the telomerase RNA target is not defined: therefore, its H/ACA motif is assigned only a stabilizing function.

A combination of deep sequencing methods and determination of the 3'-terminus of RNA (3'-RACE) has revealed the heterogeneity of the 3'-terminus of human telomerase RNA [50]. It has been found that the 3'-terminal sequence may contain from one to seven additional nucleotides corresponding to the genomic sequence, and a short oligo(A) sequence (1–10 nucleotides). Thus,

we can conclude that telomerase RNA is synthesized in the form of an elongated precursor which is processed to form the intermediate oligoadenylated form.

It is known that snRNAs containing H/ACA-motifs are processed by exosomes [51]. In mammalian cells, exosomes are attracted to their substrate by several protein complexes. The TRAMP (TRF4, ZCCHC7 and MTR4) complex is known to be involved in the degradation of noncoding RNAs and aberrant transcripts in the nucleolus. For this, the TRF4 protein oligoadenylates the transcript, which serves as a signal for degradation by exosomes [51, 52]. The NEXT complex (RBM7, ZCCHC8 and MTR4) attracts exosomes to actively transcribed RNA and the so-called PROMoter uPstream Transcripts (PROMPTs), whose synthesis begins before the coding genes promoters [53, 54]. NEXT interacts with the cap-binding complex (CBC), forming a CBCN complex and implementing co-transcriptional cap-dependent 3'-processing or degradation of RNA in the nucleus [54–57].

Inactivating mutations in the *PARN1* gene encoding poly(A) ribonuclease 1 were recently discovered in patients with severe manifestations of dyskeratosis, a disease associated with short telomeres [58]. It was found that disruption of function or knockdown of the *PARN1* gene leads to a decrease in the total amount of telomerase RNA in cells with a simultaneous increase in the proportion of non-processed oligoadenylated RNA [16, 47, 58, 59]. Baumann's group discovered that spliceostatin A, a splicing inhibitor, does not affect the processing of telomerase RNA in humans [48], whereas isoginkgetin, which blocks the operation of not only spliceosome, but also exosomes [55], inhibits the processing of the hTR, resulting in the accumulation of the 3'-elongated form. In cells with a reduced content of the RRP40 protein, the main component of exosomes, and two nucleases associated with it, RRP6 and DIS3, the 3'-elongated form and the mature form of telomerase RNA accumulate, while the amount of the oligoadenylated form decreases. Mature telomerase RNA accumulates in the case of knocked down DGCR8 processor component, as well. It has been found that DGCR8 is involved in attracting exosomes to snRNA and telomerase RNA, thus controlling their total amount in a cell [60]. Knockdown of NEXT components, as well as that of the CBC complex promotes the accumulation of the 3'-elongated form of telomerase RNA [48]. The TRF4 protein, a component of TRAMP, and the canonical poly(A) polymerases PAP α and PAP γ carry out oligoadenylation of the telomerase RNA precursor [61]. Interestingly, oligoadenylation of telomerase RNA by the TRF4 protein promotes its degradation and PAP α/γ is involved in processing, which results in the formation of mature telomerase RNA [61]. The oligoadenylated form of human telomerase RNA is stabilized by PABPN1 (nuclear poly(A)-binding protein 1), which stimulates the synthesis of poly(A) sequences and attracts PARN, whereby promoting the maturation of hTR. A free oligo(A) sequence, unprotected by PABPN1, is a signal of RNA degradation by the TRAMP-exosome complex [61].

The proteins interacting with the H/ACA domain play a major role in the processing of human telomerase RNA. Dyskerin, NOP10, NHP2, NAF1, and GAR1 are RNA chaperones, and their interaction with telomerase RNA during processing stabilizes it, preventing degradation by exosomes. Dyskerin protects telomerase RNA from degradation by nuclear 3'-5'-exosomes. Dyskerin knockdown and mutations that disrupt telomerase RNA binding to the protein result in a reduced level of mature telomerase RNA in cells, whereas double knockdown of dyskerin and PARN1 cause the accumulation of telomerase RNA in cytoplasm bodies called cyTER (cytoplasmic TER). Degradation of telomerase

RNA from the 5'-terminus by the decapping protein DCP2 and 5'-3'-exonuclease XRN1 [16] also indicate a cytoplasmic localization of telomerase RNA.

Summarizing the data on the processing of human telomerase RNA, it is possible to suggest the following general scheme for its synthesis and maturation (Fig. 4). After primary transcript synthesis by RNA-polymerase II and co-transcriptionally capping, it interacts with dyskerin, NOP10, NHP2, and NAF1, which stabilize and protect RNA from degradation [62]. Part of telomerase RNA, which is associated with dyskerin and other chaperones, undergoes processing to form mature telomerase RNA. In order to achieve this, the CBC complex attracts the NEXT-exosome complex, which shortens the long precursor in the nucleus until it meets the H/ACA motif associated with H/ACA-binding proteins [48]. This product contains from one to seven additional nucleotides at the 3'-terminus. The nuclear poly(A) polymerases PAP α , PAP γ , and TRF4, a component of the exosome-associated nuclear TRAMP complex, oligoadenylates this substrate [48, 60]. The oligoadenylated precursor interacts with PABPN1 [60], which protects it from further degradation, and attracts PARN1 [16, 48, 59, 60]. PARN1 gently shortens the oligo(A) sequence and the remaining additional nucleotides to form the mature telomerase RNA. The primary transcript which failed to form a complex with dyskerin or other chaperones is degraded by the TRAMP-exosome complex. Some of the primary transcript is exported from the nucleus to the cytoplasm, where it is decapped by the DCP2 protein and degraded by cytoplasmic 5'-3'-exonuclease XRN1 [16].

In a HeLa tumor cell line, telomerase RNA accumulates in Cajal bodies. A so-called CAB box is identified in the structure of telomerase RNA, which is responsible for its localization in the Cajal bodies, where telomerase and telomere interaction takes place [63]. Mutations in CAB-box [14], as well as mutations in the TCAB1 protein [64], disrupt human telomerase RNA localization in the Cajal bodies. TCAB1 interacts with CAB-box of telomerase RNA and ensures its location in the Cajal bodies [64]. Both the mutations and the absence of TCAB1 do not affect the enzymatic activity of telomerase, but they prevent its localization in Cajal bodies and telomeres [65]. hTERT may form a complex with hTR in both the nucleus and the cytoplasm, but the Cajal bodies and telomerase RNA direct telomerase localization at the telomere.

Recent research on the processing and localization of telomerase RNA in yeast and humans demonstrates that the amount of telomerase RNA in a cell is tightly controlled. Telomerase RNA processing and degradation are believed to be competing processes whose balance regulates the amount of telomerase RNA in a

cell. The detection of telomerase RNA in the cytoplasm raises new questions. It is unclear whether this step is necessary for the processing or assembly of telomerase or whether human telomerase RNA performs alternative cell functions, some of which have been previously described [65].

CONCLUSION

Telomerase maintains the proliferative potential of cells, which makes it one of the most important objects in studies of aging and cell transformation. Disruption of telomerase functioning leads to the development of tumors and telomeropathies. One of the essential components of telomerase is telomerase RNA, whose gene is expressed in most cell types throughout their lifetime. The expression of the *hTERT* gene which encodes the second component of telomerase is finely regulated, and the enzyme activation depends on the appearance of the hTERT protein in a cell. The mechanism of synthesis and processing of telomerase RNA has attracted the attention of scientists for more than 10 years, and recently there was a breakthrough in the study of this important stage of telomerase biogenesis. One of the most important features of telomerase RNA process-

ing is the fine regulation of the content of this molecule in the cell. Both in yeast and human cells, telomerase RNA processing involves an exosome that rapidly degrades RNA that is not protected by RNA-chaperones. It has been established that most of the telomerase RNA gene transcription product is degraded in the process of biogenesis. Disruptions in the processing result in a degradation of the telomerase RNA that causes a number of diseases classified as telomeropathies.

Despite recent progress in understanding the mechanisms of telomerase RNA processing, there are questions to which we still have no answers. A full and detailed understanding of the mechanisms of both the functioning and biogenesis of telomerase will allow us to develop new approaches to the treatment of diseases whose development is associated with an impaired telomere maintenance system. ●

The study of the mechanisms of the processing of telomerase RNA was supported by RFBR (grant № 14-04-01637 A), work on the intracellular localization of telomerase RNA was supported by RSF (grant № 16-14-10047).

REFERENCES

- Greider C.W., Blackburn E.H. // *Cell*. 1987. V. 51. № 6. P. 887–898.
- Morin G.B. // *Cell*. 1989. V. 59. № 3. P. 521–529.
- Shippen-Lentz D., Blackburn E.H. // *Science*. 1990. V. 247. № 4942. P. 546–552.
- Blackburn E.H., Collins K. // *Cold Spring Harb. Perspect. Biol.* 2011. V. 3. № 5. a003558.
- Theimer C.A., Feigon J. // *Curr. Opin. Struct. Biol.* 2006. V. 16. № 3. P. 307–318.
- Egan E.D., Collins K. // *RNA*. 2012. V. 18. № 10. P. 1747–1759.
- Schmidt J.C., Cech T.R. // *Genes Dev.* 2015. V. 29. № 11. P. 1095–1105.
- Zhang Q., Kim N.-K., Feigon J. // *Proc. Natl. Acad. Sci. USA*. 2011. V. 108. № 51. P. 20325–20332.
- Qi X., Li Y., Honda S., Hoffmann S., Marz M., Mosig A., Podlevsky J.D., Stadler P.F., Selker E.U., Chen J.J.-L. // *Nucl. Acids Res.* 2013. V. 41. № 1. P. 450–462.
- Webb C.J., Zakian V.A. // *Nat. Struct. Mol. Biol.* 2008. V. 15. № 1. P. 34–42.
- Evfratov S.A., Smekalova E.M., Golovin A.V., Logvina N.A., Zvereva M.I., Dontsova O.A. // *Acta Naturae*. 2014. V. 6. № 2. P. 41–47.
- Niederer R.O., Zappulla D.C. // *RNA*. 2015. V. 21. № 2. P. 254–261.
- Fu D., Collins K. // *Mol. Cell*. 2003. V. 11. № 5. P. 1361–1372.
- Jády B.E., Bertrand E., Kiss T. // *J. Cell Biol.* 2004. V. 164. № 5. P. 647–652.
- Kiss T., Fayet-Lebaron E., Jády B.E. // *Mol. Cell*. 2010. V. 37. № 5. P. 597–606.
- Shukla S., Schmidt J.C., Goldfarb K.C., Cech T.R., Parker R. // *Nat. Struct. Mol. Biol.* 2016. V. 23. № 4. P. 286–292.
- Chapon C., Cech T.R., Zaug A.J. // *RNA*. 1997. V. 3. № 11. P. 1337–1351.
- Smekalova E.M., Shubernetskaya O.S., Zvereva M.I., Gromenko E.V., Rubtsova M.P., Dontsova O.A. // *Biochemistry*. 2012. V. 77. № 10. P. 1120–1128.
- Jamonnak N., Creamer T.J., Darby M.M., Schaugheny P., Wheelan S.J., Corden J.L. // *RNA*. 2011. V. 17. № 11. P. 2011–2025.
- Noël J.-F., Larose S., Abou Elela S., Wellinger R.J. // *Nucl. Acids Res.* 2012. V. 40. № 12. P. 5625–5636.
- Vasiljeva L., Buratowski S. // *Mol. Cell*. 2006. V. 21. № 2. P. 239–248.
- Porrúa O., Libri D. // *Nat. Rev. Mol. Cell Biol.* 2015. V. 16. № 3. P. 190–202.
- Jia H., Wang X., Anderson J.T., Jankowsky E. // *Proc. Natl. Acad. Sci. USA*. 2012. V. 109. № 19. P. 7292–7297.
- Jia H., Wang X., Liu F., Guenther U.-P., Srinivasan S., Anderson J.T., Jankowsky E. // *Cell*. 2011. V. 145. № 6. P. 890–901.
- Wyers F., Rougemaille M., Badis G., Rousselle J.-C., Dufour M.-E., Boulay J., Régault B., Devaux F., Namane A., Séraphin B., et al. // *Cell*. 2005. V. 121. № 5. P. 725–737.
- Houseley J., LaCava J., Tollervy D. // *Nat. Rev. Mol. Cell Biol.* 2006. V. 7. № 7. P. 529–539.
- Coy S., Volanakis A., Shah S., Vasiljeva L. // *PLoS One*. 2013. V. 8. № 6. <http://www.ncbi.nlm.nih.gov/pmc/articles/PMC3675052/>.
- Mouaikel J., Verheggen C., Bertrand E., Tazi J., Bordonné R. // *Mol. Cell*. 2002. V. 9. № 4. P. 891–901.
- Gallardo F., Olivier C., Dandjinou A.T., Wellinger R.J., Chartrand P. // *EMBO J.* 2008. V. 27. № 5. P. 748–757.
- Ferrezuelo F., Steiner B., Aldea M., Fitcher B. // *Mol. Cell Biol.* 2002. V. 22. № 17. P. 6046–6055.

REVIEWS

31. Wu H., Becker D., Krebber H. // *Cell Rep.* 2014. V. 8. № 6. P. 1630–1638.
32. Box J.A., Bunch J.T., Tang W., Baumann P. // *Nature.* 2008. V. 456. № 7224. P. 910–914.
33. Smekalova E.M., Malyavko A.N., Zvereva M.I., Mardanov A.V., Ravin N.V., Skryabin K.G., Westhof E., Dontsova O.A. // *RNA.* 2013. V. 19. № 11. P. 1563–1574.
34. Qi X., Rand D.P., Podlevsky J.D., Li Y., Mosig A., Stadler P.F., Chen J.J.-L. // *Nat. Commun.* 2015. V. 6. P. 6105.
35. Wahl M.C., Will C.L., Lührmann R. // *Cell.* 2009. V. 136. № 4. P. 701–718.
36. Kannan R., Hartnett S., Voelker R.B., Berglund J.A., Staley J.P., Baumann P. // *Genes Dev.* 2013. V. 27. № 6. P. 627–638.
37. Zhang M.Q., Marr T.G. // *Nucl. Acids Res.* 1994. V. 22. № 9. P. 1750–1759.
38. Semlow D.R., Staley J.P. // *Trends Biochem. Sci.* 2012. V. 37. № 7. P. 263–273.
39. Seto A.G., Zaug A.J., Sobel S.G., Wolin S.L., Cech T.R. // *Nature.* 1999. V. 401. № 6749. P. 177–180.
40. Raker V.A., Plessel G., Lührmann R. // *EMBO J.* 1996. V. 15. № 9. P. 2256–2269.
41. Patel S.B., Bellini M. // *Nucl. Acids Res.* 2008. V. 36. № 20. P. 6482–6493.
42. Tang W., Kannan R., Blanchette M., Baumann P. // *Nature.* 2012. V. 484. № 7393. P. 260–264.
43. Kannan R., Helston R.M., Dannebaum R.O., Baumann P. // *Nat. Commun.* 2015. V. 6. P. 6104.
44. Parker R., Siliciano P.G. // *Nature.* 1993. V. 361. № 6413. P. 660–662.
45. Feng J., Funk W.D., Wang S.S., Weinrich S.L., Avilion A.A., Chiu C.P., Adams R.R., Chang E., Allsopp R.C., Yu J. // *Science.* 1995. V. 269. № 5228. P. 1236–1241.
46. Egan E.D., Collins K. // *Mol. Cell. Biol.* 2012. V. 32. № 13. P. 2428–2439.
47. Zhao J.Q., Hoare S.F., McFarlane R., Muir S., Parkinson E.K., Black D.M., Keith W.N. // *Oncogene.* 1998. V. 16. № 10. P. 1345–1350.
48. Tseng C.-K., Wang H.-F., Burns A.M., Schroeder M.R., Gaspari M., Baumann P. // *Cell Rep.* 2015. V. 13. № 10. P. 2232–2243.
49. Mitchell J.R., Collins K. // *Mol. Cell.* 2000. V. 6. № 2. P. 361–371.
50. Goldfarb K.C., Cech T.R. // *BMC Mol. Biol.* 2013. V. 14. P. 23.
51. Berndt H., Harnisch C., Rammelt C., Stöhr N., Zirkel A., Dohm J.C., Himmelbauer H., Tavanez J.-P., Hüttelmaier S., Wahle E. // *RNA.* 2012. V. 18. № 5. P. 958–972.
52. Rammelt C., Bilen B., Zavolan M., Keller W. // *RNA.* 2011. V. 17. № 9. P. 1737–1746.
53. LaCava J., Houseley J., Saveanu C., Petfalski E., Thompson E., Jacquier A., Tollervey D. // *Cell.* 2005. V. 121. № 5. P. 713–724.
54. Ntini E., Järvelin A.I., Bornholdt J., Chen Y., Boyd M., Jørgensen M., Andersson R., Hoof I., Schein A., Andersen P.R., et al. // *Nat. Struct. Mol. Biol.* 2013. V. 20. № 8. P. 923–928.
55. Andersen P.R., Domanski M., Kristiansen M.S., Storvall H., Ntini E., Verheggen C., Schein A., Bunkenborg J., Poser I., Hallais M., et al. // *Nat. Struct. Mol. Biol.* 2013. V. 20. № 12. P. 1367–1376.
56. Lubas M., Christensen M.S., Kristiansen M.S., Domanski M., Falkenby L.G., Lykke-Andersen S., Andersen J.S., Dziembowski A., Jensen T.H. // *Mol. Cell.* 2011. V. 43. № 4. P. 624–637.
57. Lubas M., Andersen P.R., Schein A., Dziembowski A., Kudla G., Jensen T.H. // *Cell Rep.* 2015. V. 10. № 2. P. 178–192.
58. Tummala H., Walne A., Collopy L., Cardoso S., de la Fuente J., Lawson S., Powell J., Cooper N., Foster A., Mohammed S., et al. // *J. Clin. Invest.* 2015. V. 125. № 5. P. 2151–2160.
59. Moon D.H., Segal M., Boyraz B., Guinan E., Hofmann I., Cahan P., Tai A.K., Agarwal S. // *Nat. Genet.* 2015. V. 47. № 12. P. 1482–1488.
60. Macias S., Cordiner R.A., Gautier P., Plass M., Cáceres J.F. // *Mol. Cell.* 2015. V. 60. № 6. P. 873–885.
61. Nguyen D., Grenier St-Sauveur V., Bergeron D., Dupuis-Sandoval F., Scott M.S., Bachand F. // *Cell Rep.* 2015. V. 13. № 10. P. 2244–2257.
62. Egan E.D., Collins K. // *Mol. Cell. Biol.* 2010. V. 30. № 11. P. 2775–2786.
63. Cristofari G., Adolf E., Reichenbach P., Sikora K., Terns R.M., Terns M.P., Lingner J. // *Mol. Cell.* 2007. V. 27. № 6. P. 882–889.
64. Venteicher A.S., Abreu E.B., Meng Z., McCann K.E., Terns R.M., Veenstra T.D., Terns M.P., Artandi S.E. // *Science.* 2009. V. 323. № 5914. P. 644–648.
65. Stern J.L., Zyner K.G., Pickett H.A., Cohen S.B., Bryan T.M. // *Mol. Cell. Biol.* 2012. V. 32. № 13. P. 2384–2395.
66. Rubtsova M.P., Vasilkova D.P., Malyavko A.N., Naraikina Y.V., Zvereva M.I., Dontsova O.A. // *Acta Naturae.* 2012. V. 4. № 2. P. 44–61.

Therapy of HIV Infection: Current Approaches and Prospects

M. M. Prokofjeva^{*}, S. N. Kochetkov, V. S. Prassolov

Engelhardt Institute of Molecular Biology, Vavilova Str., 32, Moscow, 119991, Russia

^{*}E-mail: m.prokofjeva@gmail.com

All authors contributed equally to the work

Received April 14, 2016; in final form, July 14, 2016

Copyright © 2016 Park-media, Ltd. This is an open access article distributed under the Creative Commons Attribution License, which permits unrestricted use, distribution, and reproduction in any medium, provided the original work is properly cited.

ABSTRACT The human immunodeficiency virus type 1 (HIV-1) is the causative agent of one of the most dangerous human diseases – the acquired immune deficiency syndrome (AIDS). Over the past 30 years since the discovery of HIV-1, a number of antiviral drugs have been developed to suppress various stages of the HIV-1 life cycle. This approach has enabled the suppression of virus replication in the body, which significantly prolongs the life of HIV patients. The main downside of the method is the development of viral resistance to many anti-HIV drugs, which requires the creation of new drugs effective against drug-resistant viral forms. Currently, several fundamentally new approaches to HIV-1 treatment are under development, including the use of neutralizing antibodies, genome editing, and blocking an integrated latent provirus. This review describes a traditional approach involving HIV-1 inhibitors as well as the prospects of other treatment options.

KEYWORDS HIV-1, viral life cycle inhibitors, genome editing, antiviral therapy.

ABBREVIATIONS HIV – human immunodeficiency virus; RT – reverse transcriptase; NRTI – nucleoside reverse transcriptase inhibitor; NNRTI – non-nucleoside reverse transcriptase inhibitor; HAART – highly active antiretroviral therapy; LTR – long terminal repeat.

INTRODUCTION

The development of approaches to the treatment of the HIV infection is one of the most crucial challenges facing biomedical chemistry. The medications used currently are aimed at suppressing one of the key steps of the infection: the initial contact of the virus with the cell, entry, synthesis of the DNA provirus, its transfer into the nucleus and integration into the host cell genome, and the synthesis and maturation of new virions [1]. HIV-1 is highly variable because HIV-1 reverse transcriptase (RT) lacks proofreading exonuclease activity, which results in error-associated transcription. This variability leads to the formation of many mutant viral forms, some of which are drug-resistant [2]. Because drug-resistant viral forms constantly emerge in HIV-infected individuals and are found in so-called primary patients who have undergone no previous treatment with anti-HIV drugs, the search for agents to effectively suppress HIV-1 mutant forms remains topical.

LIFE CYCLE INHIBITORS

HIV-1 life cycle

The life cycle of HIV-1 is schematically depicted in *Fig. 1A*. The initial contact of the virus with an uninfected cell occurs through non-specific binding to the

heparan sulfates located on the cell membrane surface. Following this initial contact, viral envelope proteins specifically interact with cell surface proteins (receptors). The receptor for HIV-1 is CD4 (a T cell receptor from the immunoglobulin superfamily) that interacts with the viral envelope glycoproteins gp120 and gp41. HIV-1 uses the chemokine receptors CCR5 and CXCR4 as co-receptors [3]. Mutations in the CCR5 gene can significantly affect the infectious process. For example, deletion of 32 bp in the CCR5 gene coding region ($\Delta 32$ CCR5) results in intracellular synthesis of a CCR5 truncated form that is not exposed on the cell membrane surface. These cells are resistant to HIV-1 strains that use CCR5 as a co-receptor (R5-strains) [4, 5]. The CXCR4 gene mutations that induce resistance of the cells to infection are currently unknown.

After fusion of the cell and viral membranes, the capsid enters the cytoplasm and dissociates. This step is followed by reverse transcription, when a DNA copy is synthesized on the viral genomic RNA template, which is accompanied by RNA degradation and synthesis of the second DNA strand. All three steps are implemented by one enzyme, RNA-dependent DNA polymerase, from the viral nucleocapsid. The final product of the polymerase reaction is a double-stranded DNA provirus that contains all viral genes and is flanked by long 3'- and 5'-terminal repeats (LTRs). LTR includes regu-

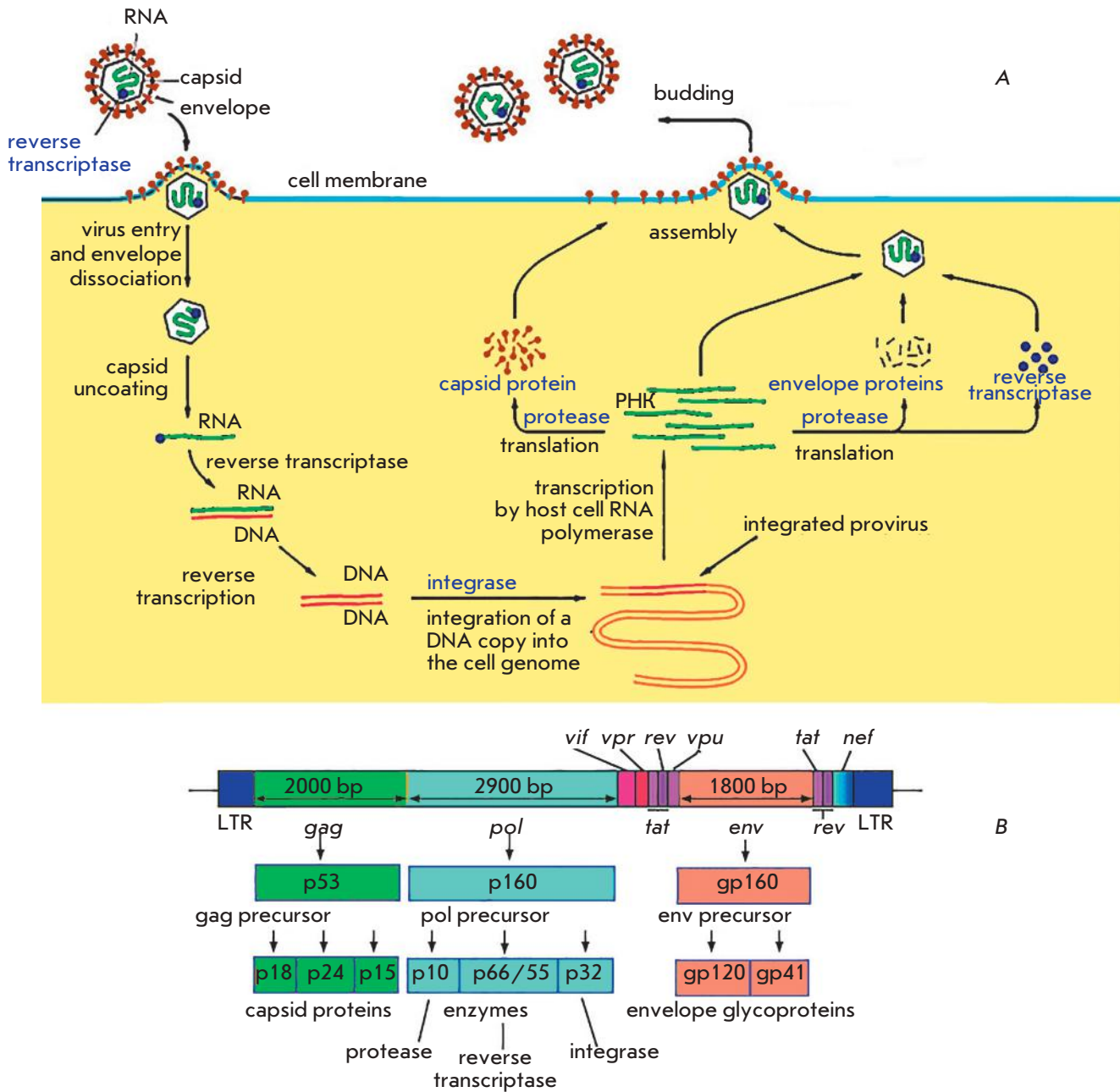


Fig. 1. The life cycle (A) and genome structure (B) of HIV-

latory elements, in particular a promoter and enhancers, which perform important functions in the retrovirus life cycle.

The DNA provirus integrates into the infected cell genome, which is required for the subsequent replication of the viral genome and permanent expression in the infected cells. The integration involves the pre-integration complex (PIC) consisting of viral integrase, RT, and a number of cellular proteins [6]. Following this integration, the integrated DNA provirus acts as a part

of the host genome, as an independent transcriptional unit. Subsequent transcription of the integrated provirus, as well as processing and splicing of the newly produced viral RNA, is performed by cellular enzymes. The synthesized viral RNA undergoes alternative splicing. The HIV-1 accessory proteins Tat, Rev, Vpu, Vpr, and Vif are translated from a double-spliced RNA (Fig. 1B). The regulatory Nef protein and the envelope protein (Env) precursor, which are necessary at later stages of the viral life cycle, are synthesized from the

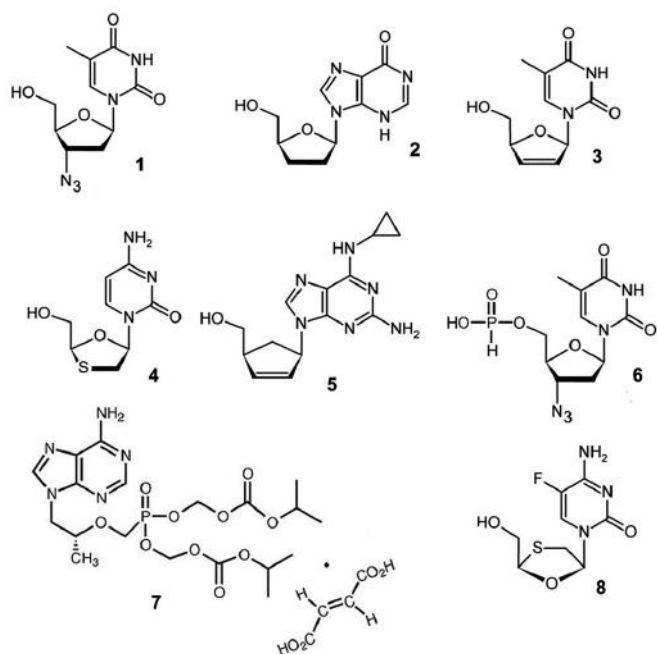


Fig. 2. Nucleoside and nucleotide HIV-1 reverse transcriptase inhibitors. The numbering corresponds to that of *Table 1*

single-spliced RNA. The unspliced viral RNA is incorporated into the capsid of the newly formed viral particles and also serves as a template for the synthesis of the Gag and Gag/Pol precursor proteins encoded by the genes *gag* (structural proteins: matrix MA (p17), capsid CA (p24), and nucleocapsid NC (p7)) and *pol* (viral enzymes: reverse transcriptase (p66/51), integrase (p32), and protease (p10)). Initially, the virus forms as a non-infectious immature virion that buds from the infected cell membrane. After budding, virus maturation occurs when precursor proteins are cleaved by viral protease and the cleavage products start performing their functions in the viral particle [7].

Reverse transcriptase inhibitors

Most of the drugs now used affect a particular HIV-1 enzyme: reverse transcriptase, integrase, or protease (*Table 1*). RT inhibitors may be conventionally divided into two groups: nucleoside and nucleotide reverse transcriptase inhibitors (NRTIs) and non-nucleoside reverse transcriptase inhibitors (NNRTIs). Nucleoside and nucleotide analogues are a group made of the earliest HIV replication inhibitors approved for clinical use [8] (*Fig. 2*). These compounds are enzyme substrate precursors, not an active form of an inhibitor. Upon entering the cell, they are converted (via phosphorylation by cellular kinases) to nucleoside triphosphate analogues

that act as substrates in the synthesis of proviral cDNA. Insertion of a NRTI into a growing cDNA chain leads to reverse transcription termination due to the lack of a 3'-hydroxyl group. Therefore, NRTIs block HIV-1 replication at the early step of its life cycle [9–11].

The first inhibitor in this class was azidothymidine (zidovudine) (**1**). This drug was synthesized in 1964 and was tested as an experimental cell cytotoxin for several years. Clinical trials in 1985 demonstrated that the drug inhibits both the infectious and cytopathic properties of HIV-1 [12]. By 2015, the FDA had approved the clinical use of seven drugs. One drug, nikavir (**6**), which was created in the laboratory of Academician A.A. Kraevskiy at the Engelhardt Institute of Molecular Biology, was approved for use in 1999 and has been widely used in Russia and the CIS countries. Each nucleoside analogue specifically competes with a cellular nucleoside: AZT (**1**), nikavir (**6**), and stavudine (d4T) (**3**) compete with dTTP; emtricitabine (FTC) (**8**) and lamivudine (3TC) (**4**) compete with dCTP; didanosine (ddI) (**2**) and tenofovir (TDF) (**7**) compete with dATP; abacavir (ABC) (**5**) competes with dGTP [13–17].

Some NRTIs are highly stable in the cell, which enables long-term virus suppression [8].

Unlike nucleoside inhibitors, nucleotide inhibitors are pre-phosphorylated: thereby the latter need one less phosphorylation step after entering the cell. Like nucleoside inhibitors, nucleotide analogues act as terminators of a growing DNA chain. They contain a phosphonate group that cannot be cleaved by cellular hydrolases, which greatly complicates 3'-5'-exonuclease-mediated excision of the nucleotide analogues inserted into a growing DNA chain compared to the excision of nucleoside analogues. The only nucleotide inhibitor used in anti-HIV therapy is tenofovir (**7**) [1].

To design and synthesize new nucleoside and nucleotide analogues is the objective of many researchers that are developing anti-HIV-1 drugs. New nucleoside analogues are needed, because HIV-1 RT undergoes point mutations, conferring drug resistance to the virus. Clinical studies have demonstrated a significant decrease in drug efficacy in HIV-1-infected patients receiving only AZT for six months [18]. There are viral strains fully resistant to AZT and other nucleoside analogues [19–21].

There are two known mechanisms of RT resistance to nucleoside. The first one is associated with a reduced affinity for artificial substrates compared to that for natural substrates. The second mechanism is based on increased phosphorolytic excision of an incorporated chain terminator [22, 23]. HIV-1 RT, even when lacking 3'-exonuclease activity, is capable of catalyzing pyrophosphorolysis, the reverse reaction of polymerization [24].

REVIEWS

Table 1. Anti-HIV drugs approved for use[†]

Russian name	Latin name	Trade name	FDA approval
Nucleoside reverse transcriptase inhibitor (NRTI)			
Zidovudine (1)	Zidovudine (azidothymidine, AZT, ZDV)	Retrovir	19/03/1987
Didanosine (2)	Didanosine (dideoxyinosine, ddI)	Videx	09/10/1991
	Delayed-release didanosine, enteric-coated didanosine, ddI EC)	Videx EC	31/10/2000
Stavudine (3)	Stavudine (d4T)	Zerit	24/06/1994
Lamivudine (4)	Lamivudine (3TC)	Epivir	17/11/1995
Abacavir (5)	Abacavir (ABC)	Ziagen	17/12/1998
Phosphazide (6)	Azidothymidine H-phosphonate	Nikavir	05/10/1999 ^{**}
Tenofovir (7)	Tenofovir disoproxil fumarate (tenofovir DF, TDF)	Viread	26/10/2001
Emtricitabine (8)	Emtricitabine (FTC)	Emtriva	02/07/2003
Non-nucleoside reverse transcriptase inhibitor (NNRTI)			
Nevirapine ^{**} (9)	Nevirapine (NVP)	Viramune	21/06/1996
Nevirapine XR ^{***} (10)	Extended-release nevirapine (NVP XR)	Viramune XR	25/03/2011
Delavirdine (11)	Delavirdine (delavirdine mesylate, DLV)	Rescriptor	04/04/1997
Efavirenz (12)	Efavirenz (EFV)	Sustiva	17/09/1998
Etravirine (13)	Etravirine (ETR)	Intelence	18/01/2008
Rilpivirine (14)	Rilpivirine (RPV)	Edurant	20/05/2011
Protease inhibitor (PI)			
Saquinavir (15)	Saquinavir (SQV)	Invirase	06/12/1995
Ritonavir (16)	Ritonavir (RTV)	Norvir	01/03/1996
Indinavir (17)	Indinavir (IDV)	Crixivan	13/03/1996
Nelfinavir (18)	Nelfinavir (NFV)	Viracept	14/03/1997
Atazanavir (19)	Atazanavir (ATV)	Reyataz	20/06/2003
Fosamprenavir (20)	Fosamprenavir (FOS-APV, FPV)	Lexiva	20/10/2003
Tipranavir (21)	Tipranavir (TPV)	Aptivus	22/06/2005
Darunavir (22)	Darunavir (DRV)	Prezista	23/06/2006
Integrase inhibitor (INI)			
Raltegravir (23)	Raltegravir (RAL)	Isentress	12/10/2007
Dolutegravir (24)	Dolutegravir (DTG)	Tivicay	13/08/2013
Elvitegravir (25)	Elvitegravir (EVG)	Vitekta	24/09/2014
Other			
Enfuvirtide ^{****} (26)	Enfuvirtide (T-20)	Fuzeon	13/03/2003
Maraviroc ^{*****} (27)	Maraviroc (MVC)	Selzentry	06/08/2007
Cobicistat ^{*****} (28)	Cobicistat, Tybost (COBI)	Tybost	24/09/2014

[†]Consecutive numbers of compounds correspond to their numbers in figures.

^{**}Approved for use in the Russian Federation.

^{***}Extended-release nevirapine.

^{****}Fusion inhibitor.

^{*****}Inhibitor of the virus-co-receptor interaction.

^{*****}A pharmacokinetic enhancer of atazanavir (**19**) or darunavir (**22**) action.

Non-nucleoside RT inhibitors (*Fig. 3*) are non-competitive inhibitors that bind in the so called hydrophobic pocket near the enzyme's catalytic site. Because of their hydrophobicity, NNRTIs can enter the cell and do not require any further reactions [25]. Five drugs of this group have been approved for clinical use: nevirapine (**10**), delavirdine (**11**), efavirenz (**12**), etravirine (**13**),

and rilpivirine (**14**). The first agent in this group, which was approved as a medication in 1996, was nevirapine [26]. Now, this drug is rarely used, because mutant HIV-1 forms resistant to nevirapine are widespread. Currently, the most commonly used medication in the group, which is prescribed to primary patients, is efavirenz [27].

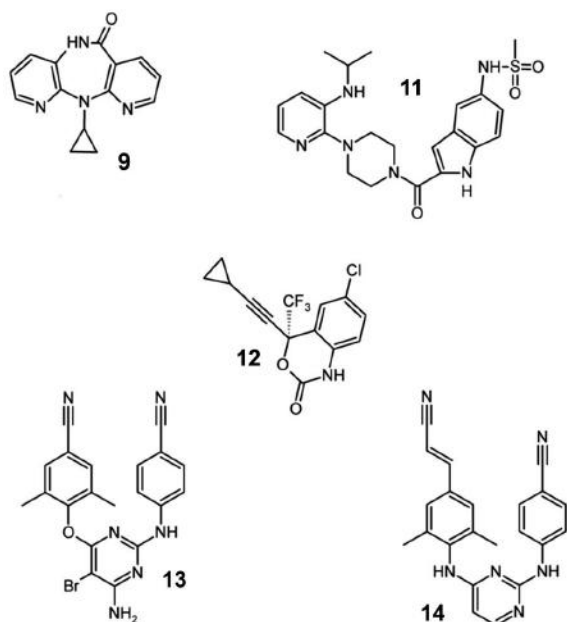


Fig. 3. Non-nucleoside HIV-1 reverse transcriptase inhibitors

The chemical structure of NNRTIs is different, but their effect on the enzyme is similar. Inhibitors in this group are specific to HIV-1 RT, but not active against other retroviruses.

Initially, NNRTIs were thought to bind only to an enzyme-substrate complex [28]. Later, NNRTIs were shown to bind to RT regardless of the substrate [29, 30], but some of them have increased affinity to the enzyme in the presence of a substrate [31]. In this case, NNRTIs do not inhibit substrate binding to the active site, but even promote it [32, 33]. This feature enables the application of NNRTIs in combination with NRTIs. Also, NNRTIs were shown to be capable of inhibiting the RNase H activity of RT [34].

Most mutations that confer resistance to NNRTIs occur in the NNRTI binding site. Over 40 mutations conferring *in vivo* and *in vitro* NNRTI resistance in RT have been found. However, if drugs that have been in use for a long time (e.g., nevirapine) are ineffective against a mutant enzyme, new drugs, the so-called second generation NNRTIs (etravirine and rilpivirine), exhibit sufficient inhibitory activity against mutant RT forms [35].

HIV-1 protease inhibitors

A second important group of clinically used inhibitors are protease inhibitors (Fig. 4). Most of these compounds are peptidomimetics that act in the same way

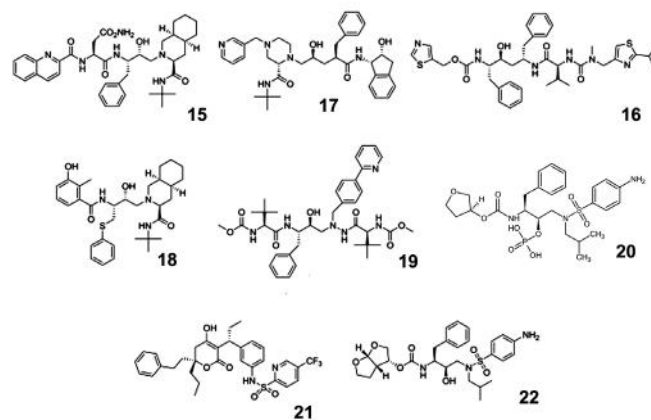


Fig. 4. HIV-1 protease inhibitors

through binding to the enzyme's active site. Unlike a natural target, inhibitors are not susceptible to proteolytic cleavage, because they contain hydroxyethylene bonds $[-CH_2-CH(OH)-]$ instead of peptide bonds $[-NH-CO-]$. Upon binding to the enzyme's active center, they compete with natural protease substrates and inhibit the enzymatic activity, which leads to a sharp decrease in the proteolytic processing of viral proteins [36–38]. The first drug in this group of inhibitors was saquinavir (**15**) [39]. Currently, eight protease inhibitors are used; this is the largest group of approved HIV-1 inhibitors (**15–21**). The mechanism inducing HIV-1 resistance to protease inhibitors is based on the replacement of an amino acid residue in the viral protease, which reduces its affinity to an inhibitor, whereas natural substrates continue to interact with the drug-resistant protease [40]. Changing the affinity to natural substrates also reduces the protease efficiency. As a consequence, drug-resistant viral forms are subject to compensatory mutations that reorganize the enzyme's efficiency and do not directly affect resistance to an inhibitor [41].

HIV-1 integrase inhibitors

Active development of inhibitors in this group began in 2000 when diketone organic acids (e.g., L-731,988) were shown to inhibit the integration and replication of HIV-1 in cell culture in particular, the step of proviral DNA integration into cellular genomic DNA [42]. This was the first indication that integrase inhibitors may be potential antiviral drugs. The first integrase inhibitor, which was approved as a drug in 2007, was raltegravir (isentriss) (**23**). Raltegravir exhibited a very high efficiency and quickly became one of the most commonly used drugs [43–45]. Three drugs from this group are now used: raltegravir, dolutegravir (**24**), and elvite-

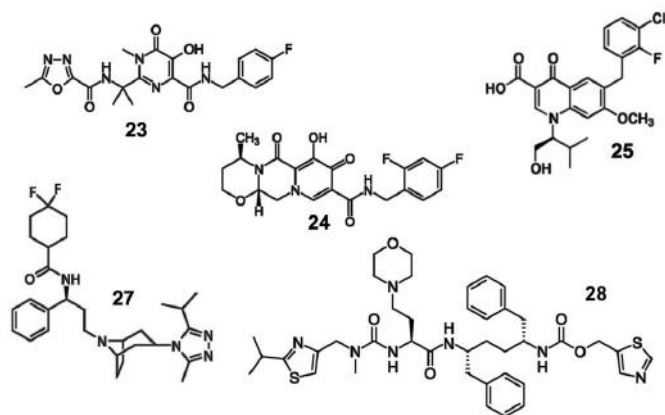


Fig. 5. Other inhibitors of the HIV life cycle

gravir (**25**) (Fig. 5); they bind to the integration complex and inhibit the integration of proviral DNA into genomic DNA.

Virus cell entry inhibitors

Besides inhibitors of HIV-1 enzymes, inhibitors affecting other steps of the viral life cycle have been developed. Virus cell entry inhibitors, which are used in the HIV infection, may be divided into two types: inhibitors of viral and cell membrane fusion and inhibitors of the binding of viral envelope proteins to receptors.

At present, only one fusion inhibitor approved as a medication, enfuvirtide (fuzeon) (**26**) (Fig. 6), is known. This is a synthetic polypeptide of 36 amino acid residues that mimics a HIV-1 gp41 transmembrane envelope glycoprotein region consisting of heptad repeats, which enables an interaction between enfuvirtide and gp41 [46, 47]. This interaction changes the gp41 conformation, which prevents the fusion of the virus and the cell. Enfuvirtide is the only synthetic polymer among all approved anti-HIV-1 drugs, which explains its high cost. Enfuvirtide is supplied as a solution for injection; it is administered twice a day, making it difficult to use.

Inhibitors of HIV-1 receptor binding need to interact with one of the CCR5 or CXCR4 co-receptors to which a HIV-1 particle binds during cell entry. Currently, this group is represented by the drug maraviroc (selzentry) (**27**) (Fig. 5) that interacts with the co-receptor CCR5 [48]. Other inhibitors in this group are under development. The main drawback of CCR5 inhibitors is their inability to affect HIV-1 X4 strains that use the CXCR4 co-receptor [1].

Marine algae polysaccharides and chitosan derivatives are considered as potential antiviral agents. These compounds that act at the virus cell entry step are effi-

cient against HIV-1 and other retroviruses *in vitro*, but they are not approved as drugs, because they do not have a homogeneous composition and a clearly defined structure [49]. Sulfated polysaccharides are structurally similar to heparan sulfates that are primary non-specific cellular receptors interacting with HIV-1. Presumably, the polysaccharides bind to a HIV-1 envelope protein and prevent its interaction with cell surface receptors. Usually, polysaccharides with a higher molecular weight and a higher degree of sulfation have a more pronounced antiviral activity [50].

Cobicistat (**28**) is another medication approved for clinical use. In contrast to the above-listed compounds, cobicistat is not an inhibitor of a particular step in the HIV-1 life cycle. Cobicistat acts as a pharmacokinetic enhancer of the action of atazanavir or darunavir. It is used as an additive to cocktails used to treat the HIV infection.

Highly active antiretroviral therapy

A combination of different inhibitor groups is usual in HIV infection therapy. First, there were nucleoside reverse transcriptase inhibitors combined with non-nucleoside reverse transcriptase inhibitors and protease inhibitors. This method was called highly active antiretroviral therapy (HAART). A combination of three or more inhibitors reduces the dose of each of them, increases the efficiency due to simultaneous action on several steps in the HIV-1 life cycle, and decreases the potential for the emergence of new drug-resistant virus forms. The use of two inhibitor types for a single enzyme, RT, in a cocktail is explained by the fact that they target different functional sites of the enzyme, which underlies enhanced inhibition of the RT function. Table 2 shows the approved anti-HIV drug cocktails used in HAART.

OTHER APPROACHES TO THE TREATMENT OF HIV-1 INFECTION

Over the past 25 years, the attention of researchers has focused primarily on the development and optimization of drugs to suppress HIV-1 replication. The antiviral treatment that is currently used, including HAART, has its limitations. Patients have to take drugs throughout their lives, while new mutant forms of the virus emerge which are resistant to a wide range of drugs. Upon long-term therapy, the drugs may cause a cumulative toxic effect. Many experts agree that a new approach is required to enable the achievement of permanent remission under milder treatment conditions. Also, life cycle inhibitors suppress HIV-1 only in cells with active viral replication, but they do not affect a latent virus. Viral genome copies integrate into the genome of memory T cells (CD4⁺ T cells) and remain

REVIEWS

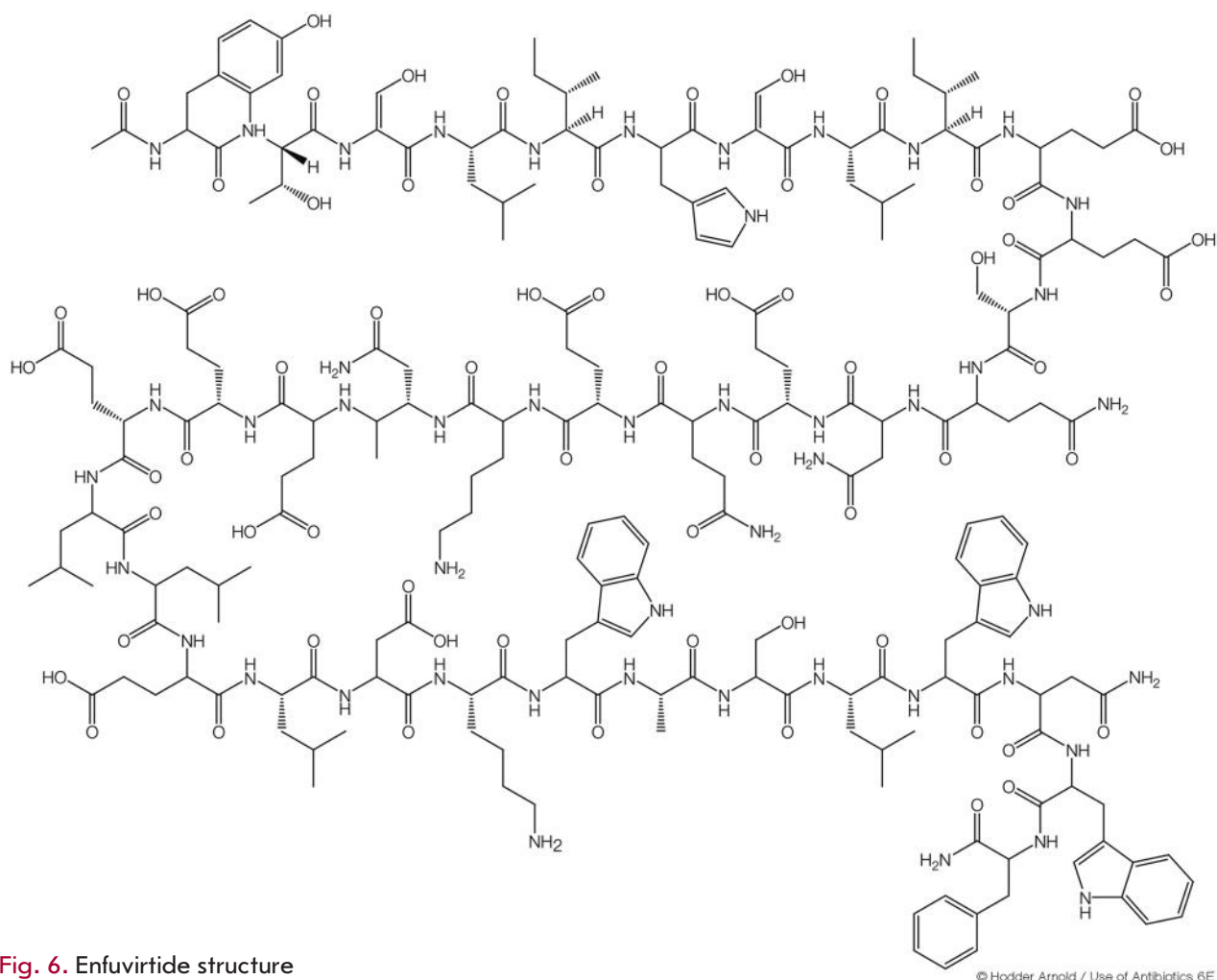


Fig. 6. Enfuvirtide structure

Table 2. Drug combinations (cocktails) used in complex treatment of a HIV infection

Combination	Trade name	FDA approval
Lamivudine/Zidovudine (3TC/ZDV)	Combivir	27/9/1997
Abacavir/Lamivudine/Zidovudine (ABC/3TC/ZDV)	Trizivir	14/11/2000
Abacavir/Lamivudine (ABC/3TC)	Epzicom	2/8/2004
Emtricitabine/Tenofovir (FTC/TDF)	Truvada	2/8/2004
Efavirenz/Emtricitabine/Tenofovir (EFV/FTC/TDF)	Atripla	12/6/2006
Emtricitabine/Rilpivirine/Tenofovir (FTC/RPV/TDF)	Complera	10/8/2011
Elvitegravir/Cobicistat/Emtricitabine/Tenofovir (QUAD, EVG/COBI/FTC/TDF)	Stribild	27/8/2012
Abacavir/Dolutegravir/Lamivudine (ABC/DTG/3TC)	Triumeq	22/8/2014
Atazanavir/Cobicistat (ATV/COBI)	Evotaz	29/1/2015
Darunavir/Cobicistat (DRV/COBI)	Prezcobix	29/1/2015
Elvitegravir/Cobicistat/Emtricitabine/Tenofovir/Alafenamide (EVG/COBI/FTC/TAF)	Genvoya	5/11/2015

invisible to the immune system [51, 52]. Induction of transcription in these cells leads to the formation of infectious viral particles [53].

The development of an anti-HIV-1 vaccine is considered as an alternative option. The first vaccine was developed in the early 2000s; however, the effectiveness of vaccination was much lower than that of classic anti-HIV drugs [54, 55]. Currently, the activity of so-called broad-spectrum neutralizing antibodies is undergoing clinical trials. The results of preliminary studies suggest that neutralizing antibodies may become promising anti-HIV drugs [56, 57].

Currently, the possibility of affecting a latent virus is being investigated. There are two approaches, called sterilizing and functional cure. The sterilizing cure means complete purging of the body of the viral genome through the destruction of cells bearing the provirus integrated into their genome; the functional cure is a complete suppression of viral activity in the body, which includes blocking latent provirus reactivation.

One of the variants of the sterilizing cure is the transplantation of bone marrow from donors resistant to the HIV infection (e.g., whose genome contains a mutant gene of HIV-1 co-receptors, $\Delta 32$ CCR5). As shown in 2009, this approach enabled a complete cure of the HIV infection; i.e., all copies of the viral genome were eliminated from the body. This event was called the “Berlin patient” [58]. The patient underwent radiation therapy and bone marrow transplantation from a donor with $\Delta 32$ CCR5. Later, after discontinuation of anti-HIV therapy, the virus could no longer be detected in his body. Initially, the case engendered great optimism among physicians. But to date, there have been cases where this approach has not had the desired effect. Therefore, the search for other therapies continues.

Latent provirus reactivation

One of the sterilizing cure variants is the “awakening” of latent proviruses. Theoretically, medication that is able to reactivate a latent provirus can successively induce the transcription of the HIV-1 genome, synthesis of viral proteins, and emergence of infectious HIV-1 particles, which would result in the death of the infected cell and decrease the number of latent HIV-1 copies in the human genome. This approach was called “shock and kill.” Cells carrying viral genome copies are supposed either to die due to the cytopathic viral effect or to be destroyed by the immune system. This approach should be combined with maintenance therapy by HIV-1 inhibitors to prevent the spread of the reactivated virus.

Vorinostat, the histone deacetylase inhibitor used in cancer therapy, was studied as a potential anti-HIV-1 drug [59]. As was demonstrated in cells derived from

patients and in clinical trials, the inhibitor can induce the transcription of viral genes in some patients. At the same time, vorinostat is cytotoxic and ineffective in all cases, which makes its wide clinical application problematic. Other histone deacetylase inhibitors are undergoing clinical trials [60, 61].

This approach has at least two disadvantages. The first is the potential side effects in the form of non-specific induction of host cell gene transcription. The second is the impossibility to predict whether all the cells harboring induced proviruses die. There is evidence that the immune system cannot recognize all these cells [62]. Progress in this direction hinges on developing a method to effectively destroy cells that harbor the activated provirus.

Along with the investigation of the possibility to “sterilize” the body from all proviral copies, there are studies that endeavor to search for a functional cure that does not require a complete elimination of all copies of the viral genome but effectively inhibits potential viral activity, which excludes the need for a constant use of HIV-1 life cycle inhibitors.

Inhibition of integrated provirus transcription

One of the potential therapeutic targets is the HIV-1 Tat protein and the Tat/TAR/P-TEFb complex. Tat is one of the HIV-1 regulatory proteins: a transcription activator. Tat binds to the so-called TAR region of 60 nucleotides located at the 5'-end of a transcribed RNA chain, which does not affect transcription initiation but increases the processivity of RNA polymerase, thereby enhancing transcription many-fold. P-TEFb kinase, the third component of the complex, may also be a target for therapy. Inhibition of the formation and activity of the complex would reduce the transcription level and prevent provirus reactivation [63, 64]. Currently, low-molecular-weight inhibitors affecting either the Tat protein or TAR are under development. Computer simulation is used for the selection of potential low-molecular-weight inhibitors.

The TAR sequence is highly conserved among HIV-1 strains, which makes it possible to select versatile drugs that interact with TAR. Quinolones are effective inhibitors of Tat-dependent transcription [65, 66]. To date, the molecular mechanism of binding to the target has been determined for only a few compounds exhibiting inhibitory activity. For example, 6-aminoquinolone WM5 inhibits the interaction between Tat and TAR through specific binding to the TAR. At the same time, some quinolone derivatives inhibit Tat-dependent transcription, but they do not interact with the TAR/Tat complex [67].

There are a number of low-molecular-weight compounds that interact with the Tat protein and block its

binding to TAR. These agents are not yet used for anti-HIV therapy. One of these, the Tat inhibitor triptolide, is undergoing clinical trials. Triptolide is a natural compound isolated from the plant *Tripterygium wilfordii*. Triptolide was demonstrated to promote rapid Tat degradation in cells, thereby inhibiting Tat-dependent transcription [68].

Genome editing

A completely new anti-HIV-1 therapy option is gene therapy that includes the editing of the integrated proviral DNA and blocking further functioning of the virus. In 2013, the CRISPR/Cas9 system was used in model HEK293 and HeLa cell lines whose genomes contained an expression cassette comprising a gene encoding GFP and a sequence encoding the HIV-1 Tat protein under the control of the HIV-1 LTR. The CRISPR/Cas9 system activity for editing the LTR sequence was shown to reduce the GFP expression level in the HEK293 cell line. Similar results were obtained on Jurkat line cells bearing a simulation of latent proviral DNA in their genome, which is an indication of the fact that the CRISPR/Cas9 system may be used to prevent latent provirus reactivation.

It was demonstrated that the TAR sequence can be used as a target for genome editing by the CRISPR/Cas9 system [69]. Another potential target is the HIV-1 co-receptor CCR5 [70–72].

However, implementation of this system in clinical practice requires the development of an effective delivery system as well as a series of pre-clinical trials. Definitely, this method is very promising.

CONCLUSION

The use of HIV-1 inhibitors for antiviral therapy is currently the only method that is actively being applied. In the case of HAART, the use of a combination of drugs aimed at inhibiting different steps of the HIV-1 life cycle minimizes the disadvantages of this approach, because HAART decreases the likelihood of a selection of drug-resistant viral forms and requires smaller doses of all of the drugs, which reduces the potential cumulative toxic effect. New treatment options, which are under development, require further research and clinical trials, but they seem promising for future use. ●

This work was supported by the Russian Foundation for Basic Research (grant 16-34-00989 mol_a).

REFERENCES

- De Clercq E. // Rev. Med. Virol. 2009. V. 19. P. 287–299.
- Roberts J.D., Bebenek K., Kunkel T.A. // Science. 1988. V. 242. № 4882. P. 1171–1173.
- Clapham P.R., McKnight A. // Br. Med. Bull. 2001. V. 58. P. 43–59.
- Benkirane M., Jin D.Y., Chun R.F., Koup R.A., Jeang K.T. // J. Biol. Chem. 1997. V. 272. P. 30603–30606.
- Wilkinson D.A., Operskalski E.A., Busch M.P., Mosley J.W., Koup R.A. // J. Infect. Dis. 1998. V. 178. P. 1163–1166.
- Depienne C., Mousnier A., Leh H., Le Rouzic E., Dormont D., Benichou S., Dargemont C. // J. Biol. Chem. 2001. V. 276. P. 18102–18107.
- Ganser-Pornillos B.K., Yeager M., Sundquist W. // Curr. Opin. Struct. Biol. 2008. V. 18. P. 203–217.
- Cihlar T., Ray A.S. // Antiviral Res. 2010. V. 85. P. 39–58.
- Lavie A., Schlichting I., Vetter I.R., Konrad M., Reinstein J., Goody R.S. // Nat. Med. 1997. V. 3. P. 922–924.
- Lavie A., Vetter I.R., Konrad M., Goody R.S., Reinstein J., Schlichting I. // Nat. Struct. Biol. 1997. V. 4. P. 601–604.
- Schneider B., Xu Y. W., Sellam O., Sarfati R., Janin J., Veron M., Deville-Bonne D. // J. Biol. Chem. 1998. V. 273. № 19. P. 11491–11497.
- Nakashima H., Matsui T., Harada S., Kobayashi N., Matsuda A., Ueda T., Yamamoto N. // Antimicrob. Agents Chemother. 1986. V. 30. № 6. P. 933–937.
- Doong S.L., Tsai C.H., Schinazi R.F., Liotta D.C., Cheng Y.C. // Proc. Natl. Acad. Sci. USA. 1991. V. 88. № 19. P. 8495–8499.
- Furman P.A., Davis M., Liotta D.C., Paff M., Frick L.W., Nelson D.J., Dornsife R.E., Wurster J.A., Wilson L.J., Fyfe J.A., et al. // Antimicrob. Agents Chemother. 1992. V. 36. № 12. P. 2686–2692.
- Hoong L.K., Strange L.E., Liotta D.C., Koszalka G.W., Burns C.L., Schinazi R.F. // J. Org. Chem. 1992. V. 57. P. 5563–5565.
- Schinazi R.F., McMillan A., Cannon D., Mathis R., Lloyd R.M., Peck A., Sommadossi J.P., St Clair M., Wilson J., Furman P.A., et al. // Antimicrob. Agents Chemother. 1992. V. 36. № 11. P. 2423–2431.
- Schinazi R.F., Boudinot F.D., Ibrahim S.S., Manning C., McClure H.M., Liotta D.C. // Antimicrob. Agents Chemother. 1992. V. 36. P. 2432–2438.
- Hooker D.J., Tachedjian G., Solomon A.E., Gurusinghe A.D., Land S., Birch C., Anderson J.L., Roy B.M., Arnold E., Deacon N.J. // J. Virol. 1996. V. 70. № 11. P. 8010–8018.
- Cruchaga C., Anso E., Rouzaut A., Martinez-Irujo J.J. // J. Biol. Chem. 2006. V. 281. № 38. P. 27744–27752.
- Coffin J.M. // Science. 1995. V. 267. № 5197. P. 483–489.
- Larder B.A., Darby G., Richman D.D. // Science. 1989. V. 243. № 4899. P. 1731–1734.
- Goldschmidt V., Marquet R. // Int. J. Biochem. Cell. Biol. 2004. V. 36. № 9. P. 1687–1705.
- Deval J., Courcambeck J., Selmi B., Boretto J., Canard B. // Curr. Drug Metab. 2004. V. 5. № 4. P. 305–316.
- Naeger L.K., Margot N.A., Miller M.D. // Antimicrob. Agents Chemother. 2002. V. 46. № 7. P. 2179–2184.
- de Béthune M. // Antiviral Res. 2010. V. 85. P. 75–90.
- Grob P.M., Wu J.C., Cohen K.A., Ingraham R.H., Shih C.K., Hargrave K.D., McTague T.L., Merluzzi V.J. // AIDS Res. Hum. Retroviruses. 1992. V. 8. № 2. P. 145–152.
- De Clercq E. // Chem. Biodivers. 2004. V. 1. № 1. P. 44–64.
- Debysier Z., Pauwels R., Andries K., Desmyter J., Kukla M., Janssen P.A., De Clercq E. // Proc. Natl. Acad. Sci. USA. 1991. V. 88. № 4. P. 1451–1455.
- Althaus I.W., Chou J.J., Gonzales A.J., Deibel M.R., Chou K.C., Kezdy F.J., Romero D.L., Palmer J.R., Thomas R.C.,

- Aristoff P.A., et al. // *Biochemistry*. 1993. V. 32. № 26. P. 6548–6554.
30. Ren J, Milton J, Weaver K.L., Short S.A., Stuart D.I., Stammers D.K. // *Structure*. 2000. V. 8. № 10. P. 1089–1094.
31. Fletcher R.S., Syed K., Mithani S., Dmitrienko G.I., Paraniak M.A. // *Biochemistry*. 1995. V. 34. № 13. P. 4346–4353.
32. Rittinger K., Divita G., Goody R.S. // *Proc. Natl. Acad. Sci. USA*. 1995. V. 92. № 17. P. 8046–8049.
33. Zhou Z., Madrid M., Evanseck J.D., Madura J.D. // *J. Am. Chem. Soc.* 2005. V. 127. № 49. P. 17253–17260.
34. Hang J.Q., Li Y., Yang Y., Cammack N., Mirzadegan T., Klumpp K. // *Biochem. Biophys. Res. Commun.* 2007. V. 352. № 2. P. 341–350.
35. Janssen P.A.J., Lewi P.J., Arnold E., Daeyaert F., de Jonge M., Heeres J., Koymans L., Vinkers M., Guillemont J., Pasquier E., et al. // *J. Med. Chem.* 2005. V. 48. № 6. P. 1901–1909.
36. Madruga J.V., Cahn P., Grinsztejn B., Haubrich R., Lalezari J., Mills A., Pialoux G., Wilkin T., Peeters M., Vingerhoets J., et al. // *Lancet*. 2007. V. 370. № 9581. P. 29–38.
37. Lazzarin A., Campbell T., Clotet B., Johnson M., Katlama C., Moll A., Towner W., Trottier B., Peeters M., Vingerhoets J., et al. // *Lancet*. 2007. V. 370. № 9581. P. 39–48.
38. Pauwels R. // *Antiviral Res.* 2006. V. 71. № 2–3. P. 77–89.
39. Roberts N.A., Martin J.A., Kinchington D., Broadhurst A.V., Craig J.C., Duncan I.B., Galpin S.A., Handa B.K., Kay J., Kröhn A., et al. // *Science*. 1990. V. 248. № 4953. P. 358–361.
40. Clavel F., Hance A.J. // *N. Engl. J. Med.* 2004. V. 350. № 10. P. 1023–1035.
41. Wensing A.M.J., van Maarseveen N.M., Nijhuis M. // *Antiviral Res.* 2010. V. 85. P. 59–74.
42. Hazuda D.J., Felock P., Witmer M., Wolfe A., Stillmock K., Grobler J.A., Espeseth A., Gabryelski L., Schleif W., Blau C., et al. // *Science*. 2000. V. 287. № 5453. P. 646–650.
43. Grinsztejn B., Nguyen B.Y., Katlama C., Gatell J.M., Lazzarin A., Vittecoq D., Gonzalez C.J., Chen J., Harvey C.M., Isaacs R.D., et al. // *Lancet*. 2007. V. 369. № 9569. P. 1261–1269.
44. Steigbigel R.T., Cooper D.A., Kumar P.N., Eron J.E., Schechter M., Markowitz M., Loutfy M.R., Lennox J.L., Gatell J.M., Rockstroh J.K., et al. // *N. Engl. J. Med.* 2008. V. 359. № 4. P. 339–354.
45. Cooper D.A., Steigbigel R.T., Gatell J.M., Rockstroh J.K., Katlama C., Yeni P., Lazzarin A., Clotet B., Kumar P.N., Eron J.E., et al. // *N. Engl. J. Med.* 2008. V. 359. № 4. P. 355–365.
46. Matthews T., Salgo M., Greenberg M., Chung J., DeMasi R., Bolognesi D. // *Nat. Rev. Drug Discov.* 2004. V. 3. № 3. P. 215–225.
47. Wild C., Greenwell T., Matthews T. // *AIDS Res. Hum. Retroviruses*. 1993. V. 9. № 11. P. 1051–1053.
48. Perros M. // *Adv. Antiviral Drug Design*. 2007. V. 5. P. 185–212.
49. Baba M., Snoeck R., Pauwels R., De Clercq E. // *Antimicrob. Agents Chemother.* 1988. V. 32. № 11. P. 1742–1745.
50. Prokofjeva M.M., Imbs T.I., Shevchenko N.M., Spirin P.V., Horn S., Fehse B., Zvyagintseva T.N., Prassolov V.S. // *Marine Drugs*. 2013. V. 11. № 8. P. 3000–3014.
51. Siliciano J.D., Kajdas J., Finzi D., Quinn T.C., Chadwick K., Margolick J.B., Kovacs C., Gange S.J., Siliciano R.F. // *Nat. Med.* 2003. V. 9. P. 727–728.
52. Adams M., Sharmeen L., Kimpton J., Romeo J.M., Garcia J.V., Peterlin B.M., Groudine M., Emerman M. // *Proc. Natl. Acad. Sci. USA*. 1994. V. 91. № 9. P. 3862–3866.
53. Chun T.W., Stuyver L., Mizell S.B., Ehler L.A., Mican J.A., Baseler M., Lloyd A.L., Nowak M.A., Fauci A.S. // *Proc. Natl. Acad. Sci. USA*. 1997. V. 94. № 24. P. 13193–13197.
54. Autran B., Carcelain G., Combadiere B., Debre P. // *Science*. 2004. V. 305. № 5681. P. 205–208.
55. Carcelain G., Autran B. // *Immunol Rev.* 2013. V. 254. № 1. P. 355–371.
56. Shingai M., Donau O.K., Plishka R.J., Buckler-White A., Mascola J.R., Nabel G.J., Nason M.C., Montefiori D., Moldt B., Pognard P., et al. // *J. Exp. Med.* 2014. V. 211. № 10. P. 2061–2074.
57. Caskey M., Klein F., Lorenzi J.C., Seaman M.S., West A.P. Jr., Buckley N., Kremer G., Nogueira L., Braunschweig M., Scheid J.F., et al. // *Nature*. 2015. V. 522. № 7557. P. 487–491.
58. Hutter G., Nowak D., Mossner M., Ganepola S., Mussig A., Allers K., Schneider T., Hofmann J., Kücherer C., Blau O., et al. // *N. Engl. J. Med.* 2009. V. 360. № 7. P. 692–698.
59. Archin N.M., Liberty A.L., Kashuba A.D., Choudhary S.K., Kuruc J.D., Crooks A.M., Parker D.C., Anderson E.M., Kearney M.F., Strain M.C., et al. // *Nature*. 2012. V. 487. P. 482–485.
60. Rasmussen T.A., Tolstrup M., Brinkmann C.R., Olesen R., Erikstrup C., Solomon A., Winckelmann A., Palmer S., Dinarello C., Buzon M., et al. // *Lancet HIV*. 2014. V. 1. № 1. P. e13–21.
61. Søgaard O.S., Graversen M.E., Leth S., Olesen R., Brinkmann C.R., Nissen S.K., Kjaer A.S., Schleimann M.H., Denton P.W., Hey-Cunningham W.J., et al. // *PLoS Pathog.* 2015. V. 11. № 9. P. e1005142.
62. Shan L., Deng K., Shroff N.S., Durand C.M., Rabi S.A., Yang H.C., Zhang H., Margolick J.B., Blankson J.N., Siliciano R.F. // *Immunity*. 2012. V. 36. № 3. P. 491–501.
63. Jones L.E., Perelson A.S. // *J. Acquir. Immune Defic. Syndr.* 2007. V. 45. № 5. P. 483–493.
64. Sklar P.A., Ward D.J., Baker R.K., Wood K.C., Gafoor Z., Alzola C.F., Moorman A.C., Holmberg S.D. // *AIDS*. 2002. V. 16. № 15. P. 2035–2041.
65. Cecchetti V., Parolin C., Moro S., Pecere T., Filippini E., Calistri A., Tabarrini O., Gatto B., Palumbo M., Fravolini A., et al. // *J. Med. Chem.* 2000. V. 43. № 20. P. 3799–3802.
66. Parolin C., Gatto B., Del Vecchio C., Pecere T., Tramontano E., Cecchetti V., Fravolini A., Masiero S., Palumbo M., Palu G. // *Antimicrob. Agents Chemother.* 2003. V. 47. № 3. P. 889–896.
67. Tabarrini O., Stevens M., Cecchetti V., Sabatini S., Dell’Uomo M., Manfroni G., Palumbo M., Pannecouque C., De Clercq E., Fravolini A. // *J. Med. Chem.* 2004. V. 47. № 22. P. 5567–5578.
68. Richter S.N., Palu G. // *Curr. Med. Chem.* 2006. V. 13. № 11. P. 1305–1315.
69. Ebina H., Misawa N., Kanemura Y., Koyanagi Y. // *Sci. Rep.* 2013. V. 3. P. 2510.
70. Tebas P., Stein D., Tang W.W., Frank I., Wang S.Q., Lee G., Spratt S.K., Surosky R.T., Giedlin M.A., Nichol G., et al. // *N. Engl. J. Med.* 2014. V. 370. № 10. P. 901–910.
71. Cho S.W., Kim S., Kim J.M., Kim J.S. // *Nat. Biotechnol.* 2013. V. 31. № 3. P. 230–232.
72. Wang W., Ye C., Liu J., Zhang D., Kimata J.T., Zhou P. // *PLoS One*. 2014. V. 9. № 12. P. e115987.

Synthetic Fluorophores for Visualizing Biomolecules in Living Systems

V. I. Martynov*, A. A. Pakhomov, N. V. Popova, I. E. Deyev, A. G. Petrenko

Shemyakin–Ovchinnikov Institute of Bioorganic Chemistry, Russian Academy of Sciences, Miklukho-Maklaya St., 16/10, Moscow, 117997, Russia

*E-mail: vimart@list.ru

Received December 12, 2015; in final form, April 26, 2016

Copyright © 2016 Park-media, Ltd. This is an open access article distributed under the Creative Commons Attribution License, which permits unrestricted use, distribution, and reproduction in any medium, provided the original work is properly cited.

ABSTRACT The last decade has witnessed significant advance in the imaging of living systems using fluorescent markers. This progress has been primarily associated with the discovery of different spectral variants of fluorescent proteins. However, the fluorescent protein technology has its own limitations and, in some cases, the use of low-molecular-weight fluorophores is preferable. In this review, we describe the arsenal of synthetic fluorescent tools that are currently in researchers' hands and span virtually the entire spectrum, from the UV to visible and, further, to the near-infrared region. An overview of recent advances in site-directed introduction of synthetic fluorophores into target cellular objects is provided. Application of these fluorescent probes to the solution of a wide range of biological problems, in particular, to the determination of local ion concentrations and pH in living systems, is discussed.

KEYWORDS fluorophore; fluorescence microscopy; site-directed reaction; measurement of ion concentration; measurement of local pH.

ABBREVIATIONS TCP – target cellular protein; FP – fluorescent protein; AGT – O⁶-alkylguanine transferase; eDHFR – dihydrofolate reductase; TMP – trimethoprim; DAPI – 4',6-diamidino-2-phenylindole; NBD – 4-nitrobenz-2-oxa-1,3-diazole; dansyl chloride – 5-dimethylaminonaphthalene-1-sulfonyl chloride; EDANS – 5-((2-aminoethyl)amino)naphthalene-1-sulfonic acid; FRET – Förster resonance energy transfer; SRh 101 – sulforhodamine 101; BODIPY – 4,4-difluoro-4-bora-3a,4a-diaza-s-indacene; FITC – fluorescein isothiocyanate; λ_{ex} – excitation maximum; λ_{em} – emission maximum; ϵ – extinction coefficient; Φ – quantum yield.

INTRODUCTION

Fluorescence-based molecular markers have for a long time served as a tool for *in vitro* imaging of biomolecules. Fluorescent labeling with a synthetic fluorophore was first reported in 1942, when fluorescein isothiocyanate (FITC)-labeled anti-pneumococcal antibodies were obtained [1]. Until the 1980s, fluorescent labeling was mostly used to analyze fixed biological specimens. Over the past two decades, a number of methods have been designed that allow one to insert fluorescent tags into living objects [2], in particular, as genetically encoded chimeras of target cellular proteins (TCPs) with GFP-like fluorescent proteins (FPs) [3–5]. However, in some cases, the analysis of living systems requires the use of low-molecular-weight fluorescent probes [6, 7] to directly modify TCP [8, 9]. The main advantage of these fluorophores is their small size and the availability of compounds with the desired chemical and photophysical properties.

The possibility of using a certain fluorophore depends on its chemical (reactivity, solubility, lipophilic properties, pKa, and stability) and photophysical prop-

erties (excitation maximum (λ_{ex}), emission maximum (λ_{em}), extinction coefficient (ϵ), quantum yield (Φ), lifetime of the excited state, and photostability). The extinction coefficient multiplied by the quantum yield ($\epsilon \times \Phi$) is the universal parameter used to determine the sensitivity of this method for different fluorophores. This value is directly proportional to the brightness and takes into account the amount of absorbed light and the yield of fluorophore emission.

PROPERTIES OF SYNTHETIC FLUOROPHORES

Fluorophores emitting in the UV and blue spectral ranges

Fluorophores emitting in the UV spectral range are used to label living systems not that frequently, since UV light is toxic for them. Furthermore, it is difficult to distinguish between the fluorescence signals of these tags and cell autofluorescence. Pyrene derivatives (*Fig. 1*) are a classic example of fluorophores emitting in the near-UV spectral range: they are characterized by $\lambda_{\text{ex}} = 340$ nm, $\lambda_{\text{em}} = 376$ nm, a high

quantum yield $\Phi = 0.75$, chemical stability, and long fluorescence lifetime, which allows fluorophore molecules to form excimers with a bathochromic shift in the emission spectra. These properties of pyrenes are used in the monitoring of conformational changes in the protein structure [10] and to determine the concentrations of ions in certain metals [11, 12]. Pyrene derivatives, such as 8-hydroxy-1,3,6-pyrenetrisulfonate (pyranine, Fig. 1), are used as pH indicators or sensors for Cu^+ ions [13]. The 8-O-carboxymethylpyranine derivative is characterized by $\lambda_{\text{ex}}/\lambda_{\text{em}}$ 401.5/428.5 nm and $\epsilon = 2.5 \times 10^4 \text{ M}^{-1}\text{cm}^{-1}$ (405 nm). This fluorophore can be used as a bright and photostable tag emitting in the violet spectral range for multicolor labeling of cellular objects [14].

Fluorescent markers based on coumarin derivatives are widely employed as chemosensors and in the labeling of biomolecules [15, 16]. A substituent inserted at position 7 of coumarin yields fluorophores emitting in the visible range of the spectrum: e.g., 7-hydroxy-4-methylcoumarin (Fig. 2). This fluorophore is characterized by $\lambda_{\text{ex}} = 360 \text{ nm}$, $\lambda_{\text{em}} = 450 \text{ nm}$, $\epsilon = 1.7 \times 10^3 \text{ M}^{-1}\text{cm}^{-1}$, and $\Phi = 0.63$. 7-Hydroxycoumarin derivatives act as an intracellular fluorescent sensor of phosphatase activity; its mixed carbonates are used to determine the lipase and esterase activities [17, 18]. A related compound, 7-amino-4-methylcoumarin (Fig. 2), exhibits the same spectral properties as the hydroxy derivative at $\text{pH} > 5$.

The indole derivative 4',6-diamidino-2-phenylindole (DAPI; Fig. 3) was first synthesized in 1971 at the Otto Dann's laboratory in pursuit of anti-trypanosomiasis drugs. This compound proved inefficient as medication but demonstrated DNA-binding ability [19]. Since the binding of DAPI to DNA significantly increases fluorescence in the blue spectral range ($\lambda_{\text{em}} = 461 \text{ nm}$ for DAPI bound to DNA), this marker is widely used to label DNA in living cells [20]. It has recently been shown that irradiation of DAPI with UV light or laser light with $\lambda = 405 \text{ nm}$ results in its photoconversion [21, 22]. The emission maximum of the fluorophore shifts toward the green region of the spectrum (505 nm) after argon laser excitation of the photoconverted form

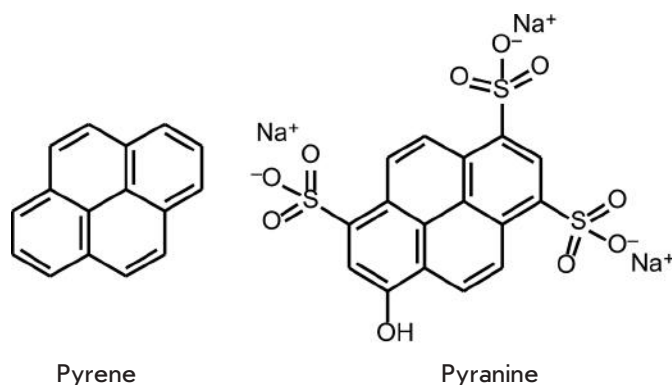


Fig. 1. Fluorophores based on condensed aromatic compounds with emission in the UV- and blue spectral ranges



7-hydroxy-4-methylcoumarin 7-amino-4-methylcoumarin

Fig. 2. Fluorophores based on coumarin derivatives

of DAPI at 458 nm. Furthermore, the photoconverted green form of the fluorophore loses its color after blue-light irradiation [22]. This property was used in single-molecule localization microscopy (the SMLM method in subdiffraction imaging) of DNA, which has made it possible to reconstruct the accurate map of distribution of these molecules in cell nuclei and chromosomes during mitosis [20].

The fluorescent dibenzimidazole derivatives were first synthesized and used by Hoechst AG company for fluorescence microscopy. The compound Hoechst 33342 (Fig. 3) fluoresces in the cyan-blue spectral range and has an emission maximum at 461 nm. It binds to DNA, easily penetrates through the cell membrane, and can be used for experiments on living cells [20].

Bimane, 1,5-diazabicyclo[3.3.0]octa-3,6-dien-2,8-dione (Fig. 3), is characterized by $\lambda_{\text{ex}} = 390 \text{ nm}$, $\lambda_{\text{em}} = 482 \text{ nm}$, and $\Phi = 0.3$. Bimane fluorescence is

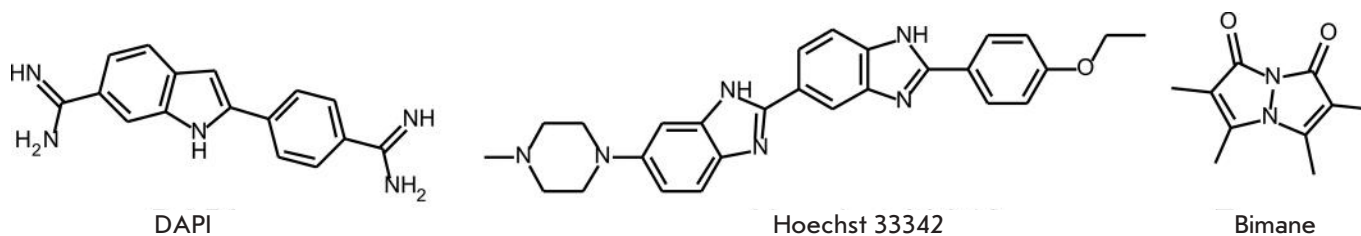


Fig. 3. Synthetic fluorophores emitting in the blue and cyan spectral ranges

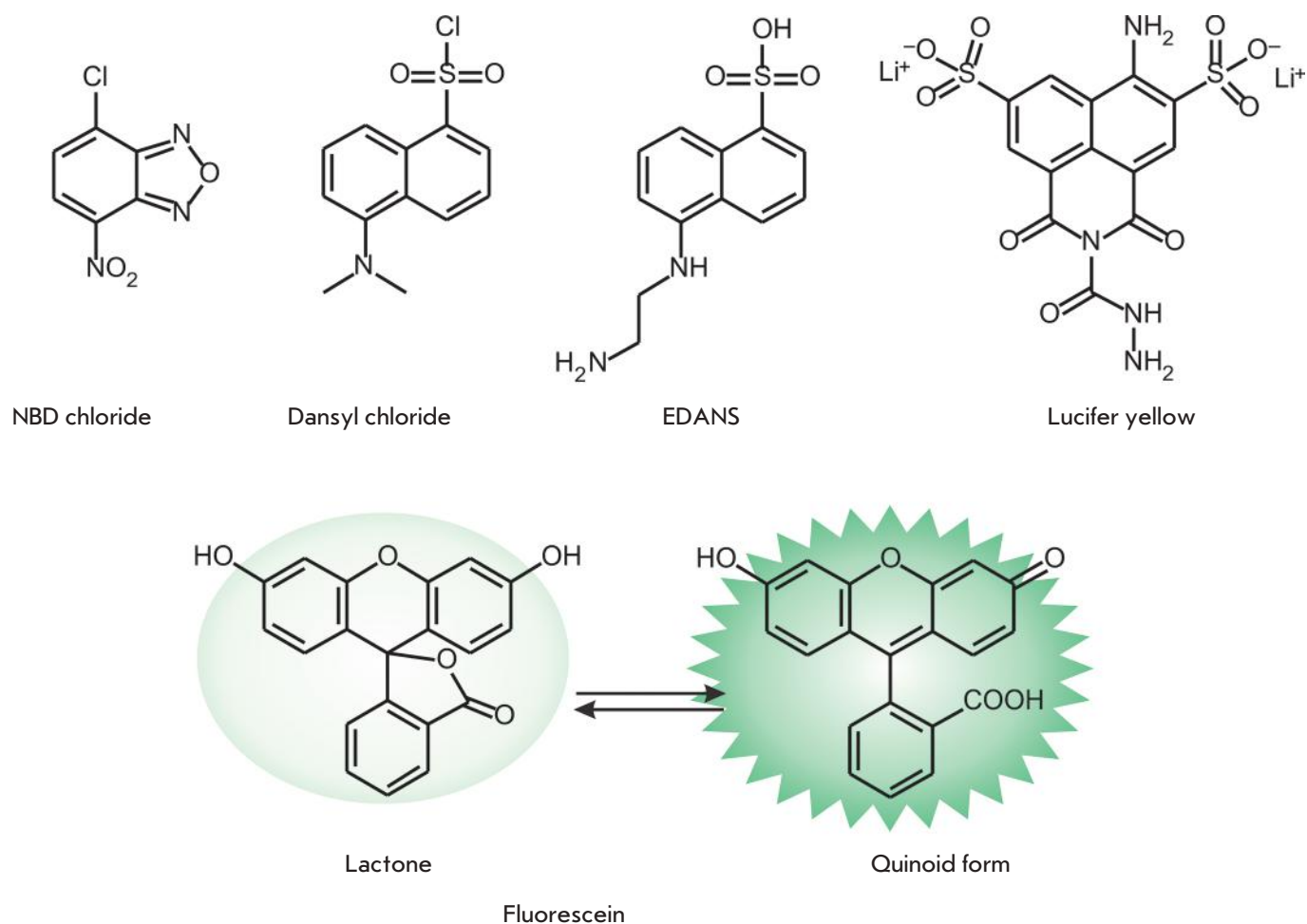


Fig. 4. Fluorophores emitting in the green-yellow spectral range

quenched in the presence of tryptophan and tyrosine; the degree of quenching depends on the distance between these two residues ($\leq 10\text{--}15$ nm). This property of the fluorophore was used for real-time detection of the conformational changes in enzymes during substrate binding [23, 24].

Fluorophores emitting in the green-yellow spectral range

NBD (4-nitrobenzo-2-oxa-1,3-diazole) and its derivatives exhibit emission in the green region of the spectrum. NBD chloride (*Fig. 4*) reacts with amino and thiol groups. Complexes between NBD chloride and primary amines have the excitation and emission maxima $\lambda_{\text{ex}} = 465$ nm, $\lambda_{\text{em}} = 535$ nm ($\epsilon = 2.2 \times 10^4$ M⁻¹cm⁻¹ and $\Phi = 0.3$). Another NBD derivative that selectively interacts with cysteine has been successfully used as a fluorescent sensor of Cys in HeLa cells [25]. The sensitivity of NBD derivatives to the microenvironment proved important in producing lipid markers [26, 27] or new kinase substrates [28]. NBD-based Cu²⁺ and S²⁻

sensors that allow one to determine the concentration of these ions in a living cell have been designed [29].

NBD-SCN was used to detect cysteine and homocysteine. Substitution of the thiocyanate group with cysteine or homocysteine increases the intensity of NBD fluorescence at 550 nm 470- and 745-fold, respectively [30]. Moreover, NBD-SCN exhibits relatively high membrane-penetrating properties and can be used to visualize changes in the concentration of cysteine and homocysteine in a living cell [30].

Naphthalene derivatives are among the most frequently used fluorophores emitting in the green spectral range. This group of tags includes dansyl chloride that reacts with amino groups and EDANS (*Fig. 4*). Derivatives of this compound are characterized by $\lambda_{\text{ex}} = 336$ nm, $\lambda_{\text{em}} = 520$ nm, $\epsilon = 6.1 \times 10^3$ M⁻¹cm⁻¹, and $\Phi = 0.27$. EDANS-based fluorescent markers are currently used in *in vivo* experiments [31]. Another fluorophore, 4-amino-3,6-disulfonylnaphthalimide, is characterized by fluorescence emission in the yellow spectral range. Its carbohydrazide, known as Lucifer yellow ($\lambda_{\text{ex}} = 428$ nm,

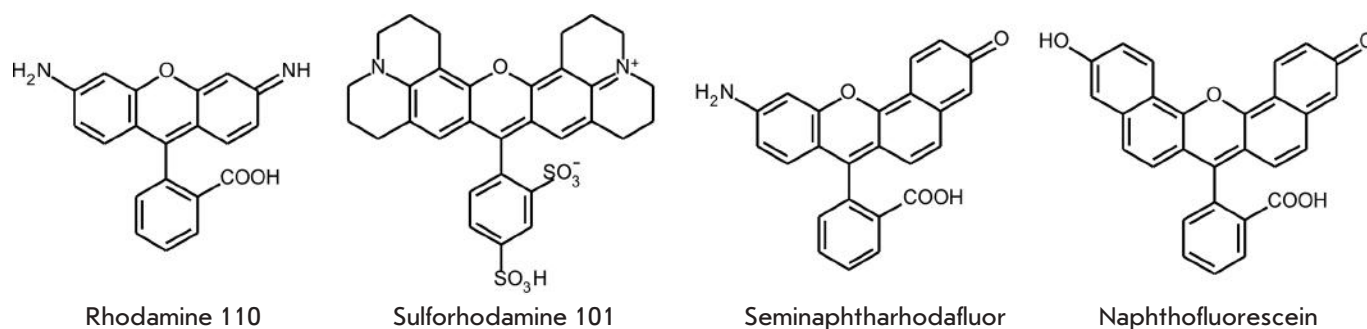


Fig. 5. Xanthene-based synthetic fluorophores

$\lambda_{em} = 534$ nm, Fig. 4), is used as a polar label and in two-photon excitation experiments [32].

Fluorophore fluorescein (Fig. 4) exhibits unique properties: it can exist in aqueous solutions in seven prototropic forms, including the most biologically important ones – the mono-anionic and dianionic forms – which interconvert with $pK_a \sim 6.4$ [33]. The dianionic form displays maximal fluorescence ($\lambda_{ex} = 490$ nm, $\lambda_{em} = 514$ nm, $\epsilon = 9.3 \times 10^4$ M⁻¹cm⁻¹, and $\Phi = 0.95$). The pH sensitivity of fluorescein derivatives was used to produce fluorescent pH indicators [34, 35]. These derivatives were employed to obtain sensors for ions of various metals: e.g., Fluo-3 for measuring the concentration of calcium ions in living cells [36, 37]. Fluorescein exists in two equilibrium forms: as lactone and the quinoid form (Fig. 4). Acylation or alkylation of phenol groups results in the fixation of a molecule as nonfluorescent lactone, which can be used to synthesize fluorogenic substrates for a number of enzymes [38, 39]. However, fluorescein-based fluorophores have significant drawbacks, as well. They are characterized by a high rate of photobleaching; the wide emission band of these fluorophores limits their application in multi-color labeling of cellular objects. Furthermore, they are prone to self-quenching at high densities of tag insertion in TCP.

Another group of synthetic fluorophores emitting in the green spectral range is based on rhodamine derivatives. Introduction of various substituents into the rhodamine structure allows one to tune its spectral characteristics. The most typical example is rhodamine 110 (Fig. 5) ($\lambda_{ex} = 497$ nm, $\lambda_{em} = 520$ nm, $\epsilon = 7.6 \times 10^4$ M⁻¹cm⁻¹, and $\Phi = 0.88$ [40]). Insertion of four-membered azetidinium rings at two nitrogen atoms substantially increases the quantum yield and brightness of the fluorophore [41], while insertion of four methyl groups at the N, N' atoms shifts the excitation and emission maxima towards the long-wavelength region ($\lambda_{ex}/\lambda_{em}$ 548/572 nm), but reduces the quantum yield of the fluorophore ($\Phi = 0.41$) in aqueous solutions [42]. Rhodamines containing rigid cyclic systems instead of amino groups are character-

ized by higher quantum yields; their spectra are shifted towards the long-wavelength region. In particular, sulforhodamine 101 (Texas Red) (Fig. 5) and its derivatives – the fluorophores that are most frequently used in cellular biology [43, 44] – are also used as photosensitizers in photodynamic therapy [45]. Together with fluorescein, rhodamine tags are components of FRET pairs [46, 47]. Substitution of both amino groups in rhodamine can yield its nonfluorescent derivative. This property is used in the synthesis of photoactivable rhodamine analogues [48] and to synthesize fluorogenic substrates when studying the mechanisms of enzyme catalysis. Rhodamine 110 derivatives have been used as substrates to determine the activity of various enzymes [49]. Hybrid fluorophores consisting of a polypeptide-linked quantum dot and rhodamine that can be cleaved by caspase-1 have been used in apoptosis assays [50]. Rhodamine derivatives are also used when designing indicators of pH and the ions of some metals [51, 52].

The compounds under the Alexa Fluor trademark are a large group of hydrophilic negatively charged tags that are represented by sulfated derivatives of various fluorophores, such as fluorescein, coumarin, cyanine, or rhodamine. The well-known rhodamine derivative Alexa Fluor 488 exhibits properties largely similar to those of FITC ($\lambda_{ex} = 493$ nm, $\lambda_{em} = 519$ nm). However, unlike FITC, Alexa Fluor 488 is characterized by higher photostability, higher brightness, and lower pH sensitivity. Optimal results in comparable experiments on specific labeling of modified histones were demonstrated by Fab fragments labeled with Alexa Fluor 488 [53]. Alexa Fluor 488 can act as a donor-fluorophore to study the structure of various cellular receptors using the FRET effect [54].

Fluorophores emitting in the red, far-red, and near-infrared spectral range

Fluorophores emitting in the far-red and near-infrared spectral ranges are of the greatest interest, since the light-exciting fluorescence of these fluorophores is

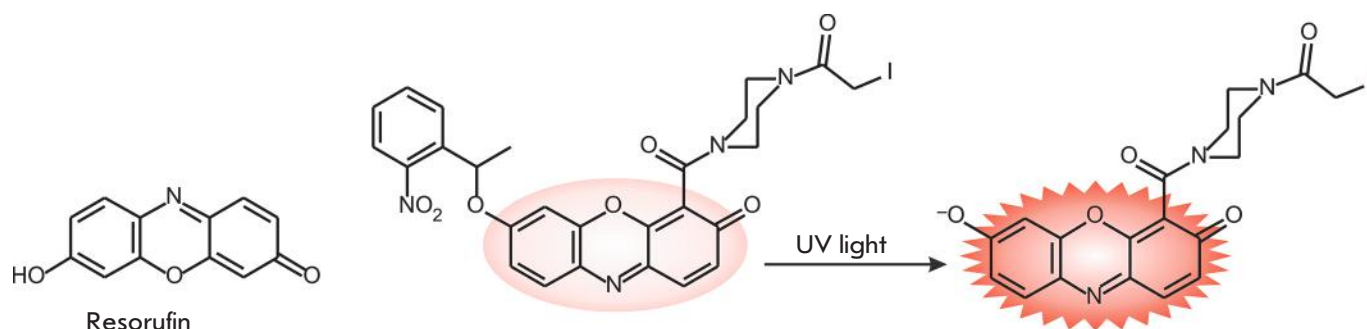


Fig. 6. Resorufin and its photoactivatable *o*-nitrobenzyl derivative

non-toxic to living systems. Furthermore, infrared rays can penetrate living tissues much deeper than shorter wave light. In addition, background autofluorescence has virtually no effect on the imaging of biomolecules in living systems using far-red and infrared fluorophores. Unfortunately, the majority of known synthetic fluorophores belonging to this group have a significant drawback: a low quantum yield of fluorescence in aqueous solutions. Probably, among the fluorophores of this group, special attention should be focused on fluorescein and rhodamine derivatives with xanthene structures modified by the addition of aromatic rings. These substituents cause a significant bathochromic shift in fluorescence spectra. One of these derivatives, naphthofluorescein (Fig. 5), fluoresces in alkaline solutions at much longer wavelengths ($\lambda_{\text{ex}}/\lambda_{\text{em}} = 595/660$ nm). However, all the advantages of this far-red fluorescent tag are outweighed by the fact that it has a lower extinction coefficient ($\epsilon = 4.4 \times 10^4 \text{ M}^{-1}\text{cm}^{-1}$) and quantum yield ($\Phi = 0.14$). This series of derivatives has been successfully used as sensors in living cells [55, 56].

In efforts to obtain rhodamine derivatives absorbing at longer wavelengths, its analogues with the oxygen atom between two aromatic cycles substituted by silicon (Si-rhodamine), germanium (Ge-rhodamine), or tin (Sn-rhodamine) atoms were synthesized [57]. The resulting derivatives retain the key characteristics of rhodamine, such as a high quantum yield in aqueous solutions, resistance to photobleaching, and high water solubility. Three new compounds – SiR680, SiR700, and SiR720 – with fluorescence in the near-infrared region (670–740 nm) were obtained by inserting additional aromatic substituents in Si-rhodamine. SiR680 and SiR700 were shown to exhibit appreciably high quantum yields in aqueous solutions ($\Phi = 0.35$ and 0.12 , respectively) [58]. Activated succinimide derivatives of SiR700 were used *in vivo* for the imaging of a tumor growth [58, 59].

Xanthene dyes with a structure containing an additional aromatic ring exhibit unique properties. Unlike the symmetric fluorescein and rhodamine derivatives,

the resonance forms of these compounds are not equivalent to each other and have different spectral properties. Hence, the asymmetry of these tags can be used to design ratiometric fluorescent indicators. The ratio between the fluorescent intensities of different forms of indicators allows one to accurately determine the intracellular concentration of various ions. Seminaphthofluorescein-based fluorophores are used as pH sensors and indicators of other ions. Rhodol-based seminaphthoxanthenes are also applied as pH indicators. The ratiometric pH sensor seminaphthorhodafluor (Fig. 5) is one of such examples [60, 61]. This compound is characterized by $\lambda_{\text{ex}} = 573$ nm, $\lambda_{\text{em}} = 631$ nm, $\epsilon = 4.4 \times 10^4 \text{ M}^{-1}\text{cm}^{-1}$, and $\Phi = 0.092$ at high pH values.

Resorufin (Fig. 6) is used, in particular, for real-time detection of endogenous phosphatase activity in living cells [62]. At pH > 7.5, resorufin exists in anionic form with fluorescence emission in the red spectral range ($\lambda_{\text{ex}} = 572$ nm, $\lambda_{\text{em}} = 585$ nm, $\epsilon = 5.6 \times 10^4 \text{ M}^{-1}\text{cm}^{-1}$, and $\Phi = 0.74$). The fluorescence intensity of this dye significantly decreases at low pH values.

Some synthetic fluorophores can be modified so that their fluorescence is “switched on” only after activation with light of a certain wavelength. These photoactivatable, or latent, fluorophores are used for space- and time-resolved dynamic imaging of processes requiring the activation of small populations of fluorescent markers. In particular, these fluorogenic markers are synthesized via reactions between a fluorophore and *o*-nitrobenzyl bromide. A molecule can be activated by irradiation at 365 nm; the *o*-nitrobenzyl group is cleaved to release the active fluorophore (Fig. 6). Active migration of microtubules during mitosis was demonstrated for the first time, and the dynamics of actin microfilaments was studied using photoactivation of a tubulin-conjugated fluorogenic probe [63]. A number of photoactivatable coumarin analogues capable of penetrating into the cell have been synthesized [64, 65]. After penetrating into the cell, a small population of coumarin molecules was activated and used as a fluo-

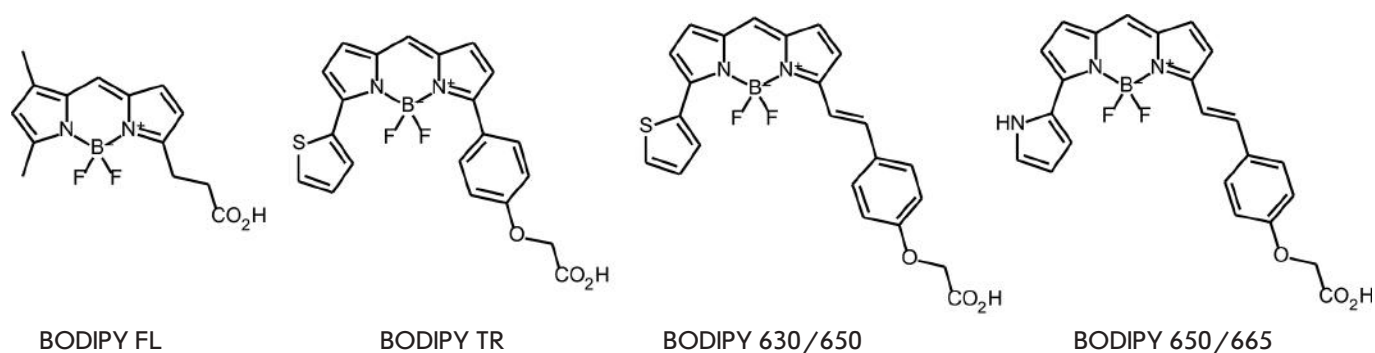


Fig. 7. BODIPY-based fluorophores

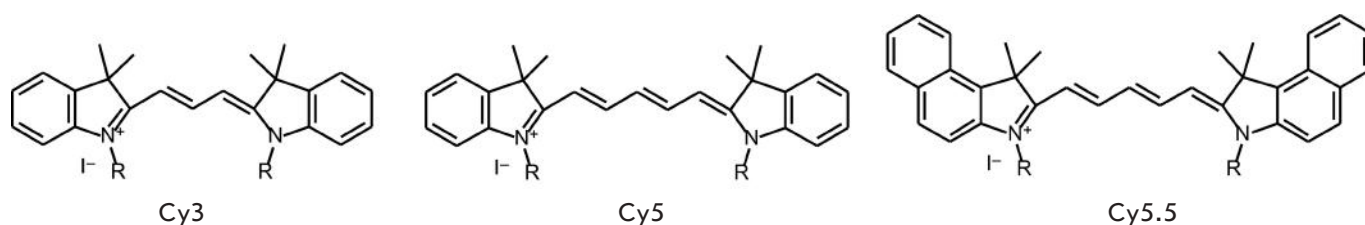


Fig. 8. Derivatives of cyanine dyes Cy3, Cy5, and Cy5.5

rescent reporter to monitor the migration of molecules through gap junctions [65].

Borodifluorodipyrromethene-based compounds widely known as BODIPY are used to synthesize fluorescent markers [66, 67], including those for labeling biomolecules in living cells [68]. They are characterized by high photostability and quantum yield, neutral charge, and narrow absorption and emission bands.

This series of dyes can be tuned to the desired wavelength using certain substituents [69]. However, wide application of these fluorophores is limited because of their poor solubility in water. Some BODIPY fluorophores (Fig. 7) exhibit spectral properties similar to those of fluorescein: e.g., BODIPY FL ($\lambda_{\text{ex}} = 505 \text{ nm}$, $\lambda_{\text{em}} = 511 \text{ nm}$, $\epsilon = 9.1 \times 10^4 \text{ M}^{-1}\text{cm}^{-1}$, and $\Phi = 0.94$). Insertion of additional aromatic substituents in the BODIPY FL molecule (Fig. 7) shifts emission towards the red and far-red regions (BODIPY TR, BODIPY 630/650 and BODIPY 650/665).

Most BODIPY-based labels are stable fluorescent markers. However, fluorophores altering their optical properties during photoactivation or upon binding to biologically important molecules have also been synthesized [70, 71]. A neutrally charged BODIPY can penetrate through the cell membrane. BODIPY and some of its derivatives exhibit appreciably high lipophilic properties and, therefore, are accumulated mostly in

the membranes of subcellular structures [72]. Hence, modified BODIPY derivatives containing hydrophilic moieties are required for the imaging of biomolecules localized in cytosol.

BODIPY and its derivatives are characterized by a small Stokes shift, which is the reason for the self-quenching of these markers at a high density of biomolecule labeling. This property is used to synthesize fluorogenic substrates for proteinases whose fluorescence intensity increases during the proteolysis of proteins labeled with this tag with a higher density [73].

Carbocyanine dyes (cyanins) are compounds with polymethine chains of different lengths that have an odd number of carbon atoms between two nitrogen atoms ($\text{R}_2\text{N}-(\text{CH}=\text{CH})_n-\text{CH}=\text{N}^+\text{R}_2$) [70] (Fig. 8). The structure of these compounds is very similar to that of the chromophores in the visual pigment rhodopsin [74]. This property was recently used to design a construct encoding a specific protein binding retinoic acid (CRABPII) that can form a complex with the fluorogenic derivative of cyanine dye. Unlike the original profluorophore, this complex is characterized by a bright fluorescence in the far-red spectral range and high quantum yield [75]. Labels with only one terminal nitrogen atom involved in the aromatic heterocycle are known as hemicyanine dyes. Hemicyanines are used as ratiometric fluorescent pH sensors in *in vivo* experi-

ments [76]. Cyanine tags in which the terminal charge-carrying atoms are directly bound to the methine chain are called streptocyanine tags. Streptocyanine dyes have been used as an indicator of superoxide dismutase activity [77].

Carbocyanine compounds are given names corresponding to the number of carbon atoms between the dihydroindole components of the molecule. In terms of its spectral characteristics, Cy3 (*Fig. 8*) is comparable to tetramethylrhodamine ($\lambda_{\text{ex}} = 554 \text{ nm}$, $\lambda_{\text{em}} = 568 \text{ nm}$). The spectra of Cy5 are shifted towards longer wavelengths ($\lambda_{\text{ex}} = 652 \text{ nm}$, $\lambda_{\text{em}} = 672 \text{ nm}$), while the more extensive constructs, such as Cy7, exhibit fluorescence emission in the near-infrared region ($\lambda_{\text{ex}} = 755 \text{ nm}$, $\lambda_{\text{em}} = 788 \text{ nm}$). Cyanines are characterized by a high extinction coefficient (up to $300,000 \text{ M}^{-1}\text{cm}^{-1}$) and high solubility in water. Absorption and emission can be shifted towards longer wavelengths either by increasing the length of the polymethine chain or by inserting an aromatic moiety of terminal heterocyclic fragments. Increasing the length of the polymethine chain by two carbon atoms shifts the absorption maximum by $\sim 100 \text{ nm}$, while insertion of the benzene ring to the terminal indole residue shifts absorption by $\sim 30 \text{ nm}$ [78]. Such structural modifications are denoted with a “5” index: e.g., Cy5.5.

The *p*-nitrobenzoyl derivative of the heptacyanine fluorophore emitting in the near-infrared region was used as a ratiometric sensor of cysteine in mitochondria under oxidative stress. It has been demonstrated that this fluorophore can be used in living mice as a sensor of Cys [79] and glutathione levels in living cells [80].

SITE-DIRECTED REACTIONS OF A SYNTHETIC FLUOROPHORE CONJUGATION TO TCP

Covalent binding reactions

Various chemical reactions are currently used to bind synthetic fluorophores to functional groups of biomolecules [81]. Succinimide ester (*Fig. 9*) is the most frequently used: its interaction with primary and secondary amino groups yields a stable amide bond. Isothiocyanate is another commonly used compound. Fluorophores modified with iodacetamide, maleimide, or dithiols are used to label sulfhydryl groups.

Bioorthogonal conjugation [82] and the so-called “click” chemistry [83–85] draw special attention. In this case, the chemical groups involved in the reaction of conjugation to a biomolecule do not react with other functional groups. These chemical groups are inserted in the molecules either via the metabolic machinery of the cell [86, 87] or due to the TCP enzymatic activity of [88, 89]. The azide moiety complies with all the requirements imposed on a bioorthogonal chemical group: it is

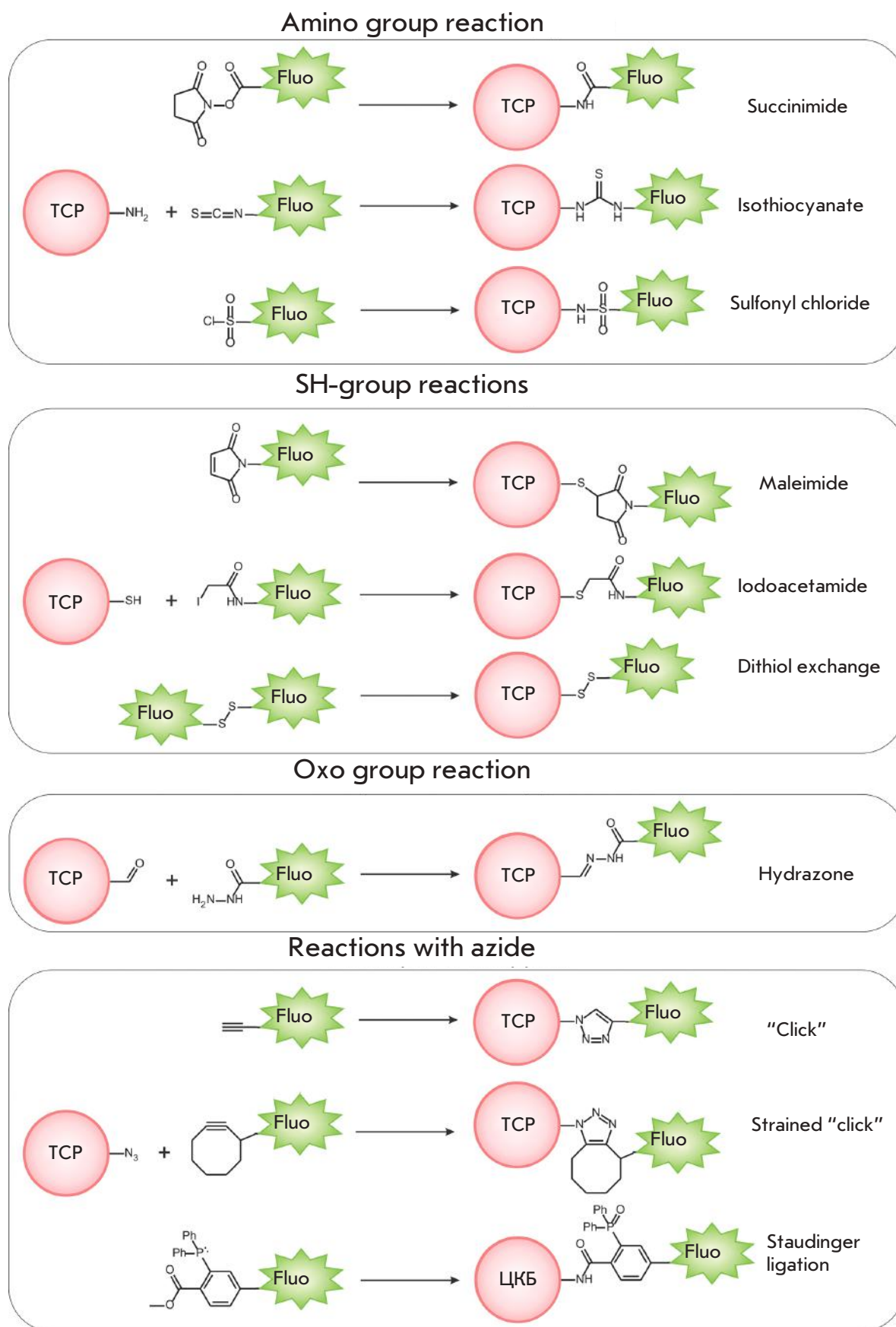
characterized by high reactivity, selectivity, stability in aqueous media, and low reactivity towards biological molecule functional groups. Insertion of a small azide moiety only results in minor structural perturbations of the biomolecule. The bioorthogonal label inserted into a cellular object can be covalently bound to the fluorophore due to highly selective click reactions: Cu-catalyzed azide–alkyne cycloaddition is a classic example of those (*Fig. 9*) [90, 91]. However, Cu-catalyzed reactions can be used mainly in *in vitro* experiments, since the catalyst needs to be delivered to the reaction site in the living systems. In addition, copper is toxic at the concentrations used for labeling. Bertozzi *et al.* [92] have developed a method of modification where an alkyne is a component of the strained eight-membered ring (*Fig. 9*). In this system, the alkyne exhibits increased reactivity and does not require a catalyst. Later on, difluorocyclooctynes [93] with much higher reactivity were obtained, allowing one to use click chemistry for azide-labeled biomolecules in living organisms [94]. The Staudinger ligation is another example of bioorthogonal reaction application for *in vivo* labeling (*Fig. 9*) [95, 96].

Reactions yielding sulfides and metal-chelate fluorophore–TCP complexes

Introduction of small amino acid sequences into the target protein is another promising approach in conjugating synthetic fluorophores to TCP. These sequences need to have an appreciably high affinity to the selected fluorescent marker. For example, the Cys-Cys-Pro-Gly-Cys-Cys sequence forms a hairpin-like structure due to the -Pro-Gly- insertion [97]. Hence, four cysteine residues form a cluster characterized by high affinity to organic arsenic compounds [98]. In particular, the arsenic-disubstituted derivative of fluorescein FAsH ($\lambda_{\text{ex}} = 508 \text{ nm}$, $\lambda_{\text{em}} = 528 \text{ nm}$) reacts with this tetracysteine sequence to form a complex with a dissociation constant that lies in the picomolar range (*Fig. 10A*) [8, 99]. Furthermore, FAsH exhibits bright green fluorescence only when bound to the tetracysteine sequence, thus significantly reducing background fluorescence. Besides FAsH, there is ReAsH ($\lambda_{\text{ex}} = 593 \text{ nm}$, $\lambda_{\text{em}} = 608 \text{ nm}$), a resorufin-based marker (*Fig. 10A*) exhibiting fluorescence in the red spectral range [8, 100].

It should be mentioned that FAsH and ReAsH are membrane-permeable labels, which facilitates their delivery to the cell. Side reactions with monothiols are a drawback common to these compounds; however, nonspecific binding can be suppressed with an excess amount of dithiotreitol. Labeling with FAsH and ReAsH is also complicated under oxidative conditions because of the oxidative reactions that the tetra-Cys sequence is involved in.

Fig. 9. Reactions of covalent bond formation with biomolecules



Metal coordination complexes are used in another method for fluorophore insertion into the TCP [101]. A polyhistidine sequence ((His)_n, where $n \geq 6$) that forms complexes with nickel nitrile triacetate (Ni²⁺-NTA) acts as a complexing agent (*Fig. 10B*). Derivatives of cyanine dyes with one or two covalently bound Ni²⁺-NTA complexes were synthesized to specifically label proteins containing the poly-His-sequence. The disubstituted derivatives Cy3 and Cy5 have demonstrated a higher affinity compared to the monosubstituted ones and were used in FRET experiments to measure the distances in DNA complexes with the poly-His-labeled protein [102].

The key disadvantage of the poly-His/Ni²⁺-NTA system for *in vivo* experiments is the low binding affinity (the K_d values lie within 1–20 μM), which negatively affects the stability of the fluorophore-TCP complex and, eventually, visualization of TCP. Piehler *et al.* synthesized fluorescein derivatives with 1–4 covalently bound NTA residues and characterized their interaction with the poly-His-sequence (His6 and His10). The stability of multivalent chelating groups to bind increased by more than four orders of magnitude, compared to that of mono-NTA and reached the subnanomolar level [103].

Poor permeability across the cell membrane is another serious limitation in using the Ni²⁺-NTA complex *in vivo*. Tampe *et al.* applied the membrane-translocating TAT-peptide (49RKKRRQRRR57) to deliver Ni²⁺-NTA inside the cell [104]. The resulting trisNTA/His6-TAT49–57 complex was used to deliver fluorescently labeled NTA into the cell (the cytosol and nucleus); trisNTA was then predominantly bound to the His10-tagged intracellular protein. The translocating peptide His6-TAT49–57 was released, since it had a higher binding affinity to His10 ($K_d = 0.1 \text{ nm}$) [103].

Sun *et al.* suggested a different approach to the synthesizing of membrane-permeable constructs [105]. They obtained a compound where NTA was covalently bound to fluorophore and aryl azide (Ni²⁺-NTA-AC). Ni²⁺-NTA-AC easily penetrated through the cell membrane and was bound to intracellular proteins carrying the poly-His tag. Light activation resulted in covalent binding of aryl azide to TCP, which increased fluorescence 13-fold and ensured stable binding to the fluorescent tag.

In addition to the tetracystein and poly-His sequences, poly-Asp ((Asp)_n, where $n = 1–3$) were also used to label TCP. Hamachi *et al.* synthesized fluorescein-tagged polynuclear Zn²⁺ complexes (a binuclear Zn²⁺ complex is shown in *Fig. 10C*) [106]. In this case, increased affinity was observed for a longer poly-Asp chain. Tetranuclear Zn²⁺ complexes were used for fluorescent labeling of the muscarinic acetylcholine receptor, and its initial activity was retained.

Site-directed labeling using enzyme reactions

Another technology of fluorophore insertion in TCP is based on enzyme reactions. The so-called SNAP-tag [107], CLIP-tag [108], HALO-tag [109], and TMP-tag [110–112] methods are used in this case.

In the SNAP-tag method, O⁶-alkylguanine transferase (AGT, *Fig. 11A*) acts as a fusion protein. AGT has a molecular weight of 20 kDa; it transfers alkyl groups from O⁶ of the alkylated guanine residue to the cysteine residue in the active site of the enzyme (see review [113]). Incubation of cells expressing AGT-TCP with the O⁶-benzylguanine substrate, in which the *p*-benzyl group carries a fluorophore, results in fluorescent labeling of AGT-TCP at cysteine in the active site of AGT [9]. Mutant forms of AGT were also obtained, catalyzing the reaction of alkyl radical transfer to AGT-TCP 50 times faster compared to the wild-type enzyme [107]. The SNAP-tag technology is currently the most commonly used to label intra- and extracellular proteins.

The CLIP-tag method is similar to SNAP-tag; it employs the mutant form of AGT, whose substrates are fluorescent analogues of O²-benzylcytosine (*Fig. 11B*) [108]. Despite the similarity between these technologies, SNAP-tag and CLIP-tag are characterized by different substrate specificities and can be used for simultaneous imaging of several cellular objects.

In the HALO-tag method, a genetically engineered variant of haloalkane dehalogenase acts as a fusion protein that specifically reacts with halogenated alkanes covalently bound to fluorophore (*Fig. 11C*) [114, 115]. This reaction, in which covalent binding is formed between the enzyme and the fluorescently labeled alkane, is highly specific and allows one to quickly insert a tag into proteins both *in vitro* and *in vivo* ($10^3–10^6 \text{ M}^{-1} \text{ s}^{-1}$) under physiological conditions; importantly, this reaction is irreversible.

In all the methods mentioned above, the unreacted tag needs to be thoroughly washed off the cells to achieve high contrast. SNAP-tag fluorogenic substrates containing an enzymatically removable fluorescent quencher were synthesized to eliminate this drawback (*Fig. 11A*). The enzymatic reaction with SNAP-tag results in cleavage of the quenching group, thus increasing the fluorescence intensity more than fiftyfold. The advantage of these no-wash fluorophores was demonstrated using the spatio-temporal dynamics of epidermal growth factor receptors during cell migration [116].

The TMP-tag carrying a mutant of dihydrofolate reductase (eDHPR L28C) from *Escherichia coli* (molecular weight of ~18 kDa) is an alternative system. As a result of the enzyme reaction, fluorescently labeled 2,4-diamino-5-(3,4,5-trimethoxybenzyl)pyrimidine

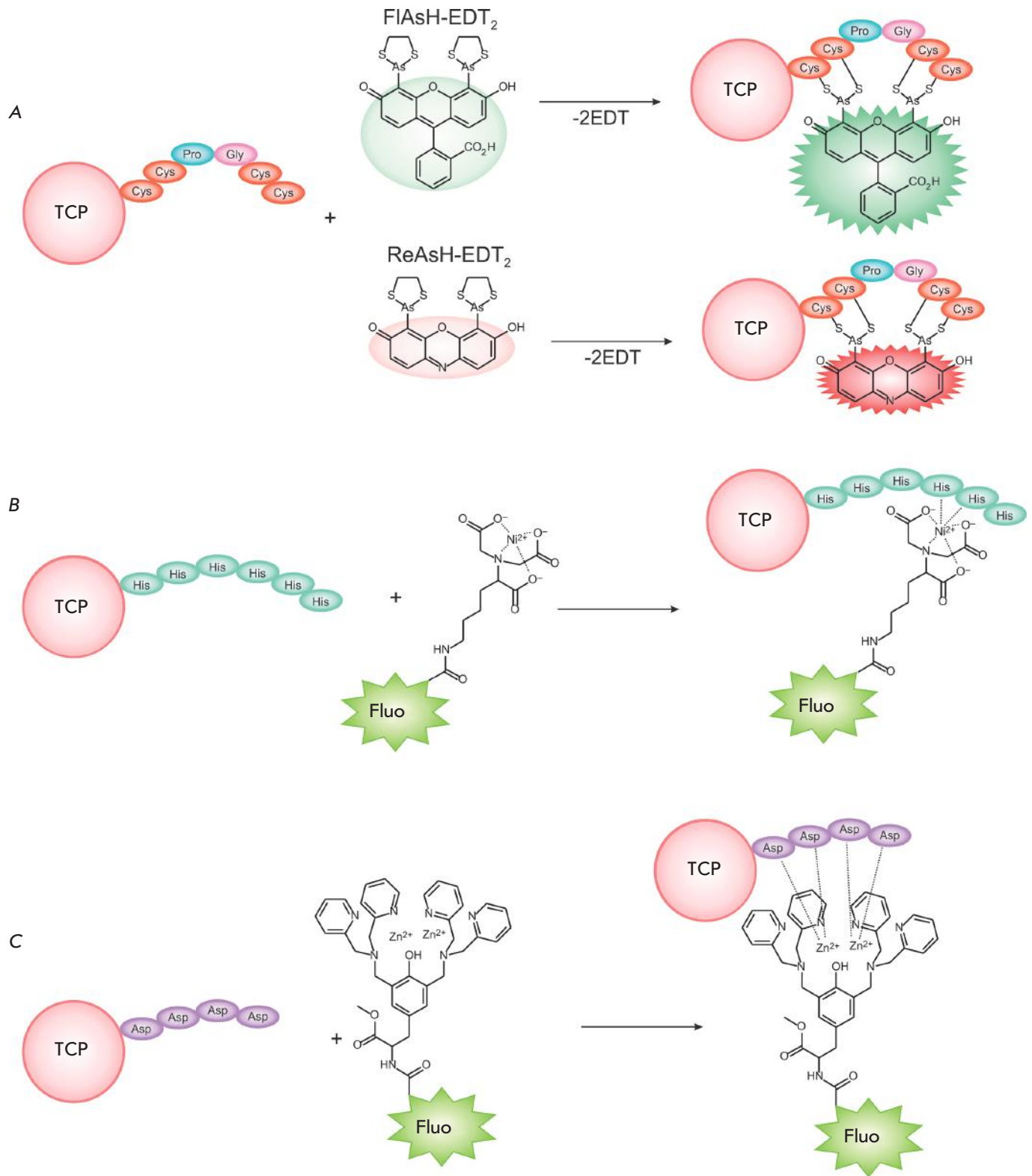


Fig. 10. Reactions of sulfide and metal-chelate complex formation between a fluorophore and a target cell protein (TCP)

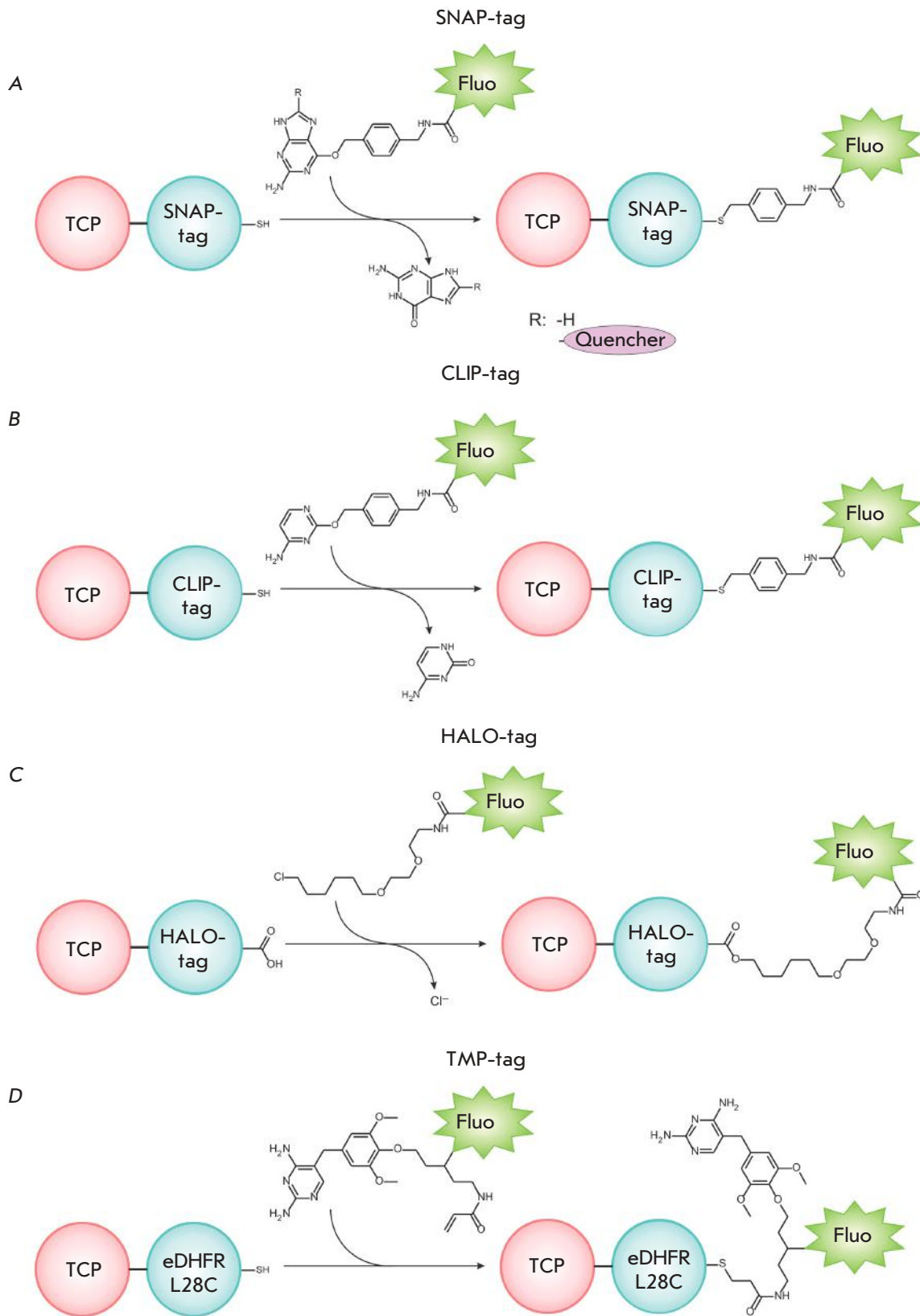


Fig. 11. Enzymatic reactions for TCP labeling using SNAP-tag (A), CLIP-tag (B), Halo-tag (C), and TMP-tag (D)

(trimethoprim, or TMP) binds to eDHPR–TCP (*Fig. 11D*) that is expressed in animal cells. The system is characterized by a relatively low background fluorescence and rapid kinetics [111]. A nonfluorescent TMP derivative containing a fluorophore and the corresponding quenching agent was produced to further reduce the background fluorescence caused by either the unbound or nonspecifically bound fluorescent tags. The TMP ligand binds to eDHPR–TCP, and the quencher is removed during the enzyme reaction. This method was shown to be efficient in labeling histones in the nuclei of HEK 903T cells [117].

CONCLUSIONS

The methods used for imaging biomolecules in living systems using synthetic fluorophores have been significantly modified in recent years. Various experimental and conceptual limitations have been overcome, primarily, for the site-directed reactions that allow one to insert a fluorescent tag into TCP. Modern technologies based on novel photoswitchable fluorophores are developing rapidly, such as subdiffraction microscopy that allows one to visualize cellular objects at resolutions in the nanometer scale.

Bioorthogonal labeling has made it possible to insert synthetic fluorophores that are much smaller than fluorescent proteins into TCP. The internal sites of TCP can be labeled using this method, as opposed to labeling N- and C-terminal regions using FPs. Furthermore, the spectral properties of synthetic fluorophores can be easier tuned compared to FPs. Synthetic fluorophores can also be used to label non-protein objects (nucleotides, lipids, glycans, metabolites, etc.).

Although the constructs used in the enzyme methods for fluorophore insertion (SNAP-tag, CLIP-tag,

HALO-tag, and TMP-tag) are of a size comparable to that of FPs, any small molecule can be inserted into TCPs using these techniques. Enzyme methods for fluorophore insertion into TCPs have been used more and more routinely to solve complex problems in modern biology and medicine. Use of these technologies in transgenic animals has been reported [118].

Today, the method involving the formation of metal–chelate complexes and sulfides is also frequently used for *in vivo* fluorescent labeling. As opposed to the previous techniques, it employs a small peptide fragment fused to TCP. New fluorophores exhibiting higher binding affinity and fluorescence intensity have been designed since the first publication that reported on the use of FIAsh. TCPs labeled with photoswitchable fluorescent tags have also been created using the metal–chelate technologies.

Taking into account the large number of application problems existing in the imaging of biomolecules in living systems, is it unlikely that a single universal fluorophore that meets all the desirable requirements can be designed. Moreover, the investigation of complex systems with several target objects requires the simultaneous use of several different fluorophores. Hence, further advance in this field solely depends on the synthesis of novel fluorophores that comply with the requirements of fluorescent microscopy, such as high photostability, low phototoxicity during long-term imaging, and the possibility of labeling multiple objects in living systems. ●

This work was supported by the Russian Science Foundation (grant no. 14-50-00131).

REFERENCES

- Coons A.H., Creech H.J., Jones R.N., Berliner E. // *J. Immunol.* 1942. V. 45. P. 159–170.
- Sung M.H., McNally J.G. // *Wiley Interdiscip. Rev. Syst. Biol. Med.* 2011. V. 3. № 2. P. 167–182.
- Chudakov D.M., Matz M.V., Lukyanov S., Lukyanov K.A. // *Physiol. Rev.* 2010. V. 90. № 3. P. 1103–1163.
- Day R.N., Davidson M.W. // *Chem. Soc. Rev.* 2009. V. 38. № 10. P. 2887–2921.
- Pakhomov A.A., Martynov V.I. // *Chem. Biol.* 2008. V. 15. № 8. P. 755–764.
- Terai T., Nagano T. // *Curr. Opin. Chem. Biol.* 2008. V. 12. № 5. P. 515–521.
- Lavis L.D., Raines R.T. // *ACS Chem. Biol.* 2014. V. 9. № 4. P. 855–866.
- Adams S.R., Campbell R.E., Gross L.A., Martin B.R., Walkup G.K., Yao Y., Llopis J., Tsien R.Y. // *J. Am. Chem. Soc.* 2002. V. 124. № 21. P. 6063–6076.
- Keppler A., Gendreizig S., Gronemeyer T., Pick H., Vogel H., Johnsson K. // *Nat. Biotechnol.* 2003. V. 21. № 1. P. 86–89.
- Bains G., Patel A.B., Narayanaswami V. // *Molecules.* 2011. V. 16. № 9. P. 7909–7935.
- Wu Y., Li C., Li Y., Li D., Li Z. // *Sens. Actuator B-Chem.* 2016. V. 222. P. 1226–1232.
- Pinheiro D., de Castro C.S., de Melo J.S.S., Oliveira E., Nunez C., Fernandez-Lodeiro A., Capelo J.L., Lodeiro C. // *Dyes Pigment.* 2014. V. 110. P. 152–158.
- Saha T., Sengupta A., Hazra P., Talukdar P. // *Photochem. Photobiol. Sci.* 2014. V. 13. № 10. P. 1427–1433.
- Legenzov E.A., Dirda N.D., Hagen B.M., Kao J.P. // *PLoS One.* 2015. V. 10. № 7. P. e0133518.
- Hara D., Komatsu H., Son A., Nishimoto S., Tanabe K. // *Bioconjug. Chem.* 2015. V. 26. № 4. P. 645–649.
- Han S., Zhang F.F., Qian H.Y., Chen L.L., Pu J.B., Xie X., Chen J.Z. // *Eur. J. Med. Chem.* 2015. V. 93. P. 16–32.
- Mizukami S., Watanabe S., Kikuchi K. // *Chembiochem.* 2009. V. 10. № 9. P. 1465–1468.
- Zadlo A., Koszelewski D., Borys F., Ostaszewski R. // *Chembiochem.* 2015. V. 16. № 4. P. 677–682.
- Morikawa K., Yanagida M. // *J. Biochem.* 1981. V. 89. № 2.

- P. 693–696.
20. Szczurek A.T., Prakash K., Lee H.K., Zurek-Biesiada D.J., Best G., Hagmann M., Dobrucki J.W., Cremer C., Birk U. // *Nucleus*. 2014. V. 5. № 4. P. 331–340.
 21. Piterburg M., Panet H., Weiss A. // *J. Microsc.* 2012. V. 246. № 1. P. 89–95.
 22. Zurek-Biesiada D., Kedracka-Krok S., Dobrucki J.W. // *Cytometry A*. 2013. V. 83. № 5. P. 441–451.
 23. J. Brunette A.M., Farrens D.L. // *Biochemistry*. 2014. V. 53. № 40. P. 6290–6301.
 24. Smirnova I., Kasho V., Kaback H.R. // *Proc. Natl. Acad. Sci. USA*. 2014. V. 111. № 23. P. 8440–8445.
 25. Wang J.M., Liao Y., Shao S.J. // *Chem. Lett.* 2015. V. 44. № 10. P. 1437–1439.
 26. Makiyama T., Nakamura H., Nagasaka N., Yamashita H., Honda T., Yamaguchi N., Nishida A., Murayama T. // *Traffic*. 2015. V. 16. № 5. P. 476–492.
 27. Gaibelet G., Allart S., Terce F., Azalbert V., Bertrand-Michel J., Hamdi S., Collet X., Orlowski S. // *PLoS One*. 2015. V. 10. № 4. e0121563.
 28. Lima S., Milstien S., Spiegel S. // *J. Lipid Res.* 2014. V. 55. № 7. P. 1525–1530.
 29. Meng Q., Shi Y., Wang C., Jia H., Gao X., Zhang R., Wang Y., Zhang Z. // *Org. Biomol. Chem.* 2015. V. 13. № 10. P. 2918–2926.
 30. Chen Y.H., Tsai J.C., Cheng T.H., Yuan S.S., Wang Y.M. // *Biosens. Bioelectron.* 2014. V. 56. P. 117–123.
 31. Urru S.A.M., Veglianese P., De Luigi A., Fumagalli E., Erba E., Diaza R.G., Carra A., Davoli E., Borsello T., Forloni G., et al. // *J. Med. Chem.* 2010. V. 53. № 20. P. 7452–7460.
 32. Kristoffersen A.S., Erga S.R., Hamre B., Frette O. // *J. Fluoresc.* 2014. V. 24. № 4. P. 1015–1024.
 33. Lavis L.D., Rutkoski T.J., Raines R.T. // *Anal. Chem.* 2007. V. 79. № 17. P. 6775–6782.
 34. Meier R.J., Simburger J.M., Soukka T., Schaferling M. // *Chem. Commun.* 2015. V. 51. № 28. P. 6145–6148.
 35. Lopez S.G., Crovetto L., Alvarez-Pez J.M., Talavera E.M., San Roman E. // *Photochem. Photobiol. Sci.* 2014. V. 13. № 9. P. 1311–1320.
 36. Minta A., Kao J.P., Tsien R.Y. // *J. Biol. Chem.* 1989. V. 264. № 14. P. 8171–8178.
 37. Cheng Z.Y., Wang X.P., Schmid K.L., Han X.G. // *Neuroscience*. 2014. V. 280. P. 254–261.
 38. Zaikova T.O., Rukavishnikov A.V., Birrell G.B., Grif-fith O.H., Keana J.F. // *Bioconjug. Chem.* 2001. V. 12. № 2. P. 307–313.
 39. Smith E.L., Bertozzi C.R., Beatty K.E. // *ChemBiochem*. 2014. V. 15. № 8. P. 1101–1105.
 40. Grimm J.B., Sung A.J., Legant W.R., Hulamm P., Matlosz S.M., Betzig E., Lavis L.D. // *ACS Chem. Biol.* 2013. V. 8. № 6. P. 1303–1310.
 41. Grimm J.B., English B.P., Chen J., Slaughter J.P., Zhang Z., Revyakin A., Patel R., Macklin J.J., Normanno D., Singer R.H., et al. // *Nat. Methods*. 2015. V. 12. № 3. P. 244–250.
 42. Vogel M., Rettig W., Sens R., Drexhage K.H. // *Chem. Phys. Lett.* 1988. V. 147. № 5. P. 452–460.
 43. Hill R.A., Grutzendler J. // *Nat. Methods*. 2014. V. 11. № 11. P. 1081–1082.
 44. Schnell C., Shahmoradi A., Wichert S.P., Mayerl S., Hagos Y., Heuer H., Rossner M.J., Hulsmann S. // *Brain Struct. Funct.* 2015. V. 220. № 1. P. 193–203.
 45. Kryman M.W., Davies K.S., Linder M.K., Ohulchansky T.Y., Detty M.R. // *Bioorg. Med. Chem.* 2015. V. 23. № 15. P. 4501–4507.
 46. Fudala R., Mummert M.E., Gryczynski Z., Gryczynski I. // *J. Photochem. Photobiol. B*. 2011. V. 104. № 3. P. 473–477.
 47. Chib R., Raut S., Fudala R., Chang A., Mummert M., Rich R., Gryczynski Z., Gryczynski I. // *Curr. Pharm. Biotechnol.* 2013. V. 14. № 4. P. 470–474.
 48. Gee K.R., Weinberg E.S., Kozlowski D.J. // *Bioorg. Med. Chem. Lett.* 2001. V. 11. № 16. P. 2181–2183.
 49. Sueyoshi K., Nogawa Y., Sugawara K., Endo T., Hisamoto H. // *Anal. Sci.* 2015. V. 31. P. 1155–1161.
 50. Moquin A., Hutter E., Choi A.O., Khatchadourian A., Castonguay A., Winnik F.M., Maysinger D. // *ACS Nano*. 2013. V. 7. № 11. P. 9585–9598.
 51. Huang Q., Zhang Q., Wang E., Zhou Y., Qiao H., Pang L., Yu F. // *Spectrochim. Acta A Mol. Biomol. Spectrosc.* 2016. V. 152. P. 70–76.
 52. Wang E., Zhou Y., Huang Q., Pang L., Qiao H., Yu F., Gao B., Zhang J., Min Y., Ma T. // *Spectrochim. Acta A Mol. Biomol. Spectrosc.* 2016. V. 152. P. 327–335.
 53. Hayashi-Takanaka Y., Stasevich T.J., Kurumizaka H., Nozaki N., Kimura H. // *PloS One*. 2014. V. 9. № 9. e106271
 54. Mahalingam M., Girgenrath T., Svensson B., Thomas D.D., Cornea R.L., Fessenden J.D. // *Structure*. 2014. V. 22. № 9. P. 1322–1332.
 55. Xue S., Ding S., Zhai Q., Zhang H., Feng G. // *Biosens. Bioelectron.* 2015. V. 68. P. 316–321.
 56. Albers A.E., Dickinson B.C., Miller E.W., Chang C.J. // *Bioorg. Med. Chem. Lett.* 2008. V. 18. № 22. P. 5948–5950.
 57. Koide Y., Urano Y., Hanaoka K., Terai T., Nagano T. // *ACS Chem. Biol.* 2011. V. 6. № 6. P. 600–608.
 58. Koide Y., Urano Y., Hanaoka K., Piao W., Kusakabe M., Saito N., Terai T., Okabe T., Nagano T. // *J. Am. Chem. Soc.* 2012. V. 134. № 11. P. 5029–5031.
 59. McCann T.E., Kosaka N., Koide Y., Mitsunaga M., Choyke P.L., Nagano T., Urano Y., Kobayashi H. // *Bioconjug. Chem.* 2011. V. 22. № 12. P. 2531–2538.
 60. Rathje M., Fang H., Bachman J.L., Anggono V., Gether U., Haganir R.L., Madsen K.L. // *Proc. Natl. Acad. Sci. USA*. 2013. V. 110. № 35. P. 14426–14431.
 61. Capellini V.K., Restini C.B., Bendhack L.M., Evora P.R., Celotto A.C. // *PLoS One*. 2013. V. 8. № 5. P. e62887.
 62. Zhang H., Xu C., Liu J., Li X., Guo L. // *Chem. Commun.* 2015. V. 51. № 32. P. 7031–7034.
 63. Theriot J.A., Mitchison T.J. // *Nature*. 1991. V. 352. № 6331. P. 126–131.
 64. Zhao Y., Zheng Q., Dakin K., Xu K., Martinez M.L., Li W.H. // *J. Am. Chem. Soc.* 2004. V. 126. № 14. P. 4653–4663.
 65. Guo Y.M., Chen S., Shetty P., Zheng G., Lin R., Li W.H. // *Nat. Methods*. 2008. V. 5. № 9. P. 835–841.
 66. Loudet A., Burgess K. // *Chem. Rev.* 2007. V. 107. № 11. P. 4891–4932.
 67. Boens N., Leen V., Dehaen W. // *Chem. Soc. Rev.* 2012. V. 41. № 3. P. 1130–1172.
 68. Kowada T., Maeda H., Kikuchi K. // *Chem. Soc. Rev.* 2015. V. 44. № 14. P. 4953–4972.
 69. Le Guennic B., Jacquemin D. // *Acc. Chem. Res.* 2015. V. 48. № 3. P. 530–537.
 70. Zhang Y., Swaminathan S., Tang S.C., Garcia-Amoros J., Boulina M., Captain B., Baker J.D., Raymo F.M. // *J. Am. Chem. Soc.* 2015. V. 137. № 14. P. 4709–4719.
 71. Yang C.D., Gong D.Y., Wang X.D., Iqbal A., Deng M., Guo Y.L., Tang X.L., Liu W.S., Qin W.W. // *Sens. Actuator B-Chem.* 2016. V. 224. P. 110–117.
 72. Uppal T., Hu X., Fronczek F.R., Maschek S., Bobadova-Parvanova P., Vicente M.G. // *Chemistry*. 2012. V. 18. № 13. P. 3893–3905.
 73. Jones L.J., Upson R.H., Haugland R.P., PanchukVoloshina

REVIEWS

- N., Zhou M.J., Haugland R.P. // *Anal. Biochem.* 1997. V. 251. № 2. P. 144–152.
74. Abdulaev N.G., Artamonov I.D., Bogachuk A.S., Feigina M.Y., Kostina M.B., Kudelin A.B., Martynov V.I., Miroshnikov A.I., Zolotarev A.S., Ovchinnikov Y.A. // *Biochem. Int.* 1982. V. 5. № 6. P. 693–703.
75. Yapici I., Lee K.S., Berbasova T., Nosrati M., Jia X., Vasileiou C., Wang W., Santos E.M., Geiger J.H., Borhan B. // *J. Am. Chem. Soc.* 2015. V. 137. № 3. P. 1073–1080.
76. Li Y., Wang Y., Yang S., Zhao Y., Yuan L., Zheng J., Yang R. // *Anal. Chem.* 2015. V. 87. № 4. P. 2495–2503.
77. Vinatier V., Guieu V., Madaule Y., Maturano M., Payrastre C., Hoffmann P. // *Anal. Biochem.* 2010. V. 405. № 2. P. 255–259.
78. Mujumdar S.R., Mujumdar R.B., Grant C.M., Waggoner A.S. // *Bioconjug. Chem.* 1996. V. 7. № 3. P. 356–362.
79. Yin K., Yu F., Zhang W., Chen L. // *Biosens. Bioelectron.* 2015. V. 74. P. 156–164.
80. Yin J., Kwon Y., Kim D., Lee D., Kim G., Hu Y., Ryu J.H., Yoon J. // *Nat. Protoc.* 2015. V. 10. № 11. P. 1742–1754.
81. Kalia J., Raines R.T. // *Curr. Org. Chem.* 2010. V. 14. № 2. P. 138–147.
82. Hao Z., Hong S., Chen X., Chen P.R. // *Acc. Chem. Res.* 2011. V. 44. № 9. P. 742–751.
83. Best M.D. // *Biochemistry.* 2009. V. 48. № 28. P. 6571–6584.
84. Kurpiers T., Mootz H.D. // *Angew. Chem. Int. Ed. Engl.* 2009. V. 48. № 10. P. 1729–1731.
85. Kolb H.C., Finn M.G., Sharpless K.B. // *Angew. Chem. Int. Ed. Engl.* 2001. V. 40. № 11. P. 2004–2021.
86. Kiick K.L., Saxon E., Tirrell D.A., Bertozzi C.R. // *Proc. Natl. Acad. Sci. USA.* 2002. V. 99. № 1. P. 19–24.
87. Kho Y., Kim S.C., Jiang C., Barma D., Kwon S.W., Cheng J., Jaunbergs J., Weinbaum C., Tamaioi F., Falck J., et al. // *Proc. Natl. Acad. Sci. USA.* 2004. V. 101. № 34. P. 12479–12484.
88. Speers A.E., Adam G.C., Cravatt B.F. // *J. Am. Chem. Soc.* 2003. V. 125. № 16. P. 4686–4687.
89. Speers A.E., Cravatt B.F. // *Chem. Biol.* 2004. V. 11. № 4. P. 535–546.
90. Rostovtsev V.V., Green L.G., Fokin V.V., Sharpless K.B. // *Angew. Chem. Int. Ed. Engl.* 2002. V. 41. № 14. P. 2596–2599.
91. Tornøe C.W., Christensen C., Meldal M. // *J. Org. Chem.* 2002. V. 67. № 9. P. 3057–3064.
92. Agard N.J., Prescher J.A., Bertozzi C.R. // *J. Am. Chem. Soc.* 2004. V. 126. № 46. P. 15046–15047.
93. Codelli J.A., Baskin J.M., Agard N.J., Bertozzi C.R. // *J. Am. Chem. Soc.* 2008. V. 130. № 34. P. 11486–11493.
94. Baskin J.M., Prescher J.A., Laughlin S.T., Agard N.J., Chang P.V., Miller I.A., Lo A., Codelli J.A., Bertozzi C.R. // *Proc. Natl. Acad. Sci. USA.* 2007. V. 104. № 43. P. 16793–16797.
95. Saxon E., Bertozzi C.R. // *Science.* 2000. V. 287. № 5460. P. 2007–2010.
96. Kohn M., Breinbauer R. // *Angew. Chem. Int. Ed. Engl.* 2004. V. 43. № 24. P. 3106–3116.
97. Madani F., Lind J., Damberg P., Adams S.R., Tsien R.Y., Graslund A.O. // *J. Am. Chem. Soc.* 2009. V. 131. № 13. P. 4613–4615.
98. Pomorski A., Krezel A. // *ChemBiochem.* 2011. V. 12. № 8. P. 1152–1167.
99. Griffin B.A., Adams S.R., Tsien R.Y. // *Science.* 1998. V. 281. № 5374. P. 269–272.
100. Chen B., Liu Q., Popowich A., Shen S., Yan X., Zhang Q., Li X.F., Weinfeld M., Cullen W.R., Le X.C. // *Metallomics.* 2015. V. 7. № 1. P. 39–55.
101. Uchinomiya S., Ojida A., Hamachi I. // *Inorg. Chem.* 2014. V. 53. № 4. P. 1816–1823.
102. Kapanidis A.N., Ebricht Y.W., Ebricht R.H. // *J. Am. Chem. Soc.* 2001. V. 123. № 48. P. 12123–12125.
103. Lata S., Reichel A., Brock R., Tampe R., Piehler J. // *J. Am. Chem. Soc.* 2005. V. 127. № 29. P. 10205–10215.
104. Wieneke R., Laboria N., Rajan M., Kollmannsperger A., Natale F., Cardoso M.C., Tampe R. // *J. Am. Chem. Soc.* 2014. V. 136. № 40. P. 13975–13978.
105. Lai Y.T., Chang Y.Y., Hu L., Yang Y., Chao A., Du Z.Y., Tanner J.A., Chye M.L., Qian C., Ng K.M., et al. // *Proc. Natl. Acad. Sci. USA.* 2015. V. 112. № 10. P. 2948–2953.
106. Ojida A., Honda K., Shinmi D., Kiyonaka S., Mori Y., Hamachi I. // *J. Am. Chem. Soc.* 2006. V. 128. № 32. P. 10452–10459.
107. Keppler A., Pick H., Arrivoli C., Vogel H., Johnsson K. // *Proc. Natl. Acad. Sci. USA.* 2004. V. 101. № 27. P. 9955–9959.
108. Gautier A., Juillerat A., Heinis C., Correa I.R., Jr., Kinnermann M., Beaufile F., Johnsson K. // *Chem. Biol.* 2008. V. 15. № 2. P. 128–136.
109. Los G.V., Encell L.P., McDougall M.G., Hartzell D.D., Karassina N., Zimprich C., Wood M.G., Learish R., Ohana R.F., Urh M., et al. // *ACS Chem. Biol.* 2008. V. 3. № 6. P. 373–382.
110. Miller L.W., Cai Y., Sheetz M.P., Cornish V.W. // *Nat. Methods.* 2005. V. 2. № 4. P. 255–257.
111. Gallagher S.S., Sable J.E., Sheetz M.P., Cornish V.W. // *ACS Chem. Biol.* 2009. V. 4. № 7. P. 547–556.
112. Wang T.Y., Friedman L.J., Gelles J., Min W., Hoskins A.A., Cornish V.W. // *Biophys. J.* 2014. V. 106. № 1. P. 272–278.
113. Correa I.R., Jr. // *Curr. Opin. Chem. Biol.* 2014. V. 20. P. 36–45.
114. Benink H.A., Urh M. // *Methods Mol. Biol.* 2015. V. 1266. P. 119–128.
115. England C.G., Luo H., Cai W. // *Bioconjug. Chem.* 2015. V. 26. № 6. P. 975–986.
116. Komatsu T., Johnsson K., Okuno H., Bito H., Inoue T., Nagano T., Urano Y. // *J. Am. Chem. Soc.* 2011. V. 133. № 17. P. 6745–6751.
117. Jing C.R., Cornish V.W. // *ACS Chem. Biol.* 2013. V. 8. № 8. P. 1704–1712.
118. Yang G., de Castro Reis F., Sundukova M., Pimpinel-la S., Asaro A., Castaldi L., Batti L., Bilbao D., Reymond L., Johnsson K., et al. // *Nat. Methods.* 2015. V. 12. № 2. P. 137–139.

From Slow to Fast: Hypogravity-Induced Remodeling of Muscle Fiber Myosin Phenotype

B. S. Shenkman

State Scientific Center of the Russian Federation – Institute of Biomedical Problems, Russian Academy of Sciences, Khoroshevskoe shosse, 76A, Moscow, 123007, Russia

E-mail: bshenkman@mail.ru

Received November 10, 2015; in final form, March 11, 2016

Copyright © 2016 Park-media, Ltd. This is an open access article distributed under the Creative Commons Attribution License, which permits unrestricted use, distribution, and reproduction in any medium, provided the original work is properly cited.

ABSTRACT Skeletal muscle consists of different fiber types arranged in a mosaic pattern. These fiber types are characterized by specific functional properties. Slow-type fibers demonstrate a high level of fatigue resistance and prolonged contraction duration, but decreased maximum contraction force and velocity. Fast-type fibers demonstrate a high contraction force and velocity, but profound fatigability. During the last decades, it has been discovered that all these properties are determined by the predominance of slow or fast myosin-heavy-chain (MyHC) isoforms. It was observed that gravitational unloading during space missions and simulated microgravity in ground-based experiments leads to the transformation of some slow-twitch muscle fibers into fast-twitch ones due to changes in the patterns of MyHC gene expression in the postural *soleus muscle*. The present review covers the facts and mechanistic speculations regarding myosin phenotype remodeling under conditions of gravitational unloading. The review considers the neuronal mechanisms of muscle fiber control and molecular mechanisms of regulation of myosin gene expression, such as inhibition of the calcineurin/NFATc1 signaling pathway, epigenomic changes, and the behavior of specific microRNAs. In the final portion of the review, we discuss the adaptive role of myosin phenotype transformations.

KEYWORDS skeletal muscle, muscle fiber type, myosin heavy chain isoform, myosin phenotype, gravitational unloading, myosin gene expression.

To the memory of K.B. Shapovalova with whom the author studied striopallidar control over the muscle myosin phenotype.

INTRODUCTION. MYOSIN PHENOTYPE.

Physiologists have investigated skeletal muscle fiber types since 1873 [1] when it was established that muscles are composed of fibers with different functional properties and arranged in a mosaic pattern. Slow-twitch fibers are characterized by high fatigue resistance and a longer duration of contraction, but lower maximum force and velocity of contraction. Fast-twitch fibers are characterized by higher contraction velocity and force, but profound fatigability. In recent decades, it has been established that these properties are determined by the predominant isoform of the myosin heavy chain (MyHC). There are four isoforms, and, therefore, four types of fibers: I, slow; IIA, fast; IId/x fast; and IIB, the fastest one, which is represented only in the muscles of small mammals [2] (*Fig. 1, Table*). Myosin isoforms, prevailing in a fiber, determine its myosin phenotype, and the ratio of different types of fib-

ers corresponds to muscle composition or the myosin phenotype. Along with fibers dominated by a certain type of MyHC isoform, muscles comprise fibers having two (or more) different MyHC isoforms. These fibers are called hybrid fibers. The expression of each of the myosin isoforms is determined by fiber innervation. Fibers innervated by one motor neuron comprise a motor unit and, in the vast majority of cases, are characterized by the same myosin phenotype [3]. Postural (tonic) muscles, having a high tone and supporting the body's posture in the Earth gravitational field, contain the largest amount of type I slow fibers. According to modern concepts, the motoneuron controls the fibers using a certain discharge frequency pattern (10 Hz for slow and 50–60 Hz for fast motor units) and secretion of the appropriate neurotrophic agents, which affects the expression of myosin genes: i.e. the myosin phenotype of the fibers [3, 4].

The myosin phenotype is very stable; however, there are impacts that can significantly alter the myosin gene expression and thereby determine the slow-to-fast transformation of fibers, or vice versa. For example,

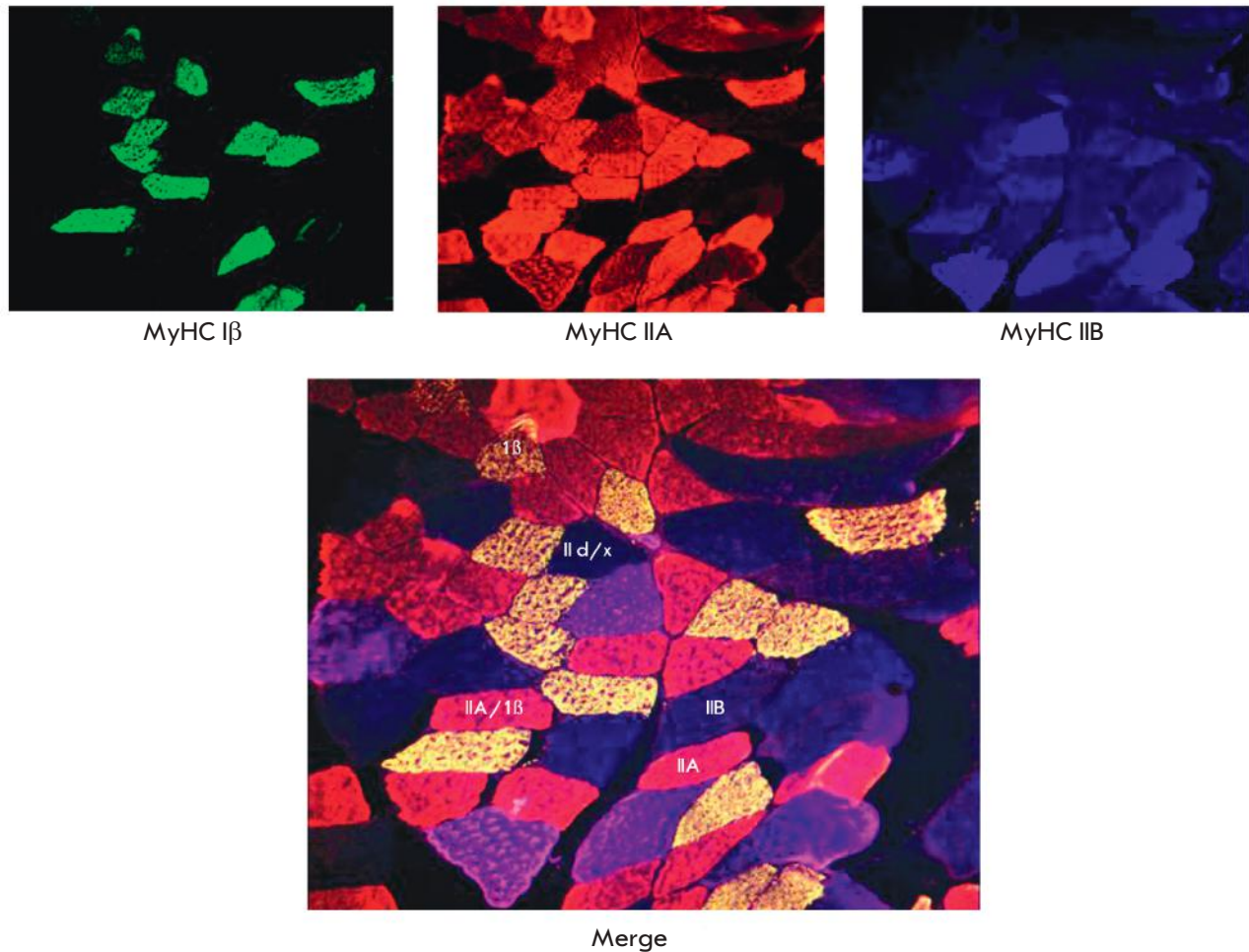


Fig. 1. Immunocytochemical detection of muscle fibers expressing MyHC Iβ isoform, MyHC IIA, and MyHC IIB in the cross-section of *m. plantaris* of rats by the triplelabeling method. The main fiber types and hybrid fibers are shown.

MyHC isoforms and muscle fiber types in mammals

MyHC isoform	β	α	Iβ	IIa	II d/x	IIb
Organ	Myocardium		Skeletal muscle			
Characteristics of species	All mammals					Small mammals
Contraction velocity	→					
Fatigue resistance	←					

low-frequency electrostimulation during several weeks leads to the formation of 30–40% slow-type fibers in predominantly fast muscles [4]. The same effect in the fast ankle plantaris muscle was observed in animals with ablated or subjected to tenotomy triceps surae muscles: i.e. during the so-called compensatory over-

load [4]. In all these cases, the leading role in myosin phenotype transformations was attributed to changes in the muscle contractile activity pattern resulting from changes in the nature of the motor neuron discharge pattern (or, in the case of direct electrical stimulation, to its pattern).

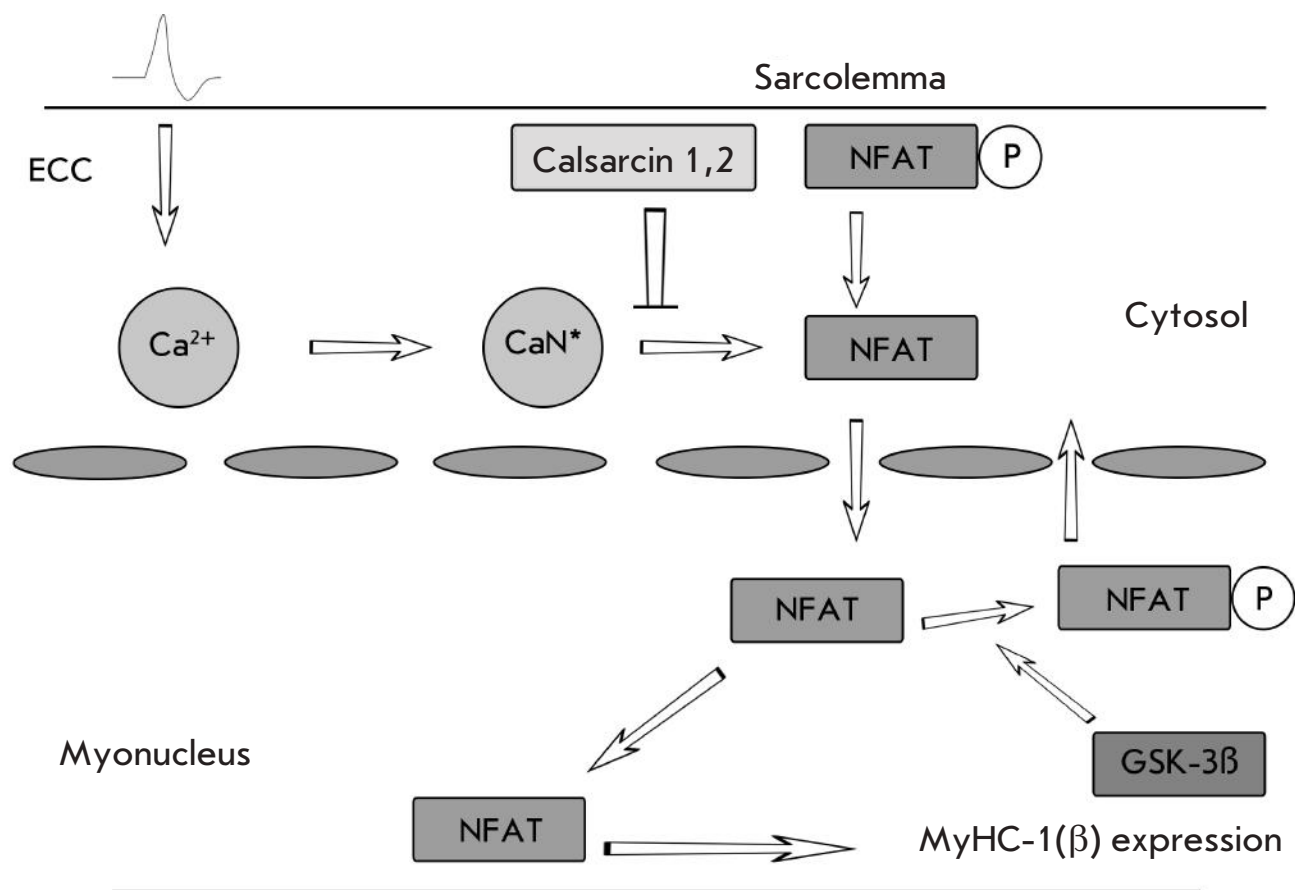


Fig. 2. Functional diagram of the calcineurin/NFATc1 signaling pathway. (According to Liu et al. [16], revised). ECC – electromechanical coupling, CaN – calcineurin. Explanations are provided in the text.

THE MECHANISMS OF ACTIVITY-DEPENDENT MYOSIN PHENOTYPE REMODELING

Chronic activity of slow-twitch fibers is associated with two phenomena: a constantly high myoplasm level of calcium ions and a low level of high-energy phosphates [4–6]. Therefore, the search for the signaling mechanisms that regulate MyHC gene expression was limited to identifying the pathways dependent on the concentration of calcium ions and high-energy phosphates. Calcineurin/NFAT is believed to be the most important signaling cascade that affects the expression of slow MyHC isoforms (and regulates the expression of many other genes). Calcineurin is a protein localized in the sarcomeric Z-disc. When interacting with the calcium-calmodulin complex, it displays phosphatase activity and dephosphorylates NFATs1 (the nuclear factor of activated T-cells), which can be translocated into myonuclei [6, 7] (*Fig. 2*). In the nucleus, this factor is either stored in heterochromatin (and gradually transferred therefrom to euchromatin) [8] or directly interacts

with MEF-2, a transcription factor specifically bound to the slow MyHC gene promoter. In this pattern, an intense transcription of slow MyHC gene is initiated [7, 8]. The NFAT dephosphorylation reaction is inhibited by Z-disc proteins, calsarcin-1, and calsarcin-2, which operate in slow-twitch and fast-twitch fibers, respectively. Knockout of the genes of these proteins results in a significant redistribution of the myosin phenotype towards the slow type [9, 10] (*Fig. 2*). Calsarcin gene expression (especially calsarcin-2) is inhibited in the case of double knockout of the E3 ubiquitin ligases MuRf-1 and MuRf-2 [11]. It can be assumed that calsarcin-2 expression is stimulated by the presence of MuRf ubiquitin ligases in the nucleus. It has been shown that alteration of the titin/connectin state results in the release/dephosphorylation of MuRf-2 caused by the titin kinase domain localized on the M-disk, which leads to its import into myonuclei [12]. It is possible that titin alteration ultimately leads to increased expression of calsarcin-2, contributes to the stabilization of the fast

myosin phenotype, and prevents any transformation towards the slow type. However, overexpression of the calsarcin gene is insufficient to completely inhibit the phosphatase activity of calcineurin. It is known that calsarcin-2 can be immobilized on the cytoskeletal components of Z-disc, α -actinin-2, and α -actinin-3, and immobilization on α -actinin-2 is more stable [13]. Therefore, in the absence of the α -actinin-3 gene or its deficit, calsarcin demonstrates stable immobilization and the slow-type phenotype of the fiber is produced (Fig. 3).

Dephosphorylation of the GSK3 β signaling protein (glycogen synthase kinase) promotes NFAT export from the nucleus and shifts the equilibrium toward the fast isoforms [14] (Fig.2). In this case, the GSK3 β inhibitory activity may be suppressed by nitric oxide through the cGMP-pathway [15].

Another mechanism of myosin phenotype regulation (also calcium-dependent) is implemented through the kinase activity of calcium-calmodulin kinase (CaMK). When activated by the calcium-calmodulin complex, this enzyme phosphorylates histone deacetylase 4 (HDAC4) and prevents it from entering the myonuclear space [16]. In the case of a low concentration of the calcium-calmodulin complex and correspondingly low kinase activity of CaMK, HDAC4 is underphosphorylated and some of its molecules are translocated to myonuclei [17]. In myonuclei, HDAC4 deacetylates not only H3 histone, but also the MEF-2 transcription factor, which interacts with the *myf7* gene promoter (i.e. MyHC I β gene) [17]. This leads to a decrease in the general transcriptional activity of the genome and expression of MyHC I β (Fig. 4). Interestingly, here again, there is an “inhibiting” mechanism: HDAC4 can be ubiquitinated and destroyed. This preserves the slow myosin phenotype [18].

The ratio of phosphorylated and non-phosphorylated high-energy phosphates, another physiological trigger of signaling processes, regulates the activity of AMP-dependent protein kinase (AMPK), which controls the main pathways of the energy metabolism of muscle fibers [19]. Additionally, AMPK phosphorylates the histone deacetylases HDAC4 and 5, which significantly facilitates the expression of the slow MyHC isoform and several other genes that control the regulatory proteins of oxidative metabolism [20, 21]. Furthermore, AMPK activity can be modulated (stimulated) by nitric oxide [22].

Another mechanism of myosin phenotype modulation provides up-regulation of MyHC I β gene expression (*myh7* gene) by means of microRNA. Besides the main MyHC I β gene (*myh7* gene), the mammalian genome comprises the *myh7b* (*myh14*) gene, which is expressed in the skeletal muscles of adult mammals

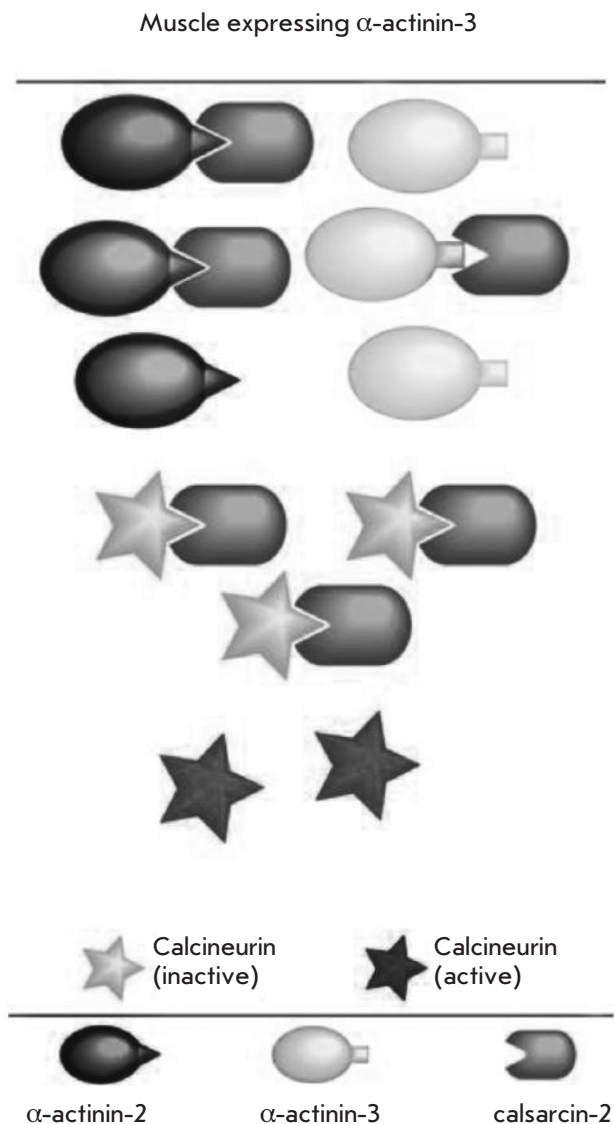


Fig. 3. Calsarcin deposition diagram in α -actinin-2 and α -actinin-3 structures. (According to Seto et al. as revised in [13]). Explanations are provided in the text.

in the form of mRNA; at the protein level, this gene is expressed only in the extraocular muscle [23]. However, its introns encode miR-499 microRNA. Expression of the *myh7b* gene is stimulated by miR-208b, which is encoded by the intron of *myh7*, the essential gene of slow myosin. In turn, miR-499 inhibits the expression of specific blockers of *myh7* gene promoters (Sox6, Pur- β , and Thrap1) [24] (Fig. 5). Interestingly, expression of the *myh7b* gene is stimulated by overexpression of MEF-2 (the basic transcriptional MyHC I β promoter) [25]. This suggests that an increase in the concentration of the calcium/calmodulin complex results in penetra-

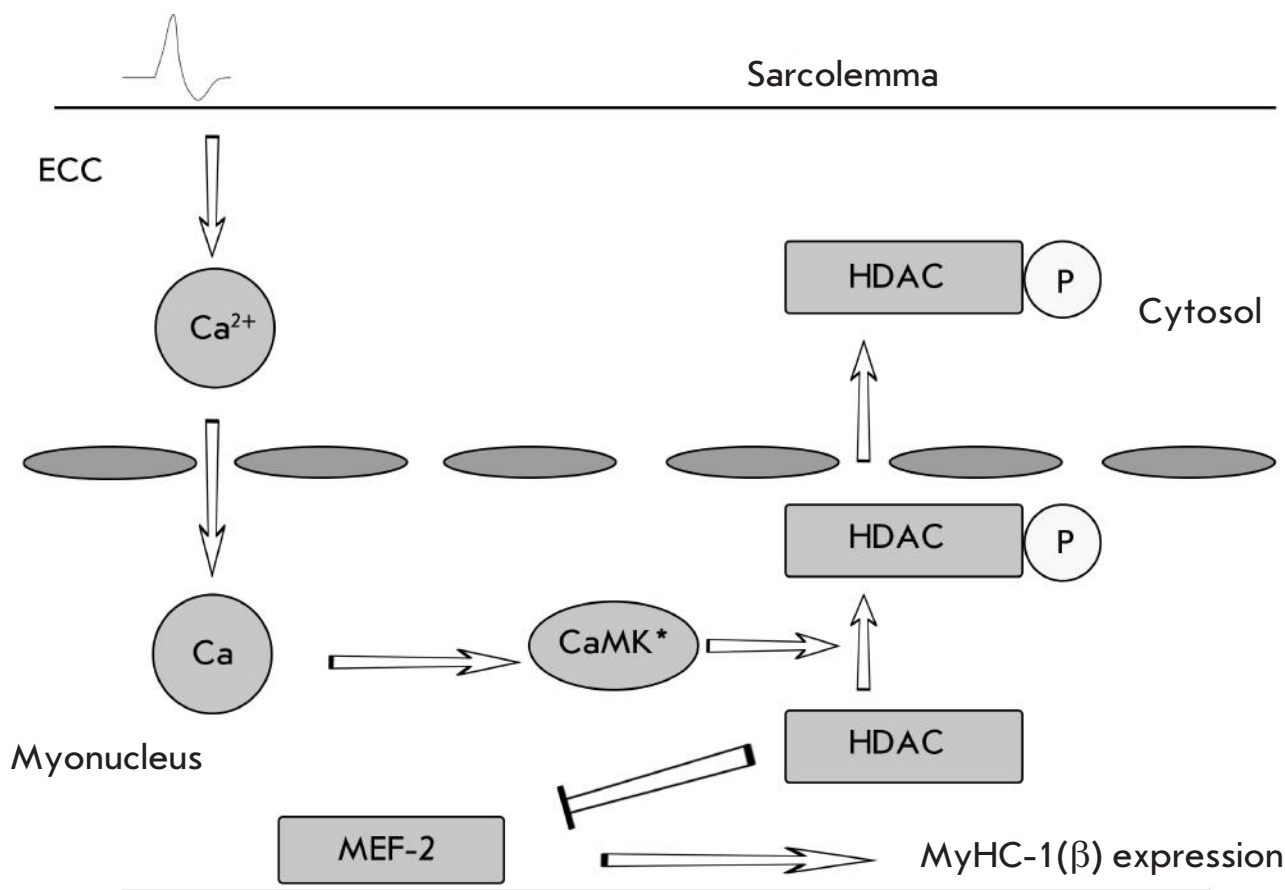


Fig. 4. Functional diagram of the calcium-calmodulin kinase/histone deacetylase 4/5 signaling pathway (according to Liu et al. [17], revised). HDAC – histone deacetylase, CaMK – calcium-calmodulin kinase, MEF-2 – transcription factor (myocyte enhancement factor).

tion of MEF-2, which can be dephosphorylated by calcineurin [26], in to the nucleus, where it regulates *myh7* expression. It also stimulates the synthesis of miR-499 that prevents the blockade of MyHC Iβ expression [25]. Thus, expression of miR-499 and miR-208b provides a smooth synthesis of slow myosin in the presence of an appropriate physiological stimulus (calcium ions).

MYOSIN PHENOTYPE UNDER GRAVITATIONAL UNLOADING CONDITIONS

Changes in the fiber myosin phenotype under gravitational unloading were observed in many laboratories. In particular, it was observed that rat hindlimb suspension results in increased content (%) of type II fibers and decreased proportion of type I fibers in *soleus muscle* [27–30] (Fig. 6).

A seven-day spaceflight resulted in a slow-to-fast shift in the fiber type ratio in *soleus* and EDL rat muscles [31, 32]. In a 12.5- to 14-day flight, a decrease in the content of type I fibers in *soleus* and adductor lon-

gus muscles was observed [33, 34]. We were the first to discover an increased proportion of type II fibers in *soleus* and *vastus lateralis muscles* in monkeys after a 12.5-day spaceflight in the Kosmos-2229 biosatellite [35]. In cases when the shift in the fiber ratio could not be detected by staining for myofibrillar ATPase, an increased amount of fibers, reactive to fast myosin antibodies and a decreased amount of fibers reactive to slow myosin antibodies, was typically observed [36–41]. Electrophoresis revealed the emergence of a new isoform of myosin-heavy chains, 2d or 2x, in a suspension experiment [40]. An increased proportion of hybrid fibers consisting of both slow and fast forms of the myosin-heavy chain, was repeatedly detected in suspension experiments and spaceflights [37, 41]. A reduced proportion of fibers expressing the slow MyHC isoform and increased proportion of fibers expressing fast isoforms was also observed in *soleus muscle* samples from astronauts after a 6-month mission [42]. A shifted ratio of MyHC isoforms towards the fast type was detected

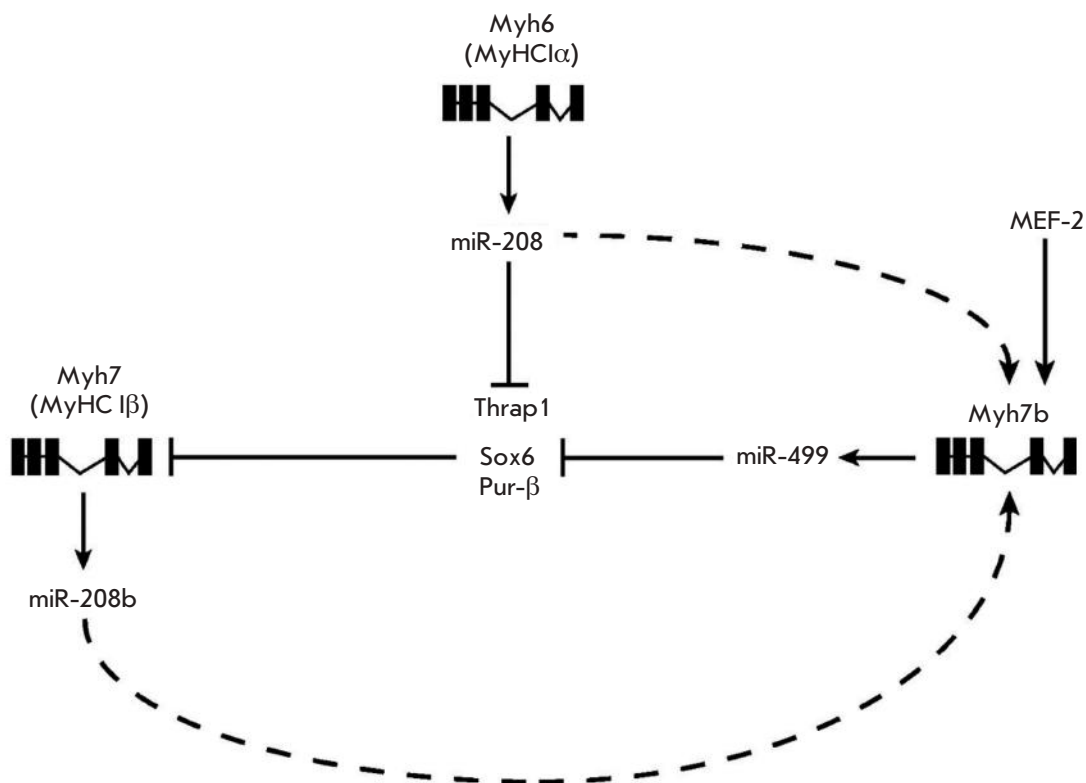


Fig. 5. Participation of microRNA in the regulation of MyHC Iβ expression (according to McCarthy et al. [25]). Explanations are provided in the text.

using an electrophoretic analysis in the *vastus lateralis muscle* of astronauts after an 11-day flight [43]. In our lab, a reduced proportion of slow MyHC fibers in human soleus was observed as early as after a 7-day exposure to dry immersion [44, 45]. Interestingly, the intensity of the myosin phenotype transformation towards the slow type usually did not exceed 15–20% of the fibers, whereas other effects of muscle unloading involved most of the muscle fibers. This fact suggests that the final stabilization of the fast phenotype under unloading conditions is achieved only in the part of the fibers being transformed.

NEURONAL MECHANISMS OF MYOSIN PHENOTYPE REGULATION DURING GRAVITATIONAL UNLOADING

Several observations suggest that the elimination of support afferentation is the main mechanism leading to the “switching-off” of the electrical activity of postural muscle motor units during gravitational unloading (see review [44]). The use of mechanical stimulation of plantar support zones under these conditions maintains the normal level of electrical activity of postural muscles. Interestingly, the use of mechanical stimulation of plantar support zones during exposure to dry immersion enabled us to avoid a decrease in the proportion of slow fibers [44, 45]. When suspending rats with one hindlimb interacting with an artificial support, *the soleus muscle* of this leg demonstrated no myosin pheno-



Fig. 6. Il'in-Novikov method of rat suspension as revised by Morey-Holton.

type transformation towards the fast type, as opposed to the contralateral limb [46]. Low-frequency chronic electrostimulation of *rat soleus muscle* combined with the conventional suspension model also prevents myosin phenotype transformation [47, 48]. The same effects were observed after chronic muscle stretching or resistive exercises during gravitational unloading (suspension or 84-day bed rest) [49–51]. The results of these studies suggest that low-intensity muscular

activity and resistive effects prevent changes in the myosin phenotype. Based on the aforementioned observations, we can suggest that the shift in myosin phenotype under gravitational unloading is caused, among other things, by changes in the neuronal control of motor unit activity. Indeed, the experiments with three-day dry immersion in humans revealed inactivation of slow-type motor units [52]. These results were confirmed in experiments with recording of the electrical activity of *soleus muscle* and fast synergists in *Macaca mulatta* during spaceflight [53] and rat hindlimb suspension, as well as their exposure under conditions of Kepler parabolic flight [54]. We can assume that it is the “switching-off” of slow motor units that leads to changes in the myosin phenotype in all of these cases. This hypothesis can be confirmed by the results obtained in the “spinal isolation” model, where all afferent and descending tracts to the lumbar spinal cord are dissected, while motor terminals are intact. In these experiments with complete “disconnection” of spinal motoneurons, myosin phenotype shift towards the fast type was observed [55]. When supplying chronic carbachol to striatopallidal structures during suspension, enhanced stability of the postural synergies in animals were even accompanied by an increase in the proportion of slow-type soleus fibers [56]. The disabling afferent activity of the tibialis anterior (TA) muscle (antagonist of *soleus muscle*) by means of tenotomy combined with hindlimb suspension prevents an increase in the proportion of fast-type fibers in murine *soleus muscle* [57]. It is conceivable that, during gravitational unloading, activation of the TA muscle [58] or the decrease in the intensity of the exciting striatopallidal effects [56] results in a decreased discharge activity of slow-type motor units of *soleus muscle* and, thus, leads to changes in the myosin phenotype of its fibers.

Another hypothetical neurophysiological mechanism of soleus motor unit inactivation under microgravity conditions is discussed in connection with the study of the muscle effects of vestibular deafferentation in animals. For this purpose, experiments with deafferentation of vestibular receptors using arsenilate injections were carried out [59]. After a month-long adaptation of rats to vestibular deafferentation, a decrease in the proportion of fibers expressing MyHC I β and their cross-sectional area, as well as an increase in the proportion of fibers expressing fast MyHC isoforms, was observed in *soleus muscle*. It is worthy of note that the discovered phenomenon is similar to the myosin phenotype transformation observed after spaceflights. This is indicative of the possibility that the functional changes in the vestibular apparatus in zero gravity state can contribute to changes in the nature of myosin isoform expression. This viewpoint is quite contestable.

First, myosin phenotype transformation towards the fast type is also observed in ground-based zero gravity simulation models, when there is only mild alteration of the vestibular apparatus function (see above). Second, a similar study conducted using surgical vestibular deafferentation (labyrinthectomy) led to opposite changes in *soleus muscle* of animals. The myosin phenotype of *soleus muscle* shifted towards an increased proportion of slow-type fibers [60, 61]. Unfortunately, our knowledge of the vestibular effects on the postural muscle myosin phenotype is limited to the aforementioned publications. Obviously, there remain many more questions than answers. Further research will contribute to filling in the blind spots in this field.

EXPRESSION OF MYOSIN GENES UNDER CONDITIONS OF GRAVITATIONAL UNLOADING

At the beginning of this review, we stated that changes in the myosin phenotype during functional unloading (disuse) are determined by a decreased expression of the slow MyHC isoform gene and increased expression of the fast MyHC isoform gene ([4], etc.). It is interesting to follow the time-course dynamics of the process. Stevens *et al.* were the first to show that a mild decrease in the content of MyHC I β mRNA occurs as early as on the 4th day in suspended Wistar rats, and on the 7th day it becomes a trend and amounts to about 20% [62]. Researchers from the University of California, Irwin, detected a statistically significant decrease in the content of MyHC I β mRNA in Sprague-Dowley rats as early as after 24-hour suspension [63]. We observed a significant decrease in MyHC I β mRNA of Wistar rats on the 7th day of suspension, but a slight downward tendency was observed earlier, on the 3rd day [64] (*Fig. 7A*). Thus, all these studies demonstrated a decrease in mRNA expression of the slow isoform of myosin heavy chains, but the speed of this process varied in different studies. Early and significant growth of the muscle content of mRNA encoding I**b** and I**d/x** isoforms of myosin heavy chains (*Fig. 7C,D*) was also observed. Interestingly, after a 3- to 4-day suspension, there was not a single “pure” slow fiber in the pools of individual fibers: i.e. each fiber undergoes gradual replacement of MyHC I β by fast-type isoforms [65]. According to our data, the time-course dynamics of the MyHC I**A** mRNA content [66] differs from the dynamics of MyHC I β mRNA, as well as MyHC I**b** and I**d/x** mRNA. The content of MyHC I**A** mRNA decreases after a 3-day suspension and further decreases up to day 7. After a 14-day suspension, the content of MyHC I**A** mRNA was found to be so high that it did not differ from the control values (*Fig. 7B*).

Thus, the changes in the myosin phenotype under gravitational unloading are preceded by changes in the

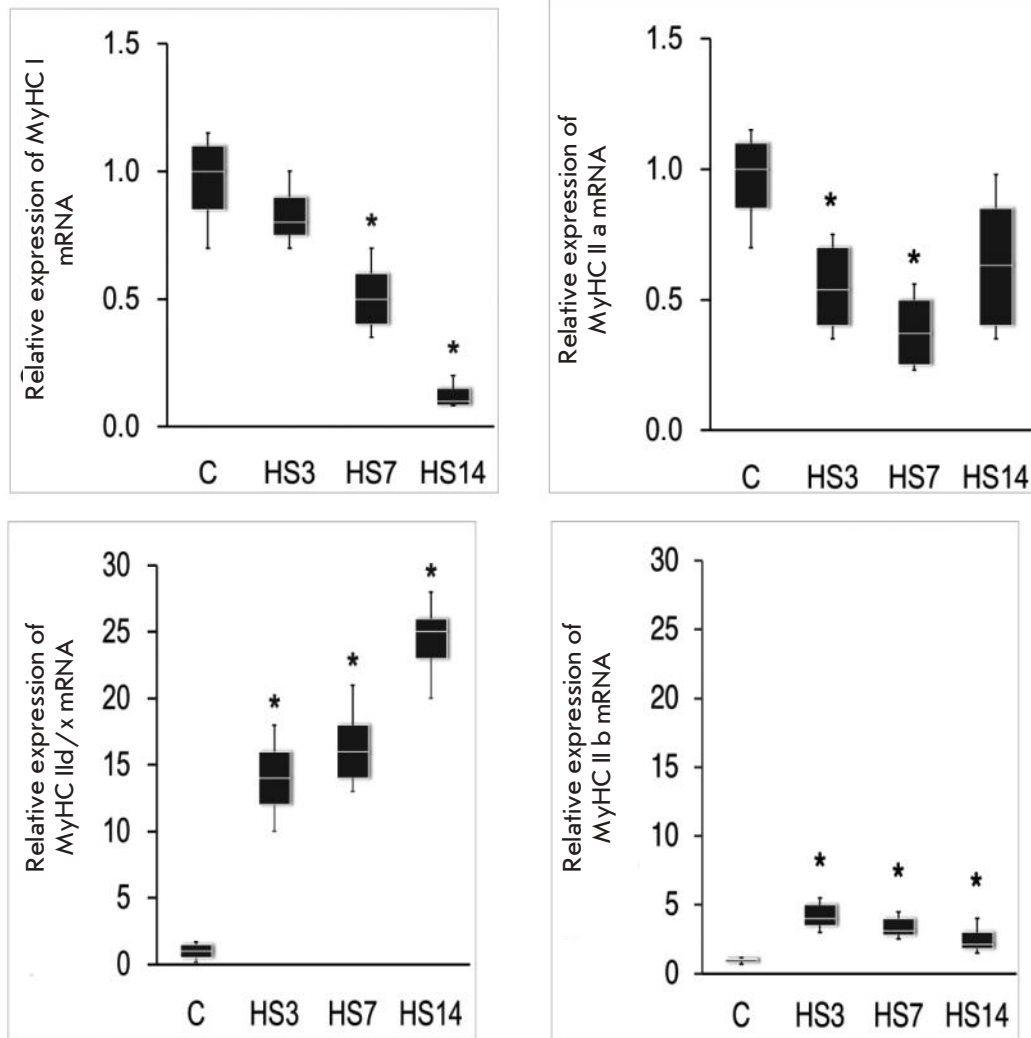


Fig. 7. The dynamics of expression of MyHC isoform mRNA in rat *m. soleus* during unloading (suspension) [64]; HS3 – 3-day suspension, HS7 – 7-day suspension, HS14 – 14-day suspension. The data were obtained by quantitative real-time PCR.

expression pattern of mRNA encoding the corresponding MyHC isoforms. For this reason, the search for the molecular mechanisms of myosin phenotype transformation largely reduces to the study of the mechanisms of myosin gene expression regulation.

Molecular regulatory mechanisms of gene expression of myosin heavy chain isoforms in postural muscles during unloading

The mechanisms of the shift in the expression of MyHC isoform genes toward the fast type are still largely unexplored. The study of the role of the calcineurin/NFATc1 signaling system during gravitational unloading revealed that intensive transportation of NFATc1 to the nuclei of rat soleus fibers [67] occurs after a 14-day suspension of Morey-Holtz rats. However, the NFATc1 content in the myonuclei of human muscles is significantly reduced after a 60-day bed rest hypokinesia [68]. Obviously, there is a contradiction between

these results. The issue of the intensity of the NFAT import to the nucleus during unloading remains unclear. Cyclosporin A, a NFATc1 dephosphorylation inhibitor [69, 70], was used in our laboratory and K.M. Baldwin's laboratory to demonstrate that expression of slow-type MyHC mRNA is further reduced under the action of cyclosporin A, a calcineurin inhibitor, during suspension. This is indicative of the potential compensatory function of this signaling pathway during unloading. Furthermore, the difference between the intensity of the decrease in slow-type MyHC mRNA expression during unloading and under the same conditions, but with underlying administration of cyclosporin A, is small, but statistically significant. The similar amount of changes in this experiment indicates that downregulation of slow-type MyHC during unloading is largely due to inhibition of the calcineurin/NFATc1 signaling pathway.

Transformation towards a fast phenotype does not occur when suspending mice knockout on both MuRF

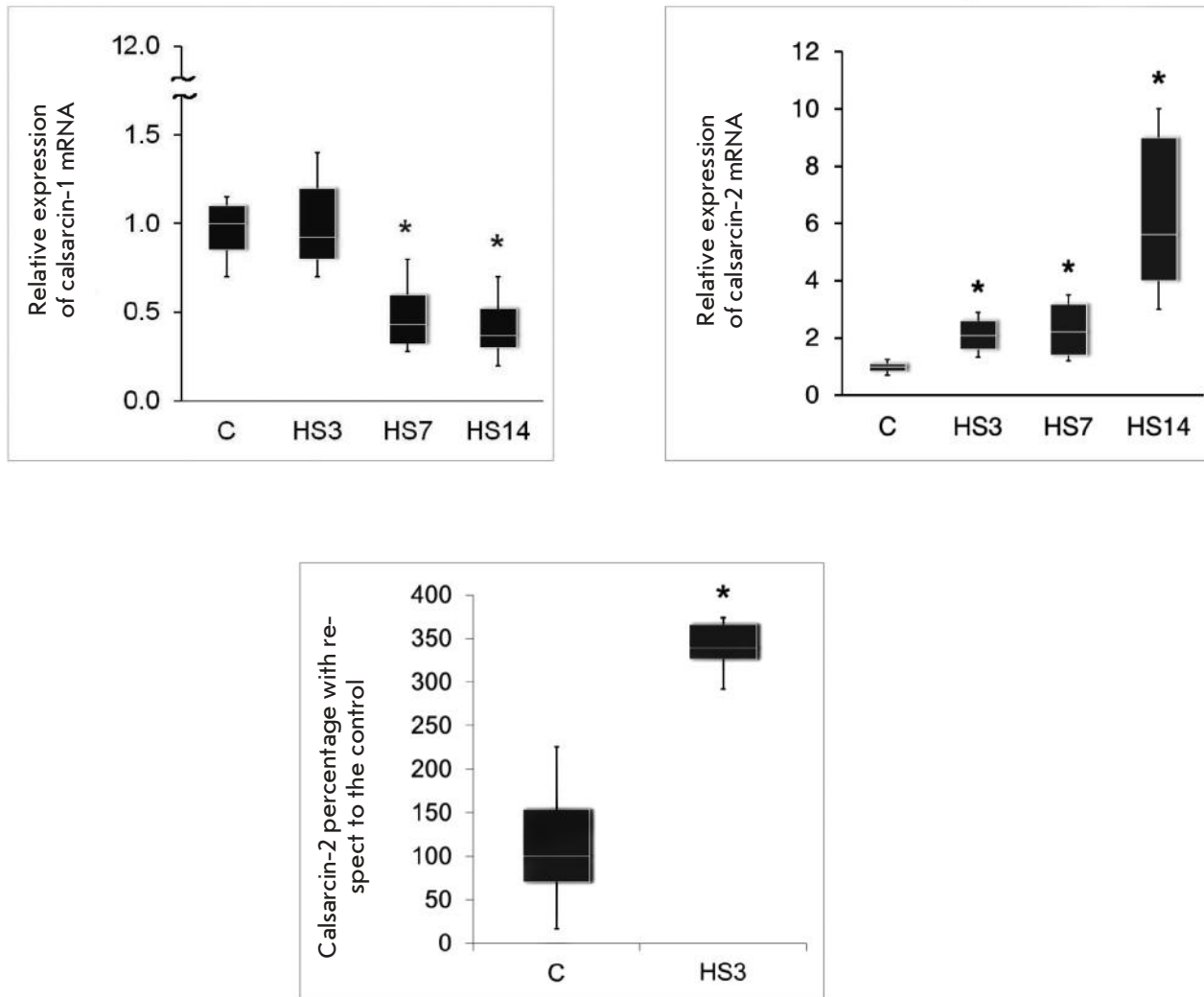


Fig. 8. mRNA expression and the level of calsarcin proteins in rat *m. soleus* during unloading (suspension) [64]. HS3 – 3-day suspension, HS7 – 7-day suspension, HS14 – 14-day suspension. The data were obtained by quantitative real-time PCR and Western blotting (third diagram).

ubiquitin ligases [71]. Therefore, MuRF-dependent expression of calsarcin-2 is probably an important element for the stabilization of the fast myosin phenotype under the influence of hypothetical mechanisms whose compensatory effect is targeted at preserving a slow phenotype. We were the first to discover the isoform-specific time-course dynamics of calsarcin mRNA expression during simulated gravitational unloading (*Fig. 8*) [66]. On the 3rd day of suspension, the level of calsarcin-1 expression was the same as in the control, and then it decreased for up to 14 days. As early as on the 3rd day, the level of calsarcin-2 mRNA was twofold higher than in the control and it continued to increase up to day 14.

In view of both published and our own results, we can assume that, in the portion of fibers containing a significant proportion of fast MyHC isoforms, increased expression of calsarcin-2 results in the prevention of compensatory activation of the calcineurin pathway and, thereby, stabilization of the fast phenotype in these fibers. In other fibers (mostly slow ones), reduced calsarcin-1 expression may intensify the calcineurin pathway and, thereby, stabilize their slow phenotype. Thus, stable populations of slow and fast fibers with a significant shift towards the fast fiber type form by day 7. Additionally, we found a statistically significant increase in the level of MuRF-1 and MuRF-2 in the nuclear fraction of *rat soleus muscle* after a 3-day

suspension; i.e., it is during this period that expression of calsarcin-2 increases [66]. This phenomenon, along with the effects of *murf* genes knockout [11], suggests the existence of a causal link between translocation of MuRF-1 and MuRF-2 to the nuclei at the initial stage of the unloading and increased calsarcin-2 expression.

It is possible that deposition of calsarcin in the structure of α -actinin-2 plays an important role in these processes. In our laboratory, a decreased content of α -actinin-2 in samples of murine *soleus muscle* was observed after a 7-day suspension of rats [72]. Therefore, it can be expected that bound calsarcin-2 is released due to α -actinin-2 degradation during simulated gravitational unloading. Cytoskeleton degradation during unloading is usually attributed to calcium-dependent cysteine proteases: calpains. It is, therefore, interesting that an increased expression of calpastatin, an endogenous calpain inhibitor, did not result in a transformation of the myosin phenotype towards the fast type in suspended mice [73]. The lack of transformation in these mice may be indicative of the fact that calpain activation can be one of the factors contributing to the transformation of the myosin phenotype during unloading. Since calpain activation during gravitational unloading is associated with the accumulation of calcium ions in the myoplasm [74–76], it is expected that blocking calcium ions delivery to the fiber when using nifedipine during gravitational unloading will result in decreased calpain activity and a less pronounced degradation of cytoskeletal proteins. Moreover, degradation of α -actinin-2 will not be as deep as in the case of suspension without additional action and the calsarcin depot will remain full. In this case, downregulation of MyHC I β will be completely or partially prevented. In support of this hypothesis, we found that there was no transformation of *rat soleus muscle* fibers in suspended rats administered chronic nifedipine [77]. However, the mechanisms of participation of calpains in MyHC expression regulation remain insufficiently studied.

In experiments on suspended rats in 2015, we observed activation (i.e., a decrease in the negative phosphorylation) of another endogenous inhibitor of the calcineurin/NFATc1 signaling pathway, glycogen synthase kinase GSK3 β , which, in the absence of negative phosphorylation, phosphorylates NFATc1 and promotes its export from the nucleus [66]. The activity of this enzyme can be inhibited with a high content of nitrogen oxide in the fiber, which acts through the guanylate cyclase mechanism [78]. We have previously shown that the nitrogen oxide level in *rat soleus* is significantly reduced during gravitational unloading [79]. At the same time, administration of *L*-arginine, which enhances nitric oxide production, prevented a reduction of the MyHC I β mRNA content. Apparent-

ly, a decreased level of nitrogen oxide in the fiber during unloading can be considered as one of the stabilizing factors of the fast phenotype, which acts through GSK3 β .

Salanova *et al.* [68] suggest that reduction in the intensity of NFATc1 import to myonuclei during functional unloading is associated with another mechanism: a decrease in Homer-1 scaffold protein expression, which was observed in human *soleus muscle* and *vastus lateralis muscle* after long-term bed rest hypokinesia. In that study, Homer-1 function is described as the scaffold support for approximation and interaction between calcineurin and NFATc1 in the postsynaptic area and Z-disc area. The mechanisms regulating the expression of this protein are not known.

The role of the ratio of high-energy phosphates in the control of the myosin phenotype under unloading conditions can be assessed only in the case when there is a significant change in this ratio at one or another stage of the process. Indeed, an early study by Ohira's group revealed that a 10-day rat hindlimb suspension does increase the level of phosphocreatine in *rat soleus muscle* [80]. It turned out that a reduced level of phosphorylated high-energy phosphates due to administration of β -guanidinopropionic acid prevents a transformation of the myosin phenotype towards the fast type in suspended animals [81]. It is known that chronic administration of β -guanidinopropionic acid acts through AMPK-dependent signaling pathways [82]. Until recently, nobody knew how AMPK activity changed during unloading. The results of two studies in this field directly contradict each other [83, 84]. In our laboratory, it was shown that gravitational unloading using the conventional "dry" immersion model for 3 days results in a significant decrease in the AMPK phosphorylation level in human *soleus muscle* [85]. It is believed that phosphorylation/dephosphorylation of HDAC molecules is the main mechanism of AMPK impact on gene expression. It can be assumed that their action (deacetylation of H3 histone and MEF2 transcription factor) occurs during simulated gravitational unloading. Indeed, acetylation of H3 histone in the gene locus of the fast myosin isoform increases in suspended rats [86]. It was recently established that no slow-to-fast fiber transformation occurs in *soleus muscle* of suspended rats subject to the action of the classical HDAC inhibitor [87].

The mechanism of microRNA-dependent regulation of myosin gene expression is also modulated under unloading conditions (see Introduction). Rat hindlimb suspension results in a reduced expression of miR-499 and miR-208b microRNA in the *soleus muscle*, and, therefore, there are conditions for the functioning of specific blockers of the *myh7* gene promoter: i.e. reduced

expression of slow myosin [25]. These data are consistent with the results of Tsika' group demonstrating an increased expression of the blockers of the *myh7* gene promoter, Pur- α , Pur- β , and SP3, and their binding to specific sites on the promoter during suspension [88, 89]. These processes may result from a reduced expression of the *myh7b* gene and miR-499. Little is known about the physiological regulators of specific blockers of *myh7* gene expression and regulatory miR-499 and miR-208b.

The data on the regulation of *myh7* gene expression provided in this review show that, despite the investigation of the molecular mechanisms that determine a reduced expression of slow MyHC isoforms under gravitational unloading, a complete picture of the functioning of these mechanisms cannot yet be built. It can be assumed that the functioning of a complex system of endogenous inhibitors of the calcineurin/NFATc1 signaling pathway is targeted at overcoming the compensatory muscle responses and fast phenotype stabilization. At the same time, it is unknown which epigenetic processes trigger the processes of *myh7* gene inactivation and reduction of slow MyHC isoform expression at the very early stage of gravitational unloading during the first 24 hours.

Even less is known about the mechanisms that stimulate the functioning of the gene promoters of the fast MyHC isoform. It is believed that, in the absence of stimulants of the slow-type MyHC isoform, DNA binding to the MyoD transcriptional regulator enhances the expression of the fast-type myosin gene [90]. At the same time, MyoD knockout hindlimb unloaded animals demonstrate no transformation towards the fast type [91]. This fact suggests that MyoD significantly affects the expression of fast MyHC isoform genes during gravitational unloading. Interestingly, the stimulatory effect of MyoD on the expression of fast myosin isoforms is inhibited by NFATc1 [92]. Another reciprocal regulation mechanism is characteristic of the expression of MyHC IIA, on the one hand, and IId/x and I Ib, on the other hand. It was found that spinal isolation results in a reduced expression of MyHC IIA and increased expression of IId/x [93]. We observed a similar phenomenon at the early stage of gravitational unloading in experiments with hindlimb suspension [66]. It has been found that the MyHC IId/x gene promoter is located next to the MyHC IIA gene and transcription from the former occurs in two directions. Transcription from the sense strand triggers transcription of the IIX gene; antisense RNA is synthesized from the complementary strand, which leads to the destruction of MyHC IIA mRNA [93]. Thus, activation of the gene expression of the fast myosin isoform results in a reduced expression of the MyHC IIA gene.

CONCLUSION

Regulation of myosin gene expression is being intensively studied at the moment. However, there is no clear picture of the long-known and still obscure phenomenon of the changing pattern of the expression of these genes during gravitational unloading. Basic questions concerning the described phenomenon will be answered in the near future. The adaptive role of the transformation of muscle fibers during gravitational unloading is not covered in numerous publications related to this problem. Hypogravity results in the “disabling” of mostly postural extensors, especially *soleus muscle*, and therein the fibers expressing the slow MyHC isoform and thus implementing slow “tonic” contractile activity. The changing nature of postural synergies under real and simulated zero gravity conditions leads to the elimination of the “tonic” component of the motor function. Therefore, the shift of the myosin phenotype towards the fast type can be an integral part of these adaptive rearrangements of the motor control system in mammals. Another view of the adaptive role of the myosin phenotype shift is based on the well-known differences in trophic mechanisms; i.e., the mechanisms that maintain the structure and metabolism of slow-type and fast-type muscle fibers. The elegant work of Ohira's group [94] demonstrated that denervation of *rat soleus muscle*, combined with hindlimb suspension exposure, does not lead to an increase in atrophic changes, i.e. reduction of the fiber cross-sectional area. Under the same conditions, atrophy of the plantaris muscle was significantly less pronounced than atrophy of *soleus muscle*, but it was much more pronounced when the muscle was denervated. This is indicative of the fact that neurotrophic effects in the fast fiber effectively prevent the intensive development of atrophic processes. This strategy is not specific to slow-type fibers, whose structure is entirely determined by the intensity and duration of the contractile activity. It can be assumed that the transformation of the myosin phenotype of slow-type fibers changing them into fast ones can increase the amount of fibers, preserving the volume of the myofibrillar apparatus during inactivity due to neurotrophic effects. ●

I am very grateful to my teacher I.B. Kozlovskaya, who contributed to the formation of my interest in the topic under discussion during our collaboration and creative dialogue. I would also like to thank S.A. Tyganov for assistance in preparing the manuscript for publication.

This work was supported by a grant from the Russian Science Foundation No 14-15-00358.

REFERENCES

1. Ranvier L. // *CR Acad. Sci. Paris*. 1873. V. 77. P. 1030–1034.
2. Schiaffino S., Reggiani C. // *Physiol. Rev.* 2010. V. 91. P. 1447–1531.
3. Burke R.E. // *J. Physiol.* 1967. V. 193. № 1. P. 141–160.
4. Pette D. // *Skeletal muscle plasticity in health and disease* / Eds Bottinelli R., Reggiani C. Springer, 2006. P. 1–27.
5. Tavi P., Westerblad H. // *J. Physiol.* 2011. V. 589. Pt 21. P. 5021–5031.
6. Chin E.R. // *Exerc. Sport Sci. Rev.* 2010. V. 38. № 2. P. 76–85.
7. Schiaffino S. // *Acta Physiol. (Oxf.)*. 2010. V. 199. № 4. P. 451–463.
8. Shen T., Liu Y., Contreras M., Hernández-Ochoa E.O., Randall W.R., Schneider M.F. // *Histochem. Cell Biol.* 2010. V. 134. № 4. P. 387–402.
9. Frey N., Frank D., Lippl S., Kuhn C., Kögler H., Barrientos T., Rohr C., Will R., Müller O.J., Weiler H., Bassel-Duby R., Katus H.A., Olson E.N. // *J. Clin. Invest.* 2008. V. 118. P. 3598–3608.
10. Frey N., Richardson J.A., Olson E.N. // *Proc. Natl. Acad. Sci. USA*. 2000. V. 97. P. 14632–14637.
11. Moriscot A., Baptista I.L., Bogomolovas J., Krohne C., Hirner S., Granzier H., Labeit S. // *J. Struct. Biol.* 2010. V. 170. № 2. P. 344–353.
12. Lange S., Xiang F., Yakovenko A., Vihola A., Hackman P., Rostkova E., Kristensen J., Brandmeier B., Franzen G., Hedberg B., et al. // *Science*. 2005. V. 308. P. 1599–1603.
13. Seto J.T., Quinlan K.G., Lek M., Zheng X.F., Garton F., MacArthur D.G., Hogarth M.W., Houweling P.J., Gregorevic P., Turner N., Cooney G.J., Yang N., North K.N. // *J. Clin. Invest.* 2013. V. 123. № 10. P. 4255–4263.
14. Shen T., Cseresnyes Z., Liu Y., Randall W.R., Schneider M.F. // *J. Physiol.* 2007. V. 579. № 2. P. 535–551.
15. Martins K.J., St-Louis M., Murdoch G.K., MacLean I.M., McDonald P., Dixon W.T., Putman C.T., Michel R.N. // *J. Physiol.* 2012. V. 590. № 6. P. 1427–1442.
16. Liu Y., Shen T., Randall W.R., Schneider M.F. // *J. Muscle Res. Cell Motility*. 2005. V. 26. P. 13–21.
17. Liu Y., Randall W.R., Martin F., Schneider M.F. // *J. Cell Biol.* 2005. V. 168. № 6. P. 887–897.
18. Potthoff M.J., Wu H., Arnold M.A., Shelton J.M., Backs J., McAnally J., Richardson J.A., Bassel-Duby R., Olson E.N. // *J. Clin. Invest.* 2007. V. 117. P. 2459–2467.
19. Sanchez A.M., Candau R.B., Csibi A., Pagano A.F., Raibon A., Bernardi H. // *Amer. J. Physiol. Cell Physiol.* 2012. V. 303. № 5. P. C475–485.
20. Röckl K.S., Hirshman M.F., Brandauer J., Fujii N., Witters L.A., Goodyear L.J. // *Diabetes*. 2007. V. 56. № 8. P. 2062–2069.
21. McGee S.L., Hargreaves M. // *Clin. Sci. (London)*. 2010. V. 118. № 8. P. 507–518.
22. Lira V.A., Brown D.L., Lira A.K., Kavazis A.N., Soltow Q.A., Zeanah E.H., Criswell D.S. // *J. Physiol.* 2010. V. 588. № 18. P. 3551–3566.
23. Rossi A.C., Mammucari C., Argentini C., Reggiani C., Schiaffino S. // *J. Physiol.* 2010. V. 588. № 2. P. 353–364.
24. Van Rooij E., Quiat D., Johnson B.A., Sutherland L.B., Qi X., Richardson J.A., Kelm R.J.Jr., Olson E.N. // *Dev. Cell*. 2009. V. 17. P. 662–673.
25. McCarthy J.J., Esser K.A., Peterson C.A., Dupont-Versteegden E.E. // *Physiol. Genomics*. 2009. V. 39. № 3. P. 219–226.
26. Dunn S.E., Simard A.R., Bassel-Duby R., Williams R.S., Michel R.N. // *J. Biol. Chem.* 2001. V. 276. № 48. P. 45243–45254.
27. Templeton G.H., Sweeney H.L., Timson B.F., Padalino M., Dudenhoefter G.A. // *J. Appl. Physiol.* (1985). 1988. V. 65. № 3. P. 1191–1195.
28. Desplanches D., Mayet M.H., Sempore B., Flandrois R. // *J. Appl. Physiol.* (1985). 1987. V. 63. № 2. P. 558–563.
29. Riley D.A., Slocum G.R., Bain J.L., Sedlak F.R., Sowa T.E., Mellender J.W. // *J. Appl. Physiol.* (1985). 1990. V. 69. № 1. P. 58–66.
30. Desplanches D., Kayar S.R., Sempore B., Flandrois R., Hoppeler H. // *J. Appl. Physiol.* (1985). 1990. V. 69. № 2. P. 504–508.
31. Martin T.P., Edgerton V.R., Grindeland R.E. // *J. Appl. Physiol.* (1985). 1988. V. 65. № 5. P. 2318–2325.
32. Desplanches D., Mayet M.H., Ilyina-Kakueva E.I., Sempore B., Flandrois R. // *J. Appl. Physiol.* (1985). 1990. V. 68. № 1. P. 48–52.
33. Desplanches D., Mayet M.H., Ilyina-Kakueva E.I., Frutoso J., Flandrois R. // *Eur. J. Appl. Physiol.* 1991. V. 63. P. 288–292.
34. Miu B., Martin T.P., Roy R.R., Oganov V.S., Ilyina-Kakueva E.I., Marini J.F., Leger J.J., Bodine-Fowler S., Edgerton V.R. // *FASEB J.* 1990. V. 4. P. 64–72.
35. Shenkman B.S., Kozlovskaya I.B., Kuznetsov S.L., Nemirovskaya T.L., Desplanches D. // *J. Gravit. Physiol.* 1994. V. 1. № 1. P. P64–P66.
36. Baldwin K.M., Herrick R., Ilyina-Kakueva E.I., Oganov V.S. // *FASEB J.* 1990. V. 4. P. 79–83.
37. Ohira Y., Jiang B., Roy R.R., Oganov V., Ilyina-Kakueva E., Marini J.F., Edgerton V.R. // *J. Appl. Physiol.* (1985). 1992. V. 73. № 2. Suppl. P. 51S–57S.
38. Guezennec C.Y., Gilson E., Serrurier B. // *Eur. J. Appl. Physiol.* 1990. V. 60. № 6. P. 430–435.
39. Campione M., Ausoni S., Guezennec C., Schiaffino S. // *J. Appl. Physiol.* 1993. V. 74. № 3. P. 1156–1160.
40. Takahashi H., Wada M., Katsuta S. // *Acta Physiol. Scand.* 1991. V. 143. № 1. P. 131–132.
41. Thomason D., Morrison P.R., Oganov V., Ilyina-Kakueva E.I., Booth F.W., Baldwin K.M. // *J. Appl. Physiol.* 1992. V. 73. № 2. Suppl. P. 90S–93S.
42. Trappe S., Costill D., Gallagher P., Creer A., Peters J.R., Evans H., Riley D.A., Fitts R.H. // *J. Appl. Physiol.* (1985). 2009. V. 106. № 4. P. 1159–1168.
43. Zhou M.Y., Klitgaard H., Saltin B., Roy R.R., Edgerton V.R., Gollnick P.D. // *J. Appl. Physiol.* (1985). 1995. V. 78. № 5. P. 1740–1744.
44. Grigor'ev A.I., Kozlovskaya I.B., Shenkman B.S. [The role of support afferents in organisation of the tonic muscle system]. // *Russ Fiziol Zh Im I M Sechenova*. 2004. V. 90. № 5. P. 508–521.
45. Shenkman B.S., Podlubnaia Z.A., Vikhliantsev I.M., Litvinova K.S., Udaltsov S.N., Nemirovskaya T.L., Lemesheva Iu.S., Mukhina A.M., Kozlovskaya I.B. [Human soleus fibers contractile characteristics and sarcomeric cytoskeletal proteins after gravitational unloading. Contribution of support stimulus]. // *Biofizika*. 2004. V. 49. № 5. P. 881–890.
46. Nemirovskaya T.L., Shenkman B.S. // *Eur. J. Appl. Physiol.* 2002. V. 87. № 2. P. 120–126.
47. Leterme D., Falempin M. // *Pflug. Arch.* 1994. V. 426. P. 155–160.
48. Dupont E., Cieniewski-Bernard C., Bastide B., Stevens L. // *Am. J. Physiol. Regul. Integr. Comp. Physiol.* 2011. V. 300. P. R408–R417.
49. Falempin M., Mounier Y. // *Acta Astronautics*. 1998. V. 42. № 1–8. P. 489–501.

50. Podlubnaia Z.A., Vikhliantsev I.M., Mukhina A.M., Nemirovskaia T.L., Shenkman B.S. [Sarcomeric cytoskeletal proteins and myosin phenotype in stretched soleus of hind-limb-suspended rats]. // *Biofizika*. 2004 V.49. № 3 P. 424–429.
51. Gallagher P., Trappe S., Harber M., Creer A., Mazzetti S., Trappe T., Alkner B., Tesch P. // *Acta Physiol. Scand*. 2005. V. 185. P. 61–69.
52. Kirenskaia A.V., Kozlovskaya I.B., Sirota M.G. [Effect of immersion hypokinesia on the characteristics of the rhythmic activity of the motor units of the soleus muscle]. // *Fiziol Cheloveka*. 1986. V. 12. № 4. P.627–632.
53. Roy R.R., Hodgson J.A., Aragon J., Day M.K., Kozlovskaya I., Edgerton V.R. // *J. Gravit. Physiol*. 1996. V. 3. № 1. P. 11–15.
54. Kawano F., Nomura T., Ishihara A., Nonaka I., Ohira Y. // *Neurosci*. 2002. V. 114. № 4. P. 1133–1138.
55. Huey K.A., Roy R.R., Baldwin K.M., Edgerton V.R. // *Muscle Nerve*. 2001. V. 24. № 4. P. 517–526.
56. Shenkman B.S., Shapovalova K.B., Mukhina A.M., Kozlovskaya I.B., Nemirovskaia T.L., Kamkina Iu.V. Activation of neostriatum muscarinic receptors prevents changes in the myosin phenotype of musculus soleus fibers under gravitational unloading. // *Dokl Biol Sci*. 2006. V. 407. № 6. P. 842–844.
57. Shenkman B.S., Nemirovskaia T.L., Mukhina A.M., Podlubnaya Z.A., Vikhlyantsev I.M., Ardabyevskaya A.V., Kozlovskaya I.B., Grigoriev A.I. Effects of inactivation of the antagonist muscle on the atrophic processes in rat soleus muscle under conditions of gravitational unloading. // *Dokl. Akad. Nauk*. 2005. V. 400. № 6. P. 840–843.
58. Yuganov E.M., Kasyan I.I., Tcherepakhin M.A., Gorshkov A.I. [On some human responses under conditions of reduced weight-bearing.] // *Probl. Kosm. Biol*. 1962. V. 2. P. 206–214.
59. Luxa N., Salanova M., Schiff G., Gutschmann M., Besnard S., Denise P., Clarke A., Blottner D. // *J. Vestib. Res*. 2013. V. 23. P. 187–193.
60. Fuller Ch. // XII Conf. on space biology and aerospace medicine, Moscow. 2002. P. 449–450.
61. Kasri M., Picquet F., Falempin M. // *Exp. Neurol*. 2004. V. 185. № 1. P. 143–153.
62. Stevens L., Sultan K.R., Peuker H., Gohlsch B., Mounier Y., Pette D. // *Am. J. Physiol. Cell Physiol*. 1999. V. 46. P. 1044–1049.
63. Giger J.M., Bodell P.W., Zeng M., Baldwin K.M., Haddad F. // *J. Appl. Physiol*. (1985). 2009. V. 107. № 4. P. 1204–1212.
64. Shenkman B.S., Lomonosova Y.N. Expression of calsarcin isoforms and myosin phenotype stabilization in transitional unloaded muscle. // *Dokl Biochem Biophys*. 2014. V. 459. P. 214–216
65. Stevens L., Gohlsch B., Mounier Y., Pette D. // *FEBS Lett*. 1999. V. 463. P. 15–18.
66. Lomonosova Y.N., Turtikova O.V., Shenkman B.S. // *J. Muscle Res. Cell Motility*. 2016. V. 37. № 1. P. 7–16. doi: 10.1007/s10974-015-9428-y.
67. Dupont-Versteegden E.E., Knox M., Gurley C.M., Houle J.D., Peterson C.A. // *Am. J. Physiol. Cell Physiol*. 2002. V. 282. P. C1387–C1395.
68. Salanova M., Bortoloso E., Schiff G., Gutschmann M., Belavy D.L., Felsenberg D., Sandra Furlan S., Volpe P., Blottner D. // *FASEB J*. 2011. V. 25. P. 4312–4325.
69. Lomonosova Y.N., Shenkman B.S., Nemirovskaia T.L. [Calcineurin-mediated regulation of myosin heavy chain expression in rat soleus muscle under conditions of reduced motor activity.] // *Ross Fiziol Zh Im I M Sechenova*. 2009. V. 95. № 9. P. 969–974.
70. Pandorf C.E., Jiang W.H., Qin A.X., Bodell P.W., Baldwin K.M., Haddad F. // *Am. J. Physiol. Regul. Integr. Comp. Physiol*. 2009. V. 297. № 4. P. R1037–R1048.
71. Labeit S., Kohl C.H., Witt C.C., Labeit D., Jung J., Granzier H. // *J. Biomed. Biotechnol*. 2010. V. 2010. Article 693741.
72. Mirzoev T.M., Shenkman B.S., Ushakov I.B., Ogneva I.V. Desmin and α -actinin-2 content in rat soleus muscle in the dynamics of gravitational unloading and subsequent reloading. // *Dokl Biochem Biophys*. 2012. V. 444. P. 216–218.
73. Tidball J.G., Spencer M.J. // *J. Physiol*. 2002. V. 545. № 3. P. 819–828.
74. Ingalls C.P., Warren G.L., Armstrong R.B. // *J. Appl. Physiol*. 1999. V. 87. № 1. P. 386–390.
75. Ingalls C.P., Wenke J.C., Armstrong R.B. // *Aviat. Space Environ. Med*. 2001. V. 72. № 5. P. 471–476.
76. Kandarian S.C., Stevenson E.J. // *Exerc. Sport Sci. Rev*. 2002. V. 30. № 3. P. 111–116.
77. Mukhina A.M., Altaeva E.G., Nemirovskaia T.L., Shenkman B.S. [Role of L-type Ca channels in Ca²⁺ accumulation and changes in distribution of myosin heavy chain and SERCA isoforms in rat M. soleus under gravitational unloading]. // *Ross Fiziol Zh Im I M Sechenova*. 2006. V. 92. № 11. P. 1285–1295.
78. Drenning J.A., Lira V.A., Simmons C.G., Soltow Q.A., Sellman J.E., Criswell D.S. // *Am. J. Physiol. Cell Physiol*. 2008. V. 294. P. 1088–1095.
79. Lomonosova Y.N., Kalamkarov G.R., Bugrova A.E., Shevchenko T.F., Kartashkina N.L., Lysenko E.A., Shvets V.I., Nemirovskaia T.L. Protective effect of L-Arginine administration on proteins of unloaded m. soleus. // *Biochemistry (Mosc)*. 2012. V.77. № 2. P. 208–216
80. Wakatsuki T., Ohira Y., Yasui W., Nakamura K., Asakura T., Ohno H., Yamamoto M. // *Jpn. J. Physiol*. 1994. V. 44. № 2. P. 193–204.
81. Matoba T., Wakatsuki T., Ohira Y. // *Med. Sci. Sports Exerc*. 1993. V. 25. № 5. P. S157.
82. Zong H., Ren J.M., Young L.H., Pypaert M., Mu J., Birnbaum M.J., Shulman G.I. // *Proc. Natl. Acad. Sci. USA*. 2002. V. 99. № 25. P. 15983–15987.
83. Han B., Zhu M.J., Ma C., Du M. // *Appl. Physiol. Nutr. Metab*. 2007. V. 32. P. 1115–1123.
84. Hilder T.L., Baer L.A., Fuller P.M., Fuller C.A., Grindeland R.E., Wade C.E., Graves L.M. // *J. Appl. Physiol*. 2005. V. 99. P. 2181–2188.
85. Vilchinskaya N.A., Mirzoev T.M., Lomonosova Y.N., Kozlovskaya I.B., Shenkman B.S. // *J. Musculoskelet. Neuronal Interact*. 2015. V. 15. № 3. P. 286–293.
86. Pandorf C.E., Haddad F., Wright C., Bodell P.W., Baldwin K.M. // *Am. J. Physiol. Cell Physiol*. 2009. V. 297. P. C6–C16.
87. Dupré-Aucouturier S., Castells J., Freyssen D., Desplanches D. // *J. Appl. Physiol*. 2015. V. 119. P. 342–351.
88. Tsika G., Ji J., Tsika R. // *Mol. Cell. Biol*. 2004. V. 24. № 24. P. 10777–10791.
89. Ji J., Tsika G.L., Rindt H., Schreiber K.L., McCarthy J.J., Kelm R.J., Jr., Tsika R. // *Mol. Cell. Biol*. 2007. V. 27. № 4. P. 1531–1543.
90. Wheeler M.T., Snyder E.C., Patterson M.N., Swoap S.J. // *Am. J. Physiol*. 1999. V. 276. № 5. Pt. 1. P. C1069–C1078.
91. Seward D.J., Haney J.C., Rudnicki M.A., Swoap S.J. // *Am. J. Physiol. Cell Physiol*. 2001. V. 280. № 2. P. C408–C413.
92. Ehlers M.L., Celona B., Black B.L. // *Cell Rep*. 2014. V. 8. P. 1–10.
93. Pandorf C.E., Haddad F., Roy R.R., Qin A.X., Edgerton V.R., Baldwin K.M. // *J. Biol. Chem*. 2006. V. 281. № 50. P. 38330–38342.
94. Ohira Y., Yoshinaga T., Ohara M., Kawano F., Wang X.D., Higo Y., Terada M., Matsuoka Y., Roy R.R., Edgerton V.R. // *Cells Tissues Organs*. 2006. V. 182. № 3–4. P. 129–142.

The Role of BAR Domain Proteins in the Regulation of Membrane Dynamics

T.B. Stanishneva-Konovalova¹, N.I. Derkacheva², S.V. Polevova¹, O.S. Sokolova^{1*}

¹Lomonosov Moscow State University, Faculty of Biology, Leninskie Gory 1, Bld 12, Moscow, 119234, Russia

²A.I. Evdokimov Moscow State University of Medicine and Dentistry, Department of Biochemistry, Delegatskaya Str. 20, Bld 1, Moscow, 127473, Russia

*E-mail: sokolova184@gmail.com

Received March 10, 2016; in final form, August 22, 2016

Copyright © 2016 Park-media, Ltd. This is an open access article distributed under the Creative Commons Attribution License, which permits unrestricted use, distribution, and reproduction in any medium, provided the original work is properly cited.

ABSTRACT Many cellular processes are associated with membrane remodeling. The BAR domain protein family plays a key role in the formation and detection of local membrane curvatures and in attracting other proteins, including the regulators of actin dynamics. Based on their structural and phylogenetic properties, BAR domains are divided into several groups which affect membrane in various ways and perform different functions in cells. However, recent studies have uncovered evidence of functional differences even within the same group. This review discusses the principles underlying the interactions of different groups of BAR domains, and their individual representatives, with membranes.

KEYWORDS BAR domains, lipid membranes, membrane dynamics

ABBREVIATIONS a.a. – amino acid; AH – amphipathic helix; ST – surface tension; PI(4,5)P₂ – phosphatidylinositol-4,5-bisphosphate.

INTRODUCTION

During cell movement, the coordinated processes of actin polymerization and the interaction between actin filaments and the cellular membrane push the active cell edge forward and result in filopodia formation. These processes are coordinated by actin-binding proteins. Disruptions in the function of actin-binding proteins that infringe on cell motility are a distinct feature of neoblasts. BAR family proteins act as connecting links between actin dynamics and membrane rearrangements in all eukaryotes. BAR domains were originally defined as the conserved regions of the animal proteins BIN and amphiphysin, as well as the yeast Rvs161 and Rvs167 proteins [1]. Along with the BAR domain, the proteins belonging to this family contain other domains that are required to ensure that they bind to specific proteins and lipids, which determines their function and arrangement in a cell [2] (*Fig. 1*). The preferential binding of BAR domains to curved membrane regions makes it possible to attract target proteins to membrane rearrangement sites.

There are different ways through which BAR domain proteins can affect actin polymerization. In some cases, they activate the actin nucleation factors WASP (Wiskott-Aldrich Syndrome Protein) and WAVE (Wiskott-Aldrich Verprolin Protein) [3], while other BAR domain proteins interact with Rho GTPases

[4]. Most BAR domains attract the proteins specific to a certain cellular process to the membrane thanks to SH3 domains, which can interact with a number of proteins that contain proline-rich sequences [5, 6]. This fact raises the question of which factors determine the specificity of attracting certain proteins. According to the existing hypothesis, partner proteins recognize the spatial arrangement of SH3 domains rather than individual SH3 domains [7] (see text below).

In addition to attracting partner proteins, SH3 domains often function as regulators of the BAR domain activity [8, 9]. Binding of SH3 to the BAR domain typically transforms the structure into an autoinhibited state; this state can be activated only via interaction with an activator protein [9]. In the F-BAR protein Nervous wreck (Nwk), binding of the SH3 domain to F-BAR does not block its membrane-binding ability but only increases the amount of phosphatidylinositol-4,5-bisphosphate (PI(4,5)P₂) required for the binding [10].

The PICK protein, whose functions have to do with the internalization and exposure of AMPA receptors to the cell surface, provides an interesting example of BAR domain activity regulation [11]. PICK is inhibited by another BAR domain protein, ICA69 [12]. It remains unclear whether this is caused by the formation of a heterodimer from the BAR domains

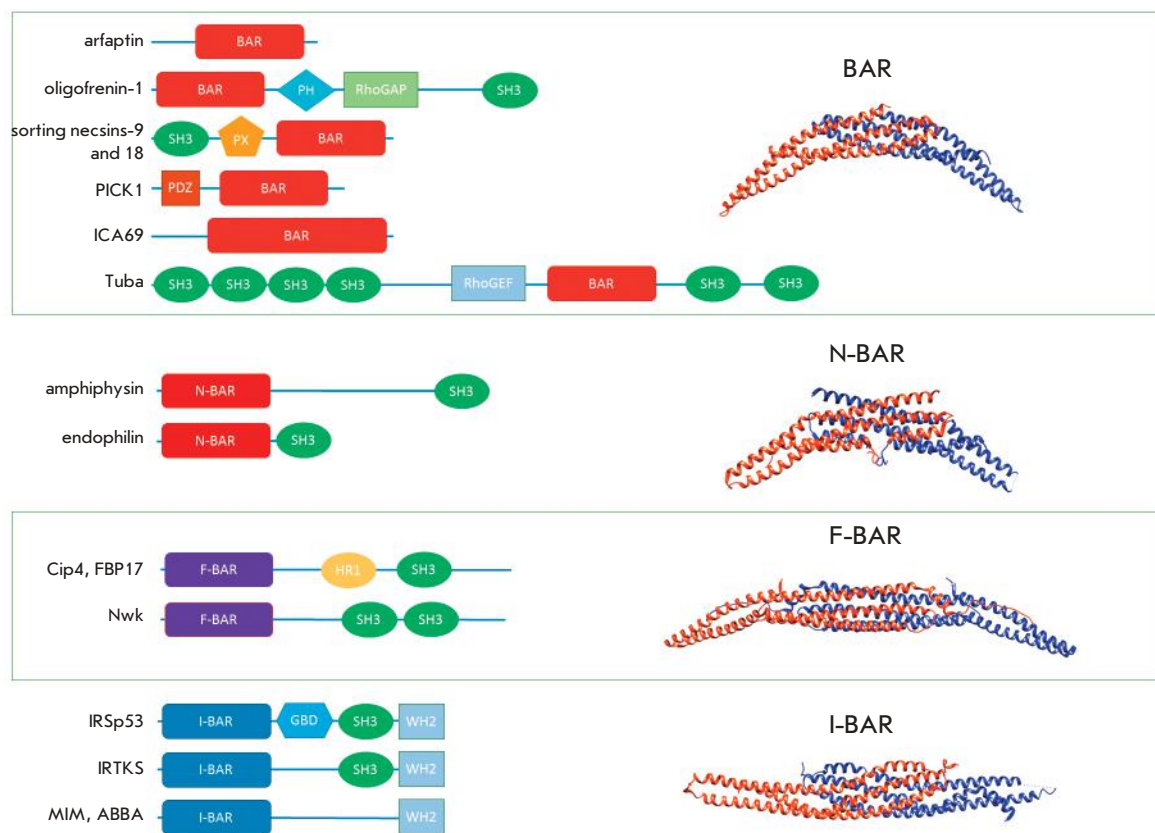


Fig. 1. The domain structures of BAR family members (left side) and the structures of BAR domain dimers (right side).

ICA69 and PICK or by the co-oligomerization of their homodimers. The second version seems more plausible, taking into account the stability of the dimers of BAR domain proteins and the potential involvement of the C-terminal region of ICA69 in the interaction.

According to the Uniprot database, the BAR family currently includes more than 220 proteins [13]; crystal structures have been obtained only for 25% of them [14]. The overarching feature of all BAR domains is that they form dimers with the positively charged surface that binds to negatively charged lipid membranes [15, 16]. BAR domains can be classified into several groups based on their structural and phylogenetic properties: classical BAR/N-BAR, F-BAR, and I-BAR (*Fig. 1*) [17].

Classical BAR domains and N-BAR domains

A classical BAR domain is a dimer where each monomer consists of three bent antiparallel α -helices [15]. The classical BAR and N-BAR dimers have a crescent shape and bind to the membrane by their concave surface. Most proteins containing the classical BAR domains are present in mammalian nerve cells, where they are involved in the formation of synaptic contacts and in the processes related to signal transduction [18].

Amphiphysins are among the best-studied BAR domain proteins; their functions are associated with

neuronal endocytosis [19]. Mammals carry two genes encoding amphiphysins. The amphiphysin II isoform, as well as drosophila amphiphysin, is expressed in muscle cells instead of neurons; it is involved in the formation and stabilization of T-tubules [20, 21]. Mutations in human amphiphysin II/BIN1 cause a hereditary neuromuscular disease known as centronuclear or myotubular neuropathy [22]. The N-terminal BAR domain is the only conserved region of different amphiphysins.

The crystal structure of the BAR domain of drosophila amphiphysin was obtained in 2004, and a prediction was made that similar domains can be found in many protein groups [15]. Based on their structural similarity, the earlier deciphered structure of the C-terminal domain of arfaptin [23] and the endophilin structure deciphered later [24] were classified as belonging to the BAR domain family. By that time, the significant role of endophilin in endocytosis and its interaction with amphiphysin and dynamin had already been reported in a number of studies [25, 26].

According to X-ray diffraction analysis data, clusters of positively charged amino acid residues (*Fig. 2*) reside at the ends of the BAR domain, between the α -helices 2 and 3 and on its concave surface. Mutations in them reduce the ability of the BAR domain to bind to the

membrane and modify liposomes *in vitro*. It has also been shown that the 26 a.a.r. N-terminal sequence of amphiphysin has an unordered structure in the solution but folds into an amphipathic helix (AH) when interacting with lipids. The insertion of an AH helps the BAR domain generate the membrane curvature [27]. AH was subsequently found in many (but not all) BAR domain proteins.

I-BAR domains

The I-BAR domain was first determined as a homologous N-terminal domain of mammalian IRSp53 and MIM proteins and called the IM domain (IRSp53/MIM) [28]. Later, due to its structural similarity to the BAR domains, this domain became known as I-BAR (Inverse BAR) [29]. I-BAR domain proteins are present both in higher and lower eukaryotes but have not been found in yeasts.

Similarly to the classical BAR domains, I-BAR domains consist of three α -helices and form dimers; many of these dimers bind to liposomes and modify their curvature in *in vitro* experiments [30–32]. The I-BAR dimer is less curved than the classical BAR (Fig. 1). Clusters of positively charged amino acids that are responsible for the binding to negatively charged lipids in the membrane reside on their convex, rather than on the concave, surface (Fig. 2) and cause membrane curvature in the opposite direction as compared to BAR's action [28, 33].

The gene encoding IRSp53 is actively expressed in various mammalian cells and tissues, especially in neurons. IRSp53 knockout mice showed impaired learning skills and memory [34]. IRSp53 contains a CRIB motif that binds to GTPase Cdc42 and an SH3 domain that interacts with WAVE. When bound into a complex with Cdc42 and the Eps8 protein, it can induce filopodia formation [35], while in complex with WAVE it causes lamellipodia formation [36]. IRSp53 is regulated by phosphorylation of two threonine residues, which results in binding of protein 14-3-3 to it and subsequent inactivation [37]. Smaller amounts of IRTKS, the closest homologue of IRSp53, were found in the brain; it was also detected in the bladder, liver, testes, heart, and lungs. Unlike IRSp53, IRTKS does not bind to Cdc42 and its expression in cells causes the formation of clusters of short actin filaments but not filopodia; however, the specific biological functions of IRTKS have not been elucidated yet [38]. MIM (Missing-In-Metastasis) was given its name due to the fact that its expression was reduced in some metastasizing cell lines [39]; however, the more recent studies have demonstrated that its expression can also be elevated in other metastasizing cell lines [40]. MIM is actively expressed in the heart, skeletal muscles,

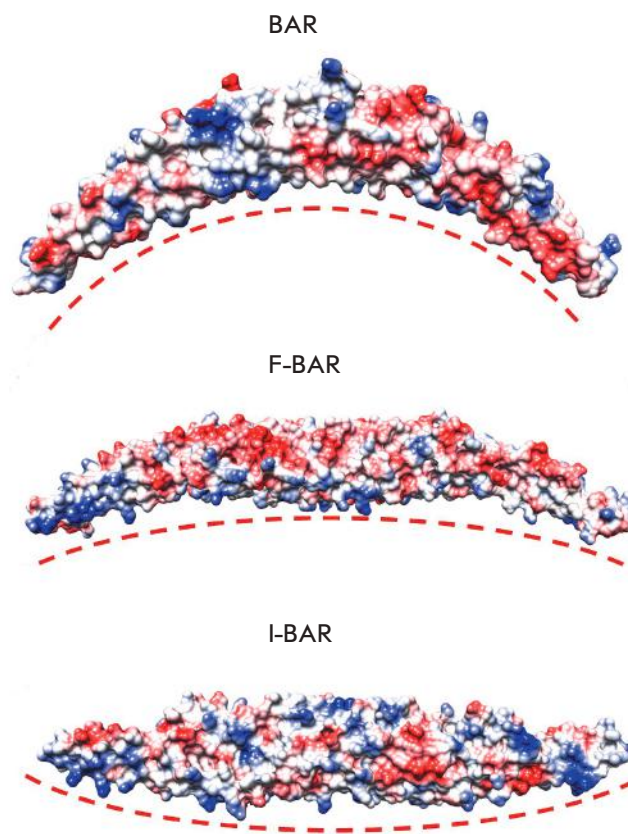


Fig. 2. Membrane deformation by BAR domains. The electrostatic surface potentials of the domains are shown with blue as positive and red as negative; the membrane surface is depicted as a red dotted line.

and the central nervous system during ontogenesis. Overexpression of MIM in mammalian cell lines leads to the disappearance of actin stress fibers and emergence of multiple small protrusions on the cell surface [41]. The activity of MIM, identically to that of IRSp53, is regulated by the phosphorylation of the residue in the central portion of the protein (outside the I-BAR domain) [42]. MIM was reported to be involved in cilia formation [43]; however, its accurate role in animal development and physiology remains unclear. The ABBA protein, the closest homologue of MIM, is expressed in glial cells of the murine central nervous system but is absent in neurons. In the glial cell line C6-R, ABBA resides within cortical actin; its knockdown results in defects in lamellipodia formation [44].

The atomic structure of the I-BAR domain of the Pinkbar (Planar Intestinal- and Kidney-specific BAR) protein was deciphered in 2011: the structure is characterized by an almost zero curvature [45]. This protein is expressed in epithelial intestinal and renal cells and partakes in membrane structuration in the intercellular contact zone. The I-BAR domain of the

Pinkbar protein, unlike the other known domains, can form flattened membrane regions and aggregate into stable flat oligomers both on the lipid membrane and in solution [29, 45]. The results of domain oligomerization include membrane deformation and clustering of charged lipids PI(4,5)P₂ in the membrane. I-BAR domains have a higher electrostatic potential compared to the classical BAR domains and can form PI(4,5)P₂ clusters at the micron scale [33].

F-BAR domains

Another broad group of BAR domain proteins contains the F-BAR domain (Fes/CIP4 homology-BAR). F-BAR proteins were found in most eukaryotes except for plants; they are considered to be the key regulators of cellular membrane curvature [46]. Most of the known F-BAR domain proteins are involved in clathrin-mediated or caveolin-dependent endocytosis. Many of them also partake in the formation of filopodia and lamellipodia: filopodia are required for the formation of axons [47], while lamellipodia inhibit this process [48]. Both these structures can ensure the migration of normal cells and be involved in the dissemination of metastasizing cells [49]. Cell division that also involves F-BAR domain proteins is another crucial process the disruption of which triggers tumor formation. Diseases associated with an altered expression level or mutations in the genes encoding proteins belonging to this family include developmental disorders, neurological and autoimmune diseases, invasive tumors, cardiac hypertrophy, carbohydrate metabolism disorder, and renal failure, thus making F-BAR domain proteins a potential therapeutic target [50].

The F-BAR domain was first discovered in the CIP4 protein (CDC42-Interacting Protein 4) [51]. The conserved N-terminal region (60 a.a.) of the CIP4 and FES proteins became known as FCH (FES/CIP4 Homology). It resides next to a domain whose structure is similar to that of the BAR domain and forms a functional unit with it (F-BAR). An analysis of the crystal structures of the F-BAR domains in mammalian FBP17 and CIP4 proteins showed that the shape of F-BAR domains is less curved and more elongated compared to that of classical BAR domains [16] (*Fig. 1*). They consist of five α -helices: the short N-terminal helix, three long and one short C-terminal helices, followed by a short sequence responsible for homodimerization. The surfaces with which monomers interact with each other mostly contain hydrophobic amino acid residues and several charged ones (*Fig. 2*). Mutations in the conserved positively charged amino acid residues on the concave side of F-BAR dimers reduce the ability of proteins to bind to the membrane and modify liposomes *in vitro* [16, 52].

Recent studies demonstrate that some F-BAR domains selectively bind to phosphoinositides [53, 54]. Thus, the yeast protein Rgd1p that activates Rho3 and Rho4 GTPases [55] was found to have a phosphoinositide-binding site that the other F-BAR domain yeast proteins Bzz1p and Hof1p do not have [56]. *In vitro* experiments have demonstrated that Rgd1p preferentially binds to liposomes containing PI(4,5)P₂. Deciphering of the crystal structure of the complex between Rgd1p and myo-inositol-1,2,3,4,5,6-hexakisphosphate (Ins P6), which acts as an analogue of the phosphoinositide lipid head, made it possible to identify which amino acid residues the phosphoinositide-binding site consists of.

The CIP4, FBP17, and FCHo2 proteins also exhibit specificity to phosphoinositides and contain a corresponding binding site [16, 52, 57]. The same site was revealed in human protein Gmip [58], which activates RhoA GTPase and plays a crucial role in cortical actin rearrangement during early mitosis [59] and in neuronal migration [60]. In both processes, phosphoinositides are important regulators. Hence, the specificity of the binding of some F-BAR domains to lipids enables the attraction of F-BAR domain proteins to certain membrane regions. Furthermore, binding of F-BAR domains limits the diffusion of lipids and, therefore, transmembrane proteins, which may be of crucial importance for the spatial arrangement of proteins in a specific cellular process [54, 61].

The interaction between BAR domain proteins and the membrane

The main functions of BAR domains include the **generation** of membrane curvature, its **propagation**, **stabilization**, and/or **sensing**, followed by the recruitment of cytosolic protein factors to a specific site in the cell [17]. Generation of the curvature and its propagation are coupled processes: local deformations of the membrane caused by one dimer facilitate the binding of other dimers.

The initial stages of **generation** of the membrane curvature take place due to the electrostatic binding of the BAR domain to the membrane and, in some cases, due to the incorporation of an N-terminal AH into the membrane [62]. Binding is based on the interaction between positively charged amino acids and negatively charged lipids; as mentioned above, some BAR domains preferentially bind to phosphoinositides [56]. The incorporation of AHs into one monolayer facilitates curvature generation due to the asymmetry emerging in the bilayer structure [63]. It was also demonstrated that AHs in some BAR proteins play a key role in the fragmenting of small liposomes [64]. However, the existing experimental data on the binding of BAR

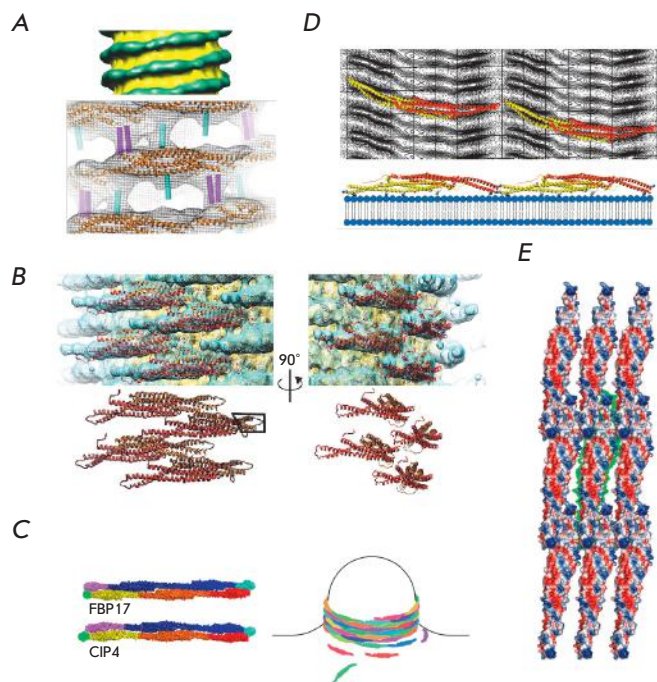


Fig. 3. Oligomerization of BAR domains on membranes. **A** – The cryo-electron microscopy model of a 28-nm membrane tubule with endophilin oligomers (top image). The BAR domain (orange) and additional helices (cyan and magenta) are fitted into the electron density [7]. **B** – Oligomerized BAR domains of amphiphysin 2 [72]. **C** – Scheme of BAR domain oligomerization and formation of membrane tubules [16]. **D** – Interactions between dimerized BAR domains of CIP4 [73]. **E** – Interactions between dimerized BAR domains of Pinkbar [45].

domains that carry no AH to membranes [65, 66] do not allow one to unambiguously answer the question about the role of AHs in the generation of membrane curvature.

Curvature **propagation** requires an interaction between many BAR domains. The structure formed by them on the membrane surface is known as a scaffold. All BAR domain proteins are believed to be capable of scaffold formation; the scaffold structure largely determines the result of the effect on the membrane. In its turn, the scaffold structure depends on the protein concentration and membrane tension. It was shown by coarse-grained molecular dynamics simulation that when present at low concentrations, N-BAR domains aggregate on flat membranes and liposomes to form a filamentary structure and networks; after a 20% surface density is achieved, they start forming a membrane protrusion [67]. N-BAR protein endophilin, whose functions are related to endocytosis, can induce tubule formation on the giant liposome at ~5% density

and low surface tension (ST). A high protein density is required for tubules to be formed at high ST values; tubule formation is completely inhibited at $ST > 0.25$ mN/m. The effect of ST on scaffold assembly is caused by the fact that the binding of dimers through their terminal regions is mediated by local membrane deformations, which are impeded by high ST values. This fact suggests that reduced ST can trigger the mechanism of activation of rapid endocytosis [68].

The sensitivity of BAR domains to membrane curvature

The investigation of the fluorescence intensity of the proteins on the membrane tubules formed by giant liposomes has shown that BAR domains can act as detectors of membrane curvature: the density of arrangement of the BAR domains bound to membrane tubules is several dozen or even hundreds of times higher than that of the BAR domains residing on a flat membrane. All the tested BAR domain proteins amphiphysin [69], endophilin [70], BIN1 [71], syndapin [65], and IRSp53 [66] have been shown to exhibit preferential binding to membrane tubules. In order to explain why BAR domains with a similar structure have different effects on membranes, let's discuss the ways in which a number of BAR domains are arranged on the membrane.

Since X-ray diffraction analysis does not provide any idea on how proteins interact with a full-size membrane, reconstructions of the oligomers of BAR domains bound to membrane tubules were obtained by cryo-electron microscopy [7, 72, 73] (Fig. 3).

Studies of the arrangement of the F-BAR domains of endophilin on the membrane tubule have demonstrated that they are oriented at a 10° angle with respect to each other [7] (Fig. 3A). The large regions of the unoccupied membrane between the neighboring bundles (~50 Å) can be attributed to the need to provide access for GTPases, with which endophilin interacts during endocytosis [74]. When full-length endophilin interacts with a membrane tubule, its SH3 domains are also arranged on the surface as dimers. This has been confirmed by experiments with cross-linking of cysteins inserted into SH3 domains [75]. It was suggested that this spatial organization can be recognized by the GTPase dynamin that carries two neighboring proline-rich sequences [75].

Another oligomeric structure that was studied using cryo-electron microscopy and helical reconstruction was the structure of the BAR domains of the amphiphysin II isoform involved in the organization of T-tubules [72] (Fig. 3B). The BAR domains of amphiphysin are more densely packed than those in the endophilin structure and in such a way that one end of the BAR domain is oriented inward into the

membrane, while the other one is oriented outwards. Unlike in endophilin, they are stably connected with one another by AHs, which presumably partake in curvature initiation. As a result, the tubules formed by amphiphysin are much more rigid. This agrees well with the biological functions of these proteins: amphiphysin forms stable T-tubules, while endophilin is involved in the formation of the dynamic structures that quickly assemble and disassemble during endocytosis [76].

X-ray crystallography was used to determine the structures of individual F-BAR domains and to propose a scheme of their interaction with membranes. In crystals, F-BAR domains form flat scaffolds where the BAR domains have a lateral orientation. The BAR domains interact with each other through the terminal and lateral regions. When interacting with the membrane, the BAR domains turn so that the curved side carrying the positively charged amino acid residues faces the membrane; the flat scaffold acquires a ring shape, and then it becomes helical and twists around the tubule being formed [16] (*Fig. 3C*). This assumption has been confirmed by cryo-electron microscopy [73] and molecular simulation data [77].

The isolated I-BAR domains can actively form the membrane curvature [33]. However, since this ability is less pronounced in full-length I-BAR proteins [41] due to autoinhibition, they can bind to the already curved membrane. The functions of membrane curvature sensing and generation are not mutually exclusive; hence, it can be assumed that protein behavior depends on its concentration: at low concentrations, they sense the existing membrane curvature and attract other proteins to it, while at high concentrations, they can aggregate into oligomers (*Fig. 3D*) and be actively involved in curvature propagation [78]. On the other hand, the I-BAR domains of the Pinkbar protein form flattened membrane regions instead of curvatures. Accordingly, although containing terminal interactions that are typical of BAR domains, their oligomers are flat (*Fig. 3E*).

Stabilization of the membrane curvature

The significance of N-terminal AHs in stabilizing interaction with lipids was established using various methods [15, 79]. In *in vitro* experiments, the absence of AHs made endophilin unable to modify liposomes and form tubules. This has also been demonstrated by molecular dynamics simulation [7]. A more recent study by electron paramagnetic resonance showed that endophilin AHs penetrate into the lipid bilayer by 8–11 Å below the level of phosphate groups and are not in direct contact with each other [80]. A hypothesis has been put forward that the importance of AHs for protein oli-

gomerization can be possibly related to the mutual coordination of lipids. Incorporation of AHs into the top lipid monolayer results in the generation of a positive membrane curvature, due to the asymmetry emerging in the bilayer structure.

The endophilin structure determined by cryo-electron microscopy indicated that the insertions of neighboring (parallel to the long axis of the tubule) dimers do not interact with each other and are oriented towards the membrane. This differentiated them from the arrangement in the crystal structure and in the liposome-bound state. The difference was later attributed to two conformational states: at high protein concentrations sufficient for oligomer formation, the N-BAR domain resides closer to the membrane, thus contributing to a deeper incorporation of AH [80], impeding spontaneous membrane curvature, and stabilizing the membrane tubule. The conformational switch between endophilin states can be associated with the phosphorylation of Ser75: the emergence of a negative charge impedes the incorporation of AH into the membrane and tubule stabilization. The mutations in LRRK2 kinase associated with Parkinson's disease are known to increase the phosphorylation of Ser75 and cause the disruption of endocytosis in synapses [81].

In addition to attracting partner proteins, the SH3 domain of endophilin regulates the activity of the N-BAR domain. It was demonstrated by a molecular dynamics simulation that the SH3 domain in solution binds to the N-terminal AH due to hydrophobic interactions and the formation of salt bridges between charged residues [8]. The negative electrostatic potential concentrates at the SH3 domain, whereas the positive potential concentrates at the AH. Hence, when a protein approaches the membrane the AH turns towards it, while the SH3 domain turns away from it. On the one hand, the SH3 domain in this autoinhibited form does not interact with other proteins in solution. On the other hand, the protein “searches” for the region in the membrane that would be suitable in terms of electrostatic potential and would have defects in lipid packing, where the AH can be incorporated.

Recently there has been evidence that not all BAR domains exhibit activity in the formation of membrane tubules or membrane invagination. The yeast protein Cdc15p involved in cytokinesis oligomerizes into filaments and does not cause membrane modification [82]. Oligomerization of Cdc15p is needed for a contractile ring to form; however, in this case the protein does not change the membrane's shape but only helps attract other proteins to it. Lack of tube-forming ability was also demonstrated for six mammalian F-BAR domains. The common function of F-BAR domain proteins possibly consists in the attraction and spatial

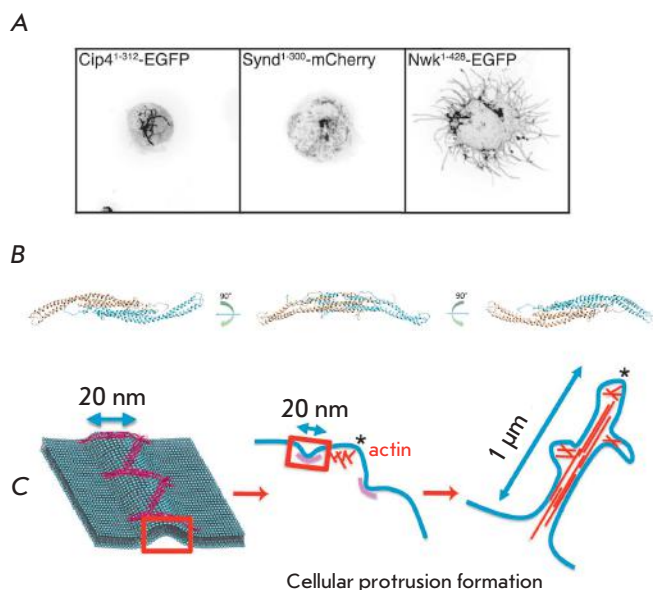


Fig. 4. Noncanonical activity of the F-BAR domain of Nwk [92]. **A** – Formation of inner membrane tubules caused by the expression of typical F-BAR domains and formation of cellular protrusions in the case of the F-BAR domain of Nwk. **B** – Model of the F-BAR domain of Nwk (monomers are shown in different colors). **C** – Model of cellular protrusion formation caused by F-BAR domain oligomerization and actin polymerization.

arrangement of other proteins near the membrane, and only in some cases do they change the membrane shape [83]. The F-BAR domain protein Nervous wreck (Nwk), whose homologues are found in many organisms, from insects to higher vertebrates, is one of such proteins. Two homologues of this protein are involved in membrane rearrangements in mammalian stereocilia and cerebellar neurons [84, 85].

Nontraditional orientation: The F-BAR domain protein Nervous wreck

Neuronal growth and the formation of new connections, the processes underlying learning and memory, are controlled by growth factors. Receptors bound to growth factors are moved inside the cell by endocytosis and sent to special cellular compartments, where they can undergo modification or degradation, or interact with other proteins [86]. Determining the mechanisms that control the rate and direction of the flow of receptor-containing endosomes is essential for understanding the signal transduction processes. The neuromuscular junction of *Drosophila melanogaster* is a convenient model for studying synaptic growth regulation, since the muscle area increases more than one hundredfold

within four days, which is accompanied by a significant increase in the number of neuronal contacts. Neuronal growth regulation includes both the retrograde signals from the muscle and anterograde signals from the neuron to the muscle cell [87]. Mutations in the proteins regulating endocytosis are known to result in excessive axon branching, since they impede the attenuation of the signal from growth factor receptors [88–90].

The F-BAR protein Nervous wreck (Nwk) exhibits limited homology to other F-BAR proteins. *In vitro* studies have shown that, unlike other F-BAR proteins, Nwk causes the formation of cellular protrusions rather than invaginations (Fig. 4A) [91].

In order to study the interaction between the Nwk F-BAR domain and the membrane, its model was built based on the known crystal structure of the homologous F-BAR domain FCHO2, which has a specific S-shape [92] (Fig. 4B). Electron microscopy was used to study the ways in which the F-BAR domains of the Cip4 and Nwk proteins were organized on lipids. As expected, the Cip4 F-BAR domains were found to aggregate into linear filaments, while the Nwk F-BAR domains were found to form higher order V-, N-shaped, and zigzag structures [92]. It is important to mention that these structures were not observed in the absence of lipids. The mechanism of interaction between Nwk and membranes was proposed based on these findings. The zigzag structures form a “ridge” on the membrane whose geometry depends on the angle between the dimers and the frequency of the dimers with the concave side facing the membrane. In cells, this ridge can form a ring marking the membrane region that is subsequently transformed into a cellular protrusion by microtubules and actin filaments (Fig. 4C) [92].

The end regions of the dimer that are responsible for oligomerization and electrostatic interactions between the membrane and the concave side of F-BAR play a crucial role in this process [92]. Protrusion formation also requires actin filament polymerization; however, the protrusions that have already formed do not respond to treatment with the actin polymerization inhibitor latrunculin B. This fact indicates that actin is required for their formation only [93]. Interestingly, the structure of the emerged protrusions differs from that of filopodia, since the protrusions contain microtubules, along with actin filaments. Treatment with the microtubule depolymerizing agent nocodazole also does not destroy the protrusions.

The functioning of Nwk in neurons is apparently ensured not only by its F-BAR domain, but also by two SH3 domains, each of them binding to certain proteins. Nwk in recycling endosomes interacts with the SNX16 protein belonging to the sorting nexin

family, which, in its turn, is bound to the presynaptic growth factor Tkv [94]. The interaction between Nwk and SNX16 reduces the signal from Tkv and is needed to ensure the receptor's return onto the membrane. Furthermore, Nwk binds to the proteins involved in endocytosis regulation (Dap160, dynamin, and Wsp). Experiments with the mutant SH3a and SH3b domains showed that SH3a binds to dynamin and Wsp, while SH3b is responsible for binding to Dap160 [95]. Wsp activates the Arp2/3 complex, which triggers actin polymerization that is required for endocytosis [96]. However, Nwk activates Wsp in a much weaker fashion than the mammalian SH3 domain proteins (e.g., Nck) activate WASP [97]. The effect can be enhanced by the co-action of Nwk and another activator of Wsp, Cdc42 GTPase. Hence, Nwk interacts with the endocytic machinery through SH3 domains and, together with Cdc42, activates Wsp/Arp2-3-dependent actin polymerization for synaptic growth regulation.

Another important function of Nwk SH3 domains is the regulation of F-BAR activity. The SH3b domain was shown to bind to F-BAR; however, this does not result in a loss of its membrane-binding ability but only increases the amount of the negatively charged lipids needed for binding [10]. Both the F-BAR domain itself and the full-length protein modify giant liposomes; however, their excessively high negative charge prevents membrane deformation [10]. One of the possible explanations is that at lower PI(4,5)P₂ concentrations, most F-BAR domains are bound to the membrane by their concave side, which facilitates deformation. On the other hand, it is quite possible that the reason lies in changes in the properties of the membrane itself. The increased PI(4,5)P₂ concentration in the membrane leads to a rise in the degree of order of lipids, which is characterized by an alignment of hydrocarbon tails, increased bilayer thickness, decreased lateral diffusion coefficient, etc. [98, 99]. The

formation of these lipids microdomains may impede membrane deformation or the dynamic migration of proteins that is required for oligomerization [100]. The membrane composition can regulate other BAR domain proteins in a similar way: the increased PI(4,5)P₂ concentration suppresses the membrane-deforming activity of the F-BAR domain FBP17 in *in vivo* experiments [101]. Binding of SH3 domains to F-BAR was previously believed to result in complete autoinhibition, which can be eliminated either by binding to other proteins [102] or by increasing the negative charge in the membrane [103]. However, the example of Nwk indicates that this mechanism is more complex and requires further research.

CONCLUSIONS

Deciphering the crystal structures of BAR domains has made it possible to describe the mechanisms of changes in the membrane shape at the molecular level, while *in vitro* studies and electron microscopy have allowed researchers to explain how the schemes of oligomerization of BAR domains result in the formation of various membrane structures. It has been demonstrated how the activity of some BAR domain proteins can be regulated by intra-protein and protein-protein interactions, as well as what the mechanism for achieving a specificity of partner protein recruitment is. However, despite the significant progress in understanding the role of BAR domain proteins in cell activity, many questions still remain to be answered. Taking into account that changes in the expression level and mutations in the genes encoding BAR domain proteins are related to many serious diseases, this field of research is of interest both for biology and medicine. ●

This work was supported by the Russian Science Foundation (grant no. 14-14-00234).

REFERENCES

1. Sakamuro D., Elliott K.J., Wechsler-Reya R., Prendergast G.C. // *Nat. Genet.* 1996. V. 14. № 1. P. 69–77.
2. Qualmann B., Koch D., Kessels M.M. // *EMBO J.* 2011. V. 30. P. 3501–3515.
3. Padrick S.B., Cheng H.C., Ismail A.M., Panchal S.C., Doolittle L.K., Kim S., Skehan B.M., Umetani J., Brautigam C.A., Leong J.M., et al. // *Mol. Cell.* 2008. V. 32. № 3. P. 426–438.
4. Itoh T., De Camilli P. // *Biochim. Biophys. Acta – Mol. Cell Biol. Lipids.* 2006. V. 1761. № 8. P. 897–912.
5. Ferguson S.M., Brasnjo G., Hayashi M., Wölfel M., Collesi C., Giovedi S., Raimondi A., Gong L., Ariel P., Paradise S., et al. // *Science.* 2007. V. 316. № 5824. P. 570–574.
6. Solomaha E., Szeto F.L., Yousef M.A., Palfrey H.C. // *J. Biol. Chem.* 2005. V. 280. № 24. P. 23147–23156.
7. Mim C., Cui H., Gawronski-Salerno J.A., Frost A., Lyman E., Voth G.A., Unger V.M. // *Cell.* 2012. V. 149. № 1. P. 137–145.
8. Vázquez F.X., Unger V.M., Voth G.A. // *Biophys. J.* 2013. V. 104. № 2. P. 396–403.
9. Rao Y., Ma Q., Vahedi-Faridi A., Sundborger A., Pechstein A., Puchkov D., Luo L., Shupliakov O., Saenger W., Haucke V. // *Proc. Natl. Acad. Sci. USA.* 2010. V. 107. № 18. P. 8213–8218.
10. Kelley C.F., Messelaar E.M., Eskin T.L., Sokolova O.S., Nicastro D., Rodal A.A., Kelley C.F., Messelaar E.M., Eskin T.L., Wang S., et al. // *CellReports.* 2015. V. 13. № 11. P. 1–13.
11. Rocca D.L., Martin S., Jenkins E.L., Hanley J.G. // *Nat. Cell Biol.* 2008. V. 10. № 3. P. 259–271.
12. Cao M., Xu J., Shen C., Kam C., Hagan R.L., Xia J. // *J. Neurosci.* 2007. V. 27. № 47. P. 12945–12956.
13. The UniProt Consortium. // *Nucl. Acids Res.* 2013. V. 41. Database issue. P. D43–D47.

REVIEWS

14. Berman H.M., Westbrook J., Feng Z., Gilliland G., Bhat T.N., Weissig H., Shindyalov I.N., Bourne P.E. // *Nucl. Acids Res.* 2000. V. 28. № 1. P. 235–242.
15. Peter B.J., Kent H.M., Mills I.G., Vallis Y., Butler P.J.G., Evans P.R., McMahon H.T. // *Science*. 2004. V. 303. № 5657. P. 495–499.
16. Shimada A., Niwa H., Tsujita K., Suetsugu S., Nitta K., Hanawa-Suetsugu K., Akasaka R., Nishino Y., Toyama M., Chen L., et al. // *Cell*. 2007. V. 129. № 4. P. 761–772.
17. Frost A., Unger V.M., De Camilli P. // *Cell*. 2009. V. 137. № 2. P. 191–196.
18. Kessels M.M., Qualmann B. // *J. Cell Sci.* 2015. P. 1–9.
19. David C., McPherson P.S., Mundigl O., de Camilli P. // *Proc. Natl. Acad. Sci. USA*. 1996. V. 93. № 1. P. 331–335.
20. Lee E., Marcucci M., Daniell L., Pypaert M., Weisz O.A., Ochoa G.-C., Farsad K., Wenk M.R., De Camilli P. // *Science*. 2002. V. 297. № 5584. P. 1193–1196.
21. Razzaq A., Robinson I.M., McMahon H.T., Skepper J.N., Su Y., Zelhof A.C., Jackson A.P., Gay N.J., Kane C.J.O. // *Genes Dev.* 2001. V. 15. P. 2967–2979.
22. Nicot A.S., Toussaint A., Tosch V., Kretz C., Wallgren-Pettersson C., Iwarsson E., Kingston H., Garnier J.M., Biancalana V., Oldfors A., Mandel J.L., Laporte J. // *Nat. Genet.* 2007. V. 39(9). P. 1134–1139.
23. Tarricone C., Xiao B., Justin N., Walker P.A., Rittinger K., Gamblin S.J., Smerdon S.J. // *Nature*. 2001. V. 411. № 6834. P. 215–219.
24. Weissenhorn W. // *J. Mol. Biol.* 2005. V. 351. № 3. P. 653–661.
25. Ringstad N., Gad H., Löw P., Di Paolo G., Brodin L., Shupliakov O., De Camilli P. // *Neuron*. 1999. V. 24. № 1. P. 143–154.
26. Guichet A., Wucherpfennig T., Dudu V., Etter S., Wilsch-Bräuniger M., Hellwig A., González-Gaitán M., Huttner W.B., Schmidt A.A. // *EMBO J.* 2002. V. 21. № 7. P. 1661–1672.
27. Gallop J.L., Jao C.C., Kent H.M., Butler P.J.G., Evans P.R., Langen R., McMahon H.T. // *EMBO J.* 2006. V. 25. № 12. P. 2898–2910.
28. Yamagishi A., Masuda M., Ohki T., Onishi H., Mochizuki N. // *J. Biol. Chem.* 2004. V. 279. № 15. P. 14929–14936.
29. Mattila P.K., Pykäläinen A., Saarikangas J., Paavilainen V.O., Vihinen H., Jokitalo E., Lappalainen P. // *J. Cell Biol.* 2007. V. 176. № 7. P. 953–964.
30. Suetsugu S., Murayama K., Sakamoto A., Hanawa-Suetsugu K., Seto A., Oikawa T., Mishima C., Shirouzu M., Takenawa T., Yokoyama S. // *J. Biol. Chem.* 2006. V. 281. № 46. P. 35347–35358.
31. Millard T.H., Bompard G., Heung M.Y., Dafforn T.R., Scott D.J., Machesky L.M., Fütterer K. // *EMBO J.* 2005. V. 24. № 2. P. 240–250.
32. Lee S.H., Kerff F., Chereau D., Ferron F., Klug A., Dominguez R. // *Structure*. 2007. V. 15. № 2. P. 145–155.
33. Saarikangas J., Zhao H., Pykäläinen A., Laurinmäki P., Mattila P.K., Kinnunen P.K.J., Butcher S.J., Lappalainen P. // *Curr. Biol.* 2009. V. 19. № 2. P. 95–107.
34. Kim M.-H., Choi J., Yang J., Chung W., Kim J.-H., Paik S.K., Kim K., Han S., Won H., Bae Y.-S., et al. // *J. Neurosci.* 2009. V. 29. № 5. P. 1586–1595.
35. Krugmann S., Jordens I., Gevaert K., Driessens M., Vandekerckhove J., Hall A. // *Curr. Biol.* 2001. V. 11. № 21. P. 1645–1655.
36. Scita G., Confalonieri S., Lappalainen P., Suetsugu S. // *Trends Cell Biol.* 2008. V. 18. P. 52–60.
37. Robens J.M., Yeow-Fong L., Ng E., Hall C., Manser E. // *Mol. Cell. Biol.* 2010. V. 30. № 3. P. 829–844.
38. Millard T.H., Dawson J., Machesky L.M. // *J. Cell Sci.* 2007. V. 120. № 9. P. 1663–1672.
39. Lee Y.-G., Macoska J.A., Korenchuk S., Pienta K.J. // *Neoplasia*. 2002. V. 4. № 4. P. 291–294.
40. Machesky L.M., Johnston S.A. // *J. Mol. Med. (Berl.)*. 2007. V. 85. № 6. P. 569–576.
41. Woodings J.A., Sharp S.J., Machesky L.M. // *Biochem. J.* 2003. V. 371. Pt 2. P. 463–471.
42. Wang Y., Zhou K., Zeng X., Lin J., Zhan X. // *J. Biol. Chem.* 2007. V. 282. № 10. P. 7624–7631.
43. Bershteyn M., Atwood S.X., Woo W.M., Li M., Oro A.E. // *Dev. Cell*. 2010. V. 19. № 2. P. 270–283.
44. Saarikangas J., Hakanen J., Mattila P.K., Grumet M., Salminen M., Lappalainen P. // *J. Cell Sci.* 2008. V. 121. P. 1444–1454.
45. Pykäläinen A., Boczkowska M., Zhao H., Saarikangas J., Rebowski G., Jansen M., Hakanen J., Koskela E.V., Peränen J., Vihinen H., et al. // *Nat. Struct. Mol. Biol.* 2011. V. 18. № 8. P. 902–907.
46. Heath R.J.W., Insall R.H. // *J. Cell Sci.* 2008. V. 121. № 12. P. 1951–1954.
47. Dent E.W., Kwiatkowski A.V., Mebane L.M., Philippart U., Barzik M., Rubinson D.A., Gupton S., van Veen J.E., Furman C., Zhang J., et al. // *Nat. Cell Biol.* 2007. V. 9. № 12. P. 1347–1359.
48. Tanaka E., Sabry J. // *Cell*. 1995. V. 83. № 2. P. 171–176.
49. Machesky L.M. // *FEBS Lett.* 2008. V. 582. № 14. P. 2102–2111.
50. Liu S., Xiong X., Zhao X., Yang X., Wang H. // *J. Hematol. Oncol.* 2015. V. 8. № 1. P. 1–14.
51. Aspenström P. // *Curr. Biol.* 1997. V. 7. № 7. P. 479–487.
52. Tsujita K., Suetsugu S., Sasaki N., Furutani M., Oikawa T., Takenawa T. // *J. Cell Biol.* 2006. V. 172. № 2. P. 269–279.
53. Wang Q., Navarro M.V.A.S., Peng G., Molinelli E., Goh S.L., Judson B.L., Rajashankar K.R., Sondermann H. // *Proc. Natl. Acad. Sci. USA*. 2009. V. 106. № 31. P. 12700–12705.
54. Zhao H., Michelot A., Koskela E.V., Tkach V., Stamou D., Drubin D.G., Lappalainen P. // *Cell Rep.* 2013. V. 4. № 6. P. 1213–1223.
55. Roumanie O., Peypouquet M.F., Bonneau M., Thoraval D., Doignon F., Crouzet M. // *Mol. Microbiol.* 2000. V. 36. № 6. P. 1403–1414.
56. Moravcevic K., Alvarado D., Schmitz K.R., Kenniston J.A., Mendrola J.M., Ferguson K.M., Lemmon M. // *Structure*. 2015. V. 23. № 2. P. 352–363.
57. Henne W.M., Kent H.M., Ford M.G., Hegde B.G., Daumke O., Butler P.J., Mittal R., Langen R., Evans P.R., McMahon H.T. // *Structure*. 2007. V. 15. № 7. P. 839–852.
58. Aresta S., de Tand-Heim M.-F., Beranger F., de Gunzburg J. // *Biochem. J.* 2002. V. 367. № 1. P. 57–65.
59. Andrieu G., Quaranta M., Leprince C., Cuvillier O., Hatzoglou A. // *Carcinogenesis*. 2014. V. 35. № 11. P. 2503–2511.
60. Ota H., Hikita T., Sawada M., Nishioka T., Matsumoto M., Komura M., Ohno A., Kamiya Y., Miyamoto T., Asai N., et al. // *Nat. Commun.* 2014. V. 5. № 5. P. 4532.
61. Tanaka-Takiguchi Y., Itoh T., Tsujita K., Yamada S., Yanagisawa M., Fujiwara K., Yamamoto A., Ichikawa M., Takiguchi K. // *Langmuir*. 2013. V. 29. № 1. P. 328–336.
62. Isas J.M., Ambroso M.R., Hegde P.B., Langen J., Langen R. // *Structure*. 2015. V. 23. № 5. P. 873–881.
63. McMahon H.T., Boucrot E. // *J. Cell Sci.* 2015. V. 128. № 6. P. 1065–1070.
64. Boucrot E., Pick A., Çamdere G., Liska N., Evergren E., McMahon H.T., Kozlov M.M. // *Cell*. 2012. V. 149. № 1.

- P. 124–136.
65. Ramesh P, Baroji Y.F, Reihani S.N.S, Stamou D, Oddershede L.B, Bendix P.M. // *Sci. Rep.* 2013. V. 3. P. 1565.
66. Prévost C., Zhao H., Manzi J., Lemichez E., Lappalainen P., Callan-Jones A., Bassereau P. // *Nat. Commun.* 2015. V. 6. P. 8529.
67. Simunovic M., Voth G.A. // *Nat. Commun.* 2015. V. 6. P. 7219.
68. Shi Z., Baumgart T. // *Nat. Commun.* 2015. V. 6. P. 5974.
69. Sorre B., Callan-Jones A., Manzi J., Goud B., Prost J., Bassereau P., Roux A. // *Proc. Natl. Acad. Sci. USA.* 2012. V. 109. № 1. P. 173–178.
70. Zhu C., Das S.L., Baumgart T. // *Biophys. J.* 2012. V. 102. № 8. P. 1837–1845.
71. Wu T., Shi Z., Baumgart T. // *PLoS One.* 2014. V. 9. № 4. P. e93060.
72. Adam J., Basnet N., Mizuno N. // *Sci. Rep.* 2015. V. 5. P. 15452.
73. Frost A., Perera R., Roux A., Spasov K., Destaing O., Egelman E.H., De Camilli P., Unger V.M. // *Cell.* 2008. V. 132. № 5. P. 807–817.
74. Ringstad N., Nemoto Y., De Camilli P. // *Proc. Natl. Acad. Sci. USA.* 1997. V. 94. № 16. P. 8569–8574.
75. Faelber K., Posor Y., Gao S., Held M., Roske Y., Schulze D., Haucke V., Noé F., Daumke O. // *Nature.* 2011. V. 477. № 7366. P. 556–560.
76. Mizuno N., Jao C.C., Langen R., Steven A.C. // *J. Biol. Chem.* 2010. V. 285. № 30. P. 23351–23358.
77. Levitsova O.V., Davletov I.D., Sokolova O.S., Shaitan K.V. // *Biophysics.* 2011. V. 56. №2. P.242–247.
78. Zhao H., Pykäläinen A., Lappalainen P. // *Curr. Opin. Cell Biol.* 2011. V. 23. № 1. P. 14–21.
79. Cui H., Mim C., Vázquez F.X., Lyman E., Unger V.M., Voth G.A. // *Biophys. J.* 2013. V. 104. № 2. P. 404–411.
80. Ambroso M.R., Hegde B.G., Langen R. // *Proc. Natl. Acad. Sci. USA.* 2014. V. 111. № 19. P. 6982–6987.
81. Matta S., van Kolen K., da Cunha R., van den Bogaart G., Mandemakers W., Miskiewicz K., De Bock P.-J., Morais V.A., Vilain S., Haddad D., et al. // *Neuron.* 2012. V. 75. № 6. P. 1008–1021.
82. McDonald N.A., Vander Kooi C.W., Ohi M.D., Gould K.L. // *Dev. Cell.* 2015. V. 35. № 6. P. 725–736.
83. Traub L.M. // *Dev. Cell.* 2015. V. 35. № 6. P. 664–666.
84. Cao H., Yin X., Cao Y., Jin Y., Wang S., Kong Y., Chen Y., Gao J., Heller S., Xu Z. // *PLoS One.* 2013. V. 8. № 2. P. 1–11.
85. Sun X., Pinacho R., Saia G., Punko D., Meana J.J., Ramos B., Gill G. // *Dev. Neurobiol.* 2015. V. 75. № 1. P. 93–108.
86. Sadowski L., Pilecka I., Miaczynska M. // *Exp. Cell Res.* 2009. V. 315. № 9. P. 1601–1609.
87. Collins C.A., DiAntonio A. // *Curr. Opin. Neurobiol.* 2007. V. 17. № 1. P. 35–42.
88. Dickman D.K., Lu Z., Meinertzhagen I.A., Schwarz T.L. // *Curr. Biol.* 2006. V. 16. № 6. P. 591–598.
89. Khodosh R., Augsburger A., Schwarz T.L., Garrity P.A. // *Development.* 2006. V. 133. № 23. P. 4655–4665.
90. Wang X., Shaw W.R., Tsang H.T.H., Reid E., O’Kane C.J. // *Nat. Neurosci.* 2007. V. 10. № 2. P. 177–185.
91. Cherbas L., Willingham A., Zhang D., Yang L., Zou Y., Eads B.D., Carlson J.W., Landolin J.M., Kapranov P., Dumais J., et al. // *Genome Res.* 2011. V. 21. № 2. P. 301–314.
92. Becalska A.N., Kelley C.F., Berciu C., Stanishneva-Kononova T.B., Fu X., Wang S., Sokolova O.S., Nicastro D., Rodal A.A. // *Mol. Biol. Cell.* 2013. V. 24. № 15. P. 2406–2418.
93. Kelley C.F., Becalska A.N., Berciu C., Nicastro D., Rodal A.A. // *Commun. Integr. Biol.* 2015. V. 8. № 2. P. e1000703.
94. Rodal A.A., Blunk A.D., Akbergenova Y., Jorquera R.A., Buhl L.K., Littleton J.T. // *J. Cell Biol.* 2011. V. 193. № 1. P. 201–217.
95. Rodal A.A., Motola-Barnes R.N., Littleton J.T. // *J. Neurosci.* 2008. V. 28. № 33. P. 8316–8325.
96. Kaksonen M., Toret C.P., Drubin D.G. // *Nat. Rev. Mol. Cell Biol.* 2006. V. 7. № 6. P. 404–414.
97. Tomasevic N., Jia Z., Russell A., Fujii T., Hartman J.J., Clancy S., Wang M., Beraud C., Wood K.W., Sakowicz R. // *Biochemistry.* 2007. V. 46. № 11. P. 3494–3502.
98. Stanishneva-Kononova T.B., Sokolova O.S. // *Comput. Theor. Chem.* 2015. V. 1058. P. 61–66.
99. Lupyan D., Mezei M., Logothetis D.E., Osman R. // *Biophys. J.* 2010. V. 98. № 2. P. 240–247.
100. Ruiz-Herrero T., Hagan M.F. // *Biophys. J.* 2015. V. 108. № 3. P. 585–595.
101. Tsujita K., Takenawa T., Itoh T. // *Nat. Cell Biol.* 2015. V. 17. № 6. P. 749–758.
102. Roberts-Galbraith R.H., Gould K.L. // *Cell Cycle.* 2010. V. 9. № 20. P. 4091–4097.
103. Wu T., Baumgart T. // *Biochemistry.* 2014. V. 53. № 46. P. 7297–7309.

Design of Stable α -Helical Peptides and Thermostable Proteins in Biotechnology and Biomedicine

A.P. Yakimov^{1,2}, A.S. Afanaseva^{1,2}, M.A. Khodorkovskiy¹, M.G. Petukhov^{1,2}

¹Peter the Great St. Petersburg Polytechnic University, Polytechnicheskaya Str., 29, St. Petersburg 195251, Russia

²Petersburg Nuclear Physics Institute, National Research Center "Kurchatov Institute", Orlova Roscha, 1, Gatchina, 188300, Russia

*E-mail: yaleks@nanobio.spbstu.ru

Received June 19, 2016; in final form, September 28, 2016

Copyright © 2016 Park-media, Ltd. This is an open access article distributed under the Creative Commons Attribution License, which permits unrestricted use, distribution, and reproduction in any medium, provided the original work is properly cited.

ABSTRACT α -Helices are the most frequently occurring elements of the secondary structure in water-soluble globular proteins. Their increased conformational stability is among the main reasons for the high thermal stability of proteins in thermophilic bacteria. In addition, α -helices are often involved in protein interactions with other proteins, nucleic acids, and the lipids of cell membranes. That is why the highly stable α -helical peptides used as highly active and specific inhibitors of protein-protein and other interactions have recently found more applications in medicine. Several different approaches have been developed in recent years to improve the conformational stability of α -helical peptides and thermostable proteins, which will be discussed in this review. We also discuss the methods for improving the permeability of peptides and proteins across cellular membranes and their resistance to intracellular protease activity. Special attention is given to the SEQOPT method (<http://mml.spbstu.ru/services/seqopt/>), which is used to design conformationally stable short α -helices.

KEYWORDS α -helix, conformational stability, factors of thermal stability, membrane permeability, resistance to intracellular proteolysis

ABBREVIATIONS SEQOPT – method for α -helix amino acid sequence optimization; MD – molecular dynamics method; HC – α -helix content, PDB – protein database; AGADIR, ALB, HELIX – the statistical mechanical models describing the conformational α -helix-coil transitions in short monomeric peptides, CD – circular dichroism spectroscopy

INTRODUCTION

Not only have the numerous studies focused on α -helical peptides that have been conducted over the past quarter century contributed to a better understanding of protein folding into the native biologically active conformation, but also they are of significant interest for designing therapeutic agents that are efficient in treating diseases associated with a disruption of the protein-protein interaction [1–3]. Since the early 1990s, a large body of experimental data on the folding and stability of α -helices in monomeric peptides has been accumulated [4, 5]. These data demonstrate that the amino acid sequences of α -helices are usually not optimal for ensuring high conformational stability. This can be an important factor in preventing the accumulation of erroneous intermediate products in the folding of globular proteins. Hence, designing short α -helical peptides and proteins with sufficient conformational stability under specified ambient conditions (tempera-

ture, pH, and ionic strength) still remains an interesting problem of practical importance in protein engineering [1, 6].

The large amount of experimental data on the physical interactions that affect the stability of α -helices in proteins and monomeric peptides allows researchers to build theoretical models that describe α -helix-coil transitions and use them to elaborate new high-efficiency computational methods for designing α -helical peptides characterized by high conformational stability.

Stabilization of α -helices has been employed repeatedly to design industrially relevant enzymes that can work at elevated temperatures [7, 8]. This review discusses various methods for enhancing the thermal stability of globular proteins, including such molecular mechanisms as changing the amino acid composition of proteins in thermophilic organisms, inserting additional ion pairs and hydrogen bonds, using amino acids with an increased propensity to α -helical conformation, for-

mation of additional disulfide bridges, strengthening of the hydrophobic interactions, introducing proline substitutions in loops, binding to metal ions, denser packing, etc.

THE MOLECULAR MECHANISMS OF THERMAL STABILITY OF PROTEINS

Thermostable enzymes are used in many biotechnological processes, both in laboratory and in large-scale industrial production [9, 10].

Hyperthermophilic microorganisms that grow optimally at 80–110°C are the natural source of thermophilic proteins. These organisms, which were originally discovered in hot springs, mainly belong to the Archaea kingdom. The enzymes in these organisms also exhibit optimum activity at high temperatures (>70°C), and some of them are active at temperatures significantly higher than 100°C. Thermostable enzymes are usually inactive at temperatures below 40°C [11].

The ability to reliably predict the key physicochemical properties of mutant proteins, such as stability and solubility in water, is of paramount importance in molecular biology and biotechnology. A number of studies have been published where factors affecting the stability and solubility of proteins were investigated and models for predicting the consequences of point mutations in proteins were elaborated [11–14]. Today, it is clear that there are many factors that can disrupt the stability or activity of a protein structure.

The features of the structural organization of thermostable proteins and enzymes that allow them to function at temperatures above 100°C have been intensively investigated both in experimental and fundamental studies, starting from the mid-1980s (according to the Medline database, a total of ~3,000 studies have been published) [12, 15–18].

The discussion is based on a comparative analysis of homologous proteins from mesophilic and thermophilic microorganisms (further in this review referred to as mesophilic and thermophilic proteins, respectively). The thermostable proteins described by that time showed no specific features in their secondary or tertiary structures that were typical only of thermophiles as compared to their mesophilic analogues. However, the differences revealed at the level of their amino acid sequences were rather diverse. Such a variety of the characteristics of thermostable proteins can be grounded in the fact that thermophilicity is determined by a summation of the effects of various factors emerging due to a suitable combination of the weak interactions involved in protein stabilization.

It has been recently demonstrated that the mechanisms of adaptation to high temperatures in different organisms may depend on their evolutionary history

[19]. Moreover, amino acid substitutions, presumably those associated with the thermal resistance of proteins, were found to often reside in α -helices [20–22]. Therefore, an analysis of the energy balance of molecular interactions inside α -helices may shed light on the reasons behind the stability of thermophilic proteins at high temperatures.

Changes in the amino acid composition of proteins in thermophilic organisms

Changes in the amino acid composition of proteins in thermophilic organisms compared to their mesophilic analogues were among the first factors affecting thermal stability that were studied [23, 24]. A statistical analysis demonstrated that glycine, serine, lysine, and the aspartic acid residues in thermophilic proteins are often replaced with alanine, threonine, arginine, and glutamic acid, respectively [25]. The function of these substitutions mainly consists in increasing the internal and reducing the external hydrophobicity of thermostable proteins. Moreover, these substitutions somewhat increase the stability of α -helices and the packing density of amino acids in thermostable proteins. A number of additional studies focused on various physical factors that can alter the amino acid composition of thermophilic proteins have recently been performed (see the review devoted to this topic [18]).

We have demonstrated in a series of studies [26–28] that the α -helices of thermostable proteins are in general more conformationally stable than the identical α -helices of highly homologous proteins in mesophilic and psychrophilic bacteria. The composition of the α -helices of thermostable proteins changes due to an increase in their content of amino acids with a high propensity to form α -helices (alanine and leucine) and, therefore, a decrease in their content of β -branched residues (valine, isoleucine, and threonine). Furthermore, a significant rise in the abundance of amino acids that can stabilize α -helices through strong interactions between their side chains and the side chains of other amino acids (e.g., glutamic acid and arginine) was detected. Similar findings were also made in a study performed by a different research group; particularly, a significant decrease in the content of β -branched residues with a low tendency to form α -helices in thermophilic proteins was also revealed [29].

Matthews et al. [30] demonstrated that the introduction of proline residues increases the thermal stability of a protein due to a decrease in the entropy of the unfolded state.

Additional hydrophobic interactions are the crucial mechanism behind structure stabilization in thermostable proteins. It has been shown that every additional methyl group inserted into a protein structure on aver-

age increases the stability of the folded protein conformation by ~ 1.3 (± 0.5) kcal/mol [31].

Ion pairs and binding to metal ions

Comparison of the spatial structures of thermophilic proteins and their analogues from mesophilic organisms has demonstrated that thermophilic proteins have a significantly higher number of ion pairs, which considerably stabilizes their structure at high temperatures [32]. One of the most vivid illustrations of this phenomenon is the content of ion pairs observed in hyperthermophilic lumazine synthase from *Aquifexae olivicus*, which was more than 90% higher than that in its mesophilic analogue from *Bacillus subtilis* [33].

It has been known for a long time that metal ions often stabilize and activate certain enzymes. Hence, xylose isomerase from *Streptomyces rubiginosus* binds to two ions from the set of Co^{2+} , Mg^{2+} or Mn^{2+} : one of them is directly involved in catalysis, while the other one predominantly participates in the stabilization of the enzyme structure [34]. Some thermostable ferredoxins have been shown to contain metal ions that are not found in their mesophilic homologues [35].

Increase in the number of noncovalent interactions

It is believed that an increase in the nonlocal noncovalent interactions (e.g., ion pairs, hydrogen bonds, and van der Waals contacts) binding the non-adjacent portions of proteins can significantly increase their thermal stability. Recently accumulated data generally prove this hypothesis. Hence, chimeras are built using the homologous proteins rubredoxins from *Pyrococcus furiosus* and *Clostridium pasteurianum* [36]. The relative stability of these chimeras as compared to rubredoxins from *P. furiosus* and *C. pasteurianum* indicate that there are interactions between the protein nucleus and one of the β -sheets via hydrogen bonding and hydrophobic interactions, which makes a considerable contribution to the thermal stability of the protein. Neither the nucleus nor the β -sheet separately ensures the required stabilization. A comparison of identical proteins from the thermophilic and mesophilic organisms (373 protein pairs http://phys.protres.ru/resources/termo_meso_base.html) has shown that the former have a closely packed water-accessible residues, while the packing of the interior parts of these proteins are almost identical in both cases [37].

Hydrogen bonds

Another factor of the type is the formation of additional hydrogen bonds that stabilize the structure of a number of thermostable proteins at high temperatures [38–40]. In particular, an investigation of the mechanism of action of hydrogen bonds on the thermal stability of RNase T1 has shown that every addi-

tional hydrogen bond increases the thermal stability of this protein by on average 1.3 kcal/mol [38]. Tanner et al. [39] revealed a strong correlation between the thermal stability of the GAPDH protein (glyceraldehyde-3-phosphate dehydrogenase) and the number of hydrogen bonds between the polar uncharged amino acid residues in it. An assumption was made that there are two main reasons that explain what effect the existence of additional hydrogen bonds may have on the thermal stability of the protein: 1) the dehydration energy of these residues is much lower than that of the charged residues in ion pairs, and 2) the gain in enthalpy for these hydrogen bonds is significantly higher due to electrostatic charge–dipole interactions.

Formation of disulfide bridges

Formation of additional disulfide bridges is another crucial factor that stabilizes the protein structure at high temperatures [41, 42]. This effect is believed to be for the most part related to the reduction of the configurational entropy of the unfolded protein state.

In some cases, the effect of inserting multiple disulfide bridges into the structure was additive [43]. In particular, mutants with disulfide bridges between the residues 3–97, 9–164 and 21–142 were designed in the bacteriophage T4 lysozyme molecule (the disulfide-free enzyme), which turned out to be significantly more thermostable than the wild-type protein.

However, no such additivity was observed in other cases [42, 44, 45]. Furthermore, formation of disulfide bonds sometimes has no effect on the thermal stability of a protein [45] or even reduces it [42], thus an indication that there are regions with different thermal sensitivities in a protein's structure. Interestingly, the magnitude of the effect of thermal stabilization of a protein using artificial disulfide bridges, at least in some cases, is approximately proportional to the logarithm of the number of amino acid residues that separate two cysteine residues forming a disulfide bridge [16, 43].

This approach to designing thermostable proteins has recently acquired additional popularity due to the elaboration of novel theoretical approaches that allow one both to calculate all the possible combinations of artificial disulfide bridges based on the known spatial structure of the protein and to roughly estimate their energy and the probability of spontaneous formation [46].

Directed evolution

Directed evolution is the main experimental method used to improve enzyme properties [47]. The key advantage of this approach is that it does not require any knowledge about the details of the structure of the

enzyme being altered. The method is based on the experimenter-controlled process of artificial, accelerated evolution of microorganisms that are intentionally exposed to harsh environmental conditions. As opposed to natural evolution, this process is more intense and selective; it has a specific purpose, is time-limited, and imitates such natural processes as random mutagenesis, recombination, and selection.

Research into directed evolution of industrially relevant proteins using chemical and radiation-induced mutagenesis was started in the early 1980s. In the 1990s, it accelerated as the era of industrial molecular biotechnology began. The intense development in this field is driven by the demand to produce new natural biocatalysts that would be more efficient and safe for humans. A novel approach, the DNA shuffling method, was proposed in 1994 [48]: it proved to be efficient and underlay a number of different modifications of the original method. Hence, this approach was used to produce thermostable subtilisin E, which is 15 times more active at 37°C than the wild-type protein from *B. subtilis* [49]. The examination of its structure showed that most of the mutations that increase the thermal stability of the protein reside in the loops connecting secondary-structure elements [50]. In a different experiment, the thermal stability and activity of *p*-nitrobenzyl esterase from *B. subtilis* were increased by five low-accuracy PCR cycles accompanied by one DNA shuffling step [51]. The thermal stability of the mutant protein increased by 10°C; its activity was higher than that of the wild-type enzyme at any temperature.

COMPUTATIONAL METHODS FOR A RATIONAL DESIGNING OF THERMOSTABLE PROTEINS

A number of theoretical models and computer-assisted algorithms based on physical and chemical principles have been proposed to predict the conformational stability of proteins and to design thermostable mutants [52–54]. The results demonstrate rather convincingly that these approaches may become reliable tools of protein engineering in the near future.

The molecular dynamics method (MD) is one of the well-proven computational approaches to the simulation of the conformational mobility of proteins and their folding into the native conformation, as well as to the rational design of proteins with altered properties [55]. In order to eliminate the need to simulate excessively long molecular dynamics trajectories, a theoretical model and the corresponding software have been developed which allow one to predict the mobile and more stable regions in a protein with a known spatial structure without simulating the detailed molecular dynamics of this protein [56].

Multiple MD trajectories of the same protein under identical conditions make it possible to determine the structure and sequence of its intermediate states during thermal unfolding [57]. These observations can provide hints about how the unfolding of the enzymes starts and which enzyme regions are the most suitable for stabilization [58].

Other approaches based on modern methods for iteration and optimization of the energy of the side-chain conformational isomers of the amino acid residues in proteins under study are also used besides MD [59]: for example, the computer-assisted global optimization algorithm based on the DEE theorem imposing conditions for revealing the rotamers that cannot be members of the conformation characterized by the global energy minimum [60]. This approach was employed to design a thermostable mutant of streptococcal protein G [61]. The melting point of the mutant protein was beyond 100°C, which is 20°C higher than that of the wild-type protein.

The energy potential for assessing the effect of point mutations on the stability of globular proteins with known spatial structures has recently been developed [62]. These computations are also available online (<http://foldx.embl.de/>). The computations include an assessment of changes in the free energy of the protein after amino acid substitution and the calculated position of charged groups, water bridges, and metal binding sites, which can also greatly affect the conformational stability of proteins.

FACTORS AFFECTING THE CONFORMATIONAL STABILITY OF α -HELICES IN SHORT PEPTIDES

Unlike in proteins, short peptides 10- to 20 amino-acid-residues-long lack many of the possibilities for structure stabilization that globular proteins have. Back in the early 1980s, it was thought that short peptides cannot maintain their stable conformation in water even at relatively low temperatures [63]. However, in the mid-1970s, Finkelstein and Ptitsyn predicted in their theoretical studies that short peptides consisting of amino acids exhibiting high proneness to the α -helical structure can have appreciably stable α -helical conformations in aqueous solutions [64–68]. These theoretical predictions were later experimentally proven by investigating synthetic peptides whose sequences repeat those of ribonuclease A α -helices [69, 70]. The theoretical model developed by Finkelstein and Ptitsyn describes the probabilities of formation of α -helices, β -structures, and turn regions in short peptides and globular proteins based on the classical Zimm-Bragg approach, with modifications that take into account some additional interactions, such as the electrostatic interactions between the charged side chains and the

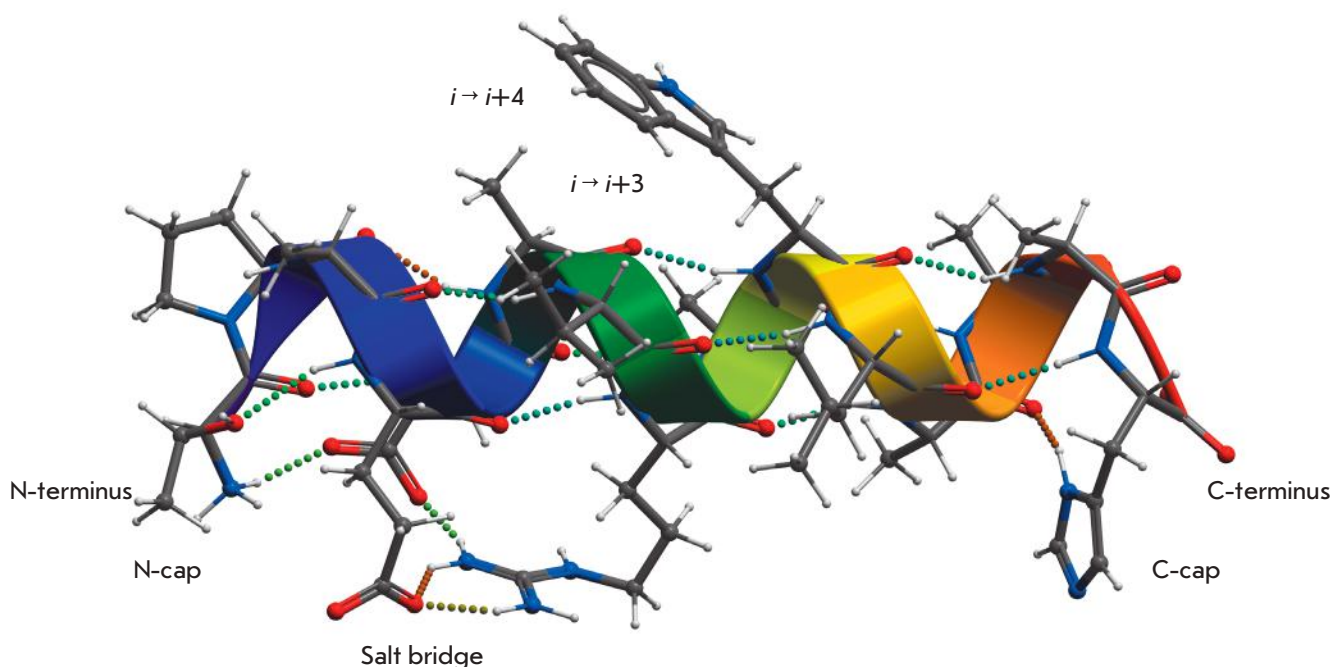


Fig. 1. The structure and factors that influence the conformational stability of the α -helix in proteins and monomeric peptides

macro-dipole of the α -helix, as well as the hydrophobic interactions between the side chains of certain amino acids. This theoretical model was employed to design software (ALB) that successfully predicts both the approximate level of conformational stability of α -helical peptides [4] and, with a $\sim 65\%$ probability, the distribution of the secondary structural elements in globular proteins [71]. The main drawback of this model is that it does not take into account certain interactions (e.g., the so-called Capping Box and/or presence of proline in the first N-terminal position of α -helix), the positional dependences of the propensities of amino acids in the first and last turn of an helix, or the effect of various special sequences of the regions in the peptide under study that are adjacent to the α -helix (as demonstrated later, these regions play a significant role in the stabilization of the α -helical conformation in proteins and peptides).

Starting in the late 1980s, and especially in the 1990s, a large number of experiments have been conducted where amino acid substitutions in short synthetic polyalanine-based peptides were used to study various interactions in α -helices [72]. This approach has allowed researchers to accumulate sufficient data and to proceed to a quantitative description of the cooperative mechanisms of conformational transitions into the α -helical conformation for peptides with random sequences [5, 73].

It is currently believed that each of the 20 natural amino acids has an intrinsic propensity to form α -helical conformations in peptides and proteins that is associated with their covalent structure (e.g., changes in the configurational entropy of the side chains of amino acids during a transition from a random conformation into the α -helical one) [74]. In addition, the stability of α -helical protein conformations is affected by the interactions between side chains (between the residues at positions $i, i+3$ and $i, i+4$), the electrostatic interactions between the charged polar residues with the macro-dipole of the α -helix, and the capping interactions between the residues adjacent to the α -helix and the unbound NH- and CO- moieties in the main chain of the protein in the first and last turn of the α -helix [5, 73].

Furthermore, local motifs of amino acid sequences that include the residues adjacent to the α -helix, which either are specifically packed against the residues of the first (N-terminal) and last (C-terminal) turn of the helix or form a network of specific hydrogen bonds with it, have also been reported [75].

It is usually assumed that the structural propensity of amino acids is independent of their positions in the α -helix [4, 76, 77]. However, the first and last turns of the α -helix are not equivalent to the remaining portion of the helix. *Figure 1* shows that the mobility of the side chain of valine at the central positions of the helix is strongly limited compared to the situation when it

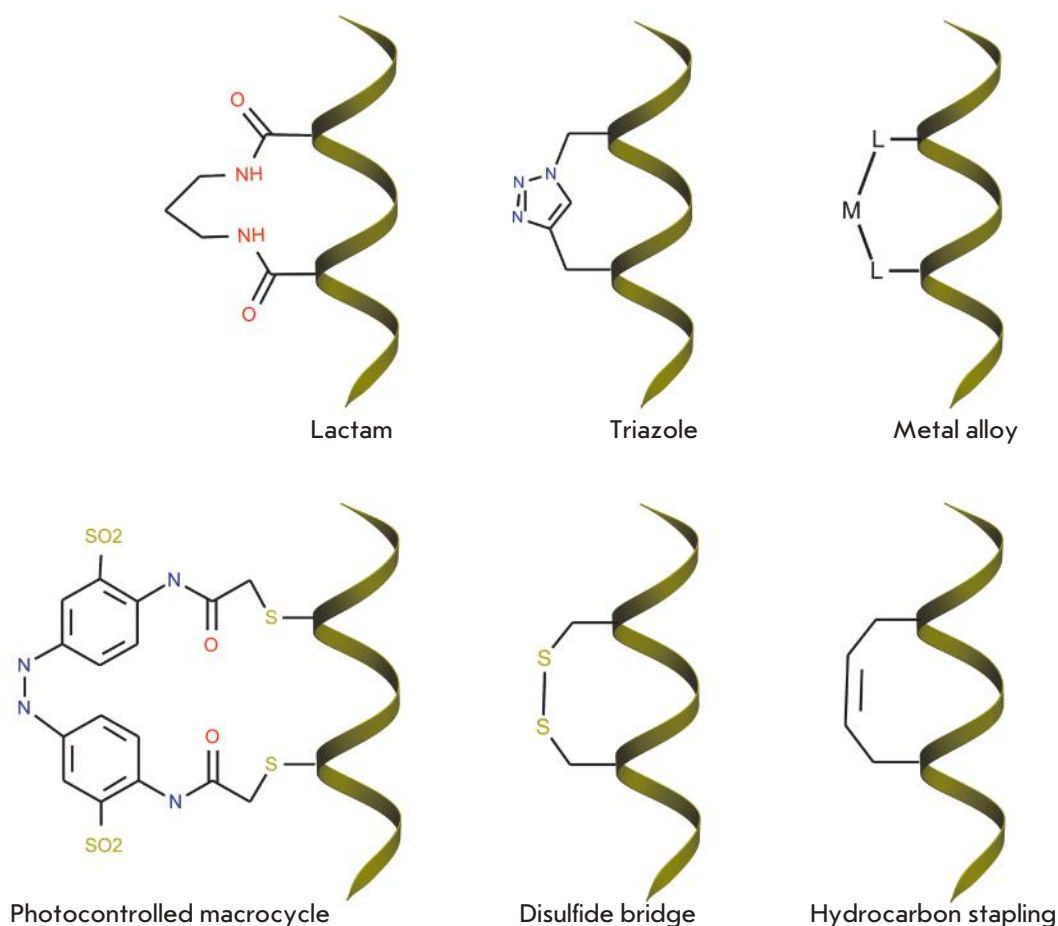


Fig. 2. The main ways of chemical modification to increase the conformational stability of α -helical structures

resides are in the first turn of the helix. The accuracy of the theoretical models of α -helix/random coil transitions in the description of experimental findings on measuring the stability of α -helical peptides with complex amino acid sequences is significantly reduced if no allowance is made for this factor [78–80].

CHEMICAL METHODS FOR THE STABILIZATION OF α -HELICAL STRUCTURES

Since α -helices often serve as a structural basis for intermolecular interfaces of protein complexes, they are frequently used to design peptide inhibitors targeted against the formation of these complexes. Targeted destruction of certain protein–protein interactions using α -helical or β -structural peptides is a topical issue in chemical biology that researchers are currently trying to solve.

However, the use of peptide inhibitors has serious limitations. First of all, there is the insufficient stability of the α -helical conformation of short peptides with amino acid sequences isolated from natural proteins. Furthermore, these proteins are characterized by poor

cell membrane penetrability and are easily degraded by proteases. Over the past 30 years, various methods for chemical modification of short α -helical peptides have been designed to increase the stability of α -helical conformations and their proteolytic stability (*Fig. 2*). Chemical modifications for stabilizing α -helical conformations include: 1) inserting residues with limited mobility, such as α - α -dialkylated residues [81], into the amino acid sequence; 2) covalent crosslinking of side chains of the amino acids residing on neighboring turns of α -helices, including the formation of covalent bridges based on disulfide bonds [82], lactam structures [83] and hydrocarbons [3]; and 3) capping the group at the N- or C-termini of the peptide [84], as well as various combinations of the aforementioned modifications [2].

The chemical modifications that stabilize α -helices turn out to also be able to improve the cell permeability of these peptides in some cases, making them good inhibitors of an intracellular target. In particular, a large body of data on increased membrane permeability in some types of human cancer cells for chemically modified α -helical peptides has been published [85].

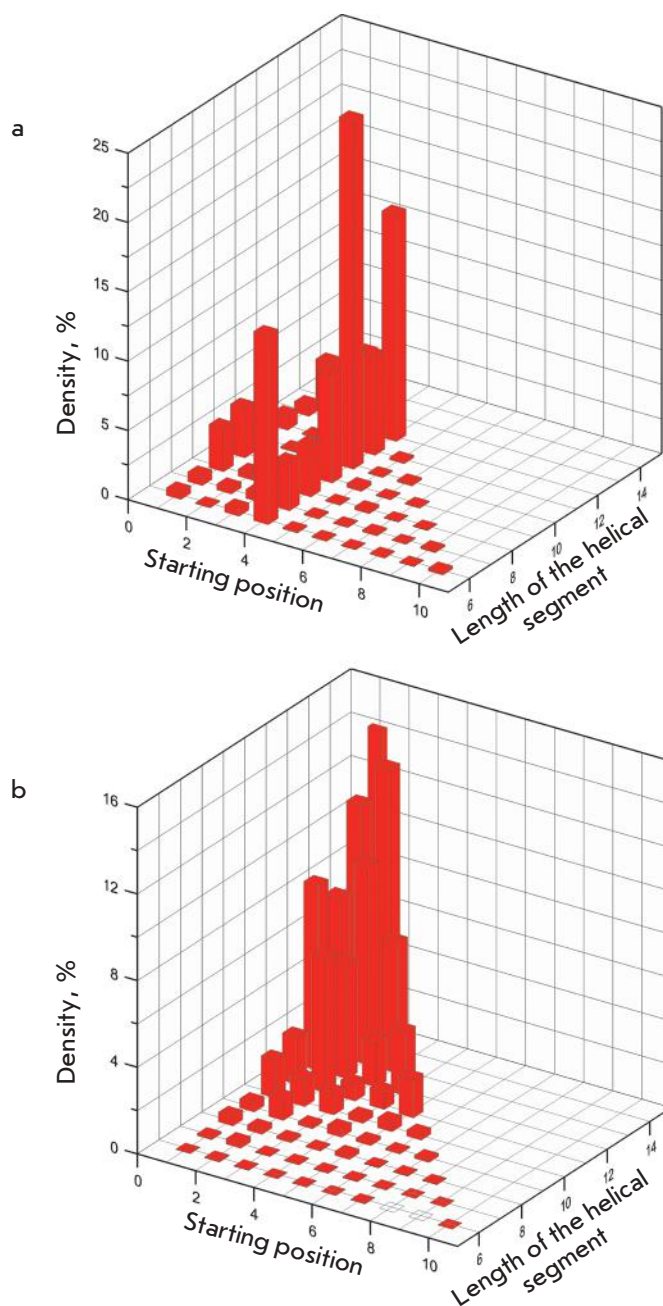


Fig. 3. The distribution of populations of all possible segments in a short peptide 13-amino-acid-residues-long (according to AGADIR [77]). *A* – the C-terminal peptide from ribonuclease A (ac-AETAAKFLRAHA-nh2) [69,70]; *B* – the peptide with an optimized sequence of the same length ac-DYMERWYRYNEF-nh2

DESIGNING STABLE α -HELICES OF PROTEINS THROUGH GLOBAL OPTIMIZATION OF THEIR AMINO ACID SEQUENCES

SEQOPT, the recently developed method for a global optimization of the amino acid sequences of α -helices in monomeric peptides and globular peptides is one of

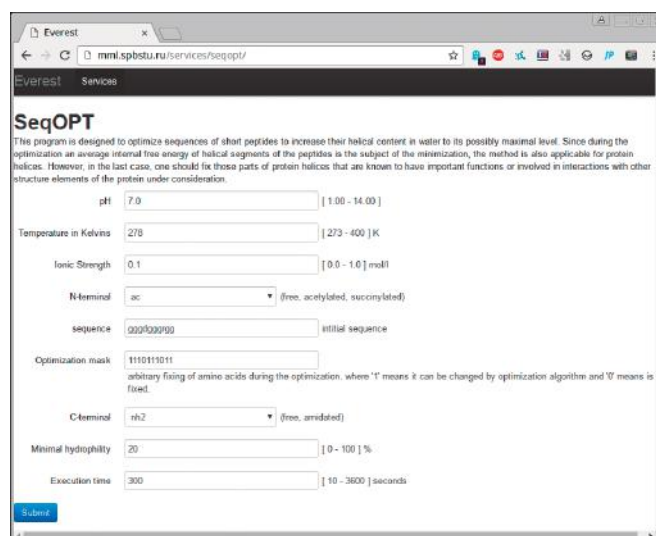


Fig. 4. The screenshot of the SEQOPT software for specifying parameters, such as pH, temperature, ionic strength, the initial sequence for the optimization and the fixed position of amino acid residues, the minimum level of solubility, and the allowed calculation time

the efficient methods for solving the problem associated with the stabilization of the structure of biologically active α -helical peptides using natural amino acids only [1]. This method allows one to design α -helices of proteins that have the maximum possible conformational stability under specific conditions (conformational environment, pH, temperature, and ionic strength of solution) using global optimization of amino acid sequences, including arbitrary fixation of any amino acid combinations. The model that theoretically underlies the proposed method is the AGADIR model, which describes the thermodynamics of folding of α -helices under various ambient conditions (temperature, pH, and ionic strength of solution, etc.) [77] and has also been used to design mutant proteins that exhibit enhanced conformational stability [7]. Its model reproduces well the existing experimental data on the stability of the α -helical conformations of a large number of short peptides [73, 77–80, 86–88].

The dependence of the energy parameters of the model on the temperature, pH, and ionic strength of the solution was included in the calculations as described in [86].

Although no guaranteed convergence to the global minimum can currently be achieved for the majority of multivariate problems that are of practical significance, the elaborated method was shown to be characterized by high efficiency in optimizing the amino acid sequences of α -helical peptides. The measured CD values

Table 1. The most commonly used peptides that exhibit antibacterial activity and can penetrate through the cell membrane

PEPTIDE	AMINO ACID SEQUENCE	SECONDARY STRUCTURE	REFERENCE
Penetratin	RQIKIWFQNRRMKWKK	α -helical	[90]
Tat	GRKKRRQRRRPPQ	nonstructural, PPII-helical	[91]
Pep-1	KETWWETWWTEWSQPKKKRKV	α -helical	[92]
S4 ₁₃ -PV	ALWKTLLKKVLKAPKKKRKV	α -helical	[93]
Magainin 2	GIGKFLHSAKKFGKAFVGEIMNS	α -helical	[94]
Buforin II	TRSSRAGLQFPVGRVHRLLRK	α -helical	[95]
Apidaecins	RP - - - - PRPPHPR	nonstructural	[96]
Transportan (TP10)	GWTLNSAGYLLGKINLKALAALAKKIL	α -helical	[97]
MAP	KLALKLALKALKAALKLA	α -helical	[98]
sC18	GLRKRLRKFRNKIKEK	α -helical	[99]
LL-37	LLGDFFRKSKEKIGKEFKRIVQRIKDFLRNLPRTES	α -helical	[100]
Bac7	PFPRPGPRPIRPLPFPRPGPRPIPRP	PPII- and α -helical	[101]

of several synthetic peptides with optimized sequences demonstrated good agreement with theoretical calculations in terms of both the absolute and relative α -helical contents [6].

It is well-known that short peptides are typically rather mobile and do not have a single dominant conformation. *Figure 3* shows the distributions of populations for all possible segments in 13 amino acid residues short peptides. The sequence (AETAAKFLRAHA) of one of these peptides (see panel 3A) corresponds to the α -helix of ribonuclease A, one of the first peptides whose significant stability of the α -helical conformation in water has been demonstrated experimentally (HC ~21%, 5°C, pH 7, ionic strength 100 mmol/L, the N- and C-termini are acetylated and amidated, respectively). The data for a peptide of the same length but with the optimized sequence DYMERWYRYNEF and HC ~ 88% are shown in *Fig. 3B* for the sake of comparison.

These figures demonstrate that in the protein with the amino acid sequence taken from the globular protein, several helical segments starting with alanine at position 4 were populated in the solution. The populations of each segment changed randomly depending on its length and, therefore, the amino acids of the C-terminal portion of this region. As a result, the first four and the last two amino acids in this peptide stand almost no chance of participating in the formation of α -helical conformation, whose average length is ~6 amino acid residues. Therefore, the helical content of this peptide is rather low: about 21%.

The optimized sequence, as opposed to the native one, behaves in completely different fashion. The helical segment covering the entire peptide sequence is characterized by the highest population. It is followed

by segments differing from the maximum segment by one or two residues that have lost their α -helical conformation at the N- and C-termini.

As a result, the total helical content of the peptide with the optimized sequence is as high as ~90%. The stability of the α -helical conformation rises with increasing peptide length and approaches 100%. The average length of the α -helical region of the peptide is also considerably greater. These results both demonstrate the potential of the SEQOPT method and indicate that the potential of 20 natural amino acids allows one to obtain appreciably stable conformations in the short α -helical peptide that are as short as 10–20 residues.

A new function of the algorithm that is of practical importance has been added in the updated SEQOPT version (web server can be accessed at <http://mml.spbstu.ru/services/seqopt/>, see *Fig. 4*). It enables to determine the minimal allowable level of solubility for α -helical peptides with optimized sequences. As far as the authors know, it is the first study in the new and promising field of global optimization of the amino acid sequences of proteins.

PERMEABILITY OF CELL MEMBRANES TO PEPTIDES

The highly stable α -helical peptides that are employed as highly active and specific inhibitors of protein–protein interactions are currently being used with increasing regularity in medicine as broad-spectrum antibiotics and to destroy certain complexes that play a key role in the activity of human cells [2]. One of the key downsides in using peptides in medicine consists in their penetrability through the cell membranes.

The cell wall prevents the penetration of foreign molecules inside the cell, thus impeding the use of the

Table 2. N-terminal peptides facilitating the penetration of microorganisms into cells

AMINO ACID SEQUENCE	<i>Candida albicans</i>	<i>Saccharomyces cerevisiae</i>	<i>Staphylococcus aureus</i>	<i>Bacillus subtilis</i>	<i>Escherichia coli</i>	Reference
VLNENPFSDP	+		+	+		[106]
YKKSNNPFSD		+		+	+	[107]
RSNNPFRAR	+	+	+			[107]
CMVSCAMPNPF					+	[108]
LLDLMD	+					[109]
LMDLAD	+				+	[109]
RQIKIWFQRRMKWKK	+					[110]
YGRKKRRQRRRCKGGAKL			+			[110]
CFFKDEL					+	[111]
GASDYQRLGC		+			+	[111]

designed highly stable peptides for therapeutic purposes. There are several approaches to solving this problem. One of these approaches is based on using special receptors that recognize certain chemical compounds and switch on the mechanisms of active transport inside the cell [89]. Another method consists in the destruction of the cell membrane and penetration through the newly opened pores.

The entire family of peptides that exhibit antimicrobial properties, can penetrate through cell membranes, and are able to carry both other peptides and chemical compounds of a different nature through the membrane is known and well-studied [102, 103]. These peptides were isolated from proteins of various organisms, ranging from viruses to higher organisms (Table 1).

Successful use of peptides that exhibit antibacterial activity to deliver therapeutic agents inside the cell has been demonstrated in a number of experiments [101, 104, 105]; there is no fundamental difference in the efficiencies of their penetration into different cells. Signal peptides belonging to another group can also penetrate into these cells. The common mechanism of their action is still to be determined [89]. Table 2 lists the amino acid sequences of peptides and indicates their ability to penetrate into the cells of single-celled microorganisms.

These peptides can be synthesized or cloned along with the required therapeutic agents.

INTRACELLULAR PROTEOLYSIS OF α -HELICAL PEPTIDES

One of the key issues hindering the development of peptide therapeutic agents is their proteolytic instability and the problems associated with delivery to molecular targets. Proteolysis typically takes place in the intestine, in microvilli on the inside walls of the small intestine, in enterocytes, hepatocytes, antigen-presenting cells, and plasma; hence, oral administration of peptide-based drugs is usually infeasible and injections are needed. However, even in the case of parenteral

administration, the degradation of peptide-based drugs in the blood, in combination with rapid renal clearance, makes this type of therapeutic agents expensive and inconvenient [112]. Furthermore, synthetic therapeutic peptides are typically non-structured and, therefore, are cleaved rapidly by intracellular proteases under natural conditions; their half-life often does not exceed a few minutes.

The proteolytic stability of α -helical peptides can be increased by inserting various factors that stabilize the conformational stability of the α -helix: additional salt-bridge bonds or other modifications, such as lactam bridges [113, 114], or formation of peptide oligomeric structures [115].

Since natural peptides are in general characterized by a relatively short lifetime in plasma, several approaches have been designed to increase it. The first approach is aimed at limiting enzyme degradation by identifying the possible peptide cleavage site, followed by structural modifications, such as amino acid substitution at the cleavage site. Peptide resistance to cleavage can also be enhanced by improving the peptide's secondary structure folding. This approach involves the use of structure-induced probes: the (SIP)-tail s, lactam bridges, and either stapling or cyclization of the peptide chain [3, 83, 116].

Another method used to increase a peptide's lifetime is to bind the peptide to circulating protein albumin as a transporter and peptide acylation [117]. Binding of polyethylene glycol to peptides is often used to increase plasma elimination the half-life of peptide-based agents [118].

CONCLUSIONS

Biologically active peptides are becoming increasingly popular as potential therapeutic agents because of their high activity, nontoxicity, and moderate cost. The problems related to their insufficient conformational

stability, penetrability through cell membranes, and rapid degradation by intracellular proteases are overcome to a significant extent through employing modern methods for the design of highly stable peptides based only on natural amino acids or using several types of their chemical modifications. SEQOPT is a recently developed computational method for designing α -helical peptides that contain only 20 natural amino acids. Peptides with the maximum possible stability of α -helical conformation can be produced using this method. It allows one to take into account the conformational envi-

ronment, the ambient conditions (pH, temperature, and ionic strength of solution), and the minimum acceptable solubility level and to arbitrarily fix any amino acid combinations needed to ensure the biological activity of the peptides. The conformational stability of monomeric peptides with an optimized structure approaches that of the α -helical regions of the secondary structure of globular proteins. ●

This work was supported by the Russian Science Foundation (research project № 14-34-00023).

REFERENCES

1. Yakimov A., Rychkov G., Petukhov M. // *Methods Mol. Biol.* 2014. V. 1216. P. 1–14.
2. Estieu-Gionnet K., Guichard G. // *Expert Opin. Drug Discov.* 2011. V. 6. № 9. P. 937–963.
3. Robertson N.S., Jamieson A.G. // *Repts Organic Chem.* 2015. V. 5. P. 65–74.
4. Finkelstein A.V., Badretdinov A.Y., Ptitsyn O.B. // *Proteins.* 1991. V. 10. № 4. P. 287–299.
5. Doig A.J. // *Biophys. Chem.* 2002. V. 101–102. P. 281–293.
6. Petukhov M., Tatsu Y., Tamaki K., Murase S., Uekawa H., Yoshikawa S., Serrano L., Yumoto N. // *J. Pept. Sci.* 2009. V. 15. № 5. P. 359–365.
7. Villegas V., Viguera A.R., Aviles F.X., Serrano L. // *Fold Des.* 1996. V. 1. № 1. P. 29–34.
8. Surzhik M.A., Churkina S.V., Shmidt A.E., Shvetsov A.V., Kozhina T.N., Firsov D.L., Firsov L.M., Petukhov M.G. // *Applied biochemistry and microbiology.* 2010. V. 46, № 2, P. 206–211.
9. Bruins M.E., Janssen A.E., Boom R.M. // *Appl. Biochem. Biotechnol.* 2001. V. 90. № 2. P. 155–186.
10. Glick B.R., Pasternak J.J. *Molecular biotechnology: Principles and applications of recombinant DNA.* (2nd ed.) Washington D.C.: ASM Press, 1998.
11. Razvi A., Scholtz J.M. // *Protein Sci.* 2006. V. 15. № 7. P. 1569–1578.
12. Trivedi S., Gehlot H.S., Rao S.R. // *Genet. Mol. Res.* 2006. V. 5. № 4. P. 816–827.
13. Mozo-Villiarías A., Querol E. // *Curr. Bioinformatics.* 2006. V. 1. № 1. P. 25–32.
14. Li W.F., Zhou X.X., Lu P. // *Biotechnol. Adv.* 2005. V. 23. № 4. P. 271–281.
15. Ladenstein R., Antranikian G. // *Adv. Biochem. Eng. Biotechnol.* 1998. V. 61. P. 37–85.
16. Vieille C., Zeikus G.J. // *Microbiol. Mol. Biol. Rev.* 2001. V. 65. № 1. P. 1–43.
17. Sterner R., Liebl W. // *Crit. Rev. Biochem. Mol. Biol.* 2001. V. 36. № 1. P. 39–106.
18. Zhou X.X., Wang Y.B., Pan Y.J., Li W.F. // *Amino Acids.* 2008. V. 34. № 1. P. 25–33.
19. Berezovsky I.N., Shakhnovich E.I. // *Proc. Natl. Acad. Sci. USA.* 2005. V. 102. № 36. P. 12742–12747.
20. Menendez-Arias L., Argos P. // *J. Mol. Biol.* 1989. V. 206. № 2. P. 397–406.
21. Wetmur J.G., Wong D.M., Ortiz B., Tong J., Reichert F., Gelfand D.H. // *J. Biol. Chem.* 1994. V. 269. № 41. P. 25928–25935.
22. Britton K.L., Baker P.J., Borges K.M., Engel P.C., Pasquo A., Rice D.W., Robb F.T., Scandurra R., Stillman T.J., Yip K.S. // *Eur. J. Biochem.* 1995. V. 229. № 3. P. 688–695.
23. Argos P., Rossman M.G., Grau U.M., Zuber H., Frank G., Tratschin J.D. // *Biochemistry.* 1979. V. 18. № 25. P. 5698–5703.
24. Bohm G., Jaenicke R. // *Int. J. Pept. Protein Res.* 1994. V. 43. № 1. P. 97–106.
25. Zeldovich K.B., Berezovsky I.N., Shakhnovich E.I. // *PLoS Comput. Biol.* 2007. V. 3. № 1. P. e5.
26. Petukhov M., Kil Y., Kuramitsu S., Lanzov V. // *Proteins.* 1997. V. 29. № 3. P. 309–320.
27. Petukhov M.G., Kil Yu.V., Lantsov V.A. // *Doklady Akademii Nauk* 1997. V. 356, № 2. P. 268–271.
28. Petukhov M.G., Baitin D.M., Kil Y.V., Lantsov V.A. // *Doklady Akademii Nauk* 1998. V. 362, № 1. P. 118–121.
29. Facchiano A.M., Colonna G., Ragone R. // *Protein Eng.* 1998. V. 11. № 9. P. 753–760.
30. Matthews B.W., Nicholson H., Becktel W.J. // *Proc. Natl. Acad. Sci. USA.* 1987. V. 84. № 19. P. 6663–6667.
31. Pace C.N. // *J. Mol. Biol.* 1992. V. 226. № 1. P. 29–35.
32. Matsui I., Harata K. // *FEBS J.* 2007. V. 274. № 16. P. 4012–4022.
33. Zhang X., Meining W., Fischer M., Bacher A., Ladenstein R. // *J. Mol. Biol.* 2001. V. 306. № 5. P. 1099–1114.
34. Whitlow M., Howard A.J., Finzel B.C., Poulos T.L., Winborne E., Gilliland G.L. // *Proteins.* 1991. V. 9. № 3. P. 153–173.
35. Fujii T., Hata Y., Oozeki M., Moriyama H., Wakagi T., Tanaka N., Oshima T. // *Biochemistry.* 1997. V. 36. № 6. P. 1505–1513.
36. Eidsness M.K., Richie K.A., Burden A.E., Kurtz D.M., Jr., Scott R.A. // *Biochemistry.* 1997. V. 36. № 34. P. 10406–10413.
37. Glyakina A.V., Garbuzynskiy S.O., Lobanov M.Y., Galzitskaya O.V. // *Bioinformatics.* 2007. V. 23. № 17. P. 2231–2238.
38. Shirley B.A., Stanssens P., Hahn U., Pace C.N. // *Biochemistry.* 1992. V. 31. № 3. P. 725–732.
39. Tanner J.J., Hecht R.M., Krause K.L. // *Biochemistry.* 1996. V. 35. № 8. P. 2597–2609.
40. Jaenicke R., Bohm G. // *Curr. Opin. Struct. Biol.* 1998. V. 8. № 6. P. 738–748.
41. Matsumura M., Matthews B.W. // *Methods Enzymol.* 1991. V. 202. P. 336–356.
42. Surzhik M.A., Schmidt A.E., Glazunov E.A., Firsov D.L., Petukhov M.G. // *Applied biochemistry and microbiology.* 2014. V. 50, № 2. P. 118–124.
43. Matsumura M., Signor G., Matthews B.W. // *Nature.* 1989. V. 342. № 6247. P. 291–293.
44. Fierobe H.P., Stoffer B.B., Frandsen T.P., Svensson B. // *Biochemistry.* 1996. V. 35. № 26. P. 8696–8704.

REVIEWS

45. Li Y., Coutinho P.M., Ford C. // *Protein Eng.* 1998. V. 11. № 8. P. 661–667.
46. Dombkowski A.A. // *Bioinformatics.* 2003. V. 19. № 14. P. 1852–1853.
47. Jackel C., Kast P., Hilvert D. // *Annu. Rev. Biophys.* 2008. V. 37. P. 153–173.
48. Stemmer W.P. // *Nature.* 1994. V. 370. № 6488. P. 389–391.
49. Zhao H., Arnold F.H. // *Protein Eng.* 1999. V. 12. № 1. P. 47–53.
50. Mamonova T.B., Glyakina A.V., Kurnikova M.G., Galzitskaya O.V. // *J. Bioinform. Comput. Biol.* 2010. V. 8. № 3. P. 377–394.
51. Giver L., Gershenson A., Freskgard P.O., Arnold F.H. // *Proc. Natl. Acad. Sci. USA.* 1998. V. 95. № 22. P. 12809–12813.
52. Lippow S.M., Tidor B. // *Curr. Opin. Biotechnol.* 2007. V. 18. № 4. P. 305–311.
53. Kang S.G., Saven J.G. // *Curr. Opin. Chem. Biol.* 2007. V. 11. № 3. P. 329–334.
54. Marti S., Andres J., Moliner V., Silla E., Tunon I., Bertran J. // *Chem. Soc. Rev.* 2008. V. 37. № 12. P. 2634–2643.
55. Morra G., Meli M., Colombo G. // *Curr. Protein Pept. Sci.* 2008. V. 9. № 2. P. 181–196.
56. Jacobs D.J., Rader A.J., Kuhn L.A., Thorpe M.F. // *Proteins.* 2001. V. 44. № 2. P. 150–165.
57. Lazaridis T., Karplus M. // *Science.* 1997. V. 278. № 5345. P. 1928–1931.
58. Lazaridis T., Lee I., Karplus M. // *Protein Sci.* 1997. V. 6. № 12. P. 2589–2605.
59. Galzitskaya O.V., Higo J., Finkelstein A.V. // *Curr. Protein Pept. Sci.* 2002. V. 3. № 2. P. 191–200.
60. Desmet J., De Maeyer M., Hazes B., Lasters I. // *Nature.* 1992. V. 356. № 6369. P. 539–542.
61. Malakauskas S.M., Mayo S.L. // *Nat. Struct. Biol.* 1998. V. 5. № 6. P. 470–475.
62. Schymkowitz J.W., Rousseau F., Martins I.C., Ferkinghoff-Borg J., Stricher F., Serrano L. // *Proc. Natl. Acad. Sci. USA.* 2005. V. 102. № 29. P. 10147–10152.
63. Shoemaker K.R., Kim P.S., Brems D.N., Marqusee S., York E.J., Chaiken I.M., Stewart J.M., Baldwin R.L. // *Proc. Natl. Acad. Sci. USA.* 1985. V. 82. № 8. P. 2349–2353.
64. Finkelstein A.V., Ptitsyn O.B. // *J. Mol. Biol.* 1976. V. 103. № 1. P. 15–24.
65. Finkelstein A.V. // *Biopolymers.* 1977. V. 16. № 3. P. 525–529.
66. Finkelstein A. V. // *Molek. Biol. (USSR).* 1977. V. 11. P. 811–819.
67. Finkelstein A. V., Ptitsyn O. B. // *Biopolymers.* 1977. V. 16. № 3. P. 469–495.
68. Finkelstein A.V., Ptitsyn O.B., Kozitsyn S.A. // *Biopolymers.* 1977. V. 16. № 3. P. 497–524.
69. Bierzynski A., Kim P.S., Baldwin R.L. // *Proc. Natl. Acad. Sci. USA.* 1982. V. 79. № 8. P. 2470–2474.
70. Kim P.S., Baldwin R.L. // *Nature.* 1984. V. 307. № 5949. P. 329–334.
71. Finkelstein A.V., Ptitsyn O.B. *Protein Physics.* London–Amsterdam: Acad. Press, 2002.
72. Scholtz J.M., Baldwin R.L. // *Annu. Rev. Biophys. Biomol. Struct.* 1992. V. 21. P. 95–118.
73. Munoz V., Serrano L. // *Nat. Struct. Biol.* 1994. V. 1. № 6. P. 399–409.
74. Creamer T.P., Rose G.D. // *Proteins.* 1994. V. 19. № 2. P. 85–97.
75. Doig A.J., Baldwin R.L. // *Protein Sci.* 1995. V. 4. № 7. P. 1325–1336.
76. Stapley B.J., Rohl C.A., Doig A.J. // *Protein Sci.* 1995. V. 4. № 11. P. 2383–2391.
77. Munoz V., Serrano L. // *J. Mol. Biol.* 1995. V. 245. № 3. P. 275–296.
78. Petukhov M., Munoz V., Yumoto N., Yoshikawa S., Serrano L. // *J. Mol. Biol.* 1998. V. 278. № 1. P. 279–289.
79. Petukhov M., Uegaki K., Yumoto N., Yoshikawa S., Serrano L. // *Protein Sci.* 1999. V. 8. № 10. P. 2144–2150.
80. Petukhov M., Uegaki K., Yumoto N., Serrano L. // *Protein Sci.* 2002. V. 11. № 4. P. 766–777.
81. Toniolo C., Crisma M., Formaggio F., Peggion C. // *Biopolymers.* 2001. V. 60. № 6. P. 396–419.
82. Ravi A., Prasad B.V.V., Balaram P. // *J. Am. Chem. Soc.* 1983. V. 105. № 1. P. 105–109.
83. Taylor J.W. // *Biopolymers.* 2002. V. 66. № 1. P. 49–75.
84. Chapman R.N., Dimartino G., Arora P.S. // *J. Am. Chem. Soc.* 2004. V. 126. № 39. P. 12252–12253.
85. Chu Q., Moellering R.E., Hilinski G.J., Kim Y.-W., Grossmann T.N., Yeh J.T.H., Verdine G.L. // *Med. Chem. Comm.* 2015. V. 6. № 1. P. 111–119.
86. Munoz V., Serrano L. // *J. Mol. Biol.* 1995. V. 245. № 3. P. 297–308.
87. Petukhov M., Yumoto N., Murase S., Onmura R., Yoshikawa S. // *Biochemistry.* 1996. V. 35. № 2. P. 387–397.
88. Lacroix E., Viguera A.R., Serrano L. // *J. Mol. Biol.* 1998. V. 284. № 1. P. 173–191.
89. Rajarao G.K., Nekhotiaeva N., Good L. // *FEMS Microbiol. Lett.* 2002. V. 215. № 2. P. 267–272.
90. Derossi D., Joliet A. H., Chassaing G., Prochiantz A. // *J. Biol. Chem.* 1994. V. 269. № 14. P. 10444–10450.
91. Vives E., Brodin P., Lebleu B. // *J. Biol. Chem.* 1997. V. 272. № 25. P. 16010–16017.
92. Morris M.C., Vidal P., Chaloin L., Heitz F., Divita G. // *Nucl. Acids Res.* 1997. V. 25. № 14. P. 2730–2736.
93. Hariton-Gazal E., Feder R., Mor A., Graessmann A., Brack-Werner R., Jans D., Gilon C., Loyter A. // *Biochemistry.* 2002. V. 41. № 29. P. 9208–9214.
94. Zasloff M. // *Proc. Natl. Acad. Sci. USA.* 1987. V. 84. № 15. P. 5449–5453.
95. Park C.B., Kim H.S., Kim S.C. // *Biochem. Biophys. Res. Commun.* 1998. V. 244. № 1. P. 253–257.
96. Casteels P., Ampe C., Jacobs F., Vaeck M., Tempst P. // *EMBO J.* 1989. V. 8. № 8. P. 2387–2391.
97. Pooga M., Hallbrink M., Zorko M., Langel U. // *FASEB J.* 1998. V. 12. № 1. P. 67–77.
98. Steiner V., Schar M., Bornsen K.O., Mutter M. // *J. Chromatogr.* 1991. V. 586. № 1. P. 43–50.
99. Neundorff I., Rennert R., Hoyer J., Schramm F., Löbner K., Kitanovic I., Wölfl S. // *Pharmaceuticals.* 2009. V. 2. № 2. P. 49.
100. Oren Z., Lerman J.C., Gudmundsson G.H., Agerberth B., Shai Y. // *Biochem. J.* 1999. V. 341 (Pt 3). P. 501–513.
101. Otvos L., Jr., Cudic M., Chua B.Y., Deliyannis G., Jackson D.C. // *Mol. Pharm.* 2004. V. 1. № 3. P. 220–232.
102. Splith K., Neundorff I. // *Eur. Biophys. J.* 2011. V. 40. № 4. P. 387–397.
103. Henriques S.T., Melo M.N., Castanho M.A. // *Biochem. J.* 2006. V. 399. № 1. P. 1–7.
104. Rousselle C., Clair P., Lefauconnier J.M., Kaczorek M., Scherrmann J.M., Tamsamani J. // *Mol. Pharmacol.* 2000. V. 57. № 4. P. 679–686.
105. Splith K., Hu W., Schatzschneider U., Gust R., Ott I., Onambele L.A., Prokop A., Neundorff I. // *Bioconjug. Chem.* 2010. V. 21. № 7. P. 1288–1296.
106. Tan P.K., Howard J.P., Payne G.S. // *J. Cell Biol.* 1996. V. 135. № 6. Pt 2. P. 1789–1800.

REVIEWS

107. Paoluzi S., Castagnoli L., Lauro I., Salcini A.E., Coda L., Fre S., Confalonieri S., Pelicci P.G., Di Fiore P.P., Cesareni G. // *EMBO J.* 1998. V. 17. № 22. P. 6541–6550.
108. Fernandez-Chacon R., Achiriloaie M., Janz R., Albanesi J.P., Sudhof T.C. // *J. Biol. Chem.* 2000. V. 275. № 17. P. 12752–12756.
109. Rosenthal J.A., Chen H., Slepnev V.I., Pellegrini L., Salcini A.E., Di Fiore P.P., De Camilli P. // *J. Biol. Chem.* 1999. V. 274. № 48. P. 33959–33965.
110. Schwartz J.J., Zhang S. // *Curr. Opin. Mol. Ther.* 2000. V. 2. № 2. P. 162–167.
111. Pap E.H., Dansen T.B., van Summeren R., Wirtz K.W. // *Exp. Cell Res.* 2001. V. 265. № 2. P. 288–293.
112. Weinstock M.T., Francis J.N., Redman J.S., Kay M.S. // *Biopolymers.* 2012. V. 98. № 5. P. 431–442.
113. Houston M.E., Jr., Campbell A.P., Lix B., Kay C.M., Sykes B.D., Hodges R.S. // *Biochemistry.* 1996. V. 35. № 31. P. 10041–10050.
114. Houston M.E., Jr., Gannon C.L., Kay C.M., Hodges R.S. // *J. Pept. Sci.* 1995. V. 1. № 4. P. 274–282.
115. Jeong W.J., Lee M.S., Lim Y.B. // *Biomacromolecules.* 2013. V. 14. № 8. P. 2684–2689.
116. Sim S., Kim Y., Kim T., Lim S., Lee M. // *J. Am. Chem. Soc.* 2012. V. 134. № 50. P. 20270–20272.
117. Bao W., Holt L.J., Prince R.D., Jones G.X., Aravindhan K., Szapacs M., Barbour A.M., Jolivet L.J., Lepore J.J., Willette R.N., et al. // *Cardiovasc. Diabetol.* 2013. V. 12. P. 148.
118. Delgado C., Francis G.E., Fisher D. // *Crit. Rev. Ther. Drug Carrier Syst.* 1992. V. 9. № 3–4. P. 249–304.

A Cascade of Thermophilic Enzymes As an Approach to the Synthesis of Modified Nucleotides

R. S. Esipov*, Yu. A. Abramchik, I. V. Fateev, I. D. Konstantinova, M. A. Kostromina,
T. I. Muravyova, K. G. Artemova, A. I. Miroshnikov

Shemyakin and Ovchinnikov Institute of Bioorganic Chemistry, Miklukho-Maklaya Str., 16/10,
Moscow, GSP-7, 117997, Russia

*Email: esipov@mx.ibch.ru

Received November 09, 2015; in final form, June 06, 2016

Copyright © 2016 Park-media, Ltd. This is an open access article distributed under the Creative Commons Attribution License, which permits unrestricted use, distribution, and reproduction in any medium, provided the original work is properly cited.

ABSTRACT We propose a new approach for the synthesis of biologically important nucleotides which includes a multi-enzymatic cascade conversion of *D*-pentoses into purine nucleotides. The approach exploits nucleic acid exchange enzymes from thermophilic microorganisms: ribokinase, phosphoribosylpyrophosphate synthetase, and adenine phosphoribosyltransferase. We cloned the ribokinase gene from *Thermus sp.* 2.9, as well as two different genes of phosphoribosylpyrophosphate synthetase (PRPP-synthetase) and the adenine phosphoribosyltransferase (APR-transferase) gene from *Thermus thermophilus* HB27 into expression vectors, generated high-yield *E. coli* producer strains, developed methods for the purification of the enzymes, and investigated enzyme substrate specificity. The enzymes were used for the conversion of *D*-pentoses into 5-phosphates that were further converted into 5-phospho- α -*D*-pentofuranose 1-pyrophosphates by means of ribokinase and PRPP-synthetases. Target nucleotides were obtained through the condensation of the pyrophosphates with adenine and its derivatives in a reaction catalyzed by APR-transferase. 2-Chloro- and 2-fluoroadenosine monophosphates were synthesized from *D*-ribose and appropriate heterobases in one pot using a system of thermophilic enzymes in the presence of ATP, ribokinase, PRPP-synthetase, and APR-transferase.

KEYWORDS enzymatic nucleotide synthesis, ribokinase, phosphoribosylpyrophosphate synthetase, adenine phosphoribosyltransferase, thermophilic microorganisms, substrate properties.

ABBREVIATIONS BSA – bovine serum albumin; IPTG – isopropyl- β -*D*-1-thiogalactopyranoside; PAAG – polyacrylamide gel; PMSF – phenylmethylsulfonyl fluoride; PCR – polymerase chain reaction; APR-transferase (*Tth*APRT) – adenine phosphoribosyltransferase from *Thermus thermophilus*; LB – Luria-Bertani medium; PRPP-synthetase (*Tth*PRPPS) – phosphoribosylpyrophosphate synthetase from *Thermus thermophilus*; RK (*Tsp*RK) – ribokinase from *Thermus sp.*; 2Cl-AMP – 2-chloroadenosine 5'-monophosphate; 2F-AMP – 2-fluoroadenosine 5'-monophosphate; Pi – inorganic phosphate; PRPP – 5-phosphoribosyl-1-pyrophosphate.

INTRODUCTION

5'-phosphorylated nucleosides are important metabolites of DNA and RNA biosynthesis, as well as co-substrates and cofactors of numerous biochemical reactions [1–3]. The important role these compounds play in a living cell underlies the interest in the synthesis of not only natural members of this class, but also their various analogues to directly affect the metabolism in normal and pathological conditions [4–8]. A large number of heterobase- and sugar-modified nucleosides are used as important antiviral and anticancer agents [9–13]. The effect of modified nucleosides is mediated through their intracellular conversion primarily into 5'-monophosphates and then usually into 5'-di- and triphosphates that act as antimetabolites. The first step in the metabolic activation of modified nucleosides –

conversion into 5'-monophosphates – is known to determine the nucleoside's biological properties. It should also be noted that heterobase- and/or sugar-modified nucleoside-5'-monophosphates are of considerable interest as starting materials for the chemical synthesis of phosphate derivatives (prodrugs) and enzymatic conversion into 5'-triphosphates for subsequent inclusion in oligonucleotides [14–16]. The development of effective biosynthetic approaches to the production of 5'-monophosphates of modified nucleosides draws the attention of researchers engaged in the development of highly efficient chemotherapeutic agents.

Mono- and multi-enzymatic synthesis of nucleoside 5'-mono- and 5'-triphosphates has been the subject of numerous publications [17–21]. Of these, we were particularly interested in the phosphoribosyltransferases

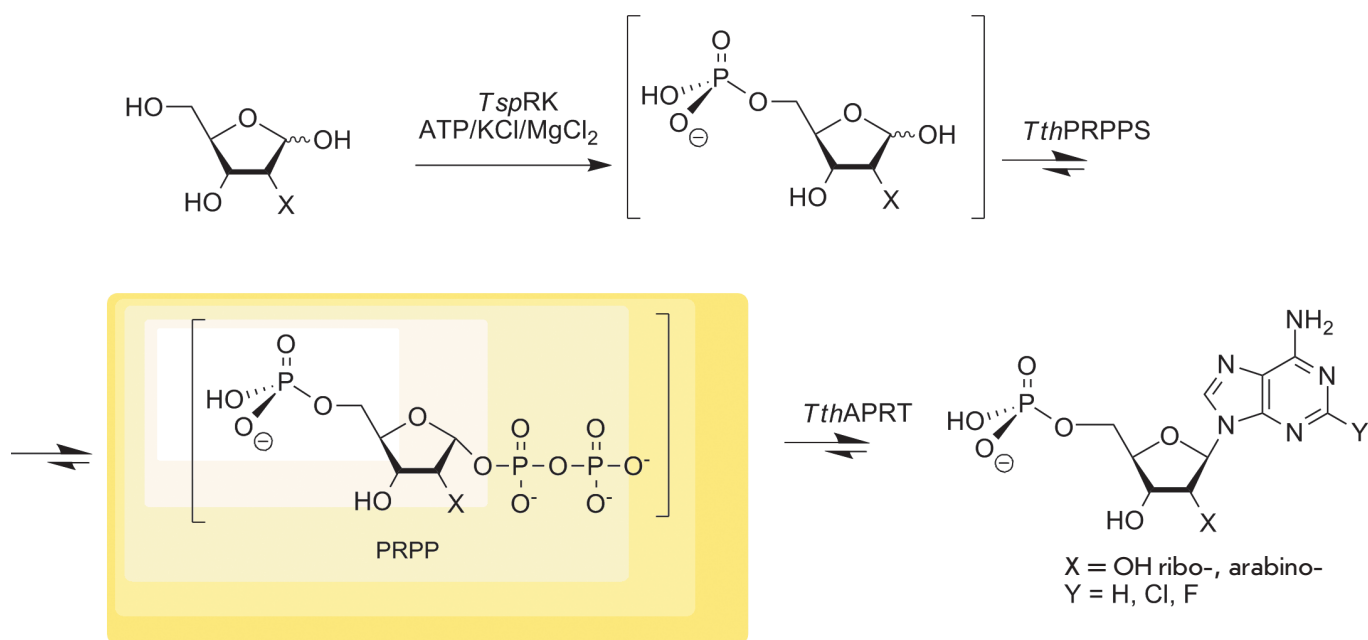


Fig. 1. A diagram of the multi-enzymatic cascade synthesis of substituted adenosine-5'-monophosphates.

that were recently successfully used in a cascade five-component synthesis of purine riboside-5'-monophosphates [22–24]. Nucleoside phosphorylases of thermophilic microorganisms are known to be less sensitive to the substrate structure [25, 26], which enables them to act at 70–80 °C and significantly increases the enzymatic reaction efficiency due to the increased solubility of heterocyclic substrates [27]. All these data aroused our interest in the purification of the recombinant enzymes ribokinase, phosphoribosylpyrophosphate synthetase, and adenine phosphoribosyltransferase from thermophilic microorganisms and in the investigation of their substrate properties to determine the applicability of these enzymes in the cascade synthesis of purine nucleoside-5-monophosphates according to the Diagram in Fig. 1.

MATERIALS AND METHODS

Cloning

Genes TT_RS05985, TT_RS06430, and TT_RS06315 encoding *TthPRPPS1*, *TthPRPPS2*, and *TthAPRT*, respectively, were amplified on the genomic DNA template of the *Thermus thermophilus* HB27 strain by a polymerase chain reaction (PCR) using synthetic primers. The QT17_05185 gene encoding RK from *Thermus* sp. 2.9 was codon-optimized for expression in *Escherichia coli* and synthesized by a chemical and enzymatic method from overlapping oligonucleotides. All genes were cloned into the expression vector pET-23d+ at

the *Nco*I and *Xho*I restriction endonuclease recognition sites.

Cultivation of producer strains

E. coli BL21(DE3), Rosetta (DE3), and C3029/pGTf2 strains were transformed with the produced expression vectors pER-PRPPS1-Tth, pER-PRPPS2-Tth, pER-APRT-Tth, and pER-RK-Tsp. Producer strains derived from *E. coli* BL21(DE3) and Rosetta(DE3) were cultured at 37 °C in a LB medium containing ampicillin (100 µg/mL). Cultivation of the producer strains derived from *E. coli* C3029/pGTf2 was carried out in a LB medium containing 50 µg/mL ampicillin, 20 µg/mL chloramphenicol, and 1 ng/mL tetracycline. After reaching a absorbance of $A_{595} = 0.8$, the cultures were added with IPTG to a final concentration of 0.4 mM and cultivation was continued at 23 and 37 °C. The cultivation duration varied from 4 to 16 h, depending on the strain. After culturing, the cell biomass was separated by centrifugation, homogenized at a 1:10 (w/v) ratio in a buffer solution (50 mM Tris-HCl, pH 8.5, 150 mM NaCl, 2 mM PMSF), and disrupted using a Labsonic P ultrasonicator (Sartorius, Germany) at 4 °C for 10 min (cycle, 0.4 sec; amplitude, 30%). The amount of target enzymes in soluble and insoluble cell fractions was determined by densitometric analysis of electrophoretic gels using the ImageLab 5.0 software (Bio-Rad, USA) [28]. The producer strains containing a maximum amount of the targeted protein in the supernatant were chosen: *E. coli* BL21(DE3)/pER-APRT-Tth

(culturing at 37 °C for 4 h after adding IPTG), *E. coli* Rosetta(DE3)/pER-PRPPS1-Tth (37 °C for 4 h), *E. coli* S3029/pGTf2/pER-PRPPS2-Tth (37 °C for 5 h), and *E. coli* S3029/pGTf2/pER-RK-Tsp (23 °C for 16 h). The strains were grown in 5–6 L of the culture medium.

Isolation and purification of *Tth*PRPPS1, *Tth*PRPPS2, and *Tsp*RK

Cell biomass of the producer strains *Tth*PRPPS1, *Tth*PRPPS2, and *Tsp*RK was re-suspended in a buffer solution (50 mM Tris-HCl, pH 8.7, 1 mM PMSF) at a 1:10 (w/v) ratio and disrupted using the Labsonic P ultrasonicator at +4 °C for 20 min (cycle, 0.5 sec; amplitude, 50%). Cell debris was removed by centrifugation at 12,000 rpm at +4 °C for 30 min on a Hermle Z383K centrifuge (HERMLE Labortechnik GmbH, Germany). In purification of *Tsp*RK, a clarified cell lysate was heat-treated at 65 °C for 10 min to precipitate contaminating proteins and DNA. The precipitate was removed by centrifugation. Further purification of the enzymes was carried out according to the same scheme. A clarified cell lysate was loaded onto a XK 16/20 column (GE Healthcare, USA) with Ni²⁺-IDA resin (Qiagen, Germany) pre-equilibrated with 50 mM Tris-HCl buffer, pH 8.7. Ballast proteins were removed by washing with 50 mM Tris-HCl buffer, pH 8.7, containing 50 mM imidazole. A target protein was eluted with a buffer solution of 50 mM Tris-HCl and 200 mM imidazole, pH 8.7. After affinity chromatography, fractions containing a target protein were added with EDTA to a concentration of 5 mM and concentrated using an Amicon 8200 200 mL stirred ultrafiltration cell (Millipore, USA) on an YM 10 kDa membrane (Millipore) when purified *Tth*PRPPS1 and *Tth*PRPPS2 and on an YM 30 kDa membrane (Millipore) when purified *Tsp*RK. Further purification was performed on a HiLoad 16/60 column with Superdex 200 resin (GE Healthcare) equilibrated with buffer containing 20 mM Tris-HCl, 1 mM ATP, 1 mM MgCl₂, 5% glycerol, 0.04% NaN₃, pH 8.5. Fractions containing a target protein were pooled and concentrated by ultrafiltration to a final concentration of 12 ± 1 mg/mL as previously described. The protein concentration was determined by the Bradford method using BSA as a standard [29]. Protein purity was determined by polyacrylamide gel electrophoresis under denaturing conditions [28]. Purified enzymes were stored at –80 °C.

Isolation and purification of *Tth*APRT

Cell biomass of the *Tth*APRT producer strain was disrupted according to the procedure described for the other enzymes. A clarified cell lysate was added with NaCl to a concentration of 300 mM and heat-treated at 65 °C for 10 min. After ballast protein precipitation by centrifugation, the lysate was applied to a PD-10 col-

umn with Sephadex G-25 Medium resin (GE Healthcare, USA) equilibrated with a buffer solution containing 20 mM Tris-HCl and 1.0 mM EDTA, pH 9.0. After desalting, the protein solution was loaded onto a XK 16/20 column with Q Sepharose XL (GE Healthcare, USA) equilibrated with the same buffer solution. A target protein was eluted with a linear concentration gradient of NaCl (0 to 400 mM). Fractions containing the target protein were pooled and loaded onto an XK 16/20 column with Phenyl Sepharose HP (GE Healthcare, USA) equilibrated with buffer containing 20 mM Tris-HCl, 1 M (NH₄)₂SO₄, 1.0 mM EDTA, pH 7.6. *Tth*APRT was eluted with a linear gradient of (NH₄)₂SO₄ (from 1 to 0 M). Fractions containing the target protein were pooled and concentrated by ultrafiltration on a PBGC 10 kDa polysulfone membrane to a final concentration of 5.0 ± 0.5 mg/mL as previously described. The final purification was performed on a HiLoad 16/60 column with Superdex 200 resin equilibrated with 20 mM Tris-HCl buffer, pH 8.0, containing 50 mM NaCl, 5% glycerol, and 0.04% NaN₃. Fractions containing the target protein were pooled and concentrated by ultrafiltration to a final concentration of 12 ± 1 mg/mL. The protein purity and concentration were determined as described previously [28, 29]. The purified enzyme was stored at –80 °C.

Enzymatic activity assay

The *Tsp*RK activity was determined radiochemically based on the formation of *D*-ribofuranosyl-5-[³²P]phosphate in the presence of [γ-³²P]ATP. A reaction mixture (0.05 mL, 20 mM Tris-HCl, pH 8.0) contained a 0.4 mM disodium ATP salt, 1 mM *D*-ribose, 5 mM MgCl₂, 50 mM KCl, 1 mM KH₂PO₄, 6 μCi of [γ-³²P]ATP, and 0.15 μg of *Tsp*RK. The mixture was incubated at 75 °C. Then, 0.8 μL aliquots were taken at 10, 20, and 40 min, applied to plates with PEI-cellulose, and eluted with 0.5 M aqueous potassium dihydrogen orthophosphate. The amount of *D*-ribofuranosyl-5-[³²P]phosphate was determined on a TRI-CARB 2100TR liquid scintillation counter (Packard BioScience Co.).

The *Tth*PRPPS1 and *Tth*PRPPS2 activity was determined in a reaction mixture containing a 1 mM disodium ATP salt, a 1 mM disodium salt of *D*-ribose-5 phosphate, 5 mM MgCl₂, 10 mM KH₂PO₄, 20 mM Tris-HCl, pH 8.0, at 75 °C. *Tth*PRPPS (0.75 μg) was added to 0.5 mL of the mixture.

The *Tth*APRT activity was determined in a reaction mixture containing 1 mM adenine, a 1 mM pentasodium salt of 5-phosphoribosyl-α-1-pyrophosphate (PRPP), 5 mM MgCl₂, and 20 mM Tris-HCl, pH 8.0, at 75 °C. *Tth*APRT (0.125 μg) was added to 0.5 mL of the reaction mixture. The amount of the product (μM) formed for 1 min was taken as the activity unit.

Determination of ribokinase kinetic parameters

A reaction mixture (0.5 mL, 20 mM Tris-HCl, pH 8.0) contained (a) a disodium salt of ATP (0.01 to 0.6 mM) and *D*-ribose (1 mM) or (b) *D*-ribose (0.01 to 8.0 mM) and ATP (1 mM) to determine the K_M and V_{max} values for ATP and *D*-ribose, respectively, 5 mM $MgCl_2$, 50 mM KCl, 10 mM KH_2PO_4 , and 0.0175 μ g of *TspRK*. Each experiment used 16 reaction mixtures. The mixtures were incubated at 75 °C for 12 min; each experiment was performed in triplicate. Then, the mean rate was determined in three experiments at the same enzyme concentration. Substrate and product concentrations were determined by HPLC under isocratic elution with 0.1 M KH_2PO_4 (water, pH 6.0, flow rate of 0.5 mL/min) with detection at 254 nm (Waters 2489 UV detector; Supelco-sil LC-18-T column, 5 μ m, 150 \times 4.6 mm).

Determination of the kinetic parameters of PRPP-synthetases

The kinetic parameters of the enzymes were determined at a ATP concentration that varied in the range of 0.005 to 0.2 mM. A similar interval was used for *D*-ribose-5 phosphate. The remaining conditions were the same as those in the enzymatic activity assay. The reaction was conducted for 2 min in triplicate. Then, the mean rate was determined in three experiments at the same concentration. Concentrations of ATP and AMP were determined by HPLC under isocratic elution with 0.1 M KH_2PO_4 (pH 6.0, flow rate of 0.5 mL/min) with detection at 254 nm (Waters 2489 detector; Supelco-sil LC-18-T column, 5 μ m, 150 \times 4.6 mm).

Determination of the kinetic parameters of APR-transferase

The kinetic parameters of APR-transferase were determined at an adenine concentration that varied in the range of 0.005 to 0.2 mM and a PRPP concentration that varied from 0.05 to 1.2 mM. The remaining conditions were the same as in the enzymatic activity assay. The reaction was conducted for 1 min in triplicate. The mean reaction rate was determined based on the results of three experiments at the same concentration. Adenine and AMP concentrations were determined by HPLC under isocratic elution with 36% aqueous methanol (flow rate of 0.5 mL/min) with detection at 254 nm (Waters 2489 detector; MZ PerfectSil 100 ODS-3 column, 5 μ m, 150 \times 4.6 mm).

The kinetic parameters were determined by a non-linear regression analysis using the SciDAVis v.0.2.4 software. The apparent catalytic constant (k_{cat}) was calculated per one subunit, whose weight was determined based on the amino acid sequence (32.0 kDa for *TspRK*, 34.5 kDa for *TthPRPPS1*, 34.6 kDa for *TthPRPPS2*, and 19.0 kDa for *TthAPRT*).

RESULTS AND DISCUSSION

To study the possibility of three-step nucleotide biosynthesis, we carried out comprehensive work on the production of recombinant enzymes of the nucleic acid metabolism (ribokinase, two PRPP-synthetases, and APR-transferase from *T. thermophilus*) and an investigation of their substrate properties.

The QT17_05185 gene encoding RK from *Thermus* sp. 2.9 was generated by a chemical-enzymatic method. Genes TT_RS05985, TT_RS06430, and TT_RS06315 encoding *TthPRPPS1*, *TthPRPPS2*, and *TthAPRT* from *T. thermophilus* HB27, respectively, were amplified from the genomic DNA by PCR. All genes were cloned into the plasmid vector pET23d+. The resulting expression vectors pER-PRPPS1-Tth, pER-PRPPS2-Tth, and pER-RK-Tsp contained hybrid genes with a reading frame including sequences encoding enzymes and an affinity tag of six histidine residues. The expression vector pER-APRT1-Tth contained an unmodified sequence encoding *TthAPRT*.

The plasmids were used to transform the *E. coli* strains BL21(DE3), Rosetta(DE3), and C3029/pGTF2. We determined the culture conditions under which producer strains synthesized target enzymes in soluble form. Producers of soluble recombinant *TspRK* and *TthPRPPS2* were derived from *E. coli* S3029/pGTF2. This strain was generated by transforming *E. coli* S3029 cells with the plasmid vector pGTF2 (Takara Bio Inc) carrying sequences encoding GroES-GroEL-Tig chaperones under the control of the Pzt-1 promoter. The choice of the *E. coli* Rosetta(DE3) strain for *TthPRPPS1* biosynthesis was based on the fact that the TT_RS05985 gene encoding *TthPRPPS1* contains codons rarely used in *E. coli* (one AGA, nine AGGs, 10 CGGs, one AUA, one CUA, and 15 CCCs). The Rosetta(DE) strain synthesizes tRNAs for these rare codons. Soluble recombinant *TthAPRT* was produced in the *E. coli* BL21(DE3) strain.

Isolation and purification of ribokinase and two PRPP-synthetases included metal chelate and gel filtration chromatography stages (Tab. 1). Heat treatment of the cell lysate during *TspRK* purification significantly enriched the target protein fraction due to aggregation of cellular proteins and DNA. A similar treatment of both *TthPRPP*-synthetases did not provide positive results, but it led to a loss of the target protein. Due to the high probability of proteolysis, metal chelate chromatography was conducted under cooling conditions, with addition of EDTA to the pooled fractions. Following the final purification step using gel filtration chromatography, all protein samples were concentrated.

Isolation and purification of *TthAPRT* included heat treatment, desalting, concentration, and anion exchange, hydrophobic interaction, and gel filtration chro-

Table 1. Steps of the isolation and purification of ribokinase, PRPP-synthetases, and APR-transferase

Purification step	Volume, mL	Protein concentration, mg/mL	Total protein, mg
Ribokinase from <i>Thermus</i> sp. 2.9			
1. Ultrasonic disintegration	150*	8.3	1245
2. Heat treatment	136	1.7	231.2
3. Metal chelate chromatography	30	1.9	57
4. Concentrating	9	6	54
5. Gel filtration chromatography	28.5	1.28	36.4
6. Concentrating	2.6	11.7	30.4
PRPP-synthetase 1 from <i>T. thermophilus</i> HB27			
1. Ultrasonic disintegration	150**	10	1500
2. Affinity chromatography	100	0.8	80
3. Concentrating	13	5.7	74.1
4. Gel filtration	50	1	50
5. Concentrating	4	12.3	49.2
PRPP-synthetase 2 from <i>T. thermophilus</i> HB27			
1. Ultrasonic disintegration	130**	11.2	1456
2. Affinity chromatography	125	0.6	75
3. Concentrating	10.3	6.2	63.9
4. Gel filtration	37.5	1.2	45
5. Concentrating	3.4	12	40.8
APR-transferase from <i>T. thermophilus</i> HB27			
1. Ultrasonic disintegration	157***	6	942
2. Heat treatment	149	1.3	193.7
3. Gel filtration	258	0.7	181
4. Anion exchange chromatography	72	1.2	86.4
5. Hydrophobic interaction chromatography	73	0.8	58.4
6. Concentrating	11	5	55
7. Gel filtration chromatography	52	0.87	45.2
8. Concentrating	3.4	12.5	42.5

* From 5.8 L of culture.

** From 5 L of culture.

*** From 6 L of culture.

matography steps (Table 1). As in the case of *Tsprk*, the first step involved heat treatment of a clarified cell lysate with addition of a salt to the solution (up to 300 mM sodium chloride), which greatly accelerated the aggregation of contaminating cell proteins and DNA.

The developed techniques provided a yield of all recombinant thermophilic enzymes not less than 8–10 mg per 1 L of the culture medium, with an electrophoretic purity of at least 95%.

Next, we determined the kinetic parameters and optimal activity conditions for the purified recombinant enzymes.

The specific activity of *Tsprk* was determined by a radiochemical method based on the formation of *D*-ribofuranosyl-5- ^{32}P]phosphate in the presence of $[\gamma\text{-}^{32}\text{P}]$ ATP. The amount of the product (μM) formed for 1 min was taken as the activity unit. The *Tsprk* activity was 5.5 U/mg.

The specific activity of *TthPRPPS1* and *TthPRPPS2* was determined indirectly via AMP formation in a reaction mixture (according to HPLC) in the presence of two substrates: ATP and *D*-ribose-5-phosphate. The activity was 0.85 U/mg for the former enzyme and 11 U/mg for the latter enzyme. Given the large differences in the enzyme activity, using the second synthetase for nucleotide synthesis seemed to be more rational, with allowance for a lower protein consumption. The *TthAPRT* properties were studied in a model reaction of adenine with 5-phosphoribosyl- α -1-pyrophosphate. The AMP formation was monitored by HPLC. The specific enzyme activity was 8.8 U/mg.

A high concentration of ribose as a substrate was found to inhibit the enzymatic activity of *Tsprk*. This effect was described for human ribokinase [30]. Therefore, the results of ATP experiments were analyzed using the Michaelis-Menten equation

Table 2. Kinetic parameters of the natural substrates of the studied enzymes

Substrate	K_M , μM	K_i , μM	V_{\max} , $\mu\text{M}/\text{min}\cdot\text{mg}$	k_{cat} , 1/s	k_{cat}/K_M , 1/M·s
Ribokinase from <i>Thermus</i> sp. 2.9					
ATP	75 ± 11	–	13 ± 1	6.8 ± 0.7	9.1×10^4
D-ribose	20 ± 6	$1,700 \pm 400$	13 ± 2	7.1 ± 1.2	3.5×10^5
PRPP-synthetase 1 from <i>T. thermophilus</i> HB27					
ATP	10 ± 2	–	0.71 ± 0.05	0.41 ± 0.03	4.3×10^4
D-ribose-5 phosphate	32 ± 6	–	0.85 ± 0.11	0.49 ± 0.06	1.5×10^4
PRPP-synthetase 2 from <i>T. thermophilus</i> HB27					
ATP	12 ± 2	–	20 ± 2	11 ± 1	9.9×10^5
D-ribose-5 phosphate	40 ± 4	–	24 ± 2	14 ± 1	3.4×10^5
APR-transferase from <i>T. thermophilus</i> HB27					
Adenine	13 ± 2	–	6.0 ± 0.4	1.9 ± 0.1	1.4×10^5
PRPP	179 ± 35	–	9.2 ± 1.1	2.9 ± 0.4	1.6×10^4

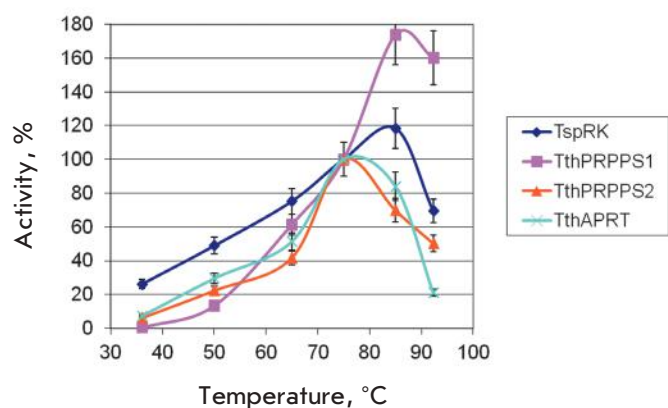


Fig. 2. The temperature dependence of the enzyme activity. The activity at 75 °C was taken as 100%. Reactions were conducted in a temperature range from 36 to 92 °C in 0.05 mL of 20 mM Tris-HCl buffer, pH 8.0, containing: 1) 0.4 mM ATP, 1 mM ribose, 1 mM KH_2PO_4 , 5 mM MgCl_2 , 50 mM KCl, 0.15 μg of *TspRK*, 2) 1 mM ATP, 1 mM D-ribose 5-phosphate, 5 mM MgCl_2 , 10 mM KH_2PO_4 , 0.75 μg of *TthPRPPS1* or *TthPRPPS2*, 3) 1 mM adenine, 1 mM PRPP, 5 mM MgCl_2 , 0.125 μg of *TthAPRT*.

$V = V_{\max} \times S / (K_M + S)$. In experiments with D-ribose, we used an equation allowing for the substrate inhibition effect due to the binding of a second molecule $V = V_{\max} \times S / (K_M + S + S^2 / K_i)$.

The kinetic parameters of natural substrates of the enzymes are listed in Tab. 2.

Figures 2–4 present the results of experiments on exploring optimal conditions for the activity of the recombinant enzymes.

The studied enzymes were active in a broad temperature range. The maximum activity of *TspRK* and *TthPRPPS1* was observed at 85°C, whereas the *TthAPRT*

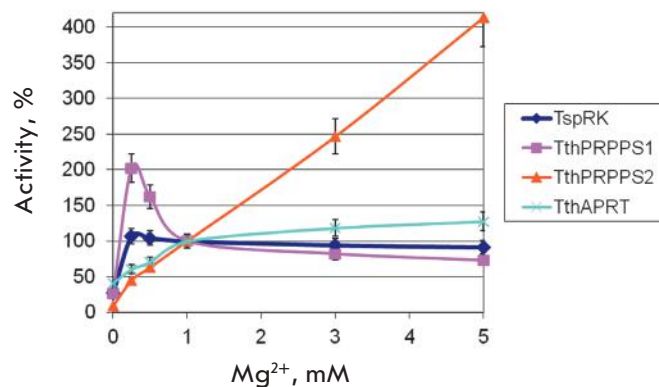


Fig. 3. The dependence of enzyme activity on the magnesium ion concentration. The activity in the presence of 1 mM Mg^{2+} was taken as 100%. Reactions were conducted at a temperature of 75°C, at a MgCl_2 concentration that varied from 0 to 5 mM, in 0.5 mL of 20 mM Tris-HCl buffer, pH 8.0, containing: 1) 0.4 mM ATP, 1 mM ribose, 1 mM KH_2PO_4 , 50 mM KCl, 0.15 μg of *TspRK*, 2) 1 mM ATP, 1 mM D-ribose 5-phosphate, 5 mM MgCl_2 , 10 mM KH_2PO_4 , 0.75 μg of *TthPRPPS1* or *TthPRPPS2*, 3) 1 mM adenine, 1 mM PRPP, 0.125 μg of *TthAPRT*.

activity at this temperature was lower by 35%. Therefore, we decided to conduct further cascade syntheses at 75°C.

The activity of the enzymes in a buffer solution lacking magnesium ions was very low. Addition of magnesium chloride to a concentration of 0.25 mM led to a considerable increase in the activity.

At higher concentrations, the dependence of enzyme activity on the magnesium ion concentration was as follows: the activity decreased in the case of *TspRK* and *TthPRPPS1*, increased in *TthAPRT*, and drastically increased in *TthPRPPS2*. Thus, the cascade reactions

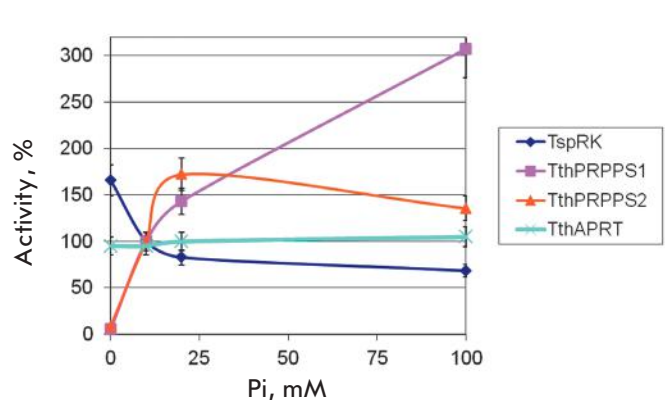


Fig. 4. The dependence of enzyme activity on the inorganic phosphate concentration. The activity in the presence of 10 mM Pi was taken as 100%. Reactions were conducted at a temperature of 75°C, at a KH_2PO_4 concentration that varied from 0 to 100 mM, in 0.5 mL of 20 mM Tris-HCl buffer, pH 8.0, 5 mM MgCl_2 , containing: 1) 0.4 mM ATP, 1 mM ribose, 50 mM KCl, 0.15 μg of *TspRK*, 2) 1 mM ATP, 1 mM *D*-ribose 5-phosphate, 0.75 μg of *TthPRPPS1* or *TthPRPPS2*, 3) 1 mM adenine, 1 mM PRPP, 0.125 μg of *TthAPRT*.

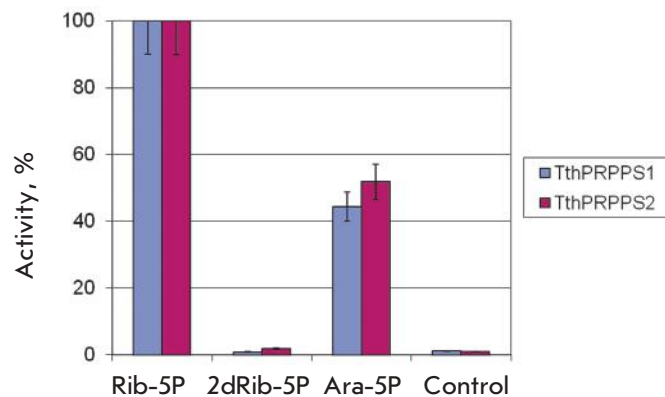


Fig. 6. Substrate specificity of PRPP synthetases toward various carbohydrate-5-phosphates. Reactions were conducted at a temperature of 75 °C in 0.5 mL of 20 mM Tris-HCl buffer, pH 8.0, containing 1 mM ATP, 1 mM carbohydrate-5-phosphate (no carbohydrates in the control reaction), 5 mM MgCl_2 , 10 mM KH_2PO_4 , 0.75 μg of PRPPS.

involving *TthPRPPS1* should be conducted at a magnesium chloride concentration of 0.25–0.5 mM; and those involving *TthPRPPS2* – at 5 mM magnesium chloride.

The enzymes responded differently to the addition of potassium orthophosphate. The activity decreased in the case of *TspRK*, remained unchanged in *TthAPRT*, and significantly increased in both *TthPRPPS*s, with the *TthPRPPS2* activity starting to decrease at a salt concentration of more than 25 mM. The optimum Pi

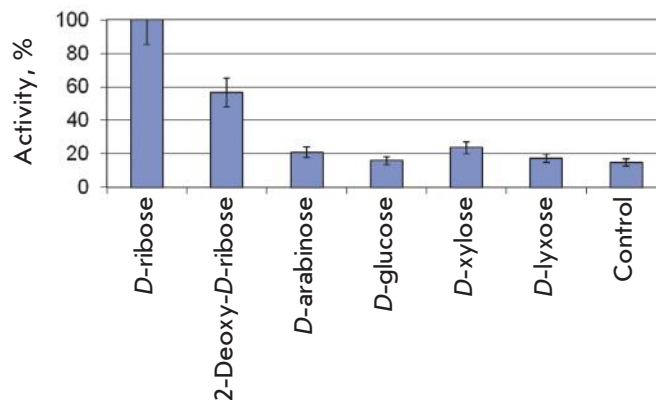


Fig. 5. Enzymatic activity of ribokinase in the presence of different carbohydrates. Reactions were conducted at a temperature of 75°C in 0.05 mL of 20 mM Tris-HCl buffer, pH 8.0, containing 0.4 mM ATP, 1 mM carbohydrate (no carbohydrates in the control reaction), 1 mM KH_2PO_4 , 5 mM MgCl_2 , 50 mM KCl, 0.15 μg of RK.

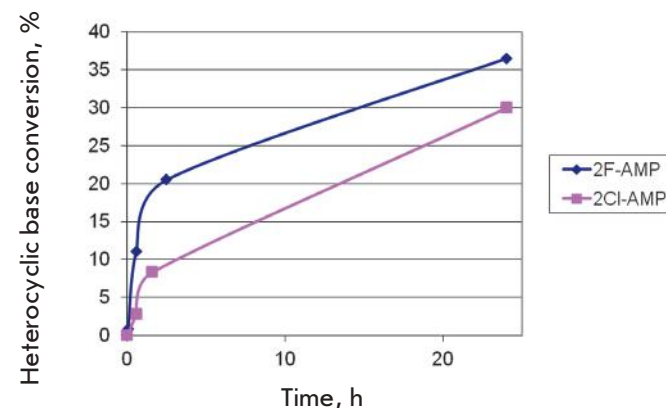


Fig. 7. Cascade synthesis of 2Cl-AMP and 2F-AMP from appropriate heterocyclic bases and *D*-ribose. Reaction conditions: 0.5 mM *D*-ribose, 1 mM ATP, 0.4 mM heterocyclic base (2-chloro- or 2-fluoroadenine), 20 mM Tris-HCl (pH 8.0), 50 mM KCl, 1 mM MgCl_2 , 10 mM KH_2PO_4 , 75°C, 0.3 μg of *TspRK*, 1.1 μg of *TthPRPPS1*, 0.25 μg of *TthAPRT* in 250 μL of the reaction mixture.

concentration for conducting cascade reactions is 10–25 mM.

The most crucial question remained the substrate specificity of each enzyme for different carbohydrates.

D-ribose and 2-deoxy-*D*-ribose are *TspRK* substrates (Fig. 5), with the activity toward deoxy-sugar being 57% of that for *D*-ribose. The activity toward *D*-arabinose and *D*-xylose was 2 times higher than the background activity, which may indicate that they can

Table 3. Substrates of APR-transferase

Base	Conversion for 24 h, %	MS of product, [M+H] ⁺
2,6-Diaminopurine	16.8	363.0786 (calc. 363.0813)
2-Chloroadenine	97.6	382.0257 (calc. 382.0314)
2-Fluoroadenine	36.5	366.0564 (calc. 366.0611)
Adenine	50.0	348.0677 (calc. 348.0704)
2-Methoxyadenine	60.9	378.0812 (calc. 378.0809)
N1-methyladenine	78.2	362.0843 (calc. 362.0800)
N6-benzyladenine	1.9	438.1117 (calc. 438.1173)
2-Aminobenzimidazole	0.1	346.0796 (calc. 346.0799)
1,2,4-Triazole-3-carboxy-N-methylamide	0	–
Guanine	0	–
Hypoxanthine	0	–
7-Deaza-2,6-diaminopurine	0	–

Note. Reaction conditions: reaction mixtures (0.5 mL; 20 mM Tris-HCl, pH 8.0, 75 °C) contained 0.4 mM heterocyclic base, 0.4 mM PRPP, 0 to 5 mM MgCl₂, 1.25 µg of *Tth*APRT.

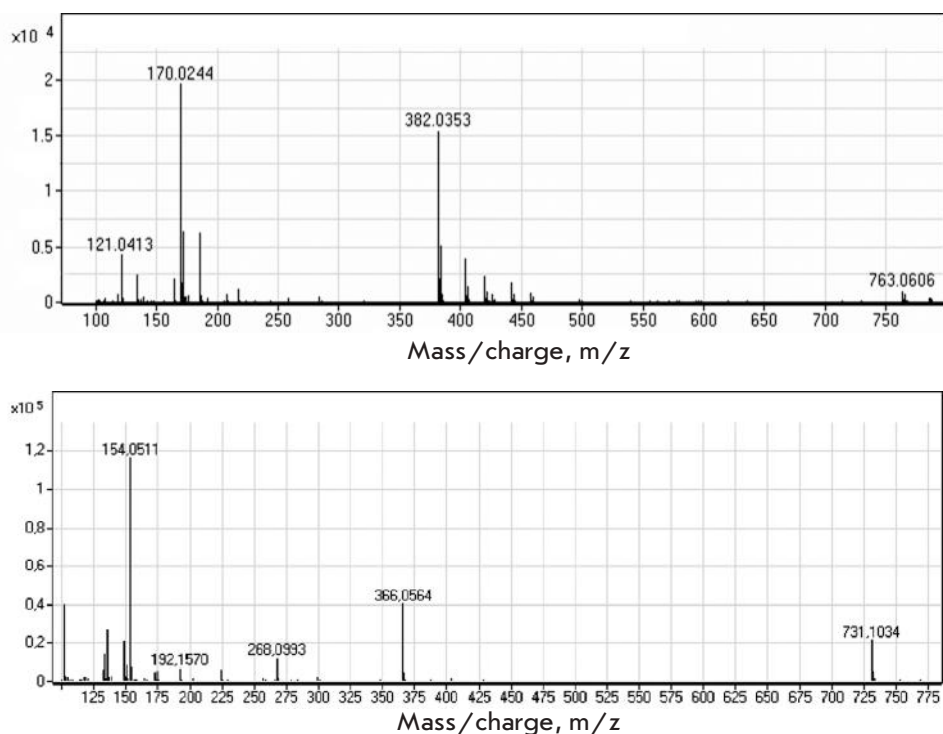


Fig. 8. a) A mass spectrum of the 2Cl-AMP nucleotide produced by cascade synthesis: C₁₀H₁₃N₅O₇P₁Cl₁, [M+H]⁺=382.0328, [M-P-Rib]⁺=170.0230. b) A mass spectrum of the 2F-AMP nucleotide synthesized by cascade synthesis: C₁₀H₁₃N₅O₇P₁F₁, [M+H]⁺=366.0564, [M-P-Rib]⁺=154.0511.

be used as substrates, but much less specific ones. Activity for *D*-glucose and *D*-lyxose was not detected.

We tested the activity of both *Tth*PRPPSs toward 2'-deoxy-ATP, GTP, and 2'-deoxy-GTP. The activity for 2'-deoxy-ATP was 80% of that for ATP. No activity toward GTP and 2'-deoxy-GTP was detected (data not

shown). It may be that these *Tth*PRPPSs are first-type enzymes [31]. All reactions were conducted under the same conditions as those for the activity assay: only the added substrate was varied. Both enzymes were able to catalyze the reaction with *D*-arabinose-5-phosphate (Fig. 6). However, activity for 2-deoxy-*D*-ribose-5

phosphate was not detected, indicating the importance of a hydroxyl group at the second sugar position to the enzymatic reaction.

We conducted several reactions to test the applicability of different heterocyclic bases for nucleotide synthesis. The data on nucleotide synthesis using *Tth*AP-RT are shown in *Tab. 3*.

The data in *Table 3* demonstrate that *Tth*APRT is specific to 6-aminopurines. 2-Chloroadenine, N1-methyladenine, and 2-methoxyadenine proved to be good substrates. No enzymatic activity was detected in reactions with hypoxanthine, guanine, N6-benzyladenine, aminobenzimidazole, and 1,2,4-triazole-3-carboxy-N-methylamide. The equilibrium in reactions with 2-chloroadenine was strongly shifted towards nucleotide formation (98% after 1 day). The reaction was conducted at 75 °C, which was preferable in the case of 2-chloroadenine because of its poor solubility. 2,6-Diaminopurine also was a substrate, while no product was detected in the reaction with its 7-deaza analogue, suggesting the need for a nitrogen atom at the seventh position of the purine.

After studying the substrate specificity of *Tth*AP-RT, we conducted a cascade synthesis of 2Cl-AMP and 2F-AMP from appropriate heterocyclic bases and *D*-

ribose. The results are shown in *Fig. 7*. The process of cascade nucleotide synthesis was monitored by a liquid chromatography-mass spectrometry analysis of the reaction mixture; samples were taken at 1, 2, 24 h from the start of the process. *Figure 8* shows the mass spectra of the target products.

Therefore, by the synthesis of 2-chloro (fluoro)-adenosine monophosphate (2Cl-AMP and 2F-AMP), we demonstrated the relevance of a thermophilic enzymatic system for the production of bioactive nucleotides.

CONCLUSION

Our findings indicate that a cascade of thermophilic enzymes of the nucleic acid metabolism (ribokinase; phosphoribosylpyrophosphate synthetase, and adenine phosphoribosyltransferase) can be used to produce modified nucleotides. This approach provides opportunities for the replacement of chemical methods of nucleotide synthesis with biocatalytic ones. ●

The authors are grateful to the Russian Science Foundation (project No. 14-50-00131) for financial support of this work.

REFERENCES

- Nelson D.L., Cox M.M. Nucleotides and Nucleic Acids. Lehninger Principles of Biochemistry, 3rd ed. N.Y.: Worth Publ., 2000. 1255 p.
- Bruce A. Molecular Biology of the Cell. N. Y.: Garland Publ., 2000. 974 p.
- Schärer O.D. // *Angew Chem. Int. Ed. Engl.* 2003. V. 42. № 26. P. 2946–2974.
- Jordheim L.P., Durantel D., Zoulim F., Dumontel C. // *Nat. Rev. Drug Discov.* 2013. V. 12. № 6. P. 447–464.
- De Clercq E. // *Rev. Med. Virol.* 2009. V. 19. № 5. P. 287–299.
- Diop-Frimpong B., Prakash T.P., Rajeev K.G., Manoharan M., Egli M. // *Nucl. Acids Res.* 2005. V. 33. № 16. P. 5297–5307.
- Famulok M., Hartig J.S., Mayer G. // *J. Chem. Rev.* 2007. V. 107. № 9. P. 3715–3743
- Peng C.G., Damha M.J. // *Nucl. Acids Res.* 2007. V. 35. № 15. P. 4977–4988.
- Golden J., Motea E., Zhang X., Choi J.S., Feng Y., Xu Y., Lee I., Berdis A.J. // *ACS Chem. Biol.* 2013. V. 8. № 11. P. 2452–2465.
- Lakshman M.K. Modified Nucleosides in Biochemistry, Biotechnology and Medicine. Weinheim: Wiley-VCH, 2008. 684 c.
- De Clercq E. // *Annu. Rev. Pharmacol. Toxicol.* 2011. V. 51. P. 1–24.
- Cen Y., Sauve A.A. // *Nucleos. Nucleotides. Nucleic Acids* 2010. V. 29. № 2. P. 113–122.
- Mikhailopulo I.A., Miroshnikov A.I. // *Mendeleev Commun.* 2011. V. 21. P. 57–68.
- Vineyard D., Zhang X., Donnelly A., Lee I., Berdis A.J. // *Org. Biomol. Chem.* 2007. V. 5. № 22. P. 3623–3630.
- Stein C.A., Cheng Y.C. // *Science.* 1993. V. 261. № 5124. P. 1004–1012.
- Motea E.A., Lee I., Berdis A.J. // *Nucl. Acids Res.* 2012. V. 40. № 5. P. 2357–2367.
- Mikhailopulo I.A. // *Curr. Org. Chem.* 2007. V. 11. № 4. P. 317–335.
- Wintersberger E. // *Biochem. Soc. Trans.* 1997. V. 25. № 1. P. 303–308.
- Tesmer J.J., Klem T.J., Deras M.L., Davisson V.J., Smith J.L. // *Nat. Struct. Biol.* 1996. V. 3. № 1. P. 74–86.
- Kim M.-J., Whitesides G.M. // *Appl. Biochem. Biotech.* 1987. V. 1. № 6. P. 95–108.
- Scism R.A., Stec D.F., Bachmann B.O. // *Org. Lett.* 2007. V. 9. № 21. P. 4179–4182.
- Scism R.A., Bachmann B.O. // *ChemBioChem.* 2010. V. 11. № 1. P. 67–70.
- Nagy M., Ribet A.M. // *Eur. J. Biochem.* 1977. V. 77. № 1. P. 77–85.
- Lee D., Moffatt B.A. // *Physiologia Plantarum.* 1993. V. 87. № 4. P. 483–492.
- Zhou X., Mikhailopulo I.A., Cruz-Bournazou N., Neubauer P. // *J. Mol. Catalysis B: Enzymatic.* 2015. V. 115. P. 119–127.
- Zhou X., Szeker K., Jiao L.-Y., Oestreich M., Mikhailopulo I.A., Neubauer P. // *Adv. Synthesis & Catalysis.* 2015. V. 357. № 6. P. 1237–1244.
- Taran S.A., Verevkina K.N., Feofanov S.A., Miroshnikov A.I. // *Russ. J. Bioorg. Chem.* 2009. V. 35. № 6. P. 739–745.
- Laemmli U.K. // *Nature.* 1970. V. 227. № 5259. P. 680–685.
- Bradford M.M. // *Anal. Biochem.* 1976. V. 72. P. 248–254.
- Park J., van Koeven P., Singh B., Gupta R.S. // *FEBS Lett.* 2007. V. 581. № 17. P. 3211–3216.
- Kadziola A., Jepsen C.H., Johansson E., McGuire J., Larsen S., Hove-Jensen B. // *J. Mol. Biol.* 2005. V. 354. № 4. P. 815–828.

Downregulation of Purkinje Cell Activity by Modulators of Small Conductance Calcium-Activated Potassium Channels In Rat Cerebellum

T. V. Karelina*, Yu. D. Stepanenko, P. A. Abushik, D. A. Sibarov, S. M. Antonov

I.M. Sechenov Institute of Evolutionary Physiology and Biochemistry of the Russian Academy of Sciences, prosp. Toreza, 44, Saint-Petersburg, 194223, Russia

*E-mail: karelina_tanja@mail.ru

Received January 20, 2016

Copyright © 2016 Park-media, Ltd. This is an open access article distributed under the Creative Commons Attribution License, which permits unrestricted use, distribution, and reproduction in any medium, provided the original work is properly cited.

ABSTRACT Small-conductance calcium-activated potassium channels (SK channels) are widely expressed in CNS tissues. Their functions, however, have not been well studied. Participation of SK channels in Purkinje cell (PC) pacemaker activity has been studied predominantly *in vitro*. Here we studied for the first time the effects of SK channel activation by NS309 or CyPPA on the PC simple spike frequency *in vivo* in adult (3 – 6 months) and aged (22 – 28 months) rats using extracellular microelectrode recordings. Both pharmacological agents caused a statistically significant decrease in the PC simple spike frequency. The maximum value of the decrease in the simple spike frequency did not depend on age, whereas a statistically significant inhibition of the spike frequency was achieved faster in aged animals than in adult ones. In experiments on cultured neurons PCs were identified by the expression of calbindin as the PC-specific marker. Registration of transmembrane currents in cerebellar neurons revealed the direct action of NS309 and CyPPA on the SK channels of PC consisted in the enhancement of outward potassium currents and action potential after-hyperpolarization. Thus, SK channel activators can compensate for age-related changes of the autorhythmic functions of the cerebellum.

KEYWORDS cerebellum, Purkinje cells, SK channels, ageing

ABBREVIATIONS PC – Purkinje cells; calbindin – calbindin-D28k; CyPPA – N-cyclohexyl-N-[2-(3,5-dimethyl-pyrazol-1-yl)-6-methyl-4-pyrimidinamine; NS309 – 6,7-dichloro-1H-indole-2,3-dione 3-oxime; SK channels – small-conductance Ca²⁺-activated K⁺ channels; VGCC – voltage-gated calcium channels

INTRODUCTION

The cerebellum is an important part of the CNS due to the variety of functions it performs. The cerebellum plays a key role in motor activity by monitoring all motor acts and minimizing the error between an intended and performed action [1]. One of the manifestations of cerebellar dysfunction is spinocerebellar ataxia, a disruption of the accuracy and coordination of voluntary movements, the development of which is often associated with the death or dysfunction of Purkinje cells (PC). In addition, the dysfunction manifested in the change in the pattern of PC activity can occur prior to the disruption of motor activity. For example, in mice with genetically determined hereditary spinocerebellar ataxia type 2, physical activity begins to deteriorate on the 8th week, the number of PC start to decrease on the 12th week, while the decrease in the PC discharge frequency can be registered as early as on week 6 of postnatal development [2]. Studies carried out on sections of the cerebellum of mice and rats have demon-

strated that pacemaker activity changes in such neurodegenerative diseases as spinocerebellar ataxia type 2 and 3, as well as episodic ataxia type 2 [3–5].

Ca²⁺-activated K⁺ channels are expressed by many neurons of the CNS and are of three types: channels of large (BK), small (SK), and intermediate (IK) conductance [6]. SK channels are voltage-independent channels which are directly activated only by Ca²⁺ at submicromolar concentrations [7], enhancing the action potential after-hyperpolarization in neurons [6]. PCs are characterized by a pronounced expression of small-conductance Ca²⁺-activated K⁺ channels of the SK2 subtype [8]. Blocking SK2 channels with apamin in PCs that have a trimodal pattern of activity causes a shortening of its cycles, while in cells with a tonic type of discharge this leads to increased frequency and occurrence of explosive discharge [9].

We have previously shown that the frequency of simple spikes increases and the depression period after a complex spike decreases in normal aging in PCs [10,

11]. A similar age-related increase in the frequency of PC discharges was shown in the study by Kasumu et al. in mutant mice with a model of spinocerebellar ataxia type 2 [12].

Almost all studies of SK channels in cerebellar PC are performed under *in vitro* conditions. However, in this case, the integrity of the cerebellum structure itself, as well as the afferent and interneuronal connections, is disturbed. Numerous papers devoted to genetically predetermined cerebellar pathologies have been based mainly on young and adult animals, whereas information on the changes in PC functions in aged animals during normal aging remains scant. For this reason, a comparative study of the features of PC function *in vivo* in late ontogenesis appears to be important. Taking into account the direct involvement of SK channels in the regulation of the pattern of cerebellar PC activity and its change during aging, as well as the contribution of SK channels to the development of various neurodegenerative diseases, the objective of this work was to perform a comparative study of the contribution of SK channels to the pattern of PC activity in adult and aged rats.

EXPERIMENTAL SECTION

Extracellular registration of cerebellar PC activity *in vivo*

This study was conducted on Wistar rat males and females. The animals were divided into two groups during the experiment: adults (3 to 6 months) and aged (21 to 24 months). For the anesthesia of the animals, urethane was used, which was administered intraperitoneally at a rate of 1,300 and 1,000 mg/kg of body weight of the adult and aged rats, respectively. PCs were registered and identified as previously described [13]. In anesthetized animals, the scalp and muscle layer were removed, and a hole 1 mm in diameter was drilled in the occipital bone above the cerebellar vermis. Next, the animal was fixed in a stereotaxic frame. For the registration of extracellular PC activity, microelectrodes made of borosilicate glass (outer diameter: 1.5 mm, inner diameter: 1.10 mm, Sutter Instrument, USA) and filled with a solution of 2.5 M NaCl were used. A microelectrode was placed in the cerebellar tissue using an automatic manipulator with a penetration step of 5 μm and a depth of up to 5 mm. PCs were identified by their characteristic pattern of activity: the presence of simple and complex spikes, as well as a pause after a complex spike before a series of simple spikes. The signal of the registered cell was amplified (AC/DC Differential Amplifier, model 3000, A-M Systems, Inc., USA) and digitized at a sampling frequency of 10,000 smp/s (ADC L-791, "L-CARD" Ltd, Russia) using the original Bioactivity Recorder v.5.3

software developed by D.A. Sibarov [<http://sibarov.ru/index.php?slab=software>] for further analysis of simple frequency spikes using the Clampfit 10.2 software (Molecular Devices Corp., USA). Active substances were loaded according to the standard method [14] by application to the exposed surface of the cerebellum in the area of microelectrode placement. First, control series of experiments were conducted in which the application of saline (0.9% NaCl) was performed. Then, a positive modulator of SK and IK channels NS309 (Tocris, USA) and selective activator of small-conductance calcium-activated potassium channels of the SK2 and SK3 subtypes, CyPPA (Tocris, USA), were used in the next series of experiments (Fig. 1). The concentrations of active substances chosen depending on the depth of microelectrode penetration were 100–200 μM for NS309 and 1–2 mM for CyPPA. Solutions of the active substances were prepared in 0.9% NaCl. Registration of PC activity was performed for 30 sec prior to substance application and then during periods of the same duration 5, 15, 30, 45 and 60 min after application.

In order to compare the control and experimental data, the frequency of simple spikes was measured in each cell for 30 sec for all the specified time points. Then, relative frequencies for each time point were calculated taking the frequency of spikes prior to application as the unit rate. The mean frequency value and standard error of mean (SEM) were calculated for each time point. Two-way ANOVA with Bonferroni's post-test was used for the assessment of the statistical significance of the differences between the control and experimental data, i. e. under the action of positive modulators. For a comparison of the original frequency with the average values at each time point in the control series of experiments, one-way ANOVA was used.

Preparation of the primary culture of cerebellar neurons

In primary cultures of neurons isolated from different parts of the embryonic brain, particularly the cer-

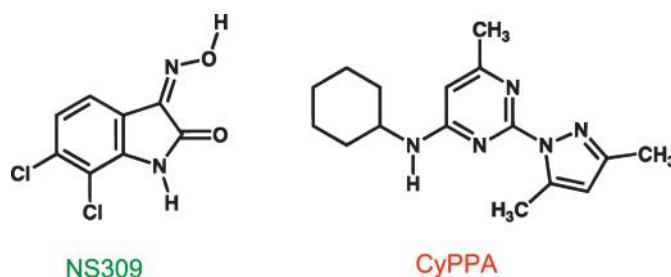


Fig. 1. Chemical structure of the activators, or allosteric modulators, of SK channels that increase their sensitivity to calcium

erebral cortex [15] and the cerebellum [16], a differentiation of the main types of neurons characteristic of these regions in the adult brain takes place. For example, a primary culture of cerebellar neurons has been successfully used to study the properties of Purkinje cells [17]. Primary cultures were prepared from the cerebellum of embryos on day 20–21 of prenatal development (E20–E21). In order to obtain a suspension of cerebellum cells, the isolated tissue was placed in a trypsin solution (0.04 mg/ml) and the cells were then treated with a DNase solution (0.04 mg/ml), trypsin inhibitor, and fetal bovine serum. After centrifugation, cell dissociation was performed by pipetting in the medium. Dispersed cells were cultured on 7-mm glasses treated with a poly-*D*-lysine in Neurobasal medium (Gibco, USA) supplemented with B27 (Gibco, USA), *L*-glutamine (Gibco, USA), and 20 mM KCl to increase the chance of survival of cerebellar neurons, including Purkinje cells and granular neurons [18].

Registration of neuronal currents by the voltage-clamp method

The direct effect of SK channel modulators on neurons in a primary culture of cerebellar neurons was confirmed using the voltage-clamp in the whole-cell configuration. In the current fixation mode, we registered the action potential shape, and in the voltage-clamp mode, we obtained the current-to-voltage characteristics of SK channels.

Experiments in cerebellar culture cells were performed on day 7–8 *in vitro* (DIV 7–8). Extracellular saline of the following composition was used in the experiments: 140 mM NaCl, 2.8 mM KCl, 2 mM CaCl, 10 mM HEPES. Intracellular solution for microelectrode filling had the following composition (mM): 9 NaCl, 17.5 KCl, 121.5 K-gluconate, 1 MgCl₂, 10 HEPES, 0.2 EGTA, 2 MgATP, 0.5 NaGTP. A MultiClamp 700B amplifier with a Digidata 1440A data collection system and the pClamp v10.2 software (Molecular Devices, USA) were used for current registration. The sampling frequency was 20,000 smp/s. The initially registered signal was subjected to preliminary analog filtering (equivalent of the 8th-order Bessel high-pass filter) with a cutoff frequency of 200 Hz. For the application of test substances (100 μM CyPPA or 10 μM NS309), a BPS-4-based system for a quick change of solutions (Ala Scientific Instruments, USA) with a multi-channel capillary perfusion was used, the tip of which was placed 200–300 μm away from the registered cell. PCs were identified by soma size, which is significantly larger than for other types of neurons (about 4-fold) and rhythmic generation of action potentials.

The current-to-voltage characteristics of the channels activated by CyPPA and NS309 were determined

based on the difference between the neuronal currents registered under the Ramp protocol: a smooth change in the potential from –100 to +60 mV in 5 seconds before and after the application of substances. The statistical significance of the changes in the after-hyperpolarization of spikes under the influence of positive modulators of SK and IK channels was evaluated using the unpaired Student's *t*-test.

Immunohistochemical staining of Purkinje cells

The presence of PC in a primary culture of rat cerebellar cells was additionally monitored using an immunocytochemistry analysis of calbindin protein expression, a marker of this type of neurons [19]. During preparation for immunocytochemical staining, the glasses with cells were fixed with a 4% formaldehyde solution and then treated with ammonium chloride (0.535 mg/ml), Triton X-100 (0.2% solution), and glycine (15 mg/ml). Non-specific binding of antibodies was blocked by treating the glasses with cells with a 2% solution of bovine serum albumin. All solutions were prepared based on PBS. For the identification of calbindin in PC, mouse primary monoclonal antibodies to this protein (Calbindin-D28k, Abcam, ab82812) were used. Immunopositive reaction was visualized using secondary antibodies conjugated to Alexa 633 fluorochrome (Molecular Probes A21052, Life Technologies, USA). In order to avoid rapid bleaching of fluorescent dyes, the glasses, treated with antibodies, were fixed on slides with an adhesive containing the Mowiol compound (Sigma-Aldrich, Germany). The fluorescence of immunopositive neurons was registered on a confocal scanning microscope Leica SP5 MP (Leica Microsystems Inc., Germany) equipped with ×63 oil immersion lens (HCX APO CS 63×/1.4; Leica Microsystems, Inc., Germany). Excitation of the Alexa 633 dye was performed using an argon laser with a wavelength of 633 nm. The dye emission range was 640–700 nm. Image processing was performed using the Leica LAS AF software (Leica Microsystems Inc., Germany).

RESULTS

Influence of positive modulators of SK channels on the PC simple spike frequency in aged rats

In our study, all afferent PC connections were preserved during the registration of PC action potentials *in vivo*, in contrast to the experiments carried out on the tissue sections, which caused irregular pulse intervals. Examples of a typical PC activity in aged animals are shown in the control and upon NS309 action, as well as in the control and upon CyPPA action (*Fig. 2A*). Application of physiological saline did not cause significant changes in the frequency of PC simple spikes in aged

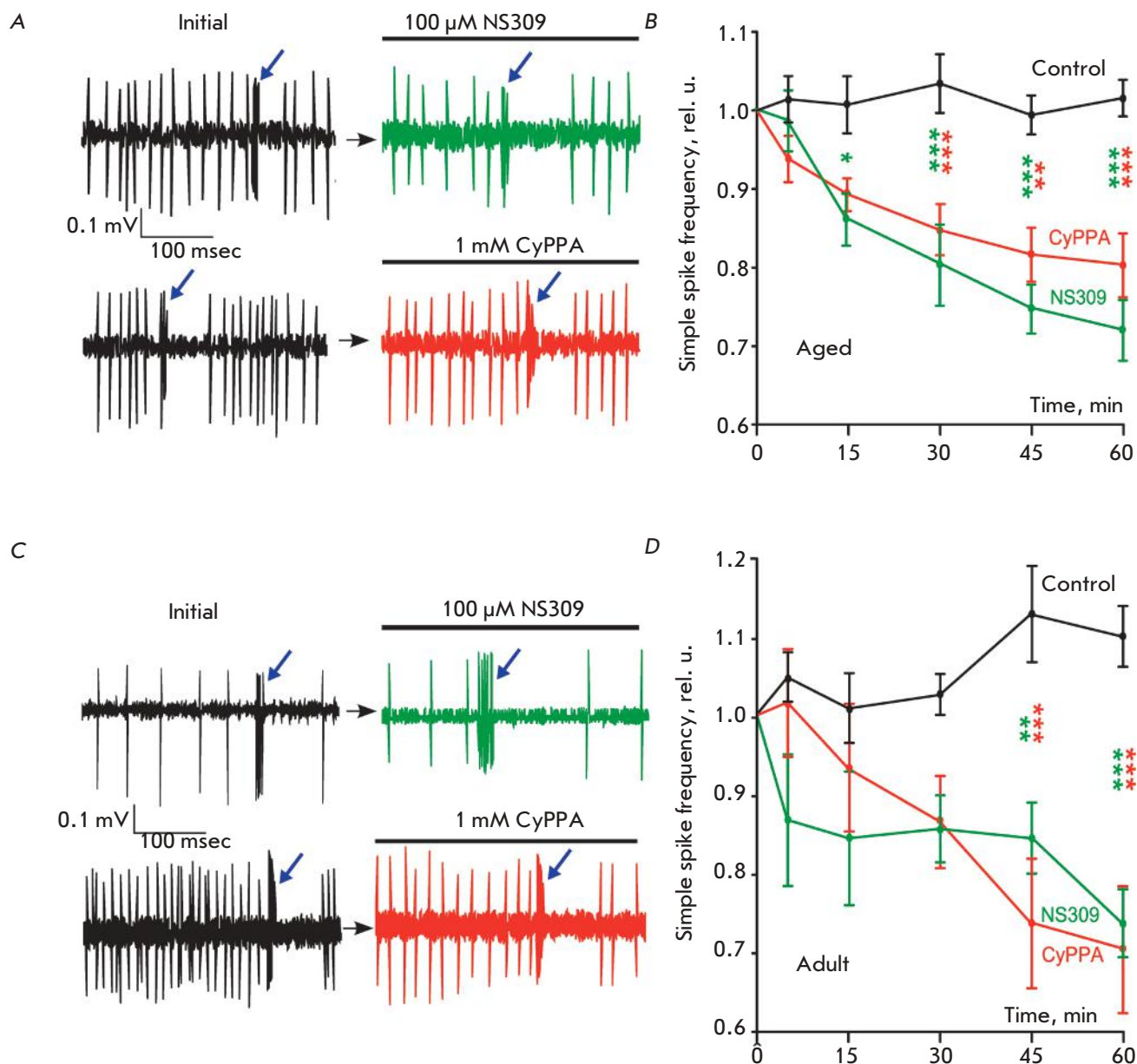


Fig. 2. Activity of rat cerebellar Purkinje cells under the influence of positive modulators of calcium-activated potassium channels. **A** – aged rats. Fragments of a recording of the activity of individual PCs prior to and after CyPPA and NS309 application. Arrows indicate episodes of occurrence of complex spikes. **B** – aged rats. Change in the medium frequency of simple spikes of cerebellar PC for 1 hour after the application of saline or SK channel activators. **C** – adult rats. Fragments of a recording of the activity of individual PCs prior to and after CyPPA and NS309 application. **D** – adult rats. Change in the medium frequency of simple spikes of cerebellar PC for 1 hour after the application of saline or SK channel activators. Green asterisks indicate a statistically significant difference from the control frequency values at the corresponding moments of NS309 application, red – CyPPA application (ANOVA, Bonferroni post-test * – $p < 0.05$, ** – $p < 0.01$, *** – $p < 0.001$)

animals for 60 minutes (15 to 43 Hz at the beginning and 16 to 48 Hz at the end, $p > 0.95$, $n = 7$, ANOVA). The increase in the average value of the relative frequency of simple spikes at certain periods of registration was 0–3% and reached its maximum value 30 min-

utes after application (Fig. 2B). These results clearly demonstrate that the application procedure did not affect the pattern of PC discharge.

NS309 caused a gradual decrease in the simple spike frequency of PCs. Significant differences in the fre-

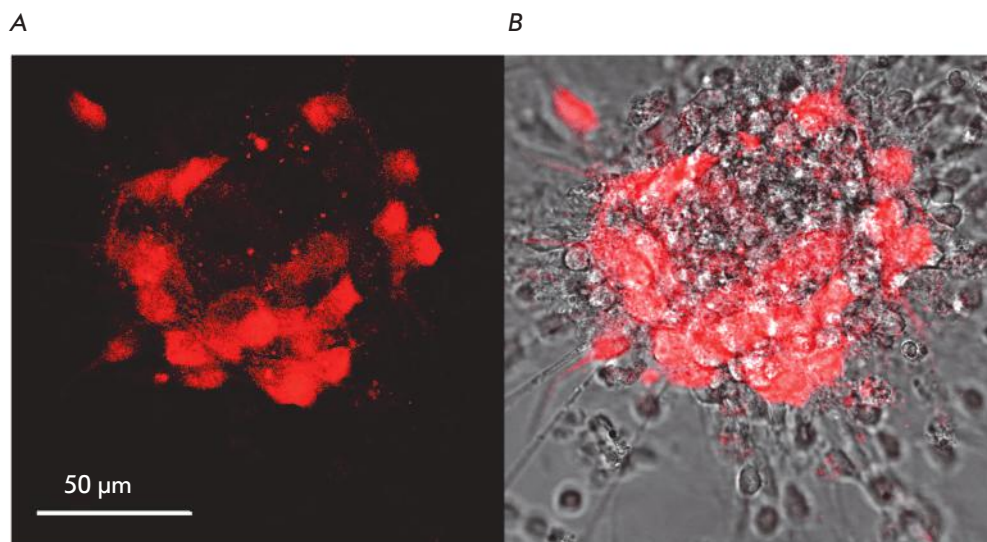


Fig. 3. Purkinje cells in a DIV 7 primary culture of rat cerebellum neurons. **A** – fluorescent image of the immunopositive response to the calbindin protein, which is expressed only in Purkinje cells. **B** – result of image superposition in transmitted light and fluorescence of the calbindin-D28k protein obtained by immunolabeling of the corresponding protein with antibodies conjugated with Alexa 633 fluorochrome

quency in the control at the appropriate time point ($p < 0.05$, $n = 10$, ANOVA, Bonferroni post-test) were revealed 15 min after application, which persisted until the end of the registration period. The lowest value of the simple spike frequency was achieved 60 min after the start of application and was on average 29% lower than the control value at this time (Fig. 2B).

Upon CyPPA action, a statistically significant decrease in the simple spike frequency of the PC discharge ($p < 0.001$, $n = 11$, ANOVA, Bonferroni post-test) occurred 30 minutes after the start of registration, i. e. later than in the case of NS309, while the maximum decrease at the end of registration was on average 21% (Fig. 2B).

Influence of positive modulators of SK channels on the PC simple spike frequency in aged rats

Figure 2B shows examples of a typical PC activity in adult animals in the control and under NS309 action, as well as in the control and under CyPPA action. In this age group, a tendency for an increase in the frequency of simple spikes was noted upon the application of saline. However, these changes were not statistically significant ($p > 0.10$, $n = 8$, ANOVA).

In adult animals, a decrease in the simple spike frequency of the PC discharge was achieved 45 min after the start of NS309 application ($p < 0.001$, $n = 9$, ANOVA, Bonferroni post-test), i. e. later than in aged mice. The maximum, 33% on average, decrease occurred at the end of the 60th minute of registration (Fig. 2D).

Upon CyPPA application, as in the case of NS309, a statistically significant decrease in the simple spike frequency of the PC discharge was achieved 45 minutes after the start ($p < 0.001$, $n = 8$, ANOVA, Bonferroni

post-test). The maximum decrease occurred after 60 minutes (a median 36% decrease) (Fig. 2D).

Despite the fact that a significant decrease in the simple spike frequency upon the action of both positive modulators of SK channels was achieved earlier in aged rats compared to the control, the maximum effect of CyPPA ($n = 11$) and NS309 ($n = 10$) did not differ in the animals regardless of age. Moreover, we did not manage to detect a statistically significant difference in the effects of NS309 and CyPPA in aged and adult rats ($p > 0.8$, ANOVA).

Electrical activity of cerebellar neurons in culture under the influence of SK channel modulators

Cerebellar cells in a primary culture form a neuronal network on day 7 of culturing, wherein immunohistochemical staining for calbindin-D28k confirmed the presence of Purkinje cells distinguished by the large size of their soma (Fig. 3). In an electrophysiological study, part of the “large” neurons were characterized by a spontaneous periodic generation of an action potential (AP) typical of Purkinje cells.

It cannot be unambiguously concluded from the *in vivo* experiments whether the studied modulators act directly on PC or whether their effect is mediated by net interactions through influence on intercalary neurons. In order to test the hypothesis on the direct action of CyPPA and NS309 on cerebellar neurons, we studied their impact on spike generation by neurons in a primary culture using local perfusion. In neurons with spontaneous generation of AP (Fig. 4A), the application of 10 μ M CyPPA caused transient depolarization followed by hyperpolarization, accompanied by an attenuation of the spontaneous generation of AP ($n = 5$). The generation of spikes caused by the injection of a current

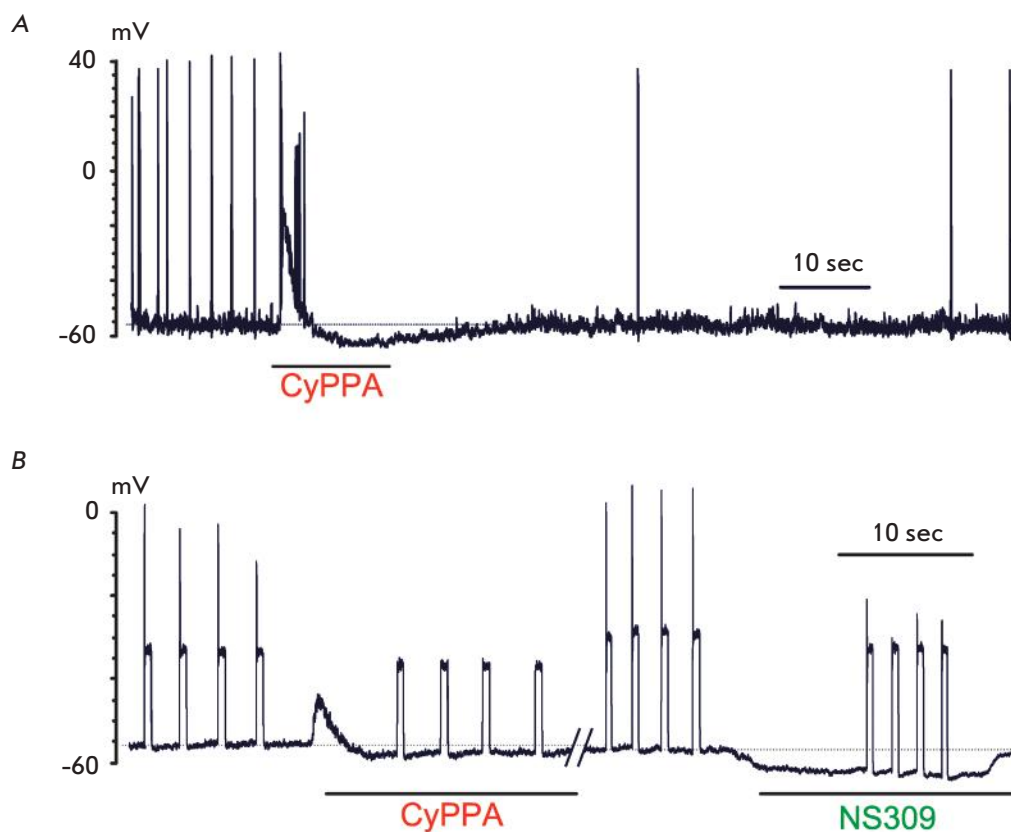


Fig. 4. Examples of the influence of CyPPA and NS309 on the spontaneous generation (A) and action potentials caused by a depolarizing stimulus (B) in cerebellar neurons. Intracellular registration of the membrane potential in the current-clamp mode. Action potentials were evoked by current injection (1.1 threshold value) through a recording electrode

of threshold amplitude in neurons without spontaneous activity was effectively suppressed by the application of both 100 μM CyPPA and 10 μM NS309 ($n = 18$, Fig. 4B). Both substances induced hyperpolarization, with the effect being more pronounced in the case of NS309. A comparison of the forms of AP of a spontaneously active neuron before and after the application of potassium channel activators showed that both substances enhance AP after-hyperpolarization (Fig. 5A). Such phenomenology is typical of the activation of SK channels. In addition, after-hyperpolarization at the point of minimum was increased by 3.1 ± 0.3 mV upon the action of CyPPA and by 6.1 ± 0.3 mV upon the action of NS309. The effect of NS309 was significantly stronger than that of CyPPA ($n = 140$; $p < 0.01$, unpaired Student's t -test). The current-to-voltage characteristics of the channels activated by CyPPA and NS309 presented in Fig. 5B are also typical of SK channels [20].

Thus, CyPPA and NS309 similarly suppress the generation of AP by Purkinje cells both *in vivo* when applied to the cerebellum surface and *in vitro* in a primary culture of neurons.

DISCUSSION

There is evidence indicating that NS309 and CyPPA, positive modulators of SK channels, change the pattern

of neuronal activity. Experiments performed on sections of the cerebellum have demonstrated a decrease in the frequency of PC discharge after NS309 application in a bath with a washing solution [3]. Similar results were obtained in *in vivo* experiments, showing that the use of CyPPA and NS309 causes a decrease in the discharge frequency of substantia nigra dopaminergic neurons [21, 22]. In our experiments conducted *in vitro* on primary cultures of cerebellar neurons, CyPPA and NS309 also effectively suppressed the generation of spontaneous and evoked spikes (Fig. 4A, B) because of an increase in the after-hyperpolarization (Fig. 5A) caused by SK channel activation (Fig. 5B) directly in the studied neurons. CyPPA is a selective activator of SK2 and SK3 channels, while only Purkinje cells are characterized by a high expression of SK2 in the cerebellar cortex in the late prenatal and postnatal periods [8], which makes these cells the primary target of the action of SK channel activators. Due to the anatomical structure of the cerebellum, activators of SK channels, when applied to the surface, first penetrate the molecular layer, where they can interact with the dendritic tree of PC and PC somas during diffusion (Fig. 6A). The roles of dendritic and somatic SK channels vary. In young rats (10–90 days of age), a blockage of somatic SK channels enhances the frequency of arrhythmic activity of PC, whereas a blockage of den-

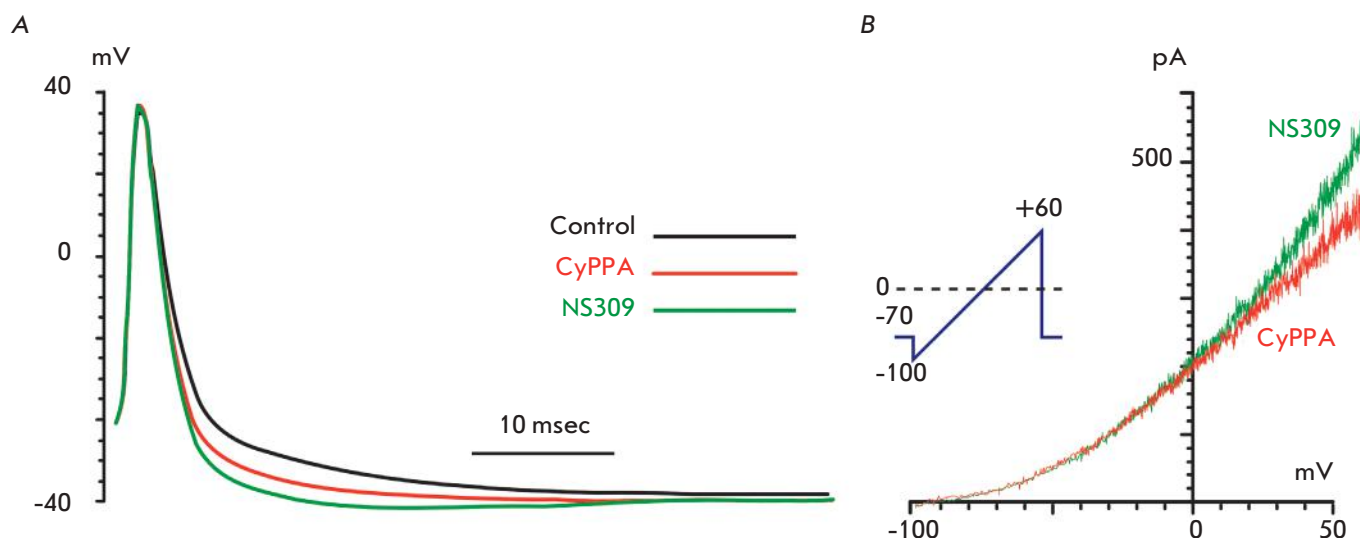


Fig. 5. Influence of CyPPA and NS309 on the after-hyperpolarization in the neurons of the cerebellum. **A** – mean action potentials in the control and in the presence of 100 μM CyPPA or 10 μM NS309 (no less than 140 AP was averaged for each condition) registered upon fixation of a neuronal current. **B** – current-voltage characteristics of the channels activated by CyPPA and NS309 in cerebellar neurons registered in the current-clamp mode. Insertion illustrates the Ramp protocol used to measure the current-to-voltage characteristics of SK channels

dritic SK channels not only enhances the frequency of simple spikes, but also reduces the leakage current and improves transmission in synaptic inputs to PC [9]. Furthermore, a blockage of only dendritic SK channels had a significantly lesser effect than a blockage of dendritic and somatic SK channels [9]. Apparently, in our experiments, the gradual diffusion of NS309 or CyPPA from PC dendrites toward the soma determines the gradual enhancement of the effect of these SK channel activators with time. In our experiments conducted *in vivo*, activation of SK channels by the positive modulators CyPPA and NS309 resulted in a change in the pattern of PC activity. In both the groups of adult and aged rats, the simple spike frequency was statistically significantly reduced compared to the control series. Although the reduction in the simple spike frequency caused by SK channel modulators was almost identical for the groups of adult and aged rats, the decrease in the frequency of simple spikes in aged rats occurred earlier compared to the control: 30 min after CyPPA application and 15 min after NS309 application. In adult rats, the decrease in the simple spike frequency under the influence of both substances was observed after 45 min.

CyPPA and NS309 in saturating concentrations enhance the sensitivity of SK channels to intracellular calcium many-fold, resulting in the fact that maximum activation of these channels is achieved at any physiological concentration of intracellular calcium [23]. In our experiments, SK channel activators achieved saturat-

ing concentrations near PC gradually during diffusion. Thus, the rate of the effect's onset could depend on the age-related features of the dynamics of intracellular calcium. Activation of SK channels in PC is determined by the entry of calcium through voltage-gated calcium channels (VGCC) (*Fig. 6B*). Reduced Cav2.1 (P/Q-type VGCC) expression and almost complete knockout of Cav1.3 (L-type VGCC) is noted in the molecular layer of the cerebellum of aged animals [24]. Cav1.3 is activated at very low values of membrane potential; i. e., it is the most sensitive to depolarization [25], whereas a deficiency of Cav2.1 can lead to ataxia type 2 [26–28], since a large proportion of the calcium in PC entering through VGCC is accounted for by Cav2.1 [29]. Under conditions of age-related partial loss of VGCC and the calcium signal associated with it, the normal activation of SK channels can be affected. Moreover, oscillations of membranous intracellular calcium modulate the activity of other types of receptors; in particular, desensitization of glutamate receptors, which provide glutamatergic synaptic transmission [30].

The study carried out *in vivo* in adult mice showed that the simple spike frequency of PC discharge upon NS309 application is reduced much more than in CyPPA application [13]. The results presented in the current paper demonstrate a similar decrease in the simple spike frequency under the influence of positive modulators of SK channels, NS309 and CyPPA, in adult rats. A tendency to a more pronounced decrease in the simple spike frequency was noted under the action of

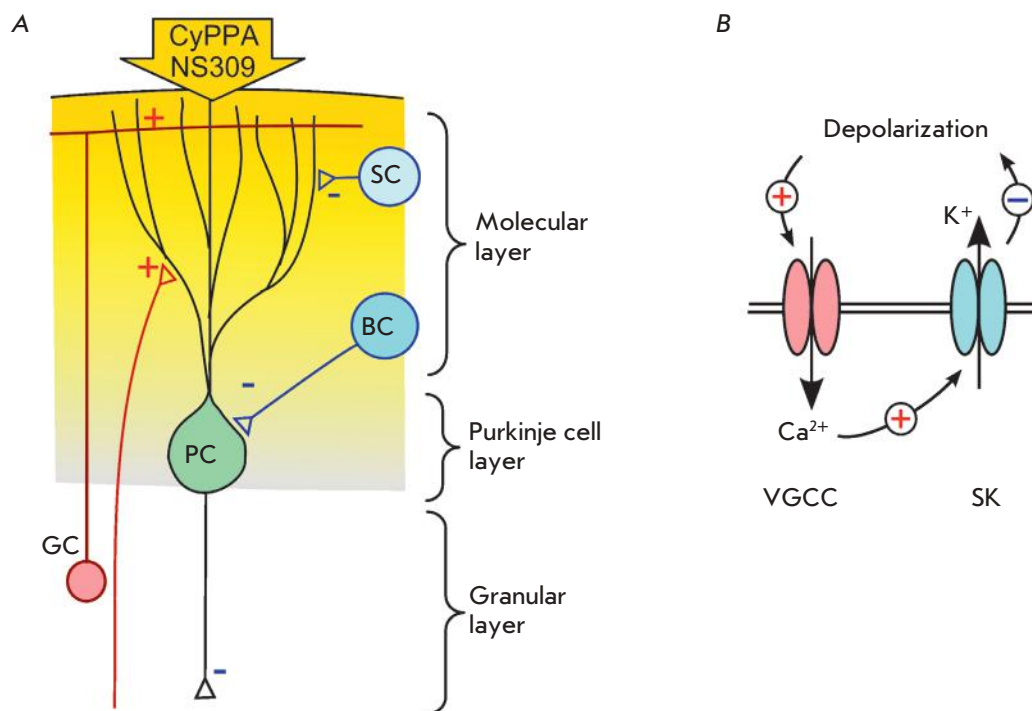


Fig. 6. The scheme of SK channel modulator action on Purkinje cells (PC) upon application to the surface of the cerebellum. **A** – simplified diagram of neuronal connections of PC in the cerebellar cortex. (+) – excitatory and (–) – inhibitory synaptic connections, PC – Purkinje cell, SC – stellate cell, BC – basket cell, GC – granule cell. **B** – relationships between the key ion channels of the PC regulating their autorhythmic activity

NS309 rather than CyPPA in the group of aged animals. Moreover, the decrease in the simple spike frequency after CyPPA application was comparable with earlier findings in mice, while NS309 had a more pronounced influence on the activity of cerebellar PC in mice than rats. CyPPA is known to be a selective modulator of SK channels, while NS309 is also an activator of the IK channels [31] expressed in PC dendrites, where they modulate temporal summation of synaptic inputs [32]. Thus, in our experiments *in vitro*, NS309 enhanced the after-hyperpolarization of PC more so than CyPPA. Apparently, due to this, a decrease in the simple spike frequency in PC is more pronounced upon NS309 action than in the case of CyPPA, which activates only SK2 channels in PC. The difference in the efficiency of the NS309 effect on the simple spike frequency of cerebellar PC discharge of mice and rats is probably due to the species differences in the expression and function of IK channel features in the cerebellum or the features of the diffusion barriers upon the specific method of application of these substances in these animals.

Application of positive modulators of SK channels in animals that serve as a model of some types of spinocerebellar ataxias leads to the restoration of an impaired pattern of PC activity and, in some cases, to the disappearance of ataxia symptoms [4, 5, 8, 9], which implies that they have a therapeutic effect. Moreover, the use of SK channel activators allows one to compensate for the age-related changes in the autorhythmic functions of cerebellar PC. The reasons for the age-related differences in the effects of SK channel activators require further study, since they could be associated to a deficit in the functions of the voltage-gated calcium channels of PC. ●

This work was supported by the Russian Foundation for Basic Research grants № 15-04-08283 and 16-04-00653 (in vivo experiments) and the Russian Science Foundation № 16-15-10192 (additional experiments using patch-clamp and immunocytochemistry methods). Immunocytochemistry was performed at the Center for Collective Use at the Institute of Evolutionary Physiology and Biochemistry RAS.

REFERENCES

- Ito M. // Brain Res. 2000. V. 886. № 1–2. P. 237–245.
- Hansen S.T., Meera P., Otis T.S., Pulst S.M. // Hum. Mol. Genet. 2013. V. 22. № 2. P. 271–283.
- Kasumu A.W., Hougaard C., Rode F., Jacobsen T.A., Sabatier J.M., Eriksen B.L., Strøbæk D., Liang X., Egorova P., Vorontsova D., et al. // Chem. Biol. 2012. V. 19. № 10. P. 1340–1353.
- Shakkottai V.G., do Carmo Costa M., Dell’Orco J.M., Sankaranarayanan A., Wulff H., Paulson H.L. // J. Neurosci. 2011. V. 31. № 36. P. 13002–13014.
- Walter J.T., Alvina K., Womack M.D., Chevez C., Khodakhah K. // Nat. Neurosci. 2006. V. 9. № 3. P. 389–397.
- Faber E.S., Sah P. // Neuroscientist. 2003. V. 9. № 3. P. 181–194.

RESEARCH ARTICLES

7. Adelman J.P., Maylie J., Sah P. // *Ann. Rev. Physiol.* 2012. № 74. P. 245–269.
8. Gymnopoulos M., Cingolani L.A., Pedarzani P., Stocker M. // *J. Comp. Neurol.* 2014. V. 522. № 5. P. 1072–1101.
9. Womack M.D., Khodakhah K. // *J. Neurosci.* 2003. V. 23. № 7. P. 2600–2607.
10. Karelina T.V., Grigorian R.A. // *J. Evol. Biochem. Physiol.* 2010. V. 46. № 3. P. 218–224.
11. Karelina T.V. Age related changes of cerebellar Purkinje cells synaptic activation with climbing and mossy fibers systems [in Russian]. PhD thesis. SPb.: UEPb RAS, 2010.
12. Kasumu A.W., Liang X., Egorova P., Vorontsova D., Bezprozvanny I. // *J. Neurosci.* 2012. V. 32. № 37. P. 12786–12796.
13. Egorova P.A., Karelina T.V., Vlasova O.L., Antovov S.M., Bezprozvanny I.B. // *J. Evol. Biochem. Physiol.* 2014. V. 50. № 2. P. 102–108.
14. Gao Z., Todorov B., Barrett C.F., van Dorp S., Ferrari M.D., van den Maagdenberg A.M., De Zeeuw C.I., Hoebeek F.E. // *J. Neurosci.* 2012. V. 32. № 44. P. 15533–15546.
15. Abushik P.A., Sibarov D.A., Eaton M.J., Skatchkov S.N., Antonov S.M. // *Cell Calcium.* 2013. V. 54. № 2. P. 95–104.
16. Weber A., Schachner M. // *Brain Res.* 1984. V. 311. P. 119–130.
17. Hirano T., Ohmori H. // *Proc. Natl. Acad. Sci. USA.* 1986. V. 83. P. 1945–1949.
18. Hockberger P.E., Tseng H.Y., Connor J.A. // *J. Neurosci.* 1989. V. 9. № 7. P. 2258–2271.
19. Bartschat S., Fieguth A., Könemann J., Schmidt A., Bode-Jänisch S. // *Forensic Sci. Int.* 2012. V. 223. № 1–3. P. 165–170.
20. Nie L., Song H., Chen M.F., Chiamvimonvat N., Beisel K.W., Yamoah E.N., Vázquez A.E. // *J. Neurophysiol.* 2004. V. 91. P. 1536–1544.
21. Herrik K.F., Christophersen P., Shepard P.D. // *J. Neurophysiol.* 2010. V. 104. № 3. P. 1726–1735.
22. Herrik K.F., Redrobe J.P., Holst D., Hougaard C., Sandager-Nielsen K., Nielsen A.N., Ji H., Holst N.M., Rasmussen H.B., Nielsen E.Ø., et al. // *Front. Pharmacol.* 2012. № 3. P. 11.
23. Hougaard C., Eriksen B.L., Jorgensen S., Johansen T.H., Dyhring T., Madsen L.S., Strobaek D., Christophersen P. // *Br. J. Pharmacol.* 2007. V. 151. P. 655–665.
24. Chung Y.H., Shin C.M., Kim M.J., Shin D.H., Yoo Y.B., Cha C.I. // *Brain Res.* 2001. V. 903. № 1–2. P. 247–252.
25. Tuckwell H.C. // *Progr. Neurobiol.* 2012. V. 96. № 1. P. 1–31.
26. Ophoff R.A., Terwindt G.M., Vergouwe M.N., van Eijk R., Oefner P.J., Hoffman S.M., Lamerdin J.E., Mohrenweiser H.W., Bulman D.E., Ferrari M., et al. // *Cell.* 1996. V. 87. P. 543–552.
27. Rose S.J., Kriener L.H., Heinzer A.K., Fan X., Raike R.S., van den Maagdenberg A.M.J. M., Hess E.J. // *Exp. Neurol.* 2014. V. 261. P. 553–562.
28. Salvi J., Bertaso F., Mausset-Bonnefont A.L., Metz A., Lemmers C., Ango F., Fagni L., Lory P., Mezghrani A. // *Neurobiol. Dis.* 2014. V. 68. P. 47–56.
29. Ovsepian S.V., Friel D.D. // *Eur. J. Neurosci.* 2008. V. 27. № 1. P. 93–103.
30. Sibarov D.A., Abushik P.A., Poguzhelskaya E.E., Bolshakov K.V., Antonov S.M. // *J. Pharmacol. Exp. Ther.* 2015. V. 355. P. 484–495.
31. Strobaek D., Teuber L., Jorgensen T.D., Ahring P.K., Kjaer K., Hansen R.S., Olesen S.P., Christophersen P., Skaaning-Jensen B. // *Biochim. Biophys. Acta.* 2004. V. 1665. P. 1–5.
32. Engbers J.D., Anderson D., Asmara H., Rehak R., Mehafey W.H., Hameed S., McKay B.E., Kruskic M., Zamponi G.W., Turner R.W. // *Proc. Natl. Acad. Sci. USA.* 2012. V. 109. P. 2601–2606.

Evolution of Tumor Clones in Adult Acute Lymphoblastic Leukemia

S. Yu. Smirnova¹, Yu. V. Sidorova¹, N. V. Ryzhikova¹, K. A. Sychevskaya², E. N. Parovichnikova¹, A. B. Sudarikov^{1*}

¹National Hematology Research Center, Novy Zykovskiy Proezd, 4a, Moscow, 125167, Russia

²Faculty of Basic Medicine, Lomonosov Moscow State University, Lomonosov Ave., 31/5, Moscow, 119192, Russia

*E-mail: dusha@blood.ru

Received February 10, 2016; in final form April 01, 2016

Copyright © 2016 Park-media, Ltd. This is an open access article distributed under the Creative Commons Attribution License, which permits unrestricted use, distribution, and reproduction in any medium, provided the original work is properly cited.

ABSTRACT Clonal instability of a tumor cell population in acute lymphoblastic leukemia (ALL) may complicate the monitoring of a minimal residual disease (MRD) by means of patient-specific targets identified at the disease onset. Most of the data concerning the possible instability of rearranged clonal *TCR* and *IG* genes during disease recurrence were obtained for ALL in children. The appropriate features of adult ALL, which are known to differ from those of childhood ALL in certain biological characteristics and prognosis, remain insufficiently studied. The aim of this study was to assess the stability of *IG* and *TCR* gene rearrangements in adult ALL. Rearrangements were identified according to the BIOMED-2 protocol (PCR followed by fragment analysis). Mismatch in clonal rearrangements at onset and relapse was identified in 83% of patients, indicating clonal instability during treatment. Clonal evolution and diversity of *IG* and *TCR* gene rearrangements may be one of the tumor progression mechanisms. New rearrangements may emerge due to residual VDJ-recombinase activity in tumor cells. Also, many clonal *IG* and *TCR* gene rearrangements may be present at different levels at a diagnosis, but less abundant clones may be “invisible” due to limited detection sensitivity. Later, major clones may disappear in the course of chemotherapy, while others may proliferate. Investigation of clonal evolution and heterogeneity in ALL and their impact on the treatment efficacy will contribute to the identification of new prognostic factors and the development of therapeutic approaches.

KEYWORDS acute lymphoblastic leukemia, relapse, PCR, *IG* and *TCR* gene rearrangements.

ABBREVIATIONS ALL – acute lymphoblastic leukemia; MRD – minimal residual disease; RT-PCR – real-time PCR; TCR – T cell receptor; TCRG – T cell receptor γ ; TCRB – T cell receptor β ; TCRD – T cell receptor δ ; IG – immunoglobulin; IGH – immunoglobulin heavy chain; IGK – light chain κ .

INTRODUCTION

Acute leukemias are a heterogeneous group of neoplastic diseases of the hematopoietic tissue, which are characterized by overproduction and accumulation of morphologically immature (blast) hematopoietic cells in the bone marrow. Depending on the hematopoietic lineage giving rise to tumor cells, acute leukemias are conventionally divided into acute lymphoblastic and acute myeloid leukemias. Untreated, the disease rapidly progresses and always results in the death of the patient. The most common causes of death are severe infectious and hemorrhagic complications arising from the replacement of normal hematopoietic tissue with blast cells.

The central goal of a treatment for any type of leukemia is the eradication of the tumor clone, restoration of normal hematopoiesis, and the achievement of long-term relapse-free survival of patients. The introduction of cytostatic drugs in clinical practice in the late

1960s enabled the achievement of complete remission in 85–95% of children with ALL [1]. In that case, an important prognostic factor is age; event-free survival of children in various age groups varies from 83–97% (1–5 years) to 49–66% (10–15 years). Recently, the Russian Research Group for the Treatment of Acute Lymphoblastic Leukemia (RALL) has demonstrated that the 5-year relapse-free survival rate in adult patients under 30 years of age is 71.5%, while this indicator in patients aged 30–55 years is lower – 61.8% [2]. Adults and children with ALL have been demonstrated to differ not only in the survival rate, but also in the biological properties and prognosis of the disease [3, 4]. In particular, a favorable prognostic group in adults includes the T cell type of the disease, whereas this type in children is considered prognostically adverse. In addition, adults are more likely to show prognostically adverse chromosomal aberrations (t(9;22), t(4;11)), myeloid antigens on the membrane of tumor cells, and hyperleu-

kocytosis at the disease onset, and they are more often diagnosed with the T-cell immunophenotype [3, 4].

Another important factor that affects the prognosis in ALL is the residual amount of tumor cells in the bone marrow, or minimal residual disease (MRD). MRD evaluation is considered not only as an independent prognostic factor, but also as a criterion for allocating patients into relapse risk groups [5–7]. The most suitable for MRD quantification are techniques with the highest sensitivity level (10^{-4} – 10^{-5}), such as real-time PCR (RT-PCR) with patient-specific primers, as well as multicolor flow cytometry. MRD evaluation in ALL patients by PCR is based on the identification of the clonal rearrangements of the T-cell receptor (TCR) and the immunoglobulin (IG) genes in the tumor cells, and the selection of patient-specific primers to the CDR3-region of the genes [8].

Clonal rearrangements of the IG and TCR genes occur in 98% of B-ALL patients and in 95% of T-ALL patients [9]. Because different chromosomal aberrations are found in tumor cells derived from different patients, only rearranged IG and TCR genes are considered to be universal markers for monitoring tumor clones in almost all patients during disease/therapy. Detection of clonality alone is not enough for ALL diagnosis. Clonal rearrangements are sometimes found also in the reactive (non-tumor) processes of inflammatory, infectious, or autoimmune genesis. A clonal product in these cases is usually detected on a polyclonal background. The differential diagnosis between tumor and non-tumor lymphoproliferation is somewhat difficult in some lymphomas, mycosis fungoides, and Sezary syndrome; however, a study of clonality in ALL when most peripheral blood lymphocytes (> 20%) are represented by tumor cells is not associated with these difficulties.

RT-PCR with patient-specific primers selected for a unique nucleotide sequence of the V-D-J-region of clonally rearranged IG or TCR genes enables a highly sensitive (10^{-4} – 10^{-5}) evaluation of the amount of residual tumor cells in ALL patients [10]. However, the data obtained from studying clonal rearrangements at the onset and relapse of ALL in children indicate that IG and TCR gene rearrangements can change during the disease: part of the identified clonal rearrangements disappears at relapse, and/or new rearrangements emerge. It should be noted that we are talking just about a partial change in clonal rearrangements, because a complete change in IG and TCR gene rearrangements at relapse indicates a development of secondary ALL [11, 12]. Partial differences in clonal rearrangements at the onset and relapse occur in 67–70% of children with B-ALL and in 45–50% of children with T-ALL [13–15]. Data on the evolution of tumor clones

in adult ALL is scant [11]. Szczepanski et al. reported on an evaluation of TCR genes in 9 adults with T-ALL [11]. The overall stability of TCR genes in the adult T-ALL was shown to be higher (97%) than that in childhood T-ALL (86%) [11]. However, IG gene rearrangements at the onset and relapse were not studied.

Alteration of clonal rearrangements, i.e. clonal evolution of the tumor, may lead to a loss of the target for MRD studies and to false negative results. Therefore, the suitability of a particular rearrangement to study MDR in ALL is determined not only by the rearrangement detection frequency, but also by its stability. The crucial data on the stability and frequency of various rearrangements in B-ALL and T-ALL are summarized in Table 1 [5–11, 15–19].

TCR δ -chain (TCRD) gene rearrangements are specific to early stages of T cells development and occur in about 55% of T-ALL cases only [20]. TCR γ -chain (TCRG) gene rearrangements occur in 95% of T-ALL patients [21]; TCR β -chain (TCRB) gene rearrangements occur in 92% of T-ALL patients. The stability of TCRB rearrangements in T-ALL relapses in children was shown to be lower than that of γ - and δ -chains – 80, 86, and 100%, respectively (Table 1) [11]. Despite a high detection rate and high stability, monoclonal rearrangements of γ -chain genes are not the best target for MRD monitoring, because they possess a short fragment of inserted nucleotides [22]. According to the published data, T-ALL is often more resistant to therapy and, therefore, MRD positive than B-ALL [23]. A high stability of IGK gene rearrangements (95%) in B-ALL children, complete V-D-J-rearrangements of the IGH (88%), TCRB (89%), and TCRD (86%) genes, a relatively high stability of TCRG gene rearrangements (75%), and a low stability of incomplete (D-J) rearrangements of IGH genes (57%) and incomplete rearrangements of TCRB genes (67%) were established (Table 1). Furthermore, oligoclonal rearrangements were initially detected in a large proportion of childhood B-ALL cases (26–30%) [13–15]. Clonal products of an incomplete gene rearrangement and derived clonal products with complete rearrangements can be present in ALL, which is explained by the action of V(D)J-recombinases and the ongoing process of immunoglobulin and TCR gene rearrangements in early progenitor cells [11, 15, 24]. Oligoclonality (presence of two or more clones) is most often detected in IGH genes: complete rearrangements – in 30–40% of cases, incomplete rearrangements – in 50–60% of cases, and TCR δ -chain gene rearrangements – in 20–25% of cases (Table 1). Oligoclonal rearrangements are not recommended for use as a target for MRD evaluation, because they are unstable and often produce false negative results.

Table 1. Stability and detection the rate of clonal rearrangements in B-ALL and T-ALL [7]

Gene	Rearrangement	B-ALL				T-ALL	
		Rate, %		Stability, %		Rate, %	Stability, %
		mono	oligo	mono	oligo		
IGH	VH-JH (complete)	93	30–40	88	47	5	NT
	DH-JH (incomplete)	20	50–60	57	38	23	NT
	All IGH	98	40	85	44	23	NT
IGK	V κ -Kde	45	5–10	95	40	0	NA
	Intron RSS-Kde	25	5–10	86	0	0	NA
	All Kde	50	5–10	95	40	0	NA
TCRB	VB-JB (complete)	21	10–15	89	60	77	79
	DB-JB (incomplete)	14	10–15	67	0	55	80
	All TCRB	33	10–15	81	43	92	80
TCRG	VG-JG	55	15	75		95	86
TCRD	VD-JD or DD-JD1	< 1	NA	NA	NA	50	100
	VD2-DD3 or DD2-DD3	40	20–25	86	26	55	100
	All TCRD	40%	20–25%	86%	26%	55%	100%

Note. NT – not tested, NA – not applicable.

The evolution of tumor cells (alteration of clonal *TCR* and *IGH* gene rearrangements) at relapse has been studied mainly in childhood ALL. Data on adult ALL is very limited. Given that adult and childhood ALLs have different biological characteristics and prognosis, the aim of our study was to examine patterns of clonal immunoglobulin and T-cell receptor gene rearrangements and how stable they are in adults with B-ALL and T-ALL who had undergone treatment at the Hematology Research Center.

MATERIALS AND METHODS

Patients and samples

The study included 63 ALL patients: 34 patients with B-cell ALL, including two patients with Ph+ ALL; 28 patients with T-cell ALL; and one patient with biphenotypic ALL (Table 2). All patients underwent a standard cytogenetic examination and a FISH-study of bone marrow cells using fluorescent probes t(9;22) and t(4;11) (Table 3). Out of the 63 patients, 20 had a normal karyotype, 17 had no mitosis, and six had different variations of chromosome 9 and/or 22. The translocation t(9;22) was detected by FISH, and the chimeric transcript BCR/ABL (p190) was identified by a molecular-genetic method (Ph+ B-ALL). In five patients, the translocation t(4; 11) was identified by FISH and the chimeric transcript MLL-EPS15 was detected by PCR. Multiple chromosomal abnormalities were found in seven patients; four patients had trisomy 21. We studied DNA from all 63 samples of bone marrow at the disease onset. The patients' age ranged from 19 to 59 years

Table 2. Brief characteristics of ALL patients

Age, years	19–59 (M, 28)
Gender, M/F	32/31
B-ALL/T-ALL/biphenotypic ALL	34/28/1
Number of relapses (B-ALL/T-ALL)	6 (4/2)
Relapse-free time, months	5.4–11.6 (M, 6.2)

Note. M – median age.

(median, 28 years). In 6 of the 63 patients, clonal rearrangements were studied at the onset and relapse. The time to relapse ranged from 5.4 to 11.6 months. The patients were observed at the Department of Chemotherapy for Hemoblastoses and Hematopoiesis Depressions of the Hematology Research Center (HRC). The diagnosis was made according to the WHO classification. All the patients enrolled in the study provided their consent to data processing. Blood from healthy donors was obtained at the HRC blood transfusion department.

Analysis of clonality using *IG/TCR* gene rearrangements

Leukocytes and DNA were isolated from peripheral blood as described previously [25]. The DNA concentration was determined spectrophotometrically. DNA samples were stored at –20 °C. B- and T-cell clonality was determined using multiplex BIOMED-2 prim-

RESEARCH ARTICLES

Table 3. Results of conventional cytogenetic testing and FISH-analysis of translocations t(4;11) and t(9;22) in ALL patients

Patient	ALL type	conventional cytogenetic testing, FISH, PCR
1	B-II	No mitosis
2	B-I	Normal karyotype
3	B-I	der(7)add(p22), -8?, der(9), i(q10), der(14), add(q32?), +mar der(9)?(17)cp/46, XX [3]
4	B-I	Additional material on the short arm of chromosome 10; trisomy of chromosomes X, 12, and 22; FISH t(4;11); MLL-EPS15 identified by PCR
5	B-I	55XX; derivatives of chromosomes 3 and 11; deletion of the short arm of chromosome 12 and the long arm of chromosome 13
6	B-I	Normal karyotype
7	B-I	Normal karyotype
8	B-I	No mitosis, FISH t(4;11), MLL-EPS15 identified by PCR
9	B-II	Additional signal from an IGH gene locus (14q32) was identified in 80% of nuclei (trisomy of chromosome 14? another translocation involving an IGH gene locus)
10	B-II	Normal karyotype
11	B-II	No mitosis
12	B-II	53XY? +X,+4,+6,+14,+21,+21,+mar [10]
13	B-II	Normal karyotype
14	B-II	No mitosis
15	B-II	No mitosis
16	B-II	In 15%, two additional signals each from loci of ABL (9q34) and BCR (22q11) genes, tetrasomy of chromosomes 9 and 22?
17	B-II	Trisomy 21
18	B-II	Normal karyotype
19	B-II	Trisomy 21
20	B-II	Trisomy 21, monosomy 13
21	B-II	Normal karyotype
22	B-II	No mitosis
23	B-II	Normal karyotype
24	B-II	Normal karyotype
25	B-II	Normal karyotype
26	B-III	Two cells with del (11), FISH t(4;11), MLL-EPS15 identified by PCR
27	B-III	Normal karyotype
28	B-III	47XX +5 (5q31)
29	B-III	54X, ?+X, Y, +4, +5, +6, ?-7, +14, +21, +22, +?mar or i(7)(q10) or i(8)(q10), +mar[19], 46XY
30	B-III	+8+11+21
31	B-Ph+	No mitosis, FISH t(9;22), BCR-ABL identified by PCR
32	B-Ph+	Normal karyotype, FISH t(9;22), BCR-ABL identified by PCR
33	B-II	No mitosis
34	B-II	No mitosis
35	T-I	46XY[2]/90-92, XXYY, =mar[10]
36	T-I	No mitosis
37	T-I	11q23 rearranged, FISH t(4;11), MLL-EPS15 identified by PCR
38	T-I	Normal karyotype
39	T-I	del9(p13)
40	T-I	No mitosis
41	T-I	Normal karyotype
42	T-I	Trisomy in 15.5%; in 45% tetrasomy in the gene locus PMLL\11q23; FISH t(4;11); MLL-EPS15 identified by PCR
43	T-I	Normal karyotype
44	T-II	Normal karyotype
45	T-II	Normal karyotype
46	T-II	Normal karyotype
47	T-II	No mitosis
48	T-II	Deletion of the long arm of chromosome 5? or translocation t(5;?), derivatives of chromosomes 2, 4, 5, 7, 22, and 17 (with involvement of the p53 gene)
49	T-II	Trisomy of chromosome 8
50	T-II	(47, XY, +8 (20))
51	T-II	Normal karyotype
52	T-II	No mitosis
53	T-III	Normal karyotype
54	T-III	47, XY+mar [20]
55	T-III	der(1)add(p36)?dup(p31p36)?{20}; momosomy 9 or deletion of locus 9q34
56	T-III	No mitosis
57	T-III	Derivative of chromosome 11, deletion of the long arm of chromosome 6
58	T-III	No mitosis
59	T-III	No mitosis
60	T-III	No mitosis
61	T-IV	t(6;17) +20
62	T-I	del 11q23
63	Biphenotypic ALL	47, XY, der(2)add(p24-25), +5, del(7)(q22), del(13)(q11-q34), +14[6]/46, XY[4]

Note: relapsed patients with identified rearrangements of T-cell receptor genes and immunoglobulin genes at the onset and relapse are shown in bold.

Table 4. Description of multiplex reactions and PCR primers according to the BIOMED-2 protocol

Gene	Primer set	Forward primers	Reverse primers (labeled)	Product length, bp
IGH	A	VH1-7 (FR1)	JHcons FAM	310–360
	B	VH1-7 (FR2)	JHcons FAM	250–295
	C	VH1-7 (FR3)	JHcons FAM	100–170
	E	DH1-6	JHcons TAMRA	110–290 and 390–420
	D	DH7	JHcons TAMRA	100–130
IGK	A	V κ 1/6-7	J κ 1-4, J κ 5 FAM	120–300
	B	V κ 1/6-7, INTR	KDE-FAM	210–390
TCRD	D1	D δ 2, V δ 1-V δ 6	J δ 1FAM, J δ 2R6G J δ 3TAMRA, J δ 4ROX	120–280
	D2	D δ 2, V δ 1-V δ 6	D δ 3FAM	130–280
TCRG	GA	V γ 1f, V γ 10	J γ 1/2FAM, J ρ 1/2 R6G	145–255
	GB	V γ 9, V γ 11	J γ 1/2FAM, J ρ 1/2 R6G	80–220
TCRB	A	V β 2-V β 24	J β 1.1, J β 1.6HEX J β 2.2, J β 2.6, J β 2.7FAM	240–285
	B	V β 2-V β 24	J β 2.1, J β 2.3, J β 2.4, J β 2.5 FAM	240–285
	C	D β 1, D β 2	J β 1.1, J β 1.6HEX J β 2.1, J β 2.7FAM	170–210 285–325

er sets for fragment analysis [26]. B-cell clonality was evaluated by IGH heavy chain (VH-JH FR1/FR2/FR3/DH-JH) and IGK κ -light chain (V κ -J κ /V κ -KDE/IntronRSS-KDE) gene rearrangements. T-cell clonality was evaluated by gene rearrangements of the T-cell receptors TCRG (VG-JG), TCRB (VB-JB/DB-JB), and TCRD (VD-JD/DD2-JD/VD-DD3/DD2-DD3). All IG and TCR gene loci were analyzed in multiplex reactions with a large number of primers clustered in several tubes according to the BIOMED-2 protocol recommendations (briefly described in *Table 4*). The TCRB genes were amplified using a TCRB Gene Clonality Assay ABI Fluorescence Detection kit (Invivoscribe Technologies, USA) according to the manufacturer's recommendations. A mixture (25 μ L) for the PCR of the IGH, IGK, TCRG, and TCRD genes contained 5 pM of each primer (Synthol, Russia), 100–200 ng of DNA, and 12.5 μ L of 2 \times PCRMasterMix (Promega, USA). Amplification was performed on a DNAEngine automated thermocycler (BioRad, USA). PCR conditions were as follows: 95 $^{\circ}$ C (7 min), then 35 cycles of 95 $^{\circ}$ C (45 s), 60 $^{\circ}$ C (45 s), 72 $^{\circ}$ C (45 s), and 72 $^{\circ}$ C (10 min). The cell lines Jurkat and Daudi were used as a positive (clonal) control. Peripheral blood mononuclear cells of healthy donors were used as a polyclonal control. A fragment analysis of PCR products was performed on an ABI PRISM 3130 Genetic Analyzer (Applied Biosystems, USA). For this purpose, 2 μ L of a 20-fold diluted PCR product was mixed with 10 μ L of Hi-Di formamide (Applied Biosystems, USA) and 0.04 μ L of a GeneScan 500-LIS Size Standard (Applied Biosystems, USA). After de-

naturation at 95 $^{\circ}$ C for 3 min and subsequent cooling, 10 μ L of the mixture was added to a well of a 96-well plate and high resolution capillary electrophoresis was performed on a POP-4 polymer (Applied Biosystems, USA). The fluorescence of amplicons and their profile were evaluated using the GeneMapper v.4.0 software (Applied Biosystems, USA).

RESULTS AND DISCUSSION

Clonal rearrangements were studied in 34 patients with B-cell ALL, 28 patients with T-cell ALL, and 1 patient with biphenotypic ALL. The frequencies of clonal TCR γ -, β -, and δ -chain and IG heavy- and light-chain gene rearrangements in B- and T-ALL are presented in *Table 5*. A biallelic rearrangement (two peaks) of TCRG genes and an oligoclonal rearrangement (four peaks) of TCRD genes were detected in the patient with biphenotypic ALL. In patients with B-cell ALL, the IG heavy-chain (82.4%) and TCR γ -chain (76.5%) gene rearrangements were the most frequent; TCR β -chain and IG κ -chain gene rearrangements were found in 38.2% of cases; TCR δ -chain gene rearrangements occurred in 55.9% of cases. In patients with T-cell ALL, TCR γ -, δ -, and β -chain gene rearrangements were detected in 89.3%, 64.3%, and 60.7% of cases, respectively. IGH rearrangements in T-ALL occurred less often (28.6%) than others. A V κ /KDE rearrangement of immunoglobulin κ -light chain genes was found in one case of T-ALL. Our data on the frequency of clonal IG and TCR gene rearrangements somewhat differ from the data obtained in international studies, which may

Table 5. Detection rate (%) of clonal TCR γ -, β -, and δ -chain gene rearrangements and IG heavy- and light-chain gene rearrangements in B- and T-ALL

Rearrangements		B-ALL (<i>n</i> = 34)	T-ALL (<i>n</i> = 28)
TCRG	VG-JG	74.3 (<i>n</i> = 26)	89.3 (<i>n</i> = 25)
TCRB	VB-JB (complete)	26.5 (<i>n</i> = 9)	50 (<i>n</i> = 14)
	DB-JB (incomplete)	23.5 (<i>n</i> = 8)	46.4 (<i>n</i> = 13)
	All TCRB	38.2 (<i>n</i> = 13)	60.7 (<i>n</i> = 17)
TCRD	VD-JD/DD2-JD	17.6 (<i>n</i> = 6)	53.6 (<i>n</i> = 15)
	VD-DD3/DD2-DD3	47.1 (<i>n</i> = 16)	32.1 (<i>n</i> = 9)
	All TCRD	55.9 (<i>n</i> = 19)	64.3 (<i>n</i> = 18)
IGH	VH-JHFR1/FR2/FR3 (complete)	73.5 (<i>n</i> = 25)	7.1 (<i>n</i> = 2)
	DH-JH (incomplete)	26.5 (<i>n</i> = 9)	25 (<i>n</i> = 7)
	All IGH	82.4 (<i>n</i> = 28)	28.6 (<i>n</i> = 8)
IGK	Vk-Jk	26.5 (<i>n</i> = 9)	0 (<i>n</i> = 0)
	Vk-KDE/Intron RSS-KDE	26.5 (<i>n</i> = 9)	3.6 (<i>n</i> = 1)
	All IGK	38.2 (<i>n</i> = 13)	3.6 (<i>n</i> = 1)

Table 6. Clonal products identified at the onset and relapse in six patients diagnosed with ALL

Patient/ diagnosis	Case 1 T-ALL		Case 2 T-ALL		Case 3 B-ALL		Case 4 B-ALL		Case 5 B-ALL		Case 6 B-ALL	
	O	R	O	R	O	R	O	R	O	R	O	R
TCRG-GA	+	+	+	+	-	-	+	-	-	+	+	+
TCRG-GB	+	+	-	-	-	-	+	-	-	+	-	+
TCRB-A	+	+	-	-	-	-	+	-	-	-	-	+
TCRB-B	-	-	-	-	-	-	-	-	-	-	+	+
TCRB-C	-	-	-	-	-	-	-	-	-	-	-	-
TCRD-D1	+	+	+	+1	+	+	+	+	+	+	-	-
TCRD-D2	+	+	-	-	-	+	+	-	+	-	-	-
IGH-A/IGH-B/IGH-C	-	-	-	-	-	+	-	-	+	+1	+	+
VK-A	-	-	-	-	-	+	+	-	-	-	+	-
VK-B	-	-	-	-	-	-	+	+	-	-	-	-

Note. "+" – monoclonal rearrangement, "-" – polyclonal rearrangement, "+1" – initial clonal rearrangement is detected along with an additional rearrangement different from the one identified at the onset, O – onset, R – relapse.

be associated with our small sample size. Oligoclonal rearrangements (three or more clonal peaks) occurred both in B-ALL (IGH in 12% (4 of 34) of patients, TCRD in 18% (6 of 34) of patients) and in T-ALL (TCRD in 32% (9 of 28) of patients).

In six patients, clonal rearrangements were investigated at the onset and relapse. A total of 17 clonal TCR and 5 clonal IG gene rearrangements were identified at

the onset. Six clonal TCR and three clonal IG gene rearrangements different from those identified at the onset were detected at relapse (Table 6).

Two patients with B-cell ALL had a loss of one of the clonal rearrangements identified at the onset, with new rearrangements simultaneously emerging (patient 5 in Fig. 1 and patient 6 in Table 6). In one patient diagnosed with early precursor T-ALL, the clonal TCR γ -, β -, and

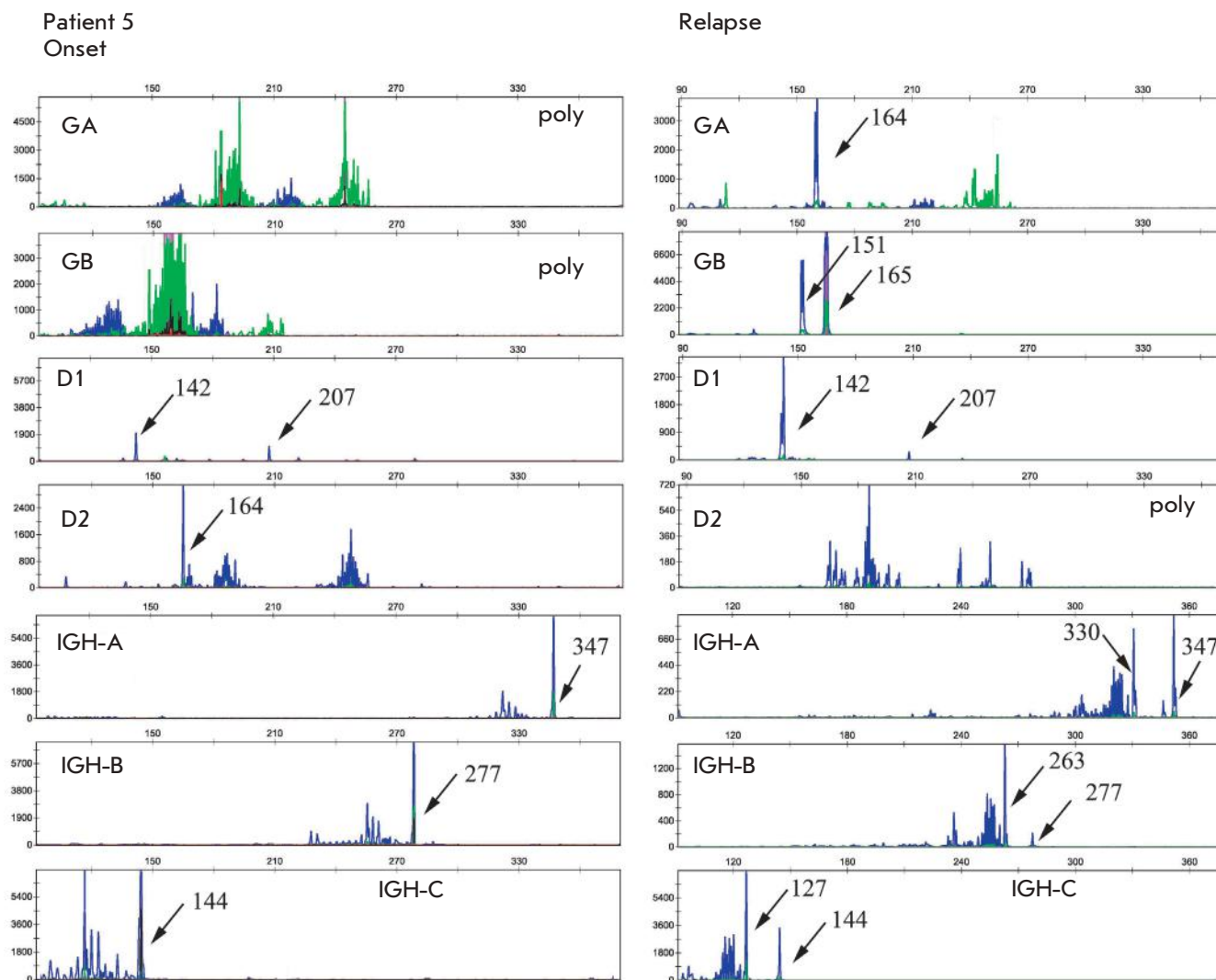


Fig. 1. Fragment analysis of *TCR*, *TCD*, and *IGH* gene amplification products in patient 5 at the onset and relapse. Two 142 and 207 bp clonal products (indicated by arrows) of *TCRD* gene rearrangements and a 347 bp clonal product of *IGH* gene rearrangements were amplified at the disease onset. In this patient, the rearrangements remained at the relapse and new clonal products were also identified (*TCRGA* – 164 bp, *TCRGB* – 151 and 165 bp; *IGHA* – 330 bp, *IGHB* – 263 bp, *IGHC* – 127 bp).

δ -chain gene rearrangements completely coincided at the onset and relapse (case 1). In one T-ALL patient, new rearrangements emerged, in addition to the clonal rearrangements identified at the onset (case 2). In one patient, only two of the seven rearrangements identified at the onset were preserved up to the relapse (Fig. 2, patient 4). In one patient, only one clonal *TCR* δ -chain gene rearrangement was detected at the B-ALL onset, which was preserved up to the relapse, but several new rearrangements emerged, including clonal *IGH* and *IG* light κ -chain gene rearrangements.

We were able to demonstrate that at least one of the initially detected clonal products was preserved up to ALL relapse in all patients (Table 6). This confirms the data showing that at least one initial clonal product is preserved even in the case of late ALL relapse in children (more than 5 years after remission achievement) [27]. In our work, differences in clonal rearrangements at the onset and relapse were found in five out of six (83%) patients. Even with this small sample size, we observed clonal evolution at relapse, which raises the issue of initial selection of the target for MRD quan-

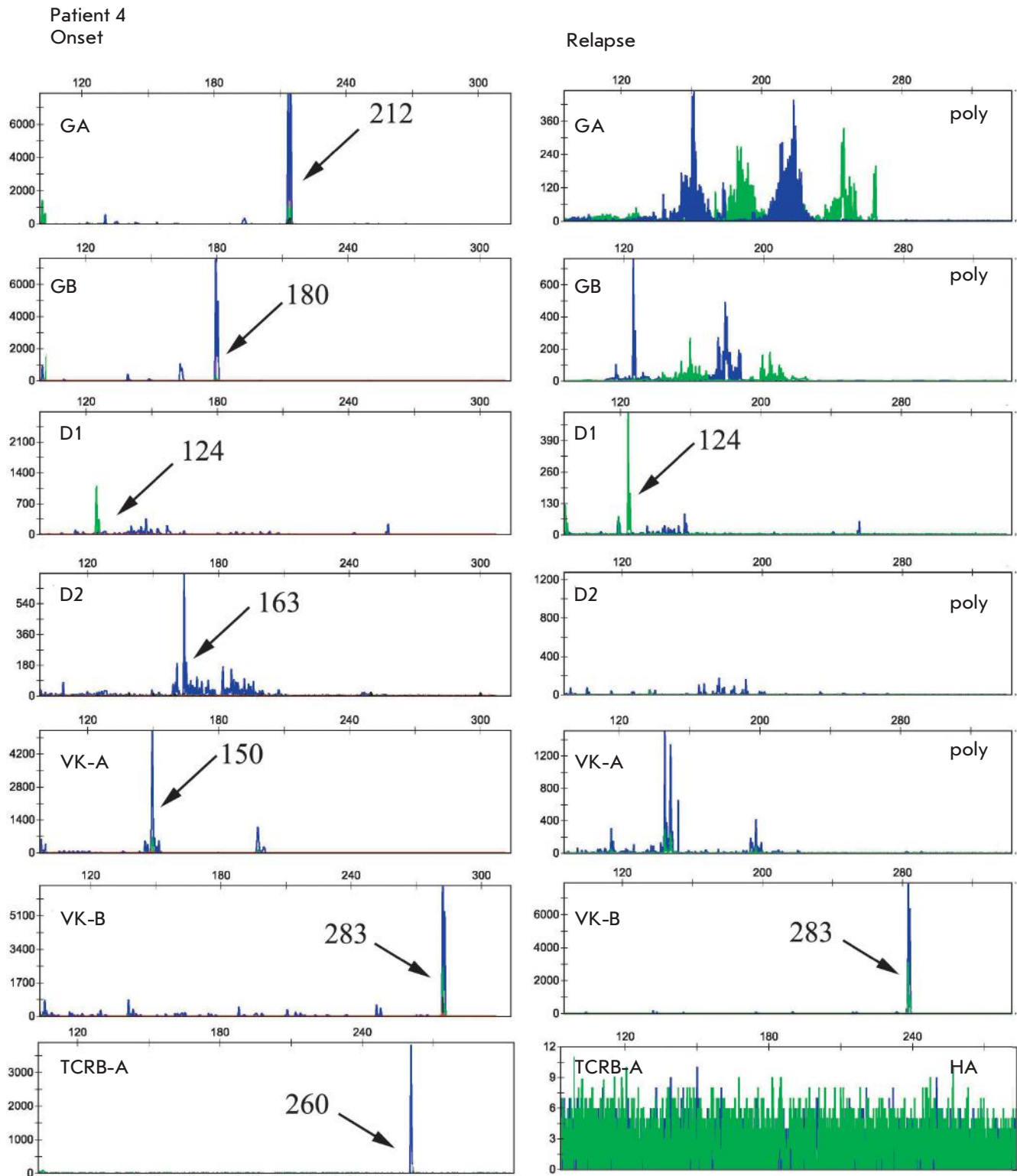


Fig. 2. Fragment analysis of *TCRG*, *TCRD*, *IGK*, and *TCRB* gene amplification products in patient 4 at the onset and relapse. Seven clonal rearrangements were identified at the diagnosis. Only two of them were preserved at the relapse (*TCRD* – 124 bp; *IGK* – 283 bp).

tification. At least two independent targets with high stability are conventionally used to minimize the risk of false positive results. However, in practice, a patient-specific primer with the desired specificity and sensitivity cannot be selected for every target. First of all, this applies to incomplete rearrangements or gene rearrangements lacking the D-segment, e.g. *TCRG* ($V\gamma$ - $J\gamma$). We found a loss of the patient-specific targets identified in three patients at the onset. To trace minor subclones at the onset and to evaluate their behavior in the presence of therapy, we decided to increase the initial sensitivity of the method. V- and J-family specific primers were used to re-examine the initial material for the presence of the clones that emerged at the relapse. The use of these primers increases the sensitivity of tumor cell detection from 10^{-1} to 10^{-2} – 10^{-3} . However, even with this sensitivity, subclones were not detected at the onset, which suggests a small size of the subclones and confirms the data of other studies. For example, in 77% (35 of 45) of childhood B-ALL cases, clones with new rearrangements at relapse were present only as small subclones at the onset [28]. The size of these resistant subclones ranged from 10^{-2} to 10^{-5} cells, and the lower the cell number was, the longer the time to relapse was [29].

Recently, acute lymphoblastic leukemias were shown to have a complex and genetically heterogeneous composition of tumor cells within one disease [30, 31]. In most ALL cases, clonal evolution is based on the reactivation of one of the minor subclones, which is resistant to therapy [29, 32, 33]. Clonal diversity is the mechanism underlying tumor progression. Some clonal cells are likely to have properties that are different from those of other cells (genetic mutations, division rate, immunological maturity), making them resistant to chemotherapy. The causes behind late reactivation of the initial tumor clone remain unknown. Perhaps, the immune surveillance and the mechanisms

of antitumor immunity weaken, or new genetic mutations emerge in tumor cells that are then reactivated. The use of quantitative methods to evaluate MRD is an independent prognostic factor and a criterion for the stratification of patients into relapse-risk groups. The spectrum of clonal rearrangements can vary during the disease. This process can occur during early induction therapy, which leads to false negative results of MRD evaluation and prevents a stratification of patients into risk groups. Successful monitoring of the minimal residual disease can be ensured only through the selection of patient-specific primers for each clonal target identified at the onset.

CONCLUSION

Five out of six (83%) patients studied had differences in clonal rearrangements at the onset and relapse, which indicates clonal instability in the presence of polychemotherapy. Tumor cells in ALL initially show a complex and genetically heterogeneous composition; while some clones disappear due to polychemotherapy, others that are unidentified because of the insufficient sensitivity of the method acquire the ability to activate. Clonal evolution is one of the mechanisms behind tumor progression and is a serious obstacle to the quantification of MRD by PCR. We have demonstrated that the absence of amplification with patient-specific primers selected for targets sequenced at the disease onset cannot fully guarantee an absence of residual disease because tumor clones were shown to be unstable in some cases of acute leukemia. Therefore, clonality should be re-examined in doubtful cases of suspected relapse and the absence of amplification with patient-specific primers. Investigation of clonal evolution mechanisms and the ability of chemotherapy to affect clonal evolution processes will contribute to the development of new prognostic factors and therapeutic approaches. ●

REFERENCES

1. Felix C. Acute lymphoblastic leukemia in infants. Washington: Education Program Book of hematology, American society of hematology, 2015. P. 285–302
2. Parovichnikova E.N., Troitskaya V.V., Sokolov A.N., Akhmerzaeva Z.Kh., Kuzmina L.A., Mendeleeva L.P., Klyasova G.A., Kravchenko S.K., Gribova E.O., Bondarenko S.N., et al. // *Oncohematology*. 2014. № 3. P. 6–15.
3. Campana D., Pui C. // *Blood*. 1995. V. 85. № 6. P. 1416–1434.
4. Copelan E., McGuire E. // *Blood*. 1995. V. 85. № 5. P. 1151–1168.
5. Flohr T., Schrauder A., Cazzaniga G., Panzer-Grümayer R., van der Velden V., Fischer S., Stanulla M., Basso G., Niggli FK, Schäfer BW // *Leukemia*. 2008. V. 22. № 4. P. 771–782.
6. Brüggemann M., Raff T., Flohr T., Gökbuget N., Nakao M., Droese J., Lüschen S., Pott C., Ritgen M., Scheuring U., et al. // *Blood*. 2006. V. 107. № 3. P. 1116–1123.
7. van Dongen J.J., van der Velden V.H., Brüggemann M., Orfao A. // *Blood*. 2015. V. 125. № 26. P. 3996–4009.
8. van der Velden V.H., Hochhaus A., Cazzaniga G., Szczepanski T., Gabert J., van Dongen J.J. // *Leukemia*. 2003. V. 17. P. 1013–1034.
9. van Dongen J.J., Langerak A.W., Brüggemann M., Evans P.A.S., Hummel M., Lavender F.L., Delabesse E., Davi F., Schuurin E., García-Sanz R. // *Leukemia*. 2003. V. 17. № 12. P. 2257–2317.
10. Pongerse-Willems M.J., Seriu T., Stolz F., d'Aniello E., Gameiro P., Pisa P., Gonzalez M., Bartram C.R., Panzer-Grümayer E.R., Biondi A. // *Leukemia*. 1999. V. 13. P. 110–118.
11. Szczepanski T., van der Velden V.H., Raff T., Jacobs D.C., van Wering E.R., Brüggemann M., Kneba M., van Dongen J.J. // *Leukemia*. 2003. V. 17. № 11. P. 2149–2156.
12. Szczepanski T., van der Velden V.H., Waanders E., Kuiper R.P., van Vlierberghe P., Gruhn B., Eckert C., Panzer-Grümayer E.R., et al. // *Blood*. 2006. V. 107. № 3. P. 1116–1123.

RESEARCH ARTICLES

- mayer R., Basso G., Cavé H., et al. // *ClinOncol.* 2011. V. 29. № 12. P. 1643–1649.
13. Beishuizen A., Verhoeven M.A., van Wering E.R., Hahlen K., Hooijkaas H., van Dongen J.J. // *Blood.* 1994. V. 83. № 8. P. 2238–2247.
14. Aihong Li Jianbiao Z., David Z., Montse R., Virginia D., Cheryl L., Lewis B.S., Stephen E. S., John G.G. // *Blood.* 2003. V. 102. № 13. P. 4520–4526.
15. Szczepański T., Willemse M.J., Brinkhof B., van Wering E.R., van der Burg M., van Dongen J.J. // *Blood.* 2002. V. 99. № 7. P. 2315–2323.
16. van der Velden V.H., Szczepanski T., Wijkhuijs J.M., Wijkhuijs J.M., Hart P.G., Hoogeveen P.G., Hop W.C.J., van Wering E.R., van Dongen J.J.M. // *Leukemia.* 2003. V. 17. № 9. P. 1834–1844.
17. Beishuizen A., Hahlen K., Hagemeijer A., Verhoeven M.A., Hooijkaas H., Adriaansen H.J., Wolvers-Tettero I.L., van Wering E.R., van Dongen J.J. // *Leukemia.* 1991. V. 5. № 8. P. 657–667.
18. Beishuizen A., de Bruijn M.A., Pongers-Willemse M.J., Verhoeven M.-A.J., van Wering E.R., Hählen K., Breit T.M., de Bruin-Versteeg S., Hooijkaas H., van Dongen J.J.M. // *Leukemia.* 1997. V. 11. № 12. P. 2200–2207.
19. Bruggemann M., van der Velden V.H., Raff T., Droese J., Ritgen M., Pott C., Wijkhuijs A.J., Gökbuget N., Hoelzer D., van Wering E.R. // *Leukemia.* 2004. V. 18. № 4. P. 709–719.
20. Breit T.M., Wolvers-Tettero I.L., Beishuizen A., Verhoeven M.A., van Wering E.R., van Dongen J.J. // *Blood.* 1993. V. 82. № 10. P. 3063–3074.
21. Szczepański T., Langerak A.W., Willemse M.J., Wolvers-Tettero I.L., van Wering E.R., van Dongen J.J. // *Leukemia.* 2000. V. 14. № 7. P. 1208–1214.
22. van der Velden V.H., Wijkhuijs J.M., Jacobs D.C., van Wering E.R., van Dongen J.J. // *Leukemia.* 2002. V. 16. № 7. P. 1372–1380.
23. Willemse M.J., Seriu T., Hettinger K., d'Aniello E., Hop W.C., Panzer-Grümayer E.R., Biondi A., Schrappe M., Kamps W.A., Masera G., et al. // *Blood.* 2002. V. 99. № 12. P. 4386–4393.
24. Germano G., del Giudice L., Palatron S., Giarin E., Cazzaniga G., Biondi A., Basso G. // *Leukemia.* 2003. V. 17. № 8. P. 1573–1582.
25. Sidorova Yu.V., Sorokina T.V., Biderman B.V., Nikulina E.E., Kisilichina D.G., Naumova E.V., Pochtar' M.E., Lugovskaya S.A., Ivanova V.L., Kovaleva L.G., et al. // *Klin Lab Diagn.* 2011. № 12. P. 22–35.
26. Dongen J.J., Langerak A.W., Bruggemann M., Evans P.A., Hummel M., Lavender F.L., Delabesse E., Davi F., Schuur-ing E., Garcia-Sanz R., et al. // *Leukemia.* 2003. V. 17. № 12. P. 2257–2317.
27. Lo Nigro L., Cazzaniga G., Di Cataldo A., Pannunzio A., D'Aniello E., Masera G. Schiliró G., Biondi A. // *Leukemia.* 1999. V. 13. P. 190–195.
28. Eckert C., Flohr T., Koehler R., Hagedorn N., Moericke A., Stanulla M., Kirschner-Schwabe R., Cario G., Stackel-berg A., Bartram C.R., et al. // *Leukemia.* 2011. V. 25. № 8. P. 1305–1313.
29. Choi S., Henderson M.J., Kwan E., Beesley A.H., Sutton R., Bahar A.Y., Giles J., Venn N.C., Pozza L.D., Baker D.L., et al. // *Blood.* 2007. V. 110. № 2. P. 632–639.
30. Mullighan C.G., Zhang J., Kasper L.H., Lerach S., Payne-Turner D., Phillips L.A., Heatley S.L., Holmfeldt L., Collins-Underwood J.R., Ma J., et al. // *Nature.* 2011. V. 471. № 7337. P. 235–239.
31. Gawad C., Pepin F., Carlton V.E., Klinger M., Logan A.C., Miklos D.B., Faham M., Dahl G., Lacayo N. // *Blood.* 2012. V. 120. № 22. P. 4407–4417.
32. Li A., Zhou J., Zuckerman D., Rue M., Dalton V., Lyons C., Silverman L.B., Sallan S.E., Gribben J.G. // *Blood.* 2003. V. 102. № 13. P. 4520–4526.
33. de Haas V., Verhagen O.J., von dem Borne A.E., Kroes W., van den Berg H., van der Schoot C.E. // *Leukemia.* 2001. V. 15. № 1. P. 134–140.

Adjuvant-Induced Arthritis in Guinea Pigs

O.S. Taranov, S.N. Yakubitskiy, T.S. Nepomnyashchikh, A.E. Nesterov, and S.N. Shchelkunov*
State Research Center of Virology and Biotechnology VECTOR, Kol'tsovo, Novosibirsk region,
630559 Russia

*E-mail: snshchel@rambler.ru; snshchel@vector.nsc.ru

Received March 28, 2016; in final form, May 30, 2016

Copyright © 2016 Park-media, Ltd. This is an open access article distributed under the Creative Commons Attribution License, which permits unrestricted use, distribution, and reproduction in any medium, provided the original work is properly cited.

ABSTRACT We propose a model of rheumatoid arthritis (RA) induced in outbred guinea pigs using a single subcutaneous injection of complete Freund's adjuvant to the hind paw. Histological examination of this model shows fibrin deposition on the surface of the synovial membrane, leukocyte infiltration of the synovial membrane and adjacent tissues, proliferation of the granulation tissue, and emergence of angioid areas, characteristic of RA. The cell response appears as an increase in the plasma cell count and development of follicle-like lymphoid infiltrates; erosion of the articular surface of the cartilage, frequently with deep cartilage destruction over large areas; and epiphyseopathy. The high reproducibility of arthritis induction in this RA model has been demonstrated. The proposed model is promising for the assessment of anti-arthritis preparations and dosage regimens.

KEYWORDS rheumatoid arthritis, adjuvant-induced arthritis, guinea pig

ABBREVIATIONS AIA, adjuvant-induced arthritis; RA, rheumatoid arthritis; CFA, complete Freund's adjuvant

INTRODUCTION

Rheumatoid arthritis (RA) is a heterogeneous autoimmune disease characterized by a systemic inflammation of the connective tissue. The morphological presentation of RA includes the inflammation of the articular capsule tissue, proliferation and hyperplasia of synovial cells, pannus formation, and structural destruction of cartilage and the subchondral bone. RA is characterized by a steadily progressive disease of the joints and internal organs, leading to early disability and shortened life expectancy. About 70 million people worldwide suffer from RA. Most often, the disease attacks older people. The reasons that cause the development of arthritis remain not well established, possibly because of their multiplicity [1–4].

Various animal models are used to study the pathogenesis of RA and develop drugs effective against the disease. The vast majority of research on the induction and therapy of RA are performed on certain lines of mice and rats [1, 2, 5, 6]. This is first of all due to the good state of knowledge on and homogeneity of these animals and the large number of available immunological reagents and test systems. However, none of these models fully reflects all aspects of the development of human RA [1, 5, 7] and, therefore, preclinical studies of potential antiarthritic drugs should be carried out in various animal models.

The genetic heterogeneity of humans and probable multiplicity of arthritis induction mechanisms actualize the use of laboratory animals that are close to humans in their physiological and immunological properties as

RA models. It is believed that guinea pigs are more appropriate models on which to study and develop treatments for various human inflammatory and infectious diseases than mice and rats [8–10].

Our work was aimed at developing a reproducible model of adjuvant-induced arthritis (AIA) in outbred guinea pigs.

EXPERIMENTAL

Animals

We used female outbred guinea pigs weighing 200–250 g (3–4 weeks of age) received from the animal kennel of the State Research Center of Virology and Biotechnology VECTOR. The animals were kept under natural light conditions with constant access to water and food.

Arthritis induction using Freund's adjuvant

The animals were subcutaneously injected with a Freund's complete adjuvant (CFA) solution into the hind paw at a dose of 50, 100, or 200 μ m, which corresponded to groups 50, 100, and 200, respectively. The control group guinea pigs (C) were administered 200 μ l of a sodium phosphate buffer (PBS). Each of the control group and group 50 consisted of 9 guinea pigs; group 100 – 14; and group 200 – 10 animals.

The width of the distal metatarsal region of both hind paws was measured one day after CFA injection and then every 3–4 days. Group C, 50, and 200 animals were taken out of the experiment (2–3 animals at a time), using ether anesthesia according to the animal

use regulations in compliance with humanity principles as stated in the European Community Directives (86/609/EEC) and Helsinki Declaration, on the 16, 28, 42, and 56th day. CFA-induced pathological changes were assessed based on a histological examination of tissues of both hind limbs of the experimental and control animals. All group 100 animals were taken out of the experiment on day 28th after CFA injection.

Histological analysis

The hind limbs of the guinea pigs were fixed in a 10% neutral formalin solution for histological examination (BioVitrum, Russia) for 48 hours. Then, bone-containing samples were decalcified using a BioDec R preparation (Bio Optica Milano, Italy) for 48–72 hours. After decalcification, the animals' hind paws were dissected in the sagittal direction as described in [2] in order to prepare histological specimens. Further material processing was performed according to the standard procedure for histological preparations: sequentially dehydrated in alcohols with increasing concentrations, soaked in a xyloparaffin mixture, and embedded in paraffin blocks. Paraffin sections (4–5 µm thick) were prepared using an automatic rotary microtome HM 360 (Germany). Sections were stained with hematoxylin and eosin. Differential staining of connective tissue was carried out using the Van Gieson's stain. Light optical examination and microphotography was performed on a AxioImager Z1 microscope (Carl Zeiss, Germany) equipped with a high resolution digital camera HRC (Carl Zeiss, Germany), using the AxioVision 4.8.2 software package (Carl Zeiss, Germany).

The statistical analysis of the results of the histological analysis of the samples obtained from group 100 animals was done using a point-based assessment of the severity of pathological manifestations of the disease in different groups. The disease severity was assessed based on four criteria: inflammatory response in articular capsule tissues, severity of synovitis (pannus formation), cartilage erosion, and destruction of the articular surface of the bone.

The inflammatory response was scored as 1 point in the case of periarticular tissue infiltration with isolated lymphocytes and granulocytes; 2 points – in the case of significant infiltration, formation of small lymphocytic-histiocytic nodules, and moderate swelling of the periarticular tissue. In the case of severe diffuse soft tissue infiltration with macrophage cells, lymphocytes, granulocytes, and plasma cells, formation of a dense infiltration, and significant edema, the inflammatory response was scored as 3 points.

The development of synovitis was assessed as follows: 1 point – there are signs of swelling of the synovial membrane and synoviocyte proliferation; 2 points –

actively proliferating granulation tissue forms pannus at the points of contact between the synovium and cartilage, forming the articular surface; 3 points – pannus “overlaps” on the articular cartilage and destroys it.

Cartilage destruction was evaluated based on damage depth: 1 point – erosion of the surface layer (articular surface) or emergence of cell-free fields, 2 points – lesions spreading to the mid-thickness of the cartilage; 3 points – destruction involves the whole cartilage.

Severity of bone destruction: 1 point – there are small areas of resorption in the epiphyseal areas of the bones that form the joint; 2 points – local injury to the peri-epiphyseal cortical layer; 3 points – extensive damage to the cortical layer, destruction of trabeculae of the cancellous bone, and bone deformity.

RESULTS

Clinical manifestations of arthritis in guinea pigs injected with CFA

Outbred guinea pigs were subcutaneously injected with CFA into the hind paw at a dose of 50, 100, or 200 µl. The width of the distal metatarsal area of both hind paws was measured, and it was found that the hind limb injected with adjuvant increased in size as a result of an inflammatory response (*Fig. 1*). The response (swelling and inflammation) to the CFA injection manifested itself as early as on the first days after the injection, swelling of the treated paw rapidly increased during the first 2 weeks, and then this value almost reached a plateau. The most severe swelling, which covered almost the entire paw, occurred in group 200 (*Fig. 2*).

Histological analysis of the hind paws of AIA guinea pigs, group 200

Pathomorphological symptoms of arthritis were similar in all groups of AIA animals. The most significant changes were observed in the left hind paw (on the side of the injection of the inducing CFA preparation) in the 200 group. For this reason, further discussion herein refers to this particular group.

By day 16th, of the experiment, a diffuse dense cellular infiltration was observed in the reticular dermis, subcutaneous fat tissue, and between muscle fibers, while the surface layers of the skin remained intact. The infiltrate was dominated by granulocytes (mostly neutrophils), macrophages, and a small amount of plasma cells. Necrotic disintegration zones were sometimes observed in the central portion of large infiltration regions. Pronounced edema, inflammatory cell infiltration (*Fig. 3C*), and hemodynamic disorders in the form of a significant plethora of small- and medium-caliber vessels, stasis, and thrombosis of small vessels of the

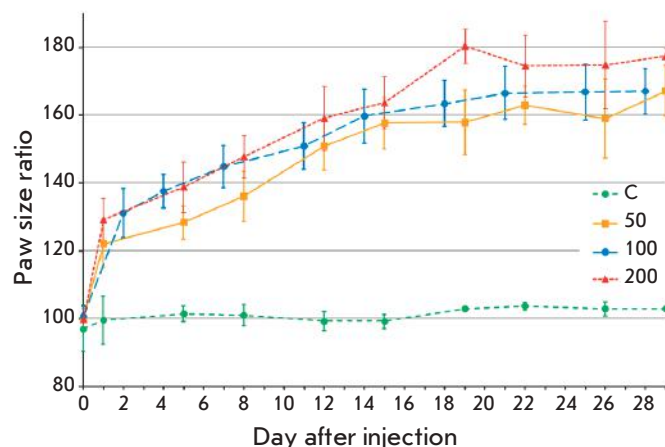


Fig. 1. Development of inflammatory response in the left hind limb of guinea pigs after the injection of the complete Freund's adjuvant at a dose of 50 (group 50), 100 (group 100), or 200 (group 200) μ l. The percentage ratio of the width of the experimental left paw to that of the intact right paw is shown (as the arithmetic mean per group \pm standard deviation); C, control animal group injected with 100 μ l PBS into the left paw.

venous bed were observed around the joints. The synovium was swollen and significantly thickened due to cell proliferation. In the marginal zone of the synovium, at the point of its contact with cartilage, development of granulation tissue and its spread to the articular surface of the cartilage was observed (Fig. 3D). Cartilage lesions were limited to variously sized erosions, cavities, and formation of cell-free zones in the cartilage (Fig. 4C). No changes in the subchondral bone tissue were observed at this stage of the experiment (Fig. 4D).

By day 28, the severity of the edema and inflammatory cell infiltration in the periarticular soft tissues increased (Fig. 3E). Joint disease progressed. The inflammatory process mainly involved large joints: ankle and talo-navicular ones. Small tarsus and metatarsus joints were damaged to a lesser degree. Dramatic thickening of the synovium covering the villi was observed, as well as proliferating synovial cells arranged in multiple layers. In some cases, the synovial cells exfoliated into the joint cavity (Fig. 3F). In the subepithelial layer, the perivascular space was dilated, there was a pronounced perivascular edema, swelling and delamination of muscular coat of the vessels, swelling and thickening of the endothelium, and margination and adhesion of neutrophils on endothelial cells. Overgrowth of granulation tissue, which "overlapped" with the cartilage in the form of pannus, was observed along the margins of the articular cartilage (Fig. 4E). There were varying degrees of cartilage lesions. Typically, rather large fields



Fig. 2. Appearance of the hind limbs of the control group (C), groups 50, and group 200 guinea pigs on day 37 after CFA injection; L and R stand for left and right paws.

of surface layer erosion and destruction areas were observed, which sometimes extended over the whole thickness of the cartilage. Thinning of the subchondral bone plate and emergence of rather extensive zones of cortical layer destruction were observed (Fig. 4F).

42 days after the CFA injection, massive infiltration of the soft tissue of the foot with necrotic areas at the central portion of the infiltration was observed on the side of the injection. Angiomatosis, congestion, and a large number of fibroblasts were observed on the periphery of infiltration foci, indicating the beginning of the active repair process of articular capsule tissue (Fig. 3G). The synovium was strongly edematous, and its hypertrophic villi deeply penetrated the articular cavity. An active process of vascular and connective tissue regeneration was observed under the synovium and in the villi (Fig. 3H). There were multiple lesions of the cartilage, which involved both large joints and small metatarsal joints. The severity of the degradation also varied from marginal deformation of the cartilage (Fig. 4G) to a complete cartilage loss over the large area of the articular surface and local destruction of bone trabeculae of the cancellous bone (Fig. 4H).

On day 56 of the experiment, a certain decrease in the activity of the inflammatory process was observed, along with progression of tissues sclerosis around the inflammatory infiltrate (Fig. 3I). In some cases, the connective tissue grew into the infiltration, forming smaller cell fibrotic granulomas surrounded by a fibrous capsule. Despite the decrease in the inflammatory response in the surrounding tissues, inflammation of the synovium remained active. Various degrees of synovitis were observed in all animals. Along the diffuse infiltration, small granulomatous nodules were often found under the synovium (Fig. 3J). Pronounced degradation of the articular cartilage (Fig. 4I) and granulation tissue growth into the cancellous bone was observed (Fig. 4K).

In the right untreated hind limbs, inflammation manifested itself in the form of small foci of inflammatory cell infiltration, mainly along small-caliber blood

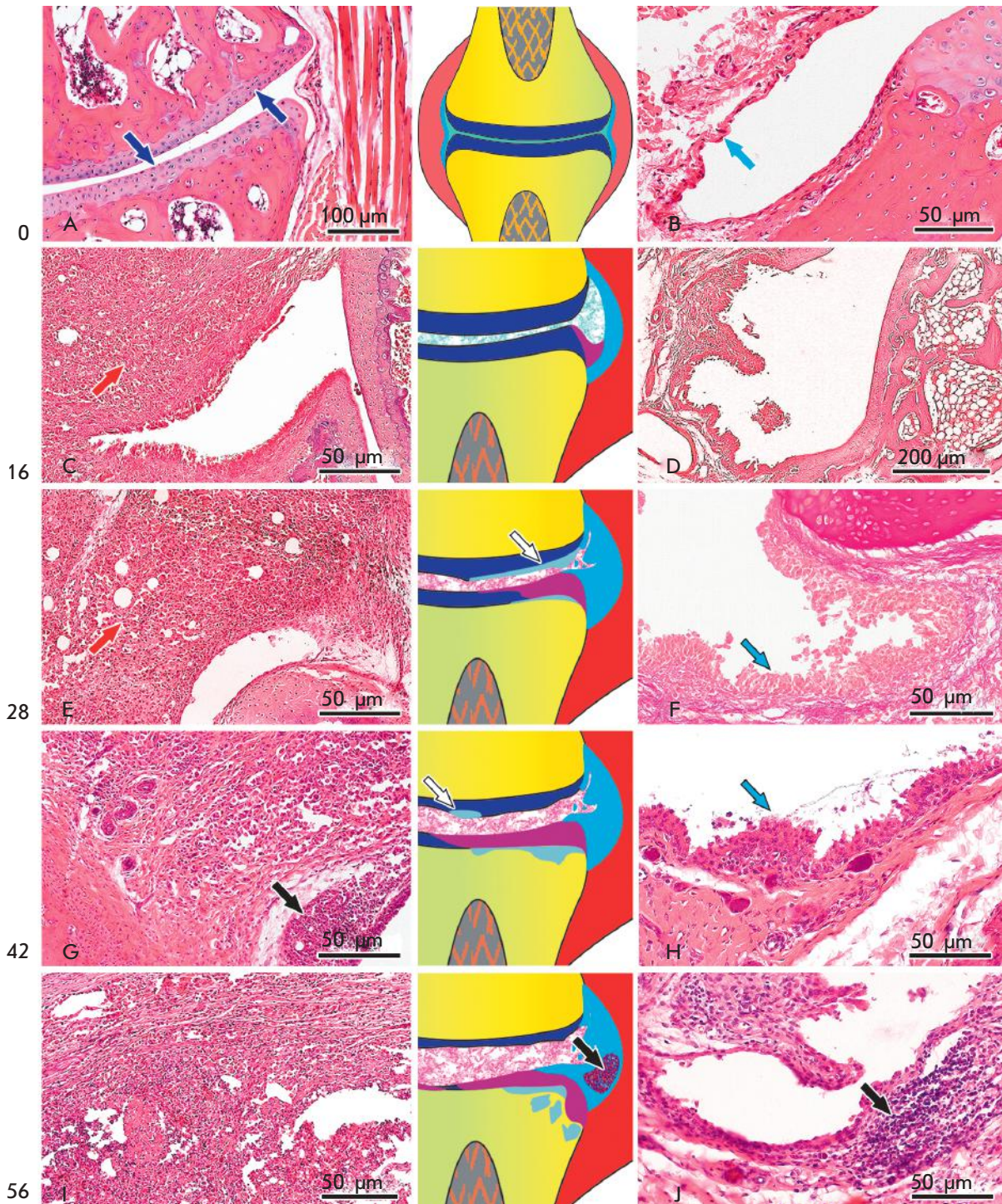


Fig. 3. The dynamics of inflammatory signs in the periarticular tissue (left column) and synovial membrane (right column); see body text for details. Hematoxylin and eosin staining (F, staining according to Van Gizon). In the schemes, the main joint elements and the pathological signs of arthritis (central column) are color-coded: bone tissue, yellow; cartilage, blue; joint capsule (inflammation), red; synovial membrane, cyan; pannus, magenta; damaged bone trabeculae in the cancellous bone, gray. The corresponding structures are indicated with arrows in micro images; arrow colors corresponds to the colors in the scheme. White arrows show erosive lesions on the articular cartilage surface and black arrows show granuloma under the synovial membrane.

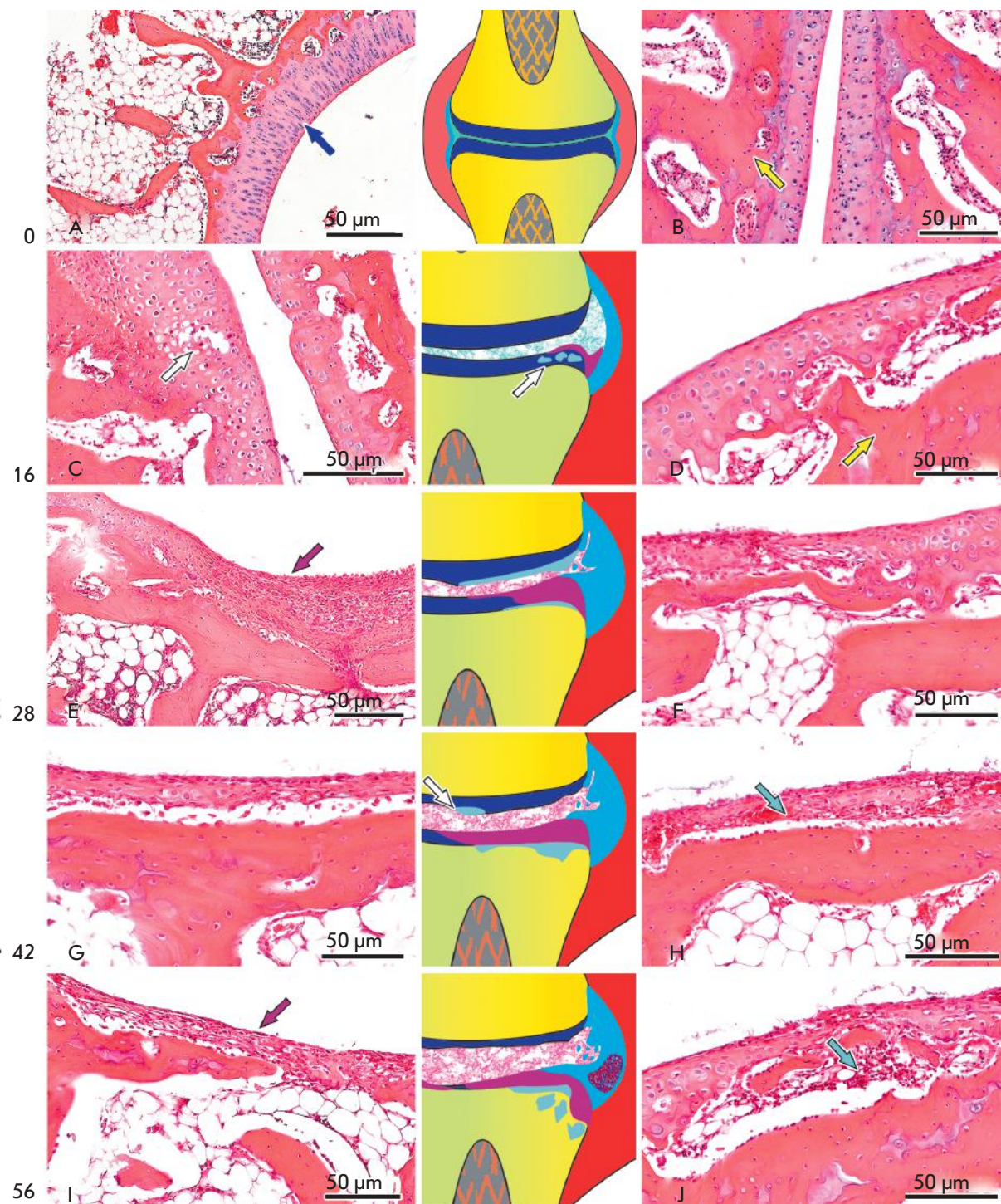


Fig. 4. The dynamics of articular cartilage (left column) and underlying bone (right column) lesions; see text for details. Hematoxylin and eosin staining. The color coding in the schemes (central column) is the same as in Figure 3.

vessels. However, synovitis symptoms were observed 42 and 56 days after the injection of adjuvant, although to a much lesser degree than on the side of the CFA injection. Moreover, erosive lesions of the articular cartilage in these extremities were observed in 56 days.

Histological analysis of the hind limbs of guinea pigs with AIA, group 50.

The pathological changes in the hind limbs of group 50 guinea pigs differed from those in group 200 mainly in their severity. In group 50, inflammation in the artic-

ular capsule and surrounding tissues attained a maximum 28 days after the CFA injection, while in group 200, the active inflammatory process continued as long as 42 days into the experiment. By day 28, the first signs of recovery around the inflammatory focus were observed in both groups in the form of vascular proliferation and proliferation of spongy irregular connective tissue. Deep cartilage erosion and destructive lesions of the cortical layer of the bone were observed in the joint, which worsened over time. However, the severity of these signs was significantly less pronounced compared to group 200. Moreover, the pathological process typically involved one joint, while in group 200, two or even three hind limb joints were involved.

Reproducibility of AIA in guinea pigs, group 100

All 14 guinea pigs in group 100, which was used to assess the reproducibility of the AIA, developed synovial and articular cartilage lesions on the side of the CFA injection (left hind paw) characteristic of rheumatoid arthritis. In addition to the cartilage surface erosion observed in all animals in this group, the destruction involved half the thickness of the articular cartilage in half of the cases. In two cases, there were portions of completely destroyed cartilage and the underlying bone was damaged. In four animals, articular cartilage of the ankle was not involved despite a rather significant inflammation in the articular capsule and synovium tissues. At the same time, in these animals, cartilage destruction was observed in other joints.

There was almost no inflammation in the limbs symmetrical to the CFA injection sites. There were only small foci of inflammatory cell infiltration along the small-caliber blood vessels. However, moderate manifestations of synovitis were observed in half of the animals, and erosive lesions of the articular cartilage were observed in two animals. Moreover, in one case, there was a limited area where cartilage tissue was destroyed over the full thickness of the articular cartilage, which, however, did not fit into the overall picture of lesions in this group of animals. The severity of various pathological manifestations in individual animals as assessed on the three-point scale (see. Experimental) is reported in the *Table*, and the average totals for the whole group 100 are shown in *Fig. 5*.

DISCUSSION

It is known that RA is a disease characterized by a diversity of molecular mechanisms and the sensitivity of individuals to different therapeutic agents. Therefore, the use of different laboratory models is advisable when testing potential antiarthritic drugs [1–3, 5, 6, 11]. Currently, the most well studied induced arthritis models are based on certain lines of mice and rats [1,

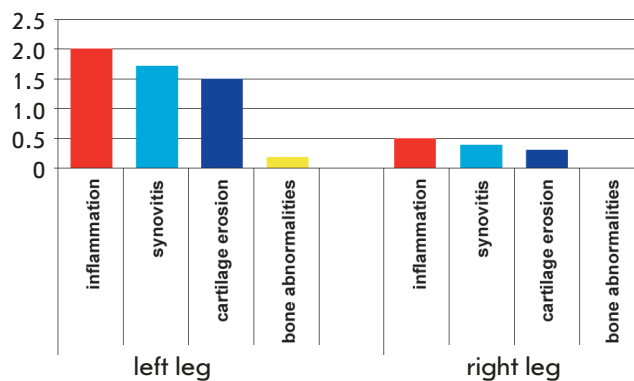


Fig. 5. Comparative characteristics of the severity of the injury to the periarticular and articular tissues in the guinea pig hind limbs: left, on the side of the CFA injection; right, in the symmetrical intact limb. The mean values for group 100 are shown.

2, 5, 6]. However, none of these models reflect all the characteristic features of RA in humans [5] and, therefore, the search for additional experimental models of RA remains relevant.

We evaluated the effectiveness of arthritis induction after subcutaneous CFA injection into the hind paw of outbred guinea pigs and a reproducible development of AIA.

It was shown that injection of arthritis-inducing CFA results in the development of a granulomatous inflammation of the soft tissues of the paw on the injection side, which involves capsules of large and small joints. The active phase of the inflammation in the periarticular tissues remits by day 42 of the experiment. Sclerosis signs develop in 28 days, and further development leads to encapsulation of the inflammation lesion. At the same time, the pathological process in the joint itself, which leads to deep destruction of the articular cartilage and underlying bone, does not stop at the end of the observation period (56 days). This may be indicative of a transformation of arthritis into chronic form. Despite a rather pronounced inflammation in the periarticular tissues, the pathological processes involve not all hind limb joints. The frequency and severity of the damage to the joint clearly depends on the administered dose. In group 200, where the inducing dose was the highest, the most severe disease joint was observed.

In this model, there are fibrin deposits on the synovial surface, leukocyte infiltration of the synovium and surrounding tissue, a productive response in the form of a proliferation of granulation tissue and emergence of angiomas areas characteristic of the acute phase

Assessment of pathological changes in the hind limb tissues of guinea pigs caused by the injection of 100 µl of CFA (see the text for details)

Animal No	On the side of CFA injection (left paw)				Intact (right paw)			
	Inflammation	Synovitis	Cartilage erosion	Bone destruction	Inflammation	Synovitis	Cartilage erosion	Bone destruction
1	3	2	2	0	0	0	0	0
2	2	1	1	0	1	0	0	0
3	2	2	3	0	0	0	0	0
4	3	1	2	1	0	0	0	0
5	2	2	1	0	1	1	0	0
6	2	2	2	0	1	0	0	0
7	3	2	2	0	0	1	0	0
8	2	2	1	0	1	0	0	0
9	1	2	1	0	0	0	0	0
10	2	1	1	0	0	0	0	0
11	2	2	2	1	1	1	1	0
12	1	1	1	0	1	1	3	0
13	2	2	1	0	1	1	0	0
14	1	2	1	0	0	0	0	0

of RA. A cellular response in the form of an increased number of plasma cells and formation of follicle-like lymphoid infiltrates, erosive lesions of the cartilage articular surface, often accompanied by deep destruction of large areas of the latter, and epiphyseal lesions, complements the picture of the systemic disease.

It is known that even the use of linear mice and rats usually does not result in the induction of experimental arthritis in all tested animals [1, 2]. This reduces the informative value of the data obtained during pre-clinical trials of new RA treatments. Therefore, the search for well reproducible modes of induced arthritis remains an important area of research [2, 11, 12]. We quantified AIA reproducibility in group 100 guinea pigs. It was shown (*Table*) that injection of CFA at a dose of 100 µl causes significant damage to joint tissue (injection side), which indicates a good reproducibility of arthritis induction in the used RA model and its potential in evaluating antiarthritic drugs and their dosage regimens. It should be noted that, in 28 days, there were no pathological changes in the right (untreated) hind paw or they were much less pronounced than in the left (treated) paw of all group 100 guinea pigs, except for animal number 12 (*Table*).

Apparently, the degenerative processes in the underlying bone tissue of group 100 animals did not have enough time to develop to a full extent by that time (28 days), so that the severity of the inflammatory process, which is quite pronounced in the joint tissues, did not always correlate with the damage to the subchondral bone. However, in a model which is used to assess the effectiveness of potential drugs, this is rather an advantage than a drawback, since the far-gone destructive process in the joint was more drug-refractory and thus complicated the assessment of the treatment results.

CONCLUSION

We have suggested a laboratory model of RA based on a subcutaneous CFA injection to outbred guinea pigs. A high effectiveness and reproducibility of AIA in these animals was shown. The developed model would facilitate pre-clinical testing of antiarthritic drugs. ●

This work was supported by the Russian Science Foundation (grant No 14-15-00050).

REFERENCES

1. Orlovskaya I.A., Tsyrendorzhiiev D.D., Shchelkunov S.N. // *Meditinskaya Immunologiya*. 2015. V. 17. P. 203–210.
2. Bolon B., Stolina M., King C., Middleton S., Gasser J., Zack D., Feige U. // *J. Biomed. Biotechnol.* 2011. V. 2011. Article ID 569068.
3. Evans C.H., Ghivizzani S.C., Robbins P.D. // *Transl. Res.* 2013. V. 161. P. 205–216.
4. Chemin K., Klareskog L., Malmstrom V. // *Curr. Opin. Rheumatol.* 2016. V. 28. P. 181–188.
5. Vincent T.L., Williams R.O., Maciewicz R., Silman A., Gar- side P. // *Rheumatology*. 2012. V. 51. P. 1931–1941.
6. Bevaart L., Vervoordeldonk M.J., Tak P.P. // *Arthritis Rheum.* 2010. V. 62. P. 2192–2205.
7. Schurgers E., Billiau A., Matthys P. // *J. Interferon Cy- tokine Res.* 2011. V. 31. P. 917–926.
8. Padilla-Carlin D.J., McMurray D.N., Hickey A.J. // *Comp. Med.* 2008. V. 58. P. 324–340.
9. Fernandez M.L., Volek J. // *Nutr. Metab.* 2006. V. 3. P. 17.
10. Thangavel R.R., Bouvier N.M. // *J. Immunol. Methods.* 2014. V. 410. P. 60–79.
11. Hu Y., Cheng W., Cai W., Yue Y., Li J., Zhang P. // *Clin. Rheumatol.* 2013. V. 32. P. 161–165.
12. Drutskaya M.S., Efimov G.A., Zvartsev R.V., Chashchina A.A., Chudakov D.M., Tillib S.V., Kruglov A.A., Nedospasov S.A. // *Biochemistry (Moscow)*. 2014. V. 79. P. 1349–1357.

Flavoprotein miniSOG Cytotoxicity Can Be Induced By Bioluminescence Resonance Energy Transfer

E.I. Shramova^{1*}, G.M. Proshkina^{1#}, S.P. Chumakov¹, Yu.M. Khodarovich¹, S.M. Deyev^{1,2}

¹Shemyakin/Ovchinnikov Institute of Bioorganic Chemistry, Russian Academy of Sciences, Miklukho-Maklaya Str., 16/10, 117997, Moscow, Russia

²National Research Tomsk Polytechnic University, Lenina av., 30, 634050, Tomsk, Russia

E-mail: *shramova.e.i@gmail.com, #gmb@ibch.ru

Received July 8, 2016; in final form, October 11, 2016

Copyright © 2016 Park-media, Ltd. This is an open access article distributed under the Creative Commons Attribution License, which permits unrestricted use, distribution, and reproduction in any medium, provided the original work is properly cited.

ABSTRACT In this study, we investigated the possibility of phototoxic flavoprotein miniSOG (photosensitizer) excitation in cancer cells by bioluminescence occurring when luciferase NanoLuc oxidizes its substrate, furimazine. We have shown that the phototoxic flavoprotein miniSOG expressed in eukaryotic cells in fusion with NanoLuc luciferase is activated in the presence of its substrate, furimazine. Upon such condition, miniSOG possesses photoinduced cytotoxicity and causes a 48% cell death level in a stably transfected cell line.

KEYWORDS bioluminescence resonance energy transfer, NanoLuc luciferase, flavoprotein miniSOG, photodynamic therapy

ABBREVIATIONS ROS – reactive oxygen species, PCR – polymerase chain reaction, PDT – photodynamic therapy, FMN – flavin mononucleotide, BRET – bioluminescence resonance energy transfer

INTRODUCTION

The properties of light as a therapeutic agent have been used by mankind for over 3,000 years [1]. The starting point of our modern approach to the study of the photosensitivity phenomenon is considered to be the work of Oscar Raab published in 1900 [2]. Raab revealed that the combination of light with certain chemicals induces the death of living cells: the acridine orange dye causes the death of ciliates on a sunny day, but not on a cloudy day [2]. Modern photodynamic therapy (PDT) appeared with the discovery of this fact.

The modern form of the photodynamic therapy is a three-component system consisting of a photosensitizer, a light of a certain wavelength, and molecular oxygen. These three key elements, each individually non-toxic, produce reactive oxygen species (ROS) when combined and, thus, induce oxygen-mediated cell death.

PDT is a promising method for the treatment of human malignant tumors, because it allows for selective and local action on the tumor.

Because photodynamic therapy requires an external light source, the method is applied only in the treatment of skin and retina tumors in clinical practice, as well as the epithelial surfaces of organs accessible to catheters and endoscopes. For example, PDT is now approved for the treatment of head and neck carcinomas [3], lung cancer [4], the upper digestive tract [5], and malignancies [6].

The main obstacle of photodynamic therapy is related to a loss of the optical activity (intensity) of the exciting light as a result of refraction, reflection, absorption and dispersion of light quanta in biological tissues. Due to the ability of tissues to absorb and disperse light, the penetrating power of visible light in tissues does not exceed 10 mm. Moreover, light absorption is determined by the biological chromophores of the tissue: almost all proteins are target chromophores in the ultraviolet region of the spectrum, oxyhemoglobin, deoxyhemoglobin, and melanin absorb light with a wavelength of 400 to 600 nm, while water absorbs light with a wavelength of 1,200 to 2,000 nm. Thus, the “optical window” of biological tissues for PDT is in the range of 650–1,200 nm [7].

With the onset of metastasis, it becomes difficult or impossible to deliver light directly to all tumor growth foci. In the case if internal light sources are developed, the light can be delivered to any body area and to any depth, which can significantly expand the scope of photodynamic therapy application [8].

The phenomenon of bioluminescence resonance energy transfer (BRET) is widely used in modern molecular and cell biology for *in vivo* and *in vitro* study of intracellular processes, as well as for bioimaging [9–11]. BRET is based on Förster resonance energy transfer between two chromophores, where a luciferase substrate serves as the donor, which is oxidized in the

presence of oxygen and emits photons in the visible spectrum, while a fluorescent protein acts as the acceptor (Fig. 1A).

With the advances in gene therapy approaches, the gene encoding luciferase can be selectively expressed in tumor cells using tumor-specific promoters [12, 13] or selectively delivered to tumor cells using such vehicles as pseudotyped viral vectors [14] targeting polyethyleneimine complexes, etc. [15]. Thus, the use of bioluminescence as an intracellular source of light for the excitation of the photosensitizer in a cancer cell may serve as a solution to the problem of light delivery to the deep regions of tissues.

The applicability of the phenomenon in therapy was first demonstrated in 1994 [16]: photosensitizer hypericin excited by luciferin bioluminescence led to *in vitro* inactivation of the equine infectious anemia virus.

However, the use of BRET in the photodynamic therapy of cancer was demonstrated only in 2003 [17]. The photosensitizer bengal red located in the cytosol in the presence of luciferin caused the death of 90% of a population of NIH 3T3 mouse fibroblasts stably expressing the luciferase gene.

According to [18], the luminescent molecule luminol can also be used as an intracellular light source for the excitation of the photosensitizer. The viability of HeLa cells treated with luminol in the presence of the photosensitizer was less than 10%. Anti-tumor therapy *in vivo* led to a 55% decrease in tumor growth in mice of the experimental group compared to the control group. In addition, luminol and the photosensitizer were injected directly into the tumors of the experimental animals.

The possibility of using BRET-mediated photodynamic therapy of deep tissue tumors and metastases was demonstrated in a mouse model in 2015 [19]. In that work, quantum dots coated with luciferase were used as an intracellular source for photodynamic therapy. The quantum dots excited the photosensitizer chlorin e6 in the presence of a luciferase substrate, leading to a regression of the primary tumor focus and metastases in the lymph nodes.

We should note that chemical photosensitizers administered intratumorally or systemically to the body were used in all of the mentioned papers.

Targeted genetically encoded protein photosensitizers with high cytotoxic activity against HER2-positive breast adenocarcinoma cells *in vitro* were previously obtained in our laboratory on the basis of the phototoxic flavoprotein miniSOG [20–23]. MiniSOG excitation occurs in the blue region of the spectrum ($\lambda_{\max} = 448 \text{ nm}$) [24], which imposes some restrictions on the use of these photosensitizers *in vivo*.

In order to solve the problem of blue light delivery *in vivo*, we propose a system where the miniSOG pho-

tosensitizer is excited during luciferase NanoLuc (Promega) oxidation of the substrate (furimazine). We have shown that NanoLuc luciferase expressed in eukaryotic cells as part of the genetic construct with miniSOG causes the excitation of phototoxic flavoprotein in the presence of the furimazine substrate. Moreover, miniSOG exhibits photoinduced cytotoxicity and causes the death of 48% of the transfected cells.

EXPERIMENTAL SECTION

Eukaryotic cell cultures

Human breast adenocarcinoma SK-BR-3 cells were used in this study. The cells were grown in a McCoy's 5A (HyClone, Belgium) or RPMI 1640 medium without phenol red (Gibco, Germany) containing 10% fetal bovine serum (HyClone, Belgium) and antibiotics (50 U/ml penicillin, 50 $\mu\text{g}/\text{ml}$ streptomycin, "PanEco", Russia) at 37°C and 5% CO₂ in high humidity. For cultivation of the cells expressing miniSOG, riboflavin ("Pharmstandart-Ufa-Vita", Russia) was added to the medium as a source of the FMN cofactor to a final concentration of 150 μM .

NanoLuc–miniSOG construction

The coding sequence of the photoactivatable cytotoxic miniSOG protein gene was cloned into pNL1.1.CMV (Promega) plasmid containing the NanoLuc luciferase gene under the control of the CMV promoter using standard techniques of genetic engineering. The coding sequence of *miniSOG* was amplified from the pDARF-miniSOG plasmid [22] using the specific primers oGP13 (5'-GCGGGTGGCGGAGGGAGCATG-GAAAAGAGCTTTGTGATTACC-3', linker sequence is underlined) and oGP14 (5'-GGTCTAGAATTAGC-CATCCAGCTGC-3', XbaI endonuclease restriction site is underlined). The coding region of the NanoLuc luciferase gene was amplified using the specific primers oGP11 (5'-CAGTTTGTTCAGAAATCTCGGGG-3', AvaI endonuclease site is underlined) and oGP12 (5'-CCATGCTCCCTCCGCCACCCGCCAGAATGCGT-TCGCACAG-3', linker sequence is underlined). The sequence underlined in the structure of primers encodes the GGGGS peptide linker inserted in order for the two functional domains (NanoLuc luciferase and miniSOG phototoxin), which are part of the fusion protein, not to experience steric constraints and retain their functional properties. PCR products encoding NanoLuc and miniSOG were combined in an equimolar ratio, heated to 90°C, and then the temperature was slowly decreased to 24°C for the complementary regions of the linker sequence to interact with each other. Next, PCR was performed using the primers oGP11 and oGP14 to obtain a complete NanoLuc–miniSOG hybrid construct. The resulting fragment was treated with the restriction endo-

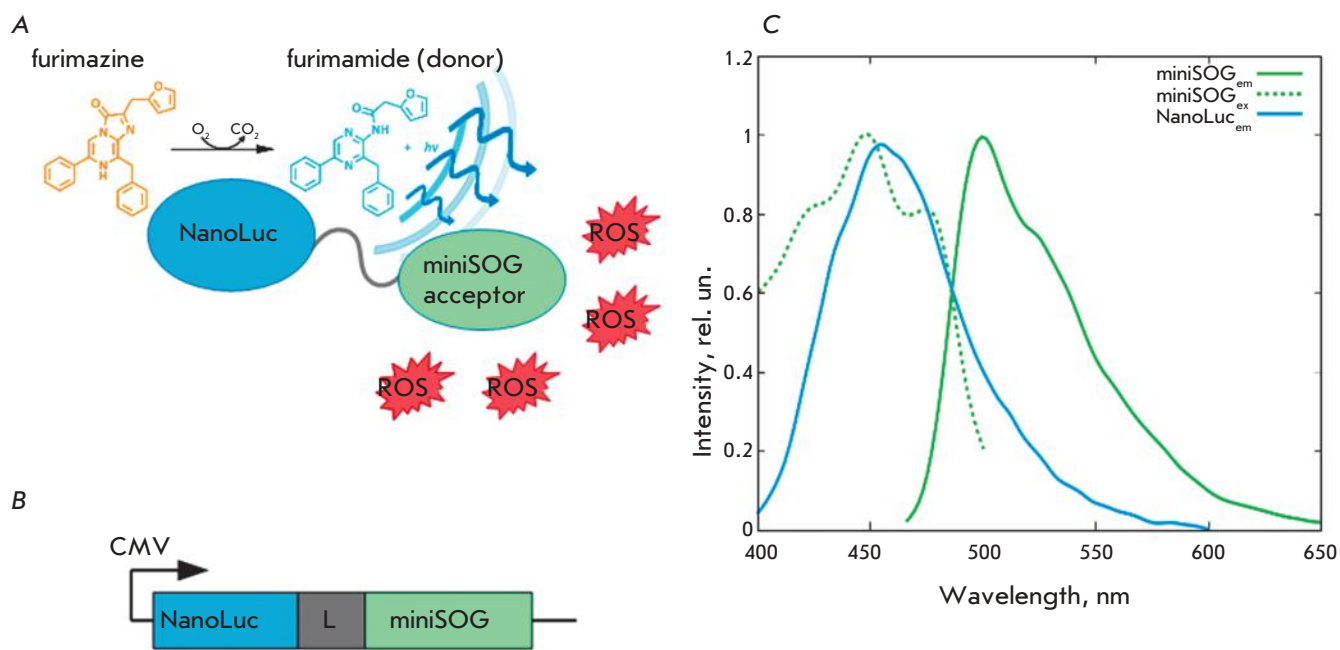


Fig. 1. Bioluminescence system based on luciferase, furimazine, and miniSOG. **A** – Schematic illustration of the BRET system for PDT. **B** – Gene construct encoding NanoLuc, peptide linker GGGGS and cytotoxic module miniSOG within one reading frame. **C** – Normalized emission spectrum of furimamide (NanoLuc_{em}) and normalized excitation (miniSOG_{ex}) and emission (miniSOG_{em}) spectra of miniSOG.

nucleases *AvaI* and *XbaI* and cloned into a pNL1.1.CMV vector digested with the same restriction enzymes. As a result, a pNanoLuc-miniSOG plasmid was obtained containing *NanoLuc*- and *miniSOG*-encoding sequences within the same reading frame connected by a linker region under the control of the constitutive promoter CMV. The accuracy of the construct was confirmed by sequencing. The scheme of the genetic construct is presented in *Fig. 1B*.

pNanoLuc-miniSOG-puro plasmid construction

To obtain cell lines that stably expressed the *NanoLuc-mSOG* fusion gene, the puromycin resistance gene was introduced into the NanoLuc-miniSOG plasmid. This gene, including the NP promoter of the human *p53* gene and polyadenylation signal, was amplified from pLCMV-puro plasmid (kindly provided by P.M. Chumakov) using the specific primers 5'-AAG-GAAAAAAGCGGCCGCTGTGAAGGAAGCCAACA-3' (NotI endonuclease site is underlined) and 5'-AAAAGTGCAGTTCCGGCTCGTATGTTGTGT-3' (PstI endonuclease site is underlined). The resulting fragment was treated with the restriction endonucleases PstI and NotI and ligated to pNanoLuc-mSOG plasmid pretreated with the same restriction enzymes.

Transfection of SK-BR-3 cells

For transfections, plasmid DNA isolated from bacterial cells with the PureLink™ kit (Invitrogen) according

to the manufacturer's instructions was used. Transfection was performed using FuGENE® HD (Promega) according to the manufacturer's recommendations (<http://www.promega.com/techserv/tools/FuGene-HdTool/>). A day before the transfection, the cells were seeded at a density of 10^5 cells/ml in a complete growth medium without antibiotics. FuGENE® HD and DNA were used in a 3: 1 ratio, and the concentration of the plasmid DNA during the formation of the complexes was $0.02 \mu\text{g}/\mu\text{l}$. The volume of the medium that was added to the cells and contained FuGENE® HD-DNA complexes was 1/20 of the total volume of the growth medium. The complexes were prepared in a medium without serum and antibiotics, cultured at room temperature for 5–10 min and added to the cells. In the case of plasmids containing *miniSOG*, riboflavin (FMN cofactor) was added to the cells 6 h after the transfection. The optimal transfection conditions were determined in preliminary experiments by evaluating miniSOG fluorescence 24–48 h after the transfection using a fluorescence microscope.

Sorting of transfected cells

Cells expressing NanoLuc-miniSOG were collected 48 h after transfection using a BD FACS Vantage sorter (BD, USA). For the sorting, the area of bright fluorescent cells was selected on a FL1-FL2 diagram so that it did not capture the cells that were fluorescent due to the presence of FMN in the medium (background FMN flu-

orescence). The sorted cells were seeded at a density of 10^5 cells/ml per well of a 96-well plate in 100 μ l of a complete growth medium containing penicillin (50 U/ml), streptomycin (50 μ g/ml), kanamycin (100 μ g/ml), and gentamicin (10 μ g/ml) (all antibiotics are produced by “PanEco” Russia).

Preparation of stable cell lines

The concentration of puromycin (Sigma, USA) that caused the death of 100% of the cells in 14 days (0.25 mg/ml for SK-BR-3 cells) was detected during preliminary experiments. The medium in the plates with cultured cells was replaced with a fresh medium containing FMN and puromycin 48 h after transfection with the pNanoLuc-miniSOG-puro plasmid. Clones of the stably transfected cells were formed by day 14–15, after which the cells were passaged in the presence of puromycin for 3 months.

Detection of NanoLuc luciferase luminescence

The luminescence of NanoLuc luciferase and the NanoLuc-miniSOG fusion protein was evaluated 48–72 h after transfection on an Infinite M1000 Pro device (Tecan, Switzerland). Measurements were carried out using living cells in a complete RPMI medium without phenol red in 96-well plates with black walls (three repeats for each sample). The luciferase substrate furimazine (Promega) was added at concentrations of 30, 43, and 75 μ M in the injection mode on an Infinite M1000 Pro device (Tecan, Switzerland). The delay after injection until the start of the analysis was 10 sec. Luminescence spectra were obtained for each experimental point in the wavelength range from 400 nm to 600 nm with a 4-nm increment and detection time of 100 msec. The obtained data were processed using the OpenOffice software, version 4.1.2. Mathematical data processing (smoothing with cubic splines) was used for the spectra plotting.

Evaluation of the cytotoxic effect of NanoLuc-miniSOG *in vitro*

The cytotoxicity of NanoLuc-miniSOG in the presence of furimazine was evaluated using the MTT test [25]. SK-BR-3 cells stably expressing the *NanoLuc-miniSOG* gene were seeded in a 96-well plate in the amount of 10^5 cells/ml of the medium in a volume of 200 μ l of suspension per cell and cultured overnight. Then, the cells were supplemented with furimazine and incubated for 48 h. The medium was removed, 100 μ l of a 3-[4,5-Dimethylthiazol-2-yl]-2,5-diphenyltetrazolium bromide (MTT, “PanEco”) solution in a McCoy’s 5A medium was added per well (0.5 mg/ml), and then the cells were incubated at 37°C and 5% CO₂ for 1 h. Next, the MTT solution was removed, 100 μ l of DMSO was added to the wells, and the plate was incubated on a

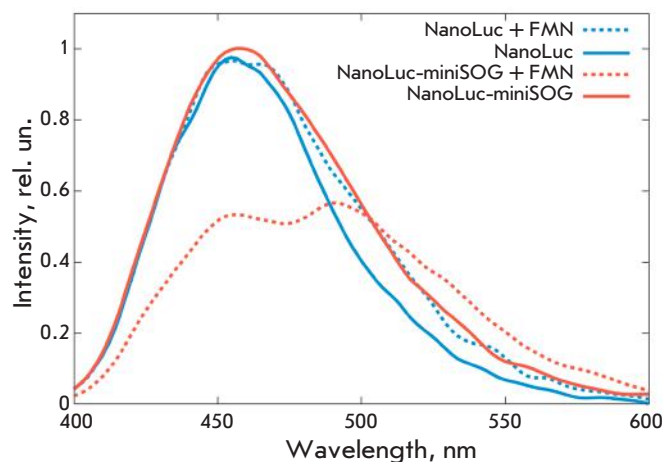


Fig. 2. Emission spectra of the bioluminescence systems NanoLuc-furimazine (NanoLuc) and NanoLuc-furimazine-miniSOG (NanoLuc-miniSOG) in the presence of FMN.

shaker until complete dissolution of the formazan crystals. The optical absorption of the content of each well was measured on a tablet spectrophotometer Infinite M1000 (Tecan, Switzerland) at two wavelengths: 570 (experimental) and 650 nm (reference). The experiments were conducted in triplicate. Cell survival after incubation with furimazine was assessed based on the amount of formazan formed as a result of the reduction of the MTT solution by the cells and dissolved in dimethylsulfoxide (the amount of formazan corresponds to the number of living cells). The data were processed using the OpenOffice software, version 4.1.2.

RESULTS AND DISCUSSION

For effective direct energy transfer from the oxidized form of the substrate to an acceptor (Förster resonance energy transfer), a number of conditions are required. First of all, an emission spectrum of the donor had to coincide as much as possible with the excitation spectrum of the acceptor. Secondly, the donor and acceptor had to be separated from each other by a distance not exceeding 10 nm [26].

Having performed an analysis of the published data, we found that the reaction of furimazine oxidation by NanoLuc luciferase of the deepwater shrimp *Ophiophorus gracilirostris* results in an emission of light in the visible spectrum with an emission maximum at 460 nm [27]. The absorption maximum of the phototoxic flavoprotein miniSOG is 448 nm [24]. Thus, the oxidized form of furimazine (furimamide) and miniSOG offer a good donor-acceptor pair for bioluminescence resonance energy transfer. Superposition of the furimamide emission and miniSOG excitation spectra is shown in Fig. 1C.

In order to bring together the donor and acceptor spatially, we obtained a construct containing NanoLuc luciferase and miniSOG phototoxin genes connected by a short linker of 15 nucleotides within the same single reading frame under the control of the constitutive CMV promoter (Fig. 1B).

The efficiency of this system was evaluated *in vitro* using a SK-BR-3 line transfected with the obtained construct. An analysis of the emission spectra of the transfected cells in the presence of furimazine demonstrated a peak at 460 nm, corresponding to the emission maximum of the oxidized form of furimazine (Fig. 2).

FMN is known to be a cofactor of all phototropins (including flavoprotein miniSOG). The phototoxicity of miniSOG directly depends on its saturation with the cofactor: FMN enters an excited state under the impact of a blue light quantum, and all the energy of the excited state of FMN transfers into the generation of reactive oxygen species [24]. Therefore, riboflavin, which penetrates through the cellular membrane and turns into FMN as a result of phosphorylation by riboflavin kinase, was added at a concentration of 150 μM to the cells transfected with the pNanoLuc-miniSOG plasmid. Addition of riboflavin to the cells transfected with pNanoLuc-miniSOG in the presence of furimazine led to a decreased intensity of the peak at 460 nm and the appearance of a peak at 500 nm (miniSOG emission maximum), which indicates energy transfer from furimamide to miniSOG. We should note that addition of FMN to cells transfected with the plasmid containing the NanoLuc luciferase gene (without miniSOG) does not lead to the appearance of a 500 nm peak (Fig. 2).

In order to evaluate the cytotoxic effect caused by the NanoLuc-furimazine-miniSOG system, SK-BR-3 cells transfected with the pNanoLuc-miniSOG plasmid were sorted using a BD FACS Vantage sorter (BD) 48 h after transfection. The selected cells were seeded in a 96-well plate for the assessment of the NanoLuc-miniSOG construct cytotoxicity in the presence of furimazine. However, the cells that had passed through the sorter and were exposed to the laser with a wavelength of 473 nm turned out to be not viable. We believe that short-time exposure to blue light (cell passage through the laser beam) was enough for miniSOG excitation and manifestation of its photoinduced cytotoxicity.

In order to circumvent this problem, we obtained a SK-BR-3 cell line stably expressing the NanoLuc-miniSOG construct. The selection of transfectants was carried out in the presence of the puromycin antibiotic as described in the “Experimental section.”

The analysis of the emission spectra of the cells containing the NanoLuc-miniSOG fusion protein in the presence of various concentrations of furimazine showed a peak at 460 nm, the intensity of which corre-

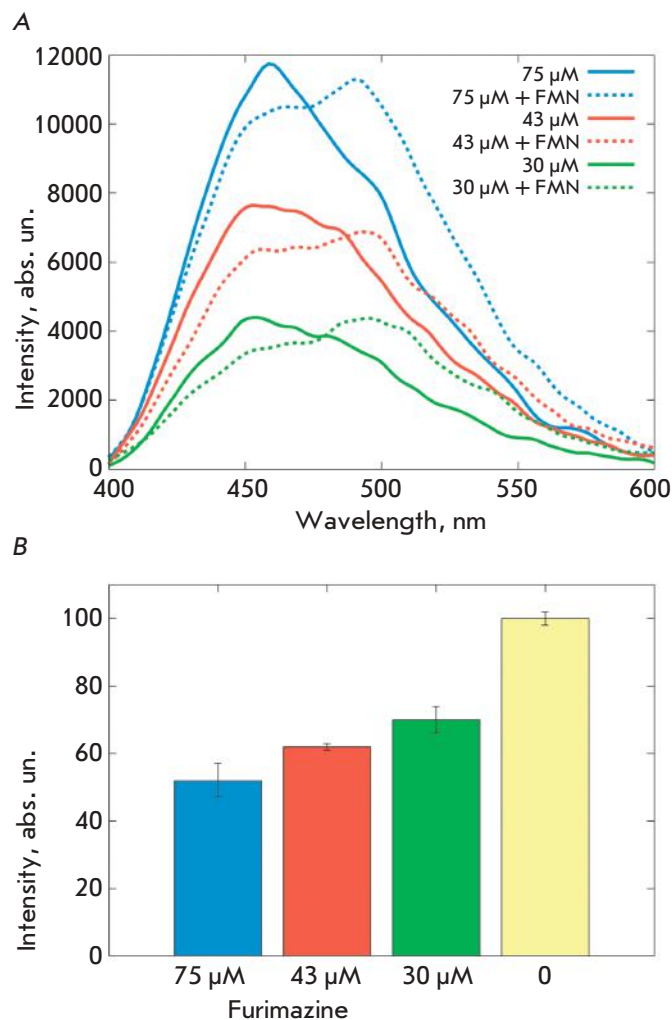


Fig. 3. Functional characteristics of the bioluminescence system NanoLuc-furimazine-miniSOG. **A** – Dependence of NanoLuc-miniSOG emission spectra on furimazine and FMN concentrations. **B** – Dependence of the cytotoxic effect of the NanoLuc-miniSOG fusion protein on the furimazine concentration.

lated with the substrate concentration (Fig. 3A). Addition of FMN to the cells led to the appearance of a peak at 500 nm, typical of a miniSOG emission maximum (Fig. 3A).

For a study of the cytotoxic effect of the “NanoLuc luciferase-furimazine-miniSOG phototoxin” system, SK-BR-3 cells stably expressing a NanoLuc-miniSOG hybrid construct were seeded in a 96-well plate and grown in the presence of FMN for 24 h. Further, furimazine was added to the cells at various concentrations and the cells were incubated at 37°C in a CO₂ atmosphere for 48 h. The cytotoxic effect at a maximum concentration of furimazine was 48% (Fig. 3B).

It is known that miniSOG localized in mitochondria or in the plasma membrane causes the death of almost

100% of HeLaKyoto cells under exposure to blue light (55 mW/cm²) [28]. Moreover, the unsaturated fatty acids contained in the plasma membrane in high amounts are the primary target for reactive oxygen species [29]. An additional factor contributing to the photo-induced damage to lipids is molecular oxygen, which is soluble in lipids. Thus, the photosensitizer is more likely to meet with molecular oxygen and generate ROS in a lipid environment than in water.

Taking into account the data in the papers [28, 29], we believe that the cytotoxic effect we identified in the course of our study can possibly be enhanced by using NanoLuc-miniSOG hybrid constructs with signals of various intracellular localization (mitochondrial, membrane, lysosomal). The systems based on a BRET-mediated activation of the photosensitizer will significantly enhance the capabilities of PDT by overcoming the problem of the “optical window” of biological tissues.

We have proved that cytotoxic flavoprotein miniSOG excitation by light emitted by the oxidized form of the luciferase substrate is possible, and shown that

this system can be used for photo-induced cell death.

CONCLUSION

This paper shows for the first time that it is possible to use bioluminescence resonance energy transfer to excite a genetically encoded photosensitizer. The light emitted by the oxidized form of the luciferase substrate renders the phototoxic protein miniSOG, which is part of the fusion with luciferase, into the excited state necessary for the generation of reactive oxygen species and cell death induction. The use of bioluminescence as an intracellular source of photosensitizer excitation in a cancer cell may become a solution to the problems of light delivery into deep regions of tissues and enhance the capabilities of photodynamic therapy of deep tissue tumors and metastasis. ●

This work was supported by the Russian Science Foundation (grant No 16-14-10321).

REFERENCES

- Ackroyd R., Kelty C., Brown N., Reed M. // *Photochem. Photobiol.* 2001. V. 74. № 5. P. 656–669.
- Raab O. // *Zeitung Biol.* 1900. V. 39. P. 524–526.
- Schweitzer V.G. // *Otolaryngol. Head Neck Surg.* 1990. V. 103. № 6. P. 981–985.
- Hayata Y., Kato H., Konaka C., Ono J., Takizawa N. // *Chest.* 1982. V. 81. № 3. P. 269–277.
- Hayata Y., Kato H., Okitsu H., Kawaguchi M., Konaka C. // *Semin. Surg. Oncol.* 1985. V. 1. № 1. P. 1–11.
- Ward B.G., Forbes I.J., Cowled P.A., McEvoy M.M., Cox L.W. // *Am. J. Obstet Gynecol.* 1982. V. 142. № 3. P. 356–357.
- Plaetzer K., Krammer B., Berlanda J., Berr F., Kiesslich T. // *Lasers Med. Sci.* 2009. V. 24. № 2. P. 259–268.
- Grebenik E.A., Deyev S.M. // *Russ. Chem. Rev.* 2016. V. 85.
- Pfleger K.D., Eidne K.A. // *Nat. Methods.* 2006. V. 3. № 3. P. 165–174.
- Baumes J.M., Gassensmith J.J., Giblin J., Lee J.J., White A.G., Culligan W.J., Leevy W.M., Kuno M., Smith B.D. // *Nat. Chem.* 2010. V. 2. № 12. P. 1025–1030.
- Takai A., Nakano M., Saito K., Haruno R., Watanabe T.M., Ohyanagi T., Jin T., Okada Y., Nagai T. // *Proc. Natl. Acad. Sci. USA.* 2015. V. 112. № 14. P. 4352–4356.
- Iyer M., Wu L., Carey M., Wang Y., Smallwood A., Gambhir S.S. // *Proc. Natl. Acad. Sci. USA.* 2001. V. 98. № 25. P. 14595–14600.
- Sieger S., Jiang S., Kleinschmidt J., Eskerski H., Schönsiegel F., Altmann A., Mier W., Haberkorn U. // *Cancer Gene Ther.* 2004. V. 11. № 1. P. 41–51.
- Adams J.Y., Johnson M., Sato M., Berger F., Gambhir S.S., Carey M., Iruela-Arispe M.L., Wu L. // *Nat. Med.* 2002. V. 8. № 8. P. 891–897.
- Hildebrandt I.J., Iyer M., Wagner E., Gambhir S.S. // *Gene Ther.* 2003. V. 10. № 9. P. 758–764.
- Carpenter S., Fehr M.J., Kraus G.A., Petrich J.W. // *Proc. Natl. Acad. Sci. USA.* 1994. V. 91. № 25. P. 12273–12277.
- Theodossiou T., Hotherall J.S., Woods E.A., Okkenhaug K., Jacobson J., MacRobert A.J. // *Cancer Res.* 2003. V. 63. № 8. P. 1818–1821.
- Yuan H., Chong H., Wang B., Zhu C., Liu L., Yang Q., Lv F., Wang S. // *J. Am. Chem. Soc.* 2012. V. 134. № 32. P. 13184–13187.
- Kim Y.R., Kim S., Choi J.W., Choi S.Y., Lee S.H., Kim H., Hahn S.K., Koh G.Y., Yun S.H. // *Theranostics.* 2015. V. 5. № 8. P. 805–817.
- Mironova K.E., Proshkina G.M., Ryabova A.V., Stremovskiy O.A., Lukyanov S.A., Petrov R.V., Deyev S.M. // *Theranostics.* 2013. V. 3. № 11. P. 831–840.
- Proshkina G.M., Mironova K.E., Deyev S.M., Petrov R.V. // *Dokl. Biochem. Biophys.* 2015. V. 460. № 2. C. 16–19.
- Proshkina G.M., Shilova O.N., Ryabova A.V., Stremovskiy O.A., Deyev S.M. // *Biochimie.* 2015. V. 118. P. 116–122.
- Shilova, O.N., Proshkina, G.M., Ryabova, A.V., Deyev, S.M. // *Moscow University Biological Sciences Bulletin.* 2016. V. 71. № 1. P. 14–18.
- Shu X., Lev-Ram V., Deerinck T.J., Qi Y., Ramko E.B., Davidson M.W., Jin Y., Ellisman M.H., Tsien R.Y. // *PLoS Biol.* 2011. V. 9. № 4. e1001041.
- Mosmann T. // *J. Immunol. Methods.* 1983. Vol. 65. № 1-2. P. 55–63.
- Carpenter S., Fehr M. J., Kraus G. A., Petrich J.W. // *Proc. Natl. Acad. Sci. USA.* 1994. V. 91. № 25. P. 12273–12277.
- Hall M.P., Unch J., Binkowski B.F., Valley M.P., Butler B.L., Wood M.G., Otto P., Zimmerman K., Vidugiris G., Machleidt T., Robers M.B., Benink H.A., Eggers C.T., Slater M.R., Meisenheimer P.L., Klaubert D.H., Fan F., Encell L.P., Wood K.V. // *ACS Chem. Biol.* 2012. V. 7. № 11. P. 1848–1857.
- Ryumina A.P., Serebrovskaya E.O., Shirmanova M.V., Snopova L.B., Kuznetsova M.M., Turchin I.V., Ignatova N.I., Klementieva N.V., Fradkov A.F., Shakhov B.E., Zagaynova E.V., Lukyanov K.A., Lukyanov S.A. // *Biochim. Biophys. Acta.* 2013. V. 1830. № 11. P. 5059–5067.
- Girotti A.W. // *J. Photochem. Photobiol.* 2001. V. 63. № 1-3. P. 103–113.

GENERAL RULES

Acta Naturae publishes experimental articles and reviews, as well as articles on topical issues, short reviews, and reports on the subjects of basic and applied life sciences and biotechnology.

The journal is published by the Park Media publishing house in both Russian and English.

The journal *Acta Naturae* is on the list of the leading periodicals of the Higher Attestation Commission of the Russian Ministry of Education and Science. The journal *Acta Naturae* is indexed in PubMed, Web of Science, Scopus and RCSI databases.

The editors of *Acta Naturae* ask of the authors that they follow certain guidelines listed below. Articles which fail to conform to these guidelines will be rejected without review. The editors will not consider articles whose results have already been published or are being considered by other publications.

The maximum length of a review, together with tables and references, cannot exceed 60,000 characters with spaces (approximately 30 pages, A4 format, 1.5 spacing, Times New Roman font, size 12) and cannot contain more than 16 figures.

Experimental articles should not exceed 30,000 symbols (approximately 15 pages in A4 format, including tables and references). They should contain no more than ten figures.

A short report must include the study's rationale, experimental material, and conclusions. A short report should not exceed 12,000 symbols (8 pages in A4 format including no more than 12 references). It should contain no more than four figures.

The manuscript and the accompanying documents should be sent to the Editorial Board in electronic form:

- 1) text in Word 2003 for Windows format;
- 2) the figures in TIFF format;
- 3) the text of the article and figures in one pdf file;
- 4) the article's title, the names and initials of the authors, the full name of the organizations, the abstract, keywords, abbreviations, figure captions, and Russian references should be translated to English;
- 5) the cover letter stating that the submitted manuscript has not been published elsewhere and is not under consideration for publication;
- 6) the license agreement (the agreement form can be downloaded from the website www.actanaturae.ru).

MANUSCRIPT FORMATTING

The manuscript should be formatted in the following manner:

- Article title. Bold font. The title should not be too long or too short and must be informative. The title should not exceed 100 characters. It should reflect the major result, the essence, and uniqueness of the work, names and initials of the authors.
- The corresponding author, who will also be working with the proofs, should be marked with a footnote *.
- Full name of the scientific organization and its departmental affiliation. If there are two or more scientific organizations involved, they should be linked by digital superscripts with the authors' names. Ab-

stract. The structure of the abstract should be very clear and must reflect the following: it should introduce the reader to the main issue and describe the experimental approach, the possibility of practical use, and the possibility of further research in the field. The average length of an abstract is 20 lines (1,500 characters).

- Keywords (3 – 6). These should include the field of research, methods, experimental subject, and the specifics of the work. List of abbreviations.

• INTRODUCTION

• EXPERIMENTAL PROCEDURES

• RESULTS AND DISCUSSION

• CONCLUSION

The organizations that funded the work should be listed at the end of this section with grant numbers in parenthesis.

• REFERENCES

The in-text references should be in brackets, such as [1].

RECOMMENDATIONS ON THE TYPING AND FORMATTING OF THE TEXT

- We recommend the use of Microsoft Word 2003 for Windows text editing software.
- The Times New Roman font should be used. Standard font size is 12.
- The space between the lines is 1.5.
- Using more than one whole space between words is not recommended.
- We do not accept articles with automatic referencing; automatic word hyphenation; or automatic prohibition of hyphenation, listing, automatic indentation, etc.
- We recommend that tables be created using Word software options (Table → Insert Table) or MS Excel. Tables that were created manually (using lots of spaces without boxes) cannot be accepted.
- Initials and last names should always be separated by a whole space; for example, A. A. Ivanov.
- Throughout the text, all dates should appear in the “day.month.year” format, for example 02.05.1991, 26.12.1874, etc.
- There should be no periods after the title of the article, the authors' names, headings and subheadings, figure captions, units (s – second, g – gram, min – minute, h – hour, d – day, deg – degree).
- Periods should be used after footnotes (including those in tables), table comments, abstracts, and abbreviations (mon. – months, y. – years, m. temp. – melting temperature); however, they should not be used in subscripted indexes (T_m – melting temperature; $T_{p.t}$ – temperature of phase transition). One exception is mln – million, which should be used without a period.
- Decimal numbers should always contain a period and not a comma (0.25 and not 0,25).
- The hyphen (“-”) is surrounded by two whole spaces, while the “minus,” “interval,” or “chemical bond” symbols do not require a space.
- The only symbol used for multiplication is “×”; the “×” symbol can only be used if it has a number to its

right. The “·” symbol is used for denoting complex compounds in chemical formulas and also noncovalent complexes (such as DNA·RNA, etc.).

- Formulas must use the letter of the Latin and Greek alphabets.
- Latin genera and species' names should be in italics, while the taxa of higher orders should be in regular font.
- Gene names (except for yeast genes) should be italicized, while names of proteins should be in regular font.
- Names of nucleotides (A, T, G, C, U), amino acids (Arg, Ile, Val, etc.), and phosphonucleotides (ATP, AMP, etc.) should be written with Latin letters in regular font.
- Numeration of bases in nucleic acids and amino acid residues should not be hyphenated (T34, Ala89).
- When choosing units of measurement, SI units are to be used.
- Molecular mass should be in Daltons (Da, KDa, MDa).
- The number of nucleotide pairs should be abbreviated (bp, kbp).
- The number of amino acids should be abbreviated to aa.
- Biochemical terms, such as the names of enzymes, should conform to IUPAC standards.
- The number of term and name abbreviations in the text should be kept to a minimum.
- Repeating the same data in the text, tables, and graphs is not allowed.

GUIDENESS FOR ILLUSTRATIONS

- Figures should be supplied in separate files. Only TIFF is accepted.
- Figures should have a resolution of no less than 300 dpi for color and half-tone images and no less than 500 dpi.
- Files should not have any additional layers.

REVIEW AND PREPARATION OF THE MANUSCRIPT FOR PRINT AND PUBLICATION

Articles are published on a first-come, first-served basis. The members of the editorial board have the right to recommend the expedited publishing of articles which are deemed to be a priority and have received good reviews.

Articles which have been received by the editorial board are assessed by the board members and then sent for external review, if needed. The choice of reviewers is up to the editorial board. The manuscript is sent on to reviewers who are experts in this field of research, and the editorial board makes its decisions based on the reviews of these experts. The article may be accepted as is, sent back for improvements, or rejected.

The editorial board can decide to reject an article if it does not conform to the guidelines set above.

The return of an article to the authors for improvement does not mean that the article has been accept-

ed for publication. After the revised text has been received, a decision is made by the editorial board. The author must return the improved text, together with the responses to all comments. The date of acceptance is the day on which the final version of the article was received by the publisher.

A revised manuscript must be sent back to the publisher a week after the authors have received the comments; if not, the article is considered a resubmission.

E-mail is used at all the stages of communication between the author, editors, publishers, and reviewers, so it is of vital importance that the authors monitor the address that they list in the article and inform the publisher of any changes in due time.

After the layout for the relevant issue of the journal is ready, the publisher sends out PDF files to the authors for a final review.

Changes other than simple corrections in the text, figures, or tables are not allowed at the final review stage. If this is necessary, the issue is resolved by the editorial board.

FORMAT OF REFERENCES

The journal uses a numeric reference system, which means that references are denoted as numbers in the text (in brackets) which refer to the number in the reference list.

For books: the last name and initials of the author, full title of the book, location of publisher, publisher, year in which the work was published, and the volume or issue and the number of pages in the book.

For periodicals: the last name and initials of the author, title of the journal, year in which the work was published, volume, issue, first and last page of the article. Must specify the name of the first 10 authors. Ross M.T., Grafham D.V., Coffey A.J., Scherer S., McLay K., Muzny D., Platzer M., Howell G.R., Burrows C., Bird C.P., et al. // Nature. 2005. V. 434. № 7031. P. 325–337.

References to books which have Russian translations should be accompanied with references to the original material listing the required data.

References to doctoral thesis abstracts must include the last name and initials of the author, the title of the thesis, the location in which the work was performed, and the year of completion.

References to patents must include the last names and initials of the authors, the type of the patent document (the author's rights or patent), the patent number, the name of the country that issued the document, the international invention classification index, and the year of patent issue.

The list of references should be on a separate page. The tables should be on a separate page, and figure captions should also be on a separate page.

The following e-mail addresses can be used to contact the editorial staff: vera.knorre@gmail.com, actanaturae@gmail.com, tel.: (495) 727-38-60, (495) 930-87-07

NANOTECHNOLOGIES

in Russia

Peer-review scientific journal

Nanotechnologies in Russia

(Rossiiskie Nanotekhnologii)

focuses on self-organizing structures and nanoassemblages, nanostructures including nanotubes, functional nanomaterials, structural nanomaterials, devices and facilities on the basis of nanomaterials and nanotechnologies, metrology, standardization, and testing in nanotechnologies, nanophotonics, nanobiology.

→ **Russian edition:** <http://nanoru.ru>

→ **English edition:** <http://www.springer.com/materials/nanotechnology/journal/12201>

Issued with support from:



The Ministry of Education and Science of the Russian Federation

Science and Technologies in Russia – STRF.RU



40% of scientists agree that the publication of research results helps the enlightenment of the society, leads to the growth of authority of scientific work

34% believe that wide communicating of research results helps to rise the foundation

12% hope that media communications helps them to stand out in public opinion...
...but

17% never speak to journalists*

Open your work to the world!

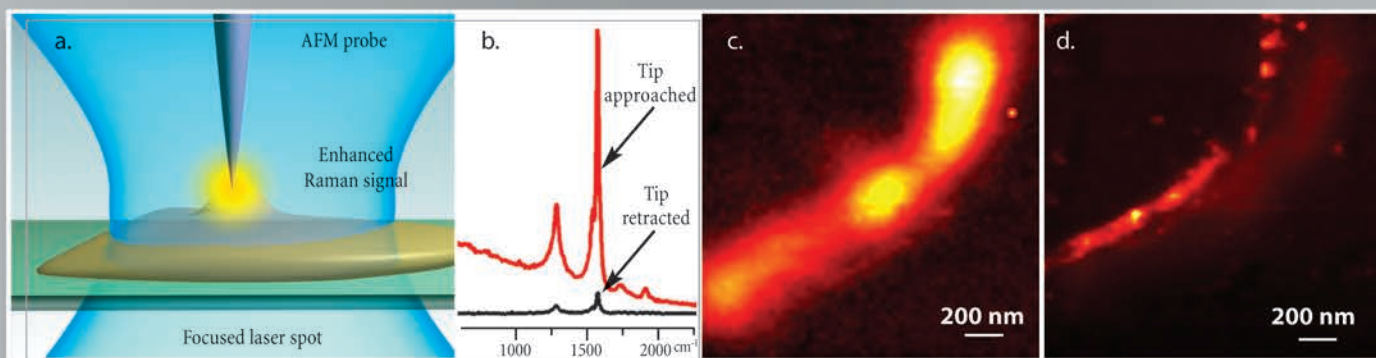
Colours do not play at nanometer scale

But you can colour molecules by their Raman spectra.



Raman mapping by TERS with ultra-high resolution

NTEGRA Spectra



a — a specially prepared AFM probe (metal coated cantilever or etched metal wire) is precisely positioned inside a tightly focused laser spot. b — intensity of carbon nanotube G- and D- Raman bands increases by several orders of magnitude when the special AFM probe is landed and positioned over a small (5 nm height) nanotube bundle - the effect of Tip enhanced Raman scattering (TERS). c — "conventional" confocal Raman image of the nanotube bundle, the observed width of the bundle is ~250 nm (diffraction limit of confocal microscopy, laser

wavelength - 633 nm). d — TERS image of the same bundle - now the observed width is ~70 nm.

Note, in this example, TERS provides more than 4-times better spatial resolution as compared to confocal microscopy. Resolution down to 10 nm and less is theoretically possible. Measurements are done with NTEGRA Spectra in Inverted configuration.

Data courtesy of Dr. S. Kharintsev, Dr. J. Loos, Dr. G. Hoffmann, Prof. G. de With, TUE, the Netherlands and Dr. P. Dorozhkin, NT-MDT Co.

* Enter the Gift code at www.nt-mdt.com and get a present from NT-MDT Co. Attention: limited quantity! Be in time to get your gift!



NT-MDT Co., building 100, Zelenograd,
124482, Moscow, Russia
tel: +7 (499) 735-0305, +7 (495) 913-5736
fax: +7 (499) 735-6410, +7 (495) 913-5739
e-mail: spm@ntmdt.ru; www.ntmdt.com

NT-MDT Europe BV, High Tech Campus 83
5656 AG Eindhoven, the Netherlands
tel: +31(0) 88 338 99 99
fax: +31(0) 88 338 99 98
e-mail: info@ntmdt.eu, www.ntmdt.com